

AD-A087 032

KANSAS UNIV/CENTER FOR RESEARCH INC LAWRENCE REMOTE --ETC F/6 17/9

RADAR BACKSCATTER STUDY OF SEA ICE.(U)

FEB 80 R G ONSTOTT, G J DOME, C V DELKER

N00014-76-C-1105

UNCLASSIFIED

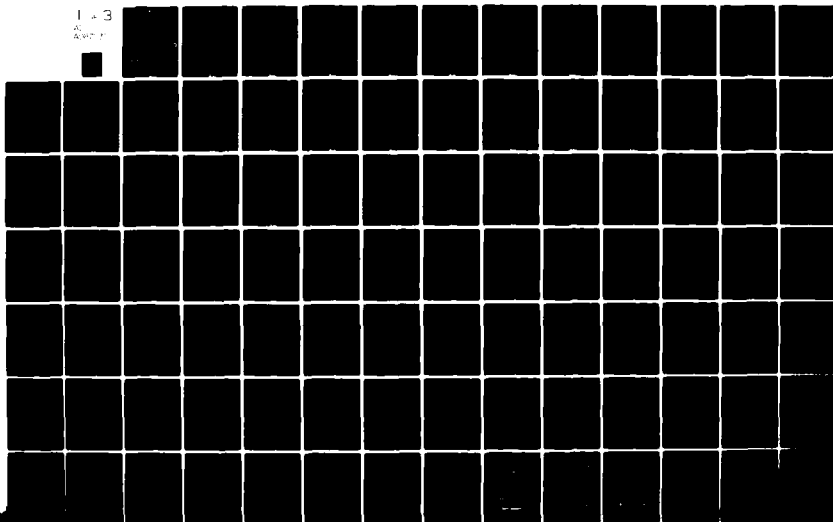
CRINC/RSL-TR-331-14

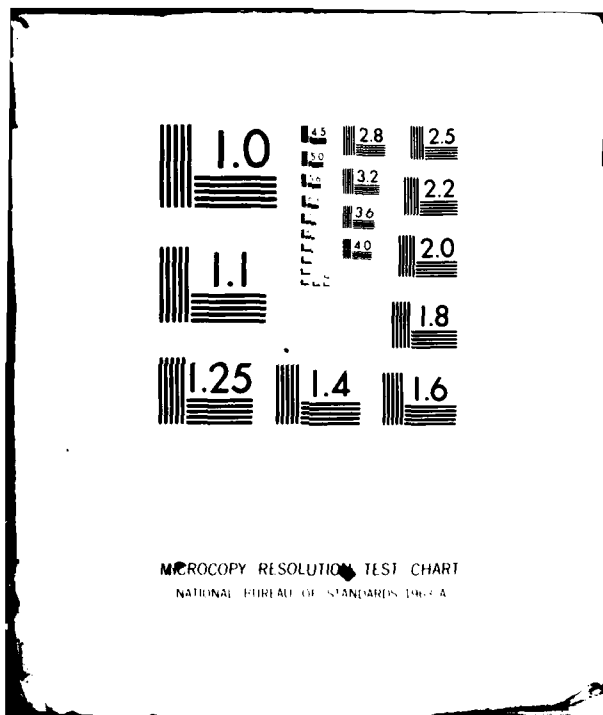
NL

1 - 3

2 - 1

3 - 1





R.K. Moore



THE UNIVERSITY OF KANSAS  
CENTER FOR RESEARCH, INC.

2291 Irving Hill Drive—Campus West  
Lawrence, Kansas 66045

ADA 087032

LEVEL

(P)

DDC FILE COPY

OTIC  
CTE  
JUL 21 1980

D



THE UNIVERSITY OF KANSAS CENTER FOR RESEARCH, INC.

2291 Irving Hill Drive—Campus West  
Lawrence, Kansas 66045

This document has been approved  
for public release and sale; its  
distribution is unlimited.

80 0 2 104

461

(P)

(6)

# RADAR BACKSCATTER STUDY OF SEA ICE

DTIC  
ELECTE  
JUL 21 1980

16  
George  
Cline  
Javed  
R.G./Onstott  
J./Dome  
V./Delker  
S./Patel  
R.K./Moore

Remote Sensing Laboratory  
Center for Research, Inc.  
The University of Kansas  
Lawrence, Kansas 66045

9  
14 CRINC / RSL Technical Report  
RSL-TR-33V-14  
Feb 1980  
11  
12 272

Supported by:

OFFICE OF NAVAL RESEARCH  
Department of the Navy  
800 N. Quincy Street  
Arlington, Virginia 22217

CONTRACT / NO0014-76-C-1105

15

This document has been approved  
for public release and sale; its  
distribution is unlimited.

### ACKNOWLEDGEMENTS

I would like to express my pleasure to have had the opportunity to have done my advanced graduate study under the guidance of Professor Richard K. Moore. Pursuing the radar study of sea ice and working under Professor Moore has been both interesting and rewarding. I would like to thank the graduate committee for their most helpful suggestions. I would also like to acknowledge Dr. W.F. Weeks for sharing his expertise in describing the physical properties of sea ice and his assistance with the on-site measurement programs.

I am very grateful for the abundance of effort and comic relief supplied by the Sea Ice Group of George J. Dome, Javed S. Patel, and Clifford V. Delker.

I would especially like to thank Julie Banhart for typing the manuscript of this dissertation and doing such a good job of it.

I wish to acknowledge the Navy Arctic Research Laboratory at Point Barrow, Alaska for its role in the success of the experiment phase of the ice measurement program.

I would like to acknowledge the support of this research by the Office of Naval Research, Contract N00014-76-C-1105.

Accession For	
NTIS GMA&I	<input checked="checked" type="checkbox"/>
DDC TAB	<input type="checkbox"/>
Unannounced	<input type="checkbox"/>
Justification	<i>Per FL-102</i>
By	<i>on file JED</i>
Distribution/	<i>1/4 Feb 80</i>
Availability Codes	
Dist	Avail and/or special
<i>A</i>	

# ABSTRACT

↙  
The ability to use radar to discriminate ice types has been investigated. Radar backscatter measurements were made of shorefast sea ice near Point Barrow, Alaska in May 1977 and April 1978, with a surface-based FM-CW scatterometer that swept from 1-2 GHz and from 8.5-17.5 GHz. The 1-2 GHz measurements showed that thick first-year and multiyear sea ice cannot be distinguished at 10°-70° incidence angles, but that undeformed sea ice can be discriminated from pressure-ridged thick first-year sea ice and lake ice. Results also indicate that frequencies between 8-18 GHz have the ability to discriminate between thick first-year sea ice, multiyear sea ice, and lake ice. The lowest frequency, 9 GHz, was found to provide the greatest separation between these ice categories with significant levels of separation existing between angles of incidence from 15° to 70°. <sup>DEG</sup> The radar cross-sections for the like polarizations, VV and HH, were very similar in absolute level and angular response. The radar cross-sections for VV-polarization were usually the highest in absolute level. Cross-polarization provided a slightly greater separation between these categories of ice. The 8.5-17.5 GHz angular responses were regressed with a straight line and had an average correlation coefficient of .97 (for 1% confidence the correlation coefficient for our measurements would need to be greater than .89) which shows the goodness of the fit. An empirical model was also developed which describes the angular and frequency variations for thick first-year sea ice, multiyear sea ice, and lake ice. The standard deviation of the model and the averaged scattering cross-section was at worst 2 dB. The individual measurements had a worst standard deviation of 3 dB about the average scattering cross-section.

## TABLE OF CONTENTS

	<u>Page</u>
ACKNOWLEDGEMENTS . . . . .	ii
ABSTRACT . . . . .	iii
1.0 INTRODUCTION . . . . .	1
1.1 Background . . . . .	2
1.2 Review of Previous Results . . . . .	7
1.2.1 J.W. Rouse (1968) . . . . .	8
1.2.2 S.K. Parashar, A.W. Biggs, A.K. Fung, and R.K. Moore (1974) . . . . .	12
1.2.3 L. Gray, J. Cihlar, and S. Parashar (1977). . . . .	19
1.2.4 Gray, Ramseier, and Campbell (1977) . . . . .	20
1.2.5 Comparison of Backscatter Return at 13.3 GHz (VV-polarization) . . . . .	23
2.0 CHARACTERISTICS OF SEA ICE. . . . .	29
2.1 Formation. . . . .	29
2.2 Physical Properties. . . . .	30
2.3 Electrical Properties. . . . .	34
2.3.1 Snow. . . . .	37
2.3.2 Fresh Water Ice . . . . .	37
2.3.3 Brine Liquid. . . . .	41
2.3.4 Sea Ice . . . . .	42
3.0 INVESTIGATION OF SEA ICE. . . . .	53
3.1 Introduction . . . . .	53
3.2 May 1977 and April 1978 Surface-Based Missions . . . . .	53
3.2.1 Microwave Remote Sensor-TRAMAS. . . . .	54
3.2.2 Experiment Description. . . . .	58
3.3 Ground Truth Information . . . . .	59
4.0 DATA ANALYSIS . . . . .	60
4.1 Introduction . . . . .	60
4.2 Scatterometer Equation . . . . .	60

	<u>Page</u>
4.3 Surface Truth. . . . .	63
4.3.1 The May 1977 Barrow Experiment	
Surface Truth Measurement . . . . .	63
4.3.1.1 Site #1: Thick First-Year	
Shorefast Sea Ice. . . . .	65
4.3.1.2 Site #2: Multiyear Sea Ice. . . . .	72
4.3.1.3 Site #3: Thick First-Year	
Shorefast Sea Ice. . . . .	87
4.3.1.4 Site #4: First-Year Pressure-	
Ridged Sea Ice . . . . .	96
4.3.1.5 Site #5: Fragment of Multiyear	
Sea Ice. . . . .	96
4.3.1.6 Site #6: Lake Ice with Ice/Water	
Interface. . . . .	105
4.3.1.7 Site #7: Lake Ice Frozen to Its	
Mud Bottom . . . . .	109
4.3.2 The April 1978 Barrow Experiment Surface Truth. .	109
4.4 L-Band Data Analysis . . . . .	126
4.4.1 Results . . . . .	126
4.4.1.1 Thick First-Year Ice . . . . .	126
4.4.1.2 Multiyear Ice. . . . .	132
4.4.1.3 Small Thick First-Year Pressure	
Ridge. . . . .	132
4.4.1.4 Lake Ice . . . . .	132
4.4.2 Comparison of Scattering Coefficients . . . . .	144
4.4.3 The Effect of Snow Depth on Backscatter	
Return. . . . .	144
4.4.4 The Effect of Temperature on Backscatter	
Return. . . . .	155
4.4.5 Relation Between Backscatter and Crystal	
Orientation . . . . .	156
4.4.6 Discussion of L-Band Results. . . . .	162
4.5 Ku-X-Band Data Analysis. . . . .	163
4.5.1 Results . . . . .	163
4.5.1.1 Thick First-Year Ice . . . . .	163
4.5.1.2 Small Thick First-Year	
Pressure Ridge . . . . .	178
4.5.1.3 Multiyear Ice. . . . .	178
4.5.1.4 Lake Ice . . . . .	183
4.5.2 Comparison of Scattering Coefficients . . . . .	193
4.5.3 The Effect of Snow Depth on Backscatter	
Return. . . . .	206
4.5.4 Temperature Effects on Backscatter	
Return. . . . .	212

	<u>Page</u>
4.6 Frequency Response . . . . .	216
4.7 Application to Ice Type/Thickness Identification . . . . .	222
5.0 MODELING OF BACKSCATTER RETURN. . . . .	227
5.1 Parashar's Backscatter Model . . . . .	227
5.2 Comparison of the Results of the Kansas Experiment with Parashar's Theoretical Model and the Results of Others. . . . .	228
5.3 An Empirical Model of Radar Backscatter From Thick First-Year Sea Ice, Multiyear Sea Ice, and Fresh Water Lake Ice. . . . .	230
5.4 A Qualitative Description of Backscatter . . . . .	237
6.0 CONCLUSIONS AND RECOMMENDATIONS . . . . .	240
6.1 Results. . . . .	240
6.2 Recommendations. . . . .	241
6.3 Sensor . . . . .	244
REFERENCES . . . . .	246

# LIST OF FIGURES

<u>Figure Number</u>	<u>Description</u>	<u>Page</u>
1.2-1	Scattering coefficient variations for multiyear and first-year ice -- line 92 (Rouse, 1968) . . . . .	9
1.2-2	Scattering coefficient variations for multiyear, first-year and ridged first-year ice -- line 94 (Rouse, 1968) . . . . .	10
1.2-3	Scattering coefficient variations for smooth first-year ice, ridged first-year ice and water -- line 91 (Rouse, 1968). . . . .	11
1.2-4	Scattering coefficient variations for first-year ice (Rouse, 1968) . . . . .	13
1.2-5	Comparison of scattering coefficient variations for multiyear ice (Rouse, 1968) . . . . .	14
1.2-6	Experimental $\sigma^0$ versus $\theta$ for different categories, 13.3 GHz, VV (Parashar et al., 1974) . . . . .	16
1.2-7	Experimental $\sigma^0$ versus ice thickness for different $\theta$ , 13.3 GHz, VV (Parashar et al., 1974) . . . . .	16
1.2-8	Experimental $\sigma^0$ versus $\theta$ for different categories, 400 MHz, VV (Parashar et al., 1974) . . . . .	17
1.2-9	Experimental $\sigma^0$ versus ice thickness for different $\theta$ , 400 MHz, VV (Parashar et al., 1974) . . . . .	17
1.2-10	Experimental $\sigma^0$ versus $\theta$ for different categories, 400 MHz, VH (Parashar et al., 1974) . . . . .	18
1.2-11	Experimental $\sigma^0$ versus ice thickness for different $\theta$ , 400 MHz, VH (Parashar et al., 1974). . . . .	18
1.2-12	Scattering coefficient $\sigma^0$ versus angle $\theta$ Forteau Bay, 13.3 GHz HH (Gray et al., 1977) . . . . .	21
1.2-13	Scattering coefficient $\sigma^0$ versus angle $\theta$ Forteau Bay, 13.3 GHz, HV (Gray et al., 1977) . . . . .	21
1.2-14	Scattering coefficient $\sigma^0$ versus angle $\theta$ Northumberland Strait, 13.3 GHz, HH (Gray et al., 1977) . . . . .	21

# LIST OF FIGURES (continued)

<u>Figure Number</u>	<u>Description</u>	<u>Page</u>
1.2-15	Scattering coefficient $\sigma^0$ versus angle $\theta$ North- umberland Strait, 13.3 GHz, HV (Gray et al., 1977). . . .	22
1.2-16	Scattering coefficient $\sigma^0$ versus angle $\theta$ Bay of Chaleur, 13.3 GHz HH (Gray et al., 1977) . . . . .	22
1.2-17	Graph illustrating the four backscattering curves as a function of incidence angle for relatively smooth, ridge-free old ice (Gray, Ramseier, and Campbell, 1977) . . . . .	24
1.2-18	Graph illustrating the four backscattering curves as a function of the incidence angle for an area of smooth young ice (Gray, Ramseier, and Campbell, 1977) . . . . .	25
1.2-19	Graph illustrating the four backscattering curves as a function of incidence angle for an area of first-year ice (Gray, Ramseier, and Campbell, 1977) . . .	26
1.2-20	Comparison of multiyear and thick first-year ice scattering cross-sections according to Rouse (1968), Parashar, et al. (1974), and Gray, et al. (1977). . . . .	27
2.2-1	Depth profiles of salinity, density, and temperature for first-year and multiyear ice obtained during April 1975 at the AIDJEX camp. The schematic of the core is shown on the left hand side of the profiles indicating the structural changes in the ice cover (Campbell, 1975). . . . .	31
2.2-2	Standard sea ice phase diagram . . . . .	33
2.2-3	Temperature dependence of the relative volume of brine liquid in sea ice . . . . .	35
2.3-1	A rudimentary four-layer scattering model of sea ice . . . . .	36
2.3-2	Dielectric properties of dry snow (Evan, 1965) . . . . .	38
2.3-3	Variation of loss tangent of snow with temperature (Cumming, 1965) . . . . .	39
2.3-4	Loss factor of fresh water ice as a function of frequency . . . . .	43

# LIST OF FIGURES (continued)

<u>Figure Number</u>	<u>Description</u>	<u>Page</u>
2.3-5	Static dielectric constant of brine and water as a function of temperature. . . . .	43
2.3-6	Relaxation time of brine and water as a function of temperature. . . . .	44
2.3-7	Conductivity of brine as a function of temperature. . . .	44
2.3-8	Dielectric constant of brine and water as a function of temperature. . . . .	45
2.3-9	Loss factor of brine as a function of temperature . . . .	45
2.3-10	Theoretical loss factor of sea ice compared to experimental data. The frequency used by Hoekstra and Cappillino (1971) was 9186 GHz, in Hallikainen (1977, 16 GHz, and in Vant et al. (1974), 10 GHz . . . . .	47
2.3-11	Theoretical loss factor of sea ice as a function of frequency. The salinity is 8 ‰ and temperature is -10° C . . . . .	48
2.3-12	Theoretical dielectric constant of sea ice compared to experimental results by Vant et al., (1974). The frequency is 10 GHz . . . . .	49
2.3-13	Dielectric constant of sea ice as a function of brine volume at 9.8 GHz. The theoretical results were obtained by using salinities from 4 ‰ to 8 ‰ and temperatures from -3° C to -16° C. . . . .	50
2.3-14	Theoretical loss factor of sea ice at 4.7 GHz as a function of temperature and salinity (random orientation model) . . . . .	51
2.3-15	Theoretical dielectric constant of sea ice at 4.7 GHz as a function of temperature and salinity (random orientation model). . . . .	52
2.3-16	Theoretical attenuation factor of sea ice at 4.7 GHz as a function of temperature and salinity (random orientation model). . . . .	52
3.2-1	The assembled transportable microwave active spectrometer (TRAMAS) . . . . .	55

# LIST OF FIGURES (continued)

<u>Figure Number</u>	<u>Description</u>	<u>Page</u>
3.2-2	Block diagram of TRAMAS system. . . . .	57
4.3-1	Offshore ice experiment locations near Barrow, Alaska, in the Chukchi Sea. . . . .	64
4.3-2	Air and ice surface temperatures for the 1977 Barrow experiment . . . . .	68
4.3-3	0-24 cm section of Site 77-1 ice core . . . . .	69
4.3-4	20-45 cm section of Site 77-1 ice core. . . . .	69
4.3-5	Horizontal thin section of Site 77-1 taken at depth 10 cm . . . . .	70
4.3-6	Horizontal thin section of Site 77-1 taken at 10 cm depth as viewed through polarizing filter . . . . .	70
4.3-7	Horizontal thin section of Site 77-1 taken at 51 cm depth . . . . .	71
4.3-8	Horizontal thin section of Site 77-1 taken at 51 cm depth as viewed through polarizing filter. . . . .	71
4.3-9	The salinity, ice temperature and brine volume profiles for the sea ice from Site 77-1 on May 14, 1977. . . . .	73
4.3-10	Salinity profile for Sites 77-1 and 77-3, thick first-year shore fast sea ice . . . . .	74
4.3-11	Complete ice core of Site 77-2 (meltpond) . . . . .	75
4.3-12	0-25 cm section of Site 77-2 (meltpond) . . . . .	75
4.3-13	21-48 cm section of Site 77-2 (meltpond). . . . .	76
4.3-14	42-68 cm section of Site 72-2 (meltpond). . . . .	76
4.3-15	64-91 cm section of Site 77-2 (meltpond). . . . .	77
4.3-16	78-100 cm section of Site 77-2 (meltpond) . . . . .	77
4.3-17	Complete ice core of Site 77-2 (hummock). . . . .	78
4.3-18	0-24 cm section of Site 77-2 (hummock). . . . .	78

# LIST OF FIGURES (continued)

<u>Figure Number</u>	<u>Description</u>	<u>Page</u>
4.3-19	20-46 cm section of Site 77-2 (hummock) . . . . .	79
4.2-20	41-67 cm section of Site 77-2 (hummock) . . . . .	79
4.3-21	64-90 cm section of Site 77-2 (hummock) . . . . .	80
4.3-22	89-110 cm section of Site 77-2 (hummock). . . . .	80
4.3-23	Horizontal thin section of Site 77-2 (meltpond) at 10 cm depth. . . . .	82
4.3-24	Horizontal thin section of Site 77-2 (meltpond) at 10 cm depth as viewed through polarizing filter. . . .	82
4.3-25	Vertical thin section of Site 77-2 (meltpond) at 78 cm depth . . . . .	83
4.3-26	Vertical thin section of Site 77-2 (meltpond) at 78 cm depth as viewed through polarizing filter . . . . .	83
4.3-27	Horizontal thin section of Site 77-2 (meltpond) at 99 cm depth. . . . .	84
4.3-28	Horizontal thin section of Site 77-2 (meltpond) at 99 cm depth as viewed through polarizing filter. . . . .	84
4.3-29	Horizontal thin section of Site 77-2 (hummock) at 5 cm depth . . . . .	85
4.3-30	Horizontal thin section of Site 77-2 (hummock) at 5 cm depth as viewed through polarizing filter. . . . .	85
4.3-31	Horizontal thin section of Site 77-2 (hummock) at 140 cm depth . . . . .	86
4.3-32	Horizontal thin section of Site 77-2 (hummock) viewed through polarizing filter. . . . .	86
4.3-33	Salinity profile for Site 77-2 and Site 77-5, multiyear sea ice . . . . .	88
4.3-34	Complete ice core of Site 77-3. . . . .	89
4.3-35	0-25 cm section of Site 77-3 ice core . . . . .	89

# LIST OF FIGURES (continued)

<u>Figure Number</u>	<u>Description</u>	<u>Page</u>
4.3-36	21-47 cm section of Site 77-3 ice core. . . . .	90
4.3-37	46-71 cm section of Site 77-3 ice core. . . . .	90
4.3-38	67-94 cm section of Site 77-3 ice core. . . . .	91
4.3-39	91 to 117 cm section of Site 77-3 ice core. . . . .	91
4.3-40	Horizontal thin section of Site 77-3 at 15 cm depth. . . . .	92
4.3-41	Horizontal thin section of Site 77-3 at 15 cm depth as viewed through polarizing filter . . . . .	92
4.3-42	Horizontal thin section of Site 77-3 at 130 cm depth. . . . .	93
4.3-43	Horizontal thin section of Site 77-3 as viewed through polarizing filter . . . . .	93
4.3-44	Vertical thin section of Site 77-3 at 122 cm depth . . . . .	94
4.3-45	Vertical thin section of Site 77-3 at 122 cm cepth as viewed through polarizing filter . . . . .	94
4.3-46	C-axis orientations measured offshore from Barrow, Alaska, in the Chukchi Sea (Weeks 77) . . . . .	95
4.3-47	Cross section of a small first-year sea ice pres- sure ridge, Site 77-4 . . . . .	97
4.3-48	Salinity profile of Site 77-4, first-year pressure- ridged sea ice. . . . .	98
4.3-49	Complete core of Site 77-5. . . . .	99
4.3-50	0-26 cm section of Site 77-5 ice core . . . . .	99
4.3-51	21-47 cm section of Site 77-5 ice core. . . . .	100
4.3-52	44-70 cm section of Site 77-5 ice core. . . . .	100
4.3-53	65-91 cm section of Site 77-5 ice core. . . . .	101
4.3-54	89-115 cm section of Site 77-5 ice core . . . . .	101

# LIST OF FIGURES (continued)

<u>Figure Number</u>	<u>Description</u>	<u>Page</u>
4.3-55	111-138 cm section of Site 77-5 ice core. . . . .	102
4.3-56	132-158 cm section of Site 77-5 ice core. . . . .	102
4.3-57	155-180 cm section of Site 77-5 ice core. . . . .	103
4.3-58	172-193 cm section of Site 77-5 ice core. . . . .	103
4.3-59	Horizontal thin section of Site 77-5 taken at 5 cm depth. . . . .	104
4.3-60	Horizontal thin section of Site 77-5 viewed through polarizing filter . . . . .	104
4.3-61	Horizontal thin section of Site 77-5 taken at 100 cm depth. . . . .	106
4.3-62	Horizontal thin section of Site 77-5 viewed through polarizing filter . . . . .	106
4.3-63	Horizontal thin section of site 77-5 taken at 170 cm depth. . . . .	107
4.3-64	Horizontal thin section of Site 77-5 viewed through polarizing filter . . . . .	107
4.3-65	Vertical thin section of Site 77-5 taken at 170 cm depth. . . . .	108
4.3-66	Vertical thin section of Site 77-5 viewed through polarizing filter . . . . .	108
4.3-67	Complete ice core of Site 77-6. . . . .	110
4.3-68	0-9 cm section of Site 77-6 ice core. . . . .	110
4.3-69	Section representative of 9-134 cm depths at Site 77-6 . . . . .	111
4.3-70	Section representative of 134-205 cm depths at Site 77-6 . . . . .	111
4.3-71	Horizontal thin section of Site 77-6 taken at 20 cm depth . . . . .	112

# LIST OF FIGURES (continued)

<u>Figure Number</u>	<u>Description</u>	<u>Page</u>
4.3-72	Horizontal thin section of Site 77-6 taken at 20 cm depth viewed through polarizing filter. . . . .	112
4.3-73	Horizontal thin section of Site 77-6 taken at 198 cm depth. . . . .	113
4.3-74	Horizontal thin section of Site 77-6 taken at 198 cm depth viewed through polarizing filter . . . . .	113
4.3-75	Salinity profile of Site 77-6, lake ice with an underlying layer of water and Site 77-7, lake ice that is frozen to its mud bottom. . . . .	115
4.3-76	Vertical thin sections of sea ice from the Chukchi Sea near Barrow, Alaska (Site 78-17). . . . .	116
4.3-77	Crystal textures and fabrics of sea ice from the Chukchi Sea near Barrow, Alaska . . . . .	117
4.3-78	Mean C-axis orientation in the horizontal plane and the standard deviation of the C-axes (as measured in the horizontal) as a function of the vertical distance measured from the upper surface of the sea ice. . .	119
4.3-79	The salinity, ice temperature and brine volume profiles for the sea ice from Site 78-17 on 8 April 1978 . . . . .	120
4.3-80	Salinity profiles for Site 78-1 and 78-2, thick first-year shorefast sea ice. . . . .	121
4.3-81	0 to 13 cm section of Site 78 ice core. . . . .	122
4.3-82	12 to 25 cm section of Site 78 ice core . . . . .	122
4.3-83	60 to 73 cm section of Site 78 ice core . . . . .	123
4.3-84	72 to 85 cm section of Site 78 ice core . . . . .	123
4.3-85	113 to 125 cm section of Site 78 ice core . . . . .	124
4.3-86	166 to 175 cm section of Site 78 ice core . . . . .	124
4.3-87	A bare ice surface is shown under study by the TRAMAS system . . . . .	125
4.3-88	Ice with an 8 cm manmade snow cover is shown under study by the TRAMAS system. . . . .	125

# LIST OF FIGURES (continued)

<u>Figure Number</u>	<u>Description</u>	<u>Page</u>
4.4-1	Scattering coefficient of thick first-year ice, Site 77-1, at 1-2 GHz, VV . . . . .	127
4.4-2	Scattering coefficient of thick first-year ice, Site 77-3, at 1-2 GHz, VV . . . . .	128
4.4-3	Scattering coefficient of thick first-year ice, Site 78, at 1-2 GHz, VV . . . . .	129
4.4-4	Scattering coefficient of thick first-year ice, Site 77-1, Site 77-3, and Site 78, at 1-2 GHz, VV . . . .	130
4.4-5	Scattering coefficient of thick first-year ice, Site 77-1, Site 77-2, and Site 78, at 1-2 GHz, VH . . . .	131
4.4-6	Comparison of average scattering coefficients for Site 77 - (1+3) and Site 78 at 1-2 GHz, VV and VH . . . .	133
4.4-7	Scattering coefficient of multiyear ice, Site 77-2, at 1-2 GHz, VV. . . . .	134
4.4-8	Scattering coefficient of mulityear ice, Site 77-5, at 1-2 GHz, VV. . . . .	135
4.4-9	Scattering coefficient of multiyear ice, Site 77-2 and Site 77-5, at 1-2 GHz, VV and VH. . . . .	136
4.4-10	Scattering coefficient of a small thick first-year pressure ridge, Site 77-4, at 1-2 GHz, VV . . . . .	137
4.4-11	Scattering coefficient of lake ice with underlying layer of water, Site 77-6, at 1-2 GHz, VV . . . . .	138
4.4-12	Scattering coefficient of lake ice frozen to its mud bottom, Site 77-7, at 1-2 GHz, VV . . . . .	139
4.4-13	Scattering coefficient of lake ice, Site 77-6 and Site 77-7, at 1-2 GHz, VV . . . . .	140
4.4-14	Scattering coefficient of thick first-year and multiyear ice at 1-2 GHz. . . . .	141
4.4-15	Scattering coefficient of thick first-year, multi- year, fresh water lake, and pressure ridge ice at 1-2 GHz . . . . .	142

# LIST OF FIGURES (continued)

<u>Figure Number</u>	<u>Description</u>	<u>Page</u>
4.4-16	Average scattering coefficient of thick first-year, multiyear, fresh water lake, and pressure ridge ice at 1-2 GHz, VH. . . . .	143
4.4-17	Average $\sigma^0$ versus angle of incidence ( $\theta$ ) curve for bare-ice and snow-covered ice, 1.5 GHz. . . . .	146
4.4-18	Scattering coefficients of thick first-year ice, Site 78-1, with a 0, 2, and 8 cm snow layer at 1-2 GHz, VV . . . . .	147
4.4-19	Scattering coefficient of thick first-year ice, Site 78-2, with a 0 and 4 cm snow layer at 1-2 GHz, VV . . . . .	148
4.4-20	Scattering coefficient of thick first-year ice, Site 78-3, with 0 and 14 cm snow cover at 1-2 GHz, VV . . . . .	149
4.4-21	Scattering coefficient of thick first-year ice, Site 78-4, with 0 and 2 cm snow cover at 1-2 GHz, VV. . . . .	150
4.4-22	Scattering coefficient of thick first-year ice, Site 78-5, with 0 and 4 cm snow cover at 1-2 GHz, VV. . . . .	151
4.4-23	To illustrate the overall effect of snow depth on radar return at 1-2 GHz, VV, the average dB return for 42, 51, 60, and 70 degree angles is plotted versus snow depth. . . . .	152
4.4-24	To illustrate the overall effect of snow depth on radar return at 1-2 GHz, VV, the average dB return for 12° is plotted versus snow depth. . . . .	153
4.4-25	The effect of ice temperature on the backscatter return from thick first-year shorefast sea ice at 1-2 GHz, VV, for 42°, 51°, 60° and 70° angles is shown. . . . .	154
4.4-26	Results of the 1977 experiment demonstrating the effects of a preferred ice crystal orientation on 1-2 GHz like-polarized (VV) radar backscatter return. . .	160

# LIST OF FIGURES (continued)

<u>Figure Number</u>	<u>Description</u>	<u>Page</u>
4.4-27	Results of 1978 experiment demonstrating the effects of a preferred ice crystal orientation on 1-2 GHz like-polarized (VV) radar backscatter return. . . . .	161
4.5-1	Scatter plot of the angular response of the radar cross-section of thick first-year ice, Site 77-1, at 9 GHz, HH. . . . .	164
4.5-2	Scatter plot of the angular response of the radar cross-section of thick first-year ice, Site 77-1, at 13 GHz, HH . . . . .	165
4.5-3	Scatter plot of the angular response of the radar cross-section of thick first-year ice, Site 77-1, at 17 GHz, HH . . . . .	166
4.5-4	Scattering coefficient of thick first-year ice, Site 77-1, at 9 GHz . . . . .	168
4.5-5	Scattering coefficient of thick first-year ice, Site 77-1, at 13 GHz. . . . .	169
4.5-6	Scattering coefficient of thick first-year ice, Site 77-1 at 17 GHz . . . . .	170
4.5-7	Scattering coefficient of thick first-year ice, Site 77-3, at 9 GHz . . . . .	172
4.5-8	Scattering coefficient of thick first-year ice, Site 77-3, at 13 GHz. . . . .	173
4.5-9	Scattering coefficient of thick first-year ice, Site 77-3, at 17 GHz. . . . .	174
4.5-10	Scattering coefficient of thick first-year ice with natural snow cover, Site 78, at 9 GHz . . . . .	175
4.5-11	Scattering coefficient of thick first-year ice with natural snow cover, Site 78, at 13 GHz. . . . .	176
4.5-12	Scattering coefficient of thick first-year ice with natural snow cover, Site 78, at 17 GHz. . . . .	177
4.5-13	A comparison of the scattering coefficients of thick first-year sea ice for Sites 77-1, 77-3, and 78 at 9 GHz, HH . . . . .	179

# LIST OF FIGURES (continued)

<u>Figure Number</u>	<u>Description</u>	<u>Page</u>
4.5-14	A comparison of the scattering coefficients of thick first-year sea ice for Sites 77-1, 77-3, and 78 at 13 GHz, HH. . . . .	180
4.5-15	A comparison of the scattering coefficients of thick first-year sea ice for Sites 77-1, 77-3, and 78 at 17 GHz, HH. . . . .	181
4.5-16	Scattering coefficient of a small thick first-year pressure ridge, Site 77-4, at 13 GHz . . . . .	182
4.5-17	Scattering coefficient of multiyear ice, Site 77-2 and Site 77-5, at 9 GHz, HH. . . . .	184
4.5-18	Scattering coefficient of multiyear ice, Site 77-2 and Site 77-5, at 13 GHz, HH . . . . .	185
4.5-19	Scattering coefficient of multiyear ice, Site 77-2 and Site 77-5, at 17 GHz. . . . .	186
4.5-20	Scattering coefficient of lake ice with underlying layer of water, Site 77-6, at 9 GHz . . . . .	187
4.5-21	Scattering coefficient of lake ice with underlying layer of water, Site 77-6, at 13 GHz. . . . .	188
4.5-22	Scattering coefficient of lake ice with underlying layer of water, Site 77-6, at 17 GHz. . . . .	189
4.5-23	Scattering coefficient of lake ice frozen to its mud bottom, Site 77-7, at 9 GHz . . . . .	190
4.5-24	Scattering coefficient of lake ice frozen to its mud bottom, Site 77-7, at 13 GHz. . . . .	191
4.5-25	Scattering coefficient of lake ice frozen to its mud bottom, Site 77-7, at 17 GHz. . . . .	192
4.5-26	Scattering coefficient of lake ice, Site 77-6 and Site 77-7 at 9 GHz, VV and Cross. . . . .	194
4.5-27	Scattering coefficient of lake ice, Site 77-6 and Site 77-7, at 13 GHz, VV and Cross. . . . .	195
4.5-28	Scattering coefficient of lake ice, Site 77-6 and Site 77-7, at 17 GHz, VV and Cross. . . . .	196
4.5-29	Scattering coefficient of thick first-year and multiyear ice at 9 GHz. . . . .	197

# LIST OF FIGURES (continued)

<u>Figure Number</u>	<u>Description</u>	<u>Page</u>
4.5-30	Scattering coefficient of thick first-year and multiyear ice at 13 GHz . . . . .	198
4.5-31	Scattering coefficient of thick first-year and multiyear ice at 17 GHz . . . . .	199
4.5-32	Scattering coefficient of thick first-year, multiyear, lake and pressure ridge ice at 9 GHz, HH . . .	201
4.5-33	Scattering coefficient of thick first-year, multiyear, fresh water lake, and pressure ridge ice at 13 GHz. . . . .	202
4.5-34	Scattering coefficient of thick first-year, multiyear, lake and pressure ridge ice at 13 GHz, VV . . . . .	203
4.5-35	Scattering coefficient of thick first-year, multiyear, lake, and pressure ridge ice at 13 GHz, HV. . . . .	204
4.5-36	Scattering coefficient of thick first-year, multiyear, lake, and pressure ridge ice at 17 GHz, HH. . . . .	205
4.5-37	Average $\sigma^0$ versus angle of incidence ( $\theta$ ) curve for bare-ice and snow-covered first-year sea ice, 9.0 GHz . .	207
4.5-38	Average $\sigma^0$ versus angle of incidence ( $\theta$ ) curve for bare-ice and snow-covered first-year sea ice, 13.0 GHz . . . . .	208
4.5-39	Average $\sigma^0$ versus angle of incidence ( $\theta$ ) curve for bare-ice and snow-covered first-year sea ice, 17.0 GHz . . . . .	209
4.5-40	Scattering coefficient of thick first-year ice, Site 78-2, with a natural 4 cm snow cover and a bare surface at 13 GHz, VV. . . . .	210
4.5-41	The response of the scattering coefficient of thick first-year ice, Site 78, as a function of snow depth at 9, 13 and 17 GHz, HH . . . . .	211
4.5-42	Effect of temperature on the scattering coefficient of thick first-year ice with no snow cover at 9 and 13 GHz, an incidence angle of 55°, and HH polarization. . . . .	213

# LIST OF FIGURES (continued)

<u>Figure Number</u>	<u>Description</u>	<u>Page</u>
4.5-43	Effect of temperature on the scattering coefficient of thick first-year ice with a 2 cm snow cover at 9 and 13 GHz, an incidence angle of 55°, and HH polarization . . . . .	214
4.5-44	Effect of temperature on the scattering coefficient of thick first-year ice with a 4 cm snow cover at 9 and 13 GHz, an angle of incidence of 55°, and HH polarization. . . . .	215
4.6-1	Scattering coefficient of thick first-year and multi-year ice at 1.5, 9.0, 13.0 and 17.0 GHz . . . . .	217
4.6-2	Scattering coefficient frequency response of thick first-year and multiyear ice. . . . .	218
4.6-3	Scattering coefficient frequency response of thick first-year and multiyear ice. . . . .	219
4.6-4	Scattering coefficient frequency response of thick first-year and multiyear ice. . . . .	220
4.6-5	Scattering coefficient frequency response of thick first-year sea ice, Site 77-3 and Site 78 . . . . .	221
4.7-1	Difference between radar cross-section of thick first-year and multiyear ice at 1.5, 9.0, 13.0 and 17.0 GHz with vertical polarization . . . . .	224
4.7-2	Difference between radar cross-section of thick first-year and multiyear ice at 1.5, 9.0, 13.0 and 17.0 GHz with cross-polarization. . . . .	224
5-1	A comparison of Parashar's theoretical results and the results of the recent Kansas experiments. . . . .	229
5-2	Comparison of multiyear and thick first-year ice scattering cross-sections (experimental) according to Rouse (1968), Parashar, et al. (1974), and Gray, et al. (1977) . . . . .	231
5-3	Scattering coefficients of multiyear, thick first-year and lake ice at 9 GHz, HH, using an empirical model developed from the recent Kansas experiments. . . . .	236
5-4	A family of radar cross-sections which illustrate the interaction of surface roughness and the volume scatter properties of ice . . . . .	238

## LIST OF TABLES

<u>Table Number</u>	<u>Description</u>	<u>Page</u>
1.2-1	Comparison of the radar cross-section $\sigma^0$ (in dB) results of Rouse (1968), Parashar (1974), and Gray (1977) for multiyear and thick first-year sea ice . . . . .	28
2.3-1	Skin depth for snow and ice . . . . .	40
3.2-1	Nominal system specifications . . . . .	56
4.3-1	Site descriptions . . . . .	66
4.3-2	Snow densities taken at Sites 77-1, 77-2, 77-4, and 77-7. . . . .	67
4.4-1	Summary of site information used in the discussion of c-axis effects on radar backscatter return . . . . .	157
5.3-1	Regression model coefficients for thick first-year sea ice, multiyear sea ice and fresh water lake ice with an underlying layer of water and little snow cover for 8-18 GHz frequencies and angles of incidence from $10^\circ$ to $70^\circ$ . . . . .	235

## 1.0 INTRODUCTION

The Arctic is the area of the far north characterized by distinctively polar conditions of climate, plant life, etc. The term Arctic is derived from the Greek word "arktos" meaning "bear" which refers to the northern constellation of the Bear. International interest in the Arctic and sub-Arctic regions has steadily increased during the twentieth century and particularly since the Second World War. Three major factors have led to this rising interest: the advantage of the North Pole route as a short-cut between important centers of population; the growing realization of economic potentialities such as minerals (especially petroleum), forest resources, and grazing areas; and the importance of the regions in the study of global meteorology.

The Arctic Ocean is partially covered with sea ice at all times. With a surface area estimated at 5,427 square miles, ice may have an extent ranging from 1/10 cover to 9/10 or 10/10 cover, depending upon the season and locality. The ice cover, pack ice, is not a static homogeneous film upon the sea surface. It consists of large and small areas of open water, areas with pressure ridges, rafted ice, etc., forming, growing, and melting and consequently covers areas of variable extension.

Due to the increasing variety of scientific and operational interests in the Arctic polar region, testing and evaluation of state-of-the-art remote sensors has been in progress for many years to determine their potential capability in sea ice studies. Development of microwave frequency radars used as remote sensors broadens prospects of remote measurements of such interesting and dynamic features of the Earth's surface. The capability of radar to provide useful

information under weather and lighting conditions unsuitable for visual sensing attracts considerable interests toward developing it into a tool to be used in sea ice reconnaissance and forecasting.

### 1.1 Background

Study and exploration of the Arctic probably began with a Greek named Pytheas, who in the fourth century BC made an astonishing voyage from the Mediterranean around Britain and reached a place he called Thule, variously identified as the Shetlands, Iceland, and Norway. His accounts of this remarkable voyage were for centuries discredited, but the idea of his Thule, shrouded in fog and believed to be the end of the Earth, caught the imagination of many. From these first glimpses of the inhabitable "frigid zone" shrouded in a mist of superstitious beliefs, primitive navigation techniques, and an obscurity resulting from inaccurate ideas of the shape of the Earth, exploration continued by men who could not quench their thirst for adventure by more calm and rudimentary methods.

A comprehensive expansion of all types of research in the Arctic Ocean took place between 1950 and 1970. Many drift ice research stations were established by the United States and the Soviet Union serving as bases for studies of atmosphere, ice, ocean waters, and crust beneath. U.S. nuclear submarines made their first voyages through the Arctic Ocean in 1957, making possible continuous profiles of many geophysical parameters. Research efforts by the U.S. recently culminated in the Arctic Ice Dynamics Joint Experiment (a study of basic processes and data collecting for use in the modeling of sea ice).

The naval military importance of the Arctic has risen significantly over the past few years. The chain of events leading to policy of energy independence and the consequent emphasis on accelerated exploration of our North Slope and offshore Alaskan oil reserves has served as one cause. As a consequence, strategists have considered the vital role of our naval forces in the protection of a new and important sea lane. A second factor has been the increasing long-range capabilities of submarine-launched ballistic missiles, making the Arctic Ocean a possible patrol and launch area. A third factor involves freedom of the seas and geographical intentions. Very recently countries bordering the Arctic have threatened to extend their rights over contiguous waters to the 200 mile limit, which could, in some measures, bottle-up the narrow eastern entrance to the Arctic Basin. The nuclear attack submarine, with its exceptional mobility in ice-infested waters, has an important potential role in all of the above considerations.

The polar regions greatly effect the environment of the Earth's surface. In the global thermodynamics cycle of atmosphere and ocean, the polar regions are the heat sinks. In the period of one revolution of the Earth, the polar regions lose more heat to space than is received from the sun. As a result, they are regions which are cold and maintain permanent ice cover of annually ranging extent. In compensation for the heat lost to space, heat from the lower latitudes is circulated into the polar regions. The vertical extent of sea ice cover is extremely small compared to its vast horizontal extent (about  $1:10^6$ ). Small perturbations in the heat balance in the ice surface may result in large alterations in the ice cover, resulting in changes of terrestrial

albedo, sea surface temperature, ocean mixing, evaporation, and so forth.

Sea ice is a dynamic obstacle of shipping. For global weather forecasting it is a prized piece of the puzzle, an integral part of the global weather model. On a large time scale ice is forming, growing, and melting; consequently it covers areas of variable extension. On a short time scale weather, mainly the wind, influences the ice cover causing movement of the ice, formation of open leads and ice ridges, etc. In order to make navigation as safe as possible and to optimize it economically by choosing the easiest routes through the ice, it is necessary to watch the ice situation. Ice cover, being a key in global weather, must be monitored. This means mapping, analyzing, and forecasting the ice situation.

For sea ice mapping may be the name of the game. Large areas of sea ice have been mapped in the past, primarily by the use of conventional aerial photographic methods using black and white, color, and infrared films. It was shown by Anderson (1970) that ages and discrimination among categories of sea ice could be determined from stereoscopic aerial photography by employing the usual photo-interpretation techniques of terrain air-photo analysis. Pattern configuration, surface features, and tone are used in the interpretation. Local weather and daytime usage limit the operational capability of this remote sensor in the uncertain weather conditions and durations of inadequate incident light characteristic of the Arctic region.

Development of remote-sensing radar systems operating in the microwave region of the frequency spectrum has broadened the prospects of remotely measuring significant features of the Earth's surface. Since

the performance of the remote-sensing radars is unaffected by poor weather conditions and lack of incident light, the application of radar in the remote sensing of sea ice appears to be particularly attractive.

The potential application of SLAR to sea ice research and reconnaissance was recognized in 1962, when the U.S. Army Cold Regions Research and Engineering Laboratory utilized a U.S. Air Force AN/APQ-56 K-band SLAR in sea ice experiments conducted during April and August of that year [1]. This study indicated that various important sea ice features could be identified on the K-band imagery, and that the SLAR system provided the capability of obtaining good-resolution image maps of large expanses of ice independent of incidence-light and weather conditions.

Since that time radar has been used extensively to monitor sea ice by Rouse (1969); Johnson and Farmer (1971); Glushkov and Komarov (1971); Ketchum and Tooma (1973); Parashar et al. (1974); Dunbar (1975); Dunbar and Weeks (1976); Gray et al. (1977); and Ketchum (1977). These studies have primarily been made at 2 and 3 cm wavelengths, although a few studies were made at 25 cm wavelengths. Most SLAR flights have used angles of incidence near grazing. These studies tend to agree that, with some reservations, the ability to detect and interpret ice age, ice drift, ice surface topography such as pressure-ridges and fractures, and to evaluate sea ice conditions, in general, was very good.

The first attempt to expand the knowledge of the parametric response of radar systems sensing sea ice began in 1967 when the National Aeronautics and Space Administration, Navy Oceanographic

Office, U.S. Army Cold Regions Research and Engineering Laboratory, Arctic Institute of North America, and the University of Kansas studied the ability of a 2.25 cm wavelength radar scatterometer to identify different ice types. The radar scatterometer is a calibrated instrument designed to measure the differential scattering coefficient  $\sigma^0$  as a function of incidence angle [11]. Analysis of the 1967 scatterometer data was carried out by Rouse [2], who demonstrated that a 2.25 cm wavelength (13.3 GHz) vertically polarized scatterometer could be used to discriminate ice types. For instance, multiyear returns were higher than thick first-year ice at all angles of incidence.

In April 1970 another joint experiment was conducted by NASA, Naval Oceanographic Office, and the University of Kansas in which systematic radar backscatter measurements of sea ice were made at 400 MHz (HH, VV, VH, and HV polarizations) and 13.3 GHz (VV polarization). The results showed that multiyear ice gave the strongest return at 13.3 GHz [12]. First-year ice and open water gave the strongest return at 400 MHz. Also discrimination of ice from open water was possible with both frequencies. Four polarization 16.5 GHz radar imagery was also analyzed. Results showed that 0-18 cm, 18-90 cm, 90-360 cm ice and open water were discriminable. These results were consistent with the scatterometer results. Cross-polarization appeared to be better in discriminating sea ice types, but problems with the images prevented a firm conclusion.

During the winter and spring of 1975-1976, measurements were made with a multi-polarized 13.3 GHz scatterometer by the Canada Centre for Remote Sensing in conjunction with Aidx and Beaufort Sea offshore

programs [9]. Results showed systematic changes in microwave backscatter which strongly correlated with gross ice type categories. Multiyear ice showed significantly higher backscatter than thick first-year ice. Typical differences in backscatter ran 8-10 dB for like-polarization and 15-18 dB for cross-polarization.

An X-band SLAR experiment was also conducted recently (May 1975) by the Naval Oceanographic Office over areas of the Lincoln Seas, Nares Strait, and Baffin Bay. The ability to interpret sea ice features and evaluate sea ice conditions was considered to be generally good in the more northerly Arctic areas. However, the young stages of ice development observed in Baffin Bay made interpretation and discrimination much more difficult due to a high homogeneous radar return. Multiyear ice was easy to discriminate due to predictable return and the well-defined shapes of the floes. Younger ice was discriminable from old ice, in a gross sense, but discrimination among the several stages of young ice development was not possible from backscatter information and pattern analysis. New ice-ridges and hummocks provided strong returns. Old weathered ridges and hummocks provided backscatter returns that were similar to returns observed in undeformed old ice suggesting that volume scattering is the major backscatter mechanism of multiyear ice.

#### 1.2 Review of Previous Results

Previous scatterometry measurements of sea ice have been detailed in papers by Rouse (1968), Parashar et al. (1974), Gray et al. (1977), and Gray et al. (1977). Each of these will be considered individually,

with brief descriptions given of the radars used, the sea ice conditions at time of measurement, and their results.

1.2.1 J.W. Rouse (1968).

Radar backscatter measurements were made at 13.3 GHz (VV polarization). These measurements were made using the NASA Ryan Redop scatterometer. The illuminated area subtended  $120^\circ$  in the along-track direction and  $3^\circ$  in the across-track direction. The measurements were made off the coast of Alaska near Point Barrow during the month of May in 1967. Ground truth was provided by black-and-white photography and color infrared photography. Some documentation was done by ground parties.

The results (of flight line 92) shown in Figure 1.2-1 are those for an old multiyear ice floe and smooth first-year ice. The multiyear ice floe was found to be several years old and was well-weathered. Hummocks were well-rounded. The smooth thick first-year ice had an average thickness of 1.35 meters, was uniform, and was covered with 1-2 cm of snow. Multiyear ice returns were found to be greater than 5 dB higher than first-year ice returns at angles greater than  $25^\circ$ . Figure 1.2-2 shows the return from another flight line (line 94). The ice types and conditions were found to be similar to the previous line. This figure shows the returns from the multiyear ice, ridged ice, and first-year ice. Figure 1.2-3 shows the returns, obtained from a third flight line (line 91), of smooth first-year ice, ridged first-year ice, and open water. These results showed that it was difficult in this case to discriminate between smooth and ridged first-year ice. It was also demonstrated that open water was discriminable from first-year ice. Figure 1.2-4 shows the variation in the return of first-year ice

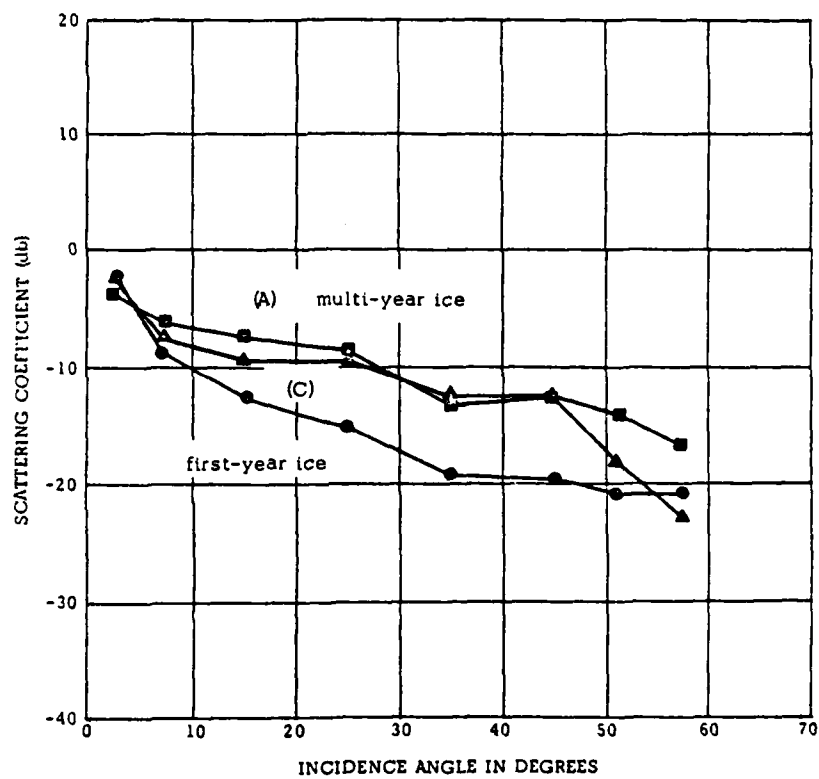


Figure 1.2-1. Scattering coefficient variations for multiyear and first-year ice -- line 92 (Rouse, 1968).

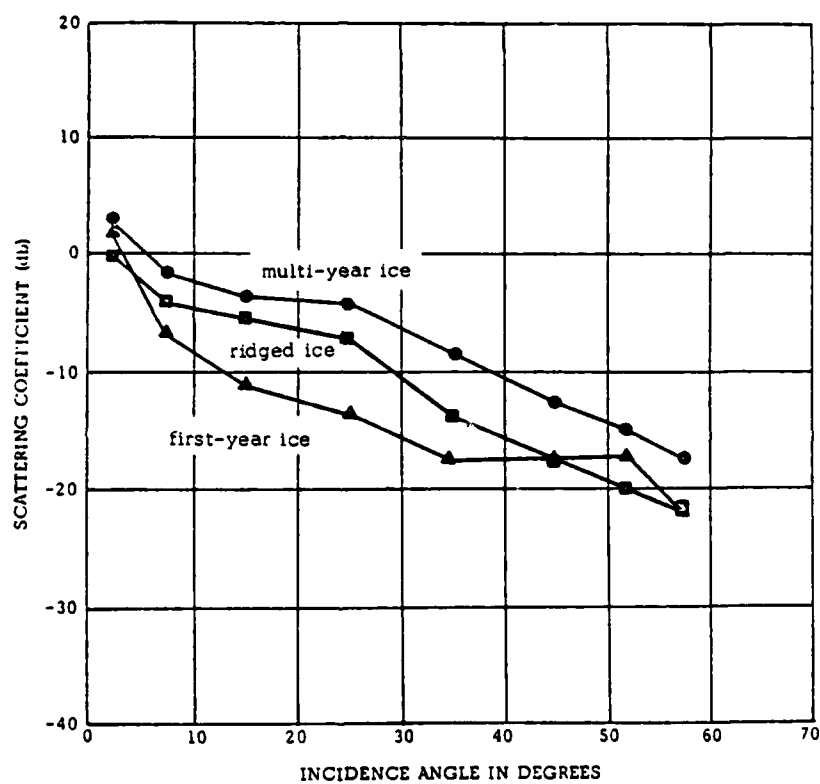


Figure 1.2-2. Scattering coefficient variations for multiyear, first-year, and ridged first-year ice -- line 94 (Rouse, 1968).

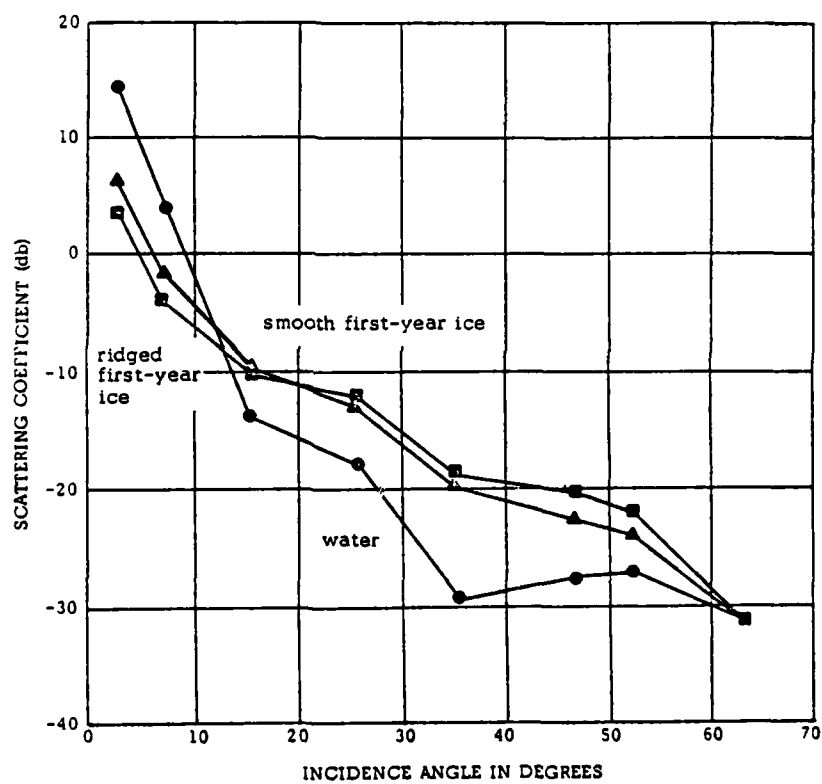


Figure 1.2-3. Scattering coefficient variations for smooth first-year ice, ridged first-year ice and water -- line 91 (Rouse, 1968).

for the three flight lines, with good agreement in shape. It was noted that the ice in line 91 was very smooth compared to the block-strewn ice of the other lines. Figure 1.2-5 shows the variation in the multi-year ice returns found in flight lines 92 and 94.

1.2.2 S.K. Parashar, A.W. Biggs, A.K. Fung and R.K. Moore (1974).

Radar backscatter measurements of sea ice were made at 400 MHz (VV, HH, VH, HV polarizations) and 13.3 GHz (VV polarization). The NASA Ryan Redop scatterometer was used in the 13.3 GHz measurement program. The illuminated area subtended  $120^\circ$  in the along-track direction and  $3^\circ$  in the across-track direction. The NASA-Emerson scatterometer system was used in the 400 MHz program. The illuminated area subtended  $120^\circ$  in the along-track direction and  $7.5^\circ$  in the across-track direction. This mission was conducted off the coast of Alaska near Point Barrow during the month of April 1970. The surface truth was provided by stereo aerial photographs. The ice surface temperature of  $-10^\circ\text{C}$  (obtained from a surface party) was assigned to all categories of ice. Seven categories were used to describe the ice conditions. These were:

- Category 1: Open water
- Category 2: New ice (0-5 cm thick)
- Category 3: Thin young ice (5-18 cm thick)
- Category 4: Thick young ice (18-30 cm thick)
- Category 5: Thin first-year ice (30-90 cm thick)
- Category 6: Thick first-year ice (90-180 cm thick)
- Category 7: Multiyear ice (180-360 cm thick)

Results with the 13.3 GHz scatterometer showed that open water gave the strongest return at near-vertical angles, whereas beyond  $15^\circ$

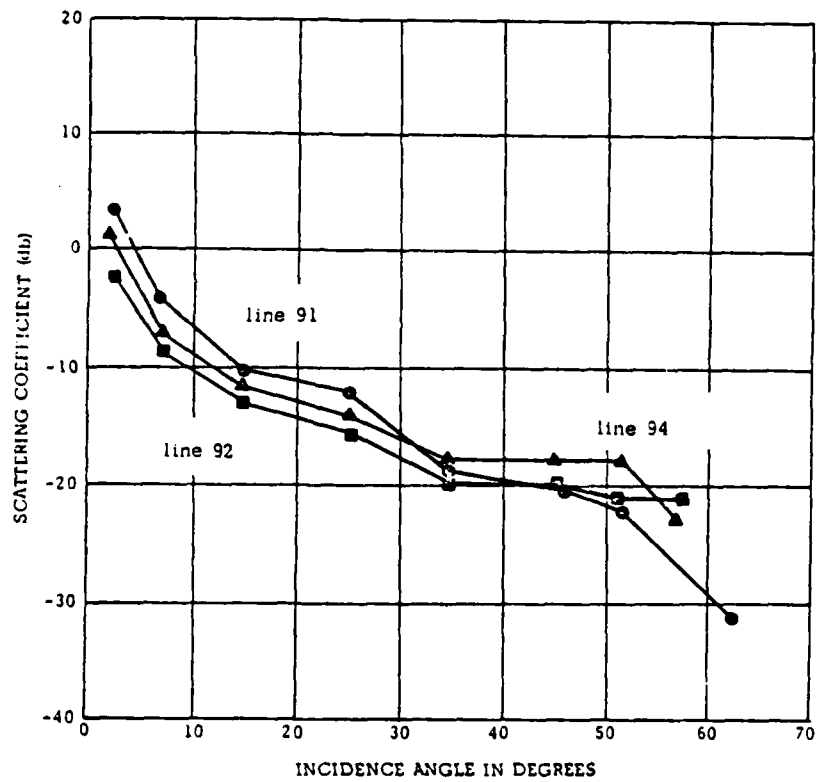


Figure 1.2-4. Scattering coefficient variations for first-year ice (Rouse, 1968).

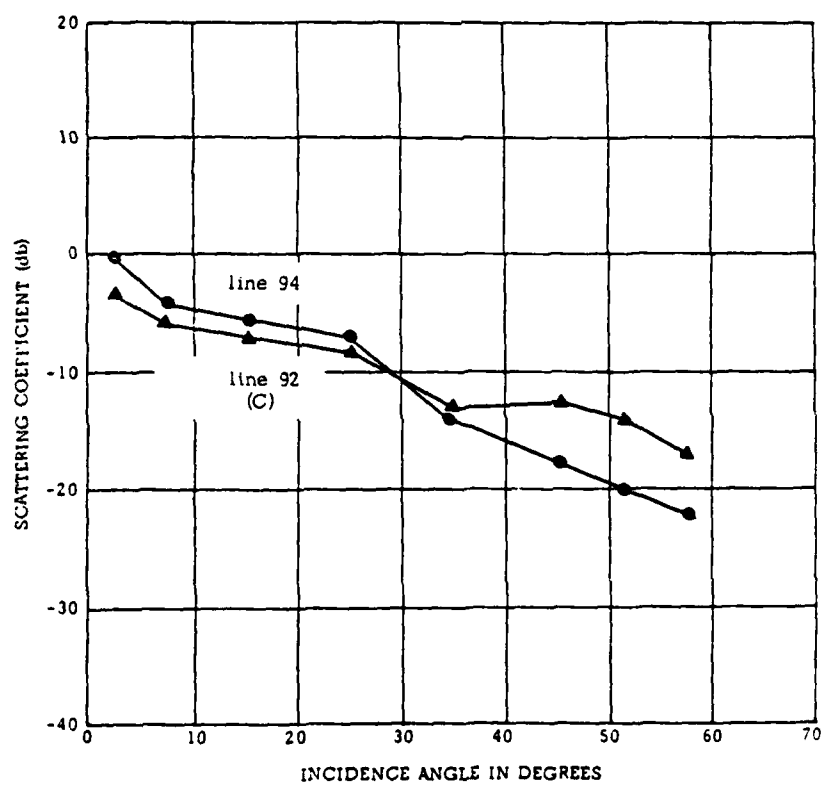


Figure 1.2-5. Comparison of scattering coefficient variations for multiyear ice (Rouse, 1968).

multiyear ice gave more return than the other categories of ice or water. Thick first-year ice was the next strongest in return at these angles and was 4 dB less strong than multiyear ice returns (see Figure 1.2-6). At the larger angles both multiyear ice and thick first-year ice were discriminable from the younger stages of ice and from open water. Also, at these angles there was some ability to discriminate between new and thin young ice and thin first-year and thick first-year ice. Radar cross-sections versus thickness curves were produced to demonstrate the ability to discriminate among ice types. These curves are shown in Figure 1.2-7. As these curves demonstrate, the ability to discriminate is a function of the angle of incidence. Also, there are ambiguities in the radar returns from ice under 18 cm thick and ice 90-180 cm thick. This ambiguity exists because the thinner ice gives more return than the moderately thick ice.

The results with the 400 MHz scatterometer for VV and VH polarizations are shown in Figures 1.2-8 and 1.2-10, respectively. For VV polarization open water gave the strongest return at all angles. New and thin young ice gave the minimum return at all angles and thin and thick first-year ice gave more return than multiyear ice. For HH polarization, open water returns were the strongest at angles less than  $20^\circ$ , whereas thin and thick first-year ice produced the strongest returns beyond  $20^\circ$ . Again, ice less than 18 cm thick gave minimum returns at all angles. For both cross-polarizations (HV and VV), open water produced at almost all angles the strongest returns. Again, ice less than 18 cm thick produced the minimum returns. Radar cross-section versus ice thickness curves are shown in Figures 1.2-9 and

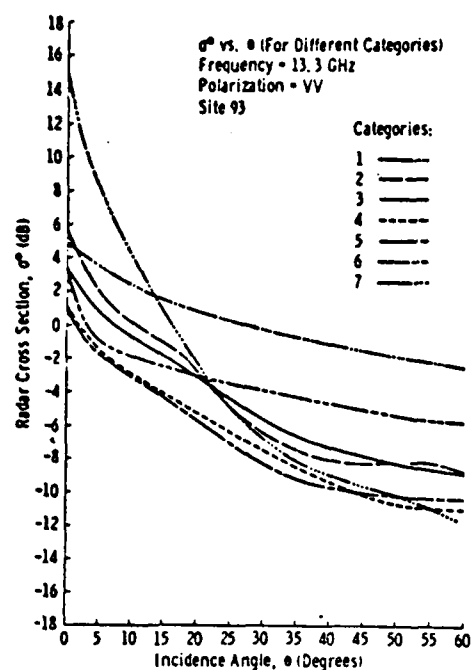


Figure 1.2-6. Experimental  $\sigma^0$  versus  $\theta$  for different categories, 13.3 GHz, VV (Parashar et al., 1974).

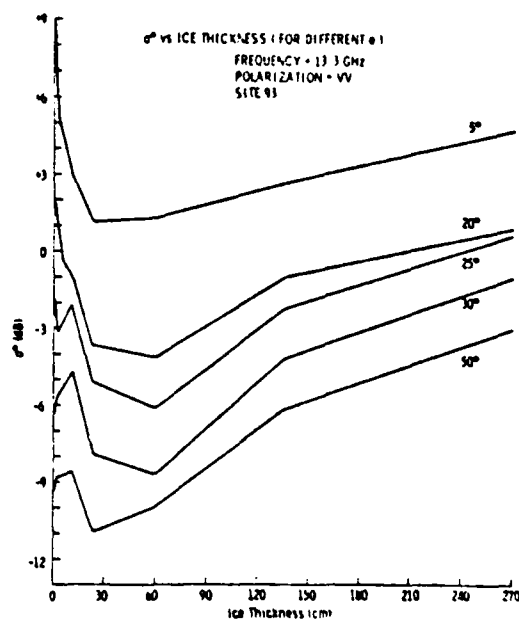


Figure 1.2-7. Experimental  $\sigma^0$  versus ice thickness for different  $\theta$ , 13.3 GHz, VV (Parashar et al., 1974).

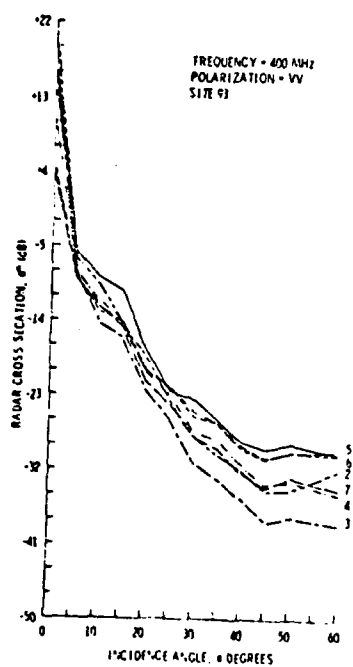


Figure 1.2-8. Experimental  $\sigma^0$  versus  $\theta$  for different categories, 400 MHz, VV (Parashar et al., 1974).

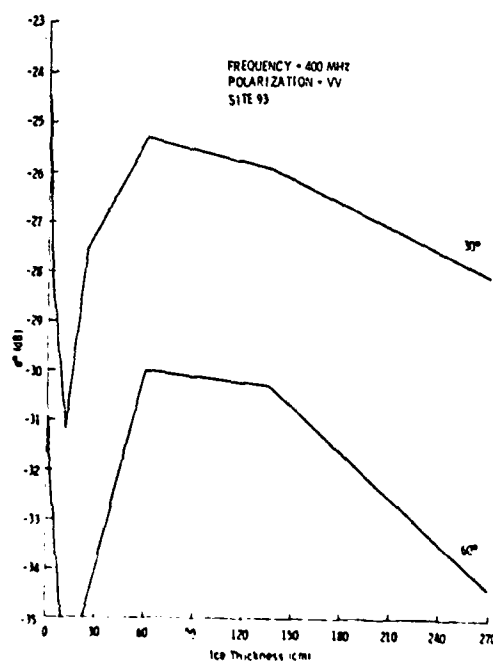


Figure 1.2-9. Experimental  $\sigma^0$  versus ice thickness for different  $\theta$ , 400 MHz, VV (Parashar et al., 1974).

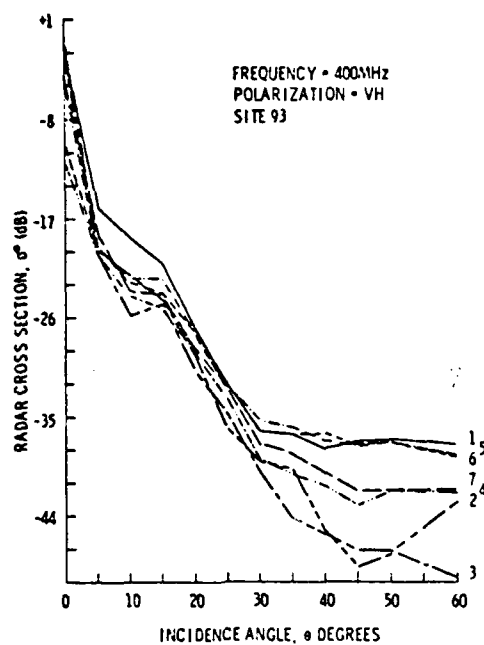


Figure 1.2-10. Experimental  $\sigma^0$  versus  $\theta$  for different categories, 400 MHz, VH (Parashar et al., 1974).

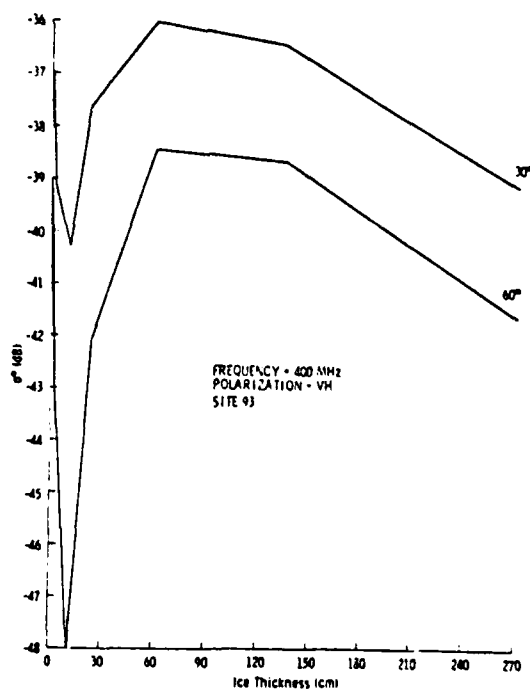


Figure 1.2-11. Experimental  $\sigma^0$  versus ice thickness for different  $\theta$ , 400 MHz, VH (Parashar et al., 1974).

1.2-11, respectively. The dynamic range in scattering cross-section was found to be greater with cross-polarization than with like-polarization.

1.2.3 L. Gray, J. Cihlar, and S. Parashar (1977).

Radar backscatter measurements of sea ice were made at 13.3 GHz (HH and HV polarizations). These measurements were made using the Ryan Model 720 dual-polarized scatterometer system. The illuminated area subtended  $120^\circ$  in the along-track direction and  $3^\circ$  in the across-track direction. The measurements were made off the east coast of Canada during the winter and spring of 1975-1976. The primary ground truth was provided by a RC-10 camera and a Daedalus infrared scanner. In-situ measurements of temperature, salinity, snow cover, and thickness of shorefast ice were made.

An area called Forteau Bay was investigated. Measurements were made of areas containing smooth, medium rough, and rough first-year ice, rafted young ice, new ice, and open water. Results showed that, as expected, open water gives the maximum return near vertical incidence and then decreases relatively rapidly with increasing angle (see Figures 1.2-12 and 1.2-13). For this group of ice types, rough first-year ice gives maximum return at angles greater than  $20^\circ$ , followed by medium rough first-year and then smooth first-year ice. Rafted young ice was found to have an angular response very similar to the response of medium rough thick first-year ice, even though the rafter ice was thinner than the thick first-year ice. It is important to note that a range of at least 20 dB was noted in the radar return from the three shorefast ice regions which were described by their surface

roughness. The results for cross-polarization were similar to those obtained for like-polarization, although the level of separation between ice type categories appeared to be slightly greater in the case of cross-polarization.

An area called Northumberland Strait was also investigated. Measurements were made of the following ice categories: thin first-year, consolidated brash, rafted young, heavily rafted nilas, rafted nilas, and open water. The angular response of the scattering coefficients are shown in Figures 1.2-14 and 1.2-15. Among these ice types thin ice gave the strongest return throughout all angles. Rafted nilas produces a relatively low return in comparison to other ice returns, whereas heavily rafted nilas produced returns that were slightly higher than those of rafted young ice. The order of return from these various ice types for cross-polarization is similar to like-polarization returns, but separation between ice categories is slightly greater than for like-polarization. In this case, rafted nilas produced returns that were significantly lower than return from open water.

#### 1.2.4 Gray, Ramseier, and Campbell (1977).

Radar backscatter measurements were made at 13.3 GHz (HH, VV, HV, VH polarizations). These measurements were made using a Ryan Model 720 scatterometer system. The illuminated area subtended 120° in the along-track direction and 3° in the across-track direction. The measurements were made in the Beaufort Sea during the month of March in 1975. Ground truth was provided by black-and-white photography and infrared imagery. Detailed dielectric constant, temperature and salinity profiles were obtained for a variety of ice types by surface parties.

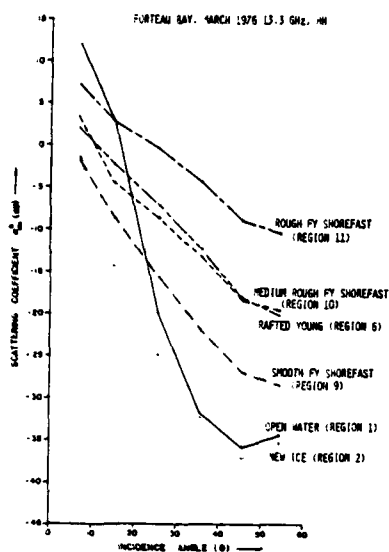


Figure 1.2-12. Scattering coefficient  $\sigma_0$  versus angle  $\theta$  Forteau Bay, 13.3 GHz HH (Gray et al., 1977).

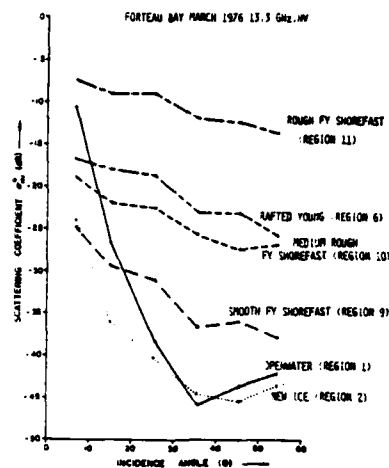


Figure 1.2-13. Scattering coefficient  $\sigma_0$  versus angle  $\theta$  Forteau Bay, 13.3 GHz, HV (Gray et al., 1977).

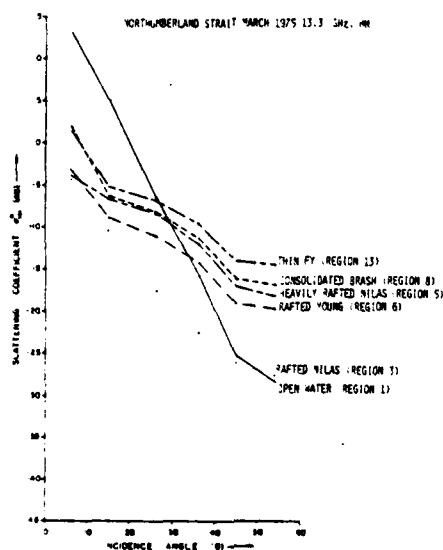


Figure 1.2-14. Scattering coefficient  $\sigma_0$  versus angle  $\theta$  Northumberland Strait, 13.3 GHz, HH (Gray et al., 1977).

THIS PAGE IS BEST QUALITY PRACTICABLE  
FROM COL 1 FILED TO LOG

THIS PAGE IS BEST QUALITY PRACTICABLE  
FROM COPY FURNISHED TO EDC

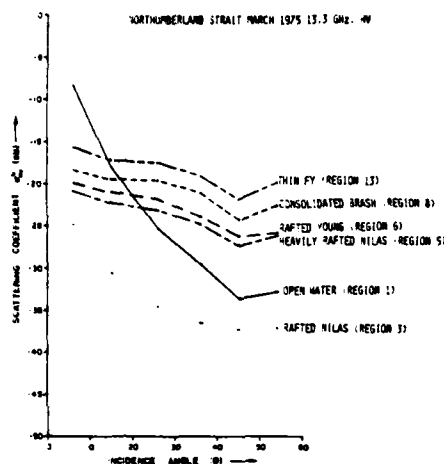


Figure 1.2-15. Scattering coefficient  $\sigma^0$  versus angle  $\theta$  Northumberland Strait, 13.3 GHz, HV (Gray et al., 1977).

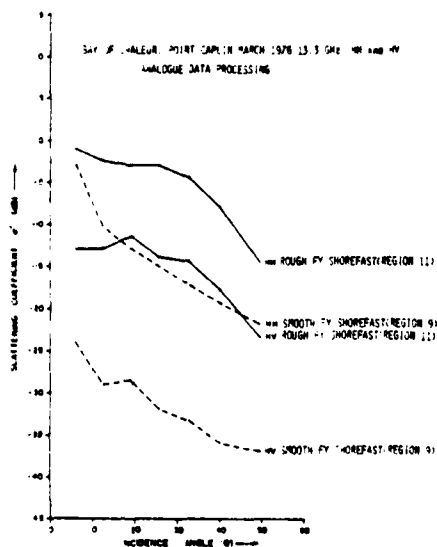


Figure 1.2-16. Scattering coefficient  $\sigma^0$  versus angle  $\theta$  Bay of Chaleur, 13.3 GHz HH (Gray et al., 1977).

Their results indicated that there was a strong correlation between the magnitude of the radar scattering cross-section and major ice types. Old ice gave significantly higher backscatter returns than first-year and young ice forms. Also, at all angles the average return for the old ice is greater than the maximum signal for the ridges on the first-year ice. The angular response for an old ice floe is shown in Figure 1.2-17. Scattering curves for smooth young ice are shown in Figure 1.2-18. The scattering curves for first-year ice is shown in Figure 1.2-19. The error bars that are plotted on the curves indicate  $\pm 1 \sigma$  spread in the results.

#### 1.2.5 Comparison of Backscatter Returns at 13.3 GHz (VV-polarization).

The angular responses of multiyear and thick first-year ice obtained by Rouse, Parashar and Gray are presented in Figure 1.2-20. In each case, at incidence angles greater than  $10^\circ$ , multiyear ice returns were higher than thick first-year ice returns. Average separations between responses for thick first-year and multiyear ice were 6.0 dB for Rouse, 3.5 dB for Parashar, and 12.0 dB for Gray. The angular responses of multiyear ice in the cases of Rouse and Gray agreed, both in level and in shape, up to incidence angles of  $40^\circ$ . The angular responses of thick first-year ice in the cases of Rouse and Gray were somewhat similar in level and shape at near-vertical angles of incidence. Significant level differences (10 dB) existed between the results of Parashar and the results of Rouse and Gray. Table 1.2-1 provides for a comparison of radar cross-section levels.

Absolute levels and the angular response of experimentally measured radar scattering cross-sections of a target may vary from sensor to sensor as was demonstrated in the above results. These variations tend to

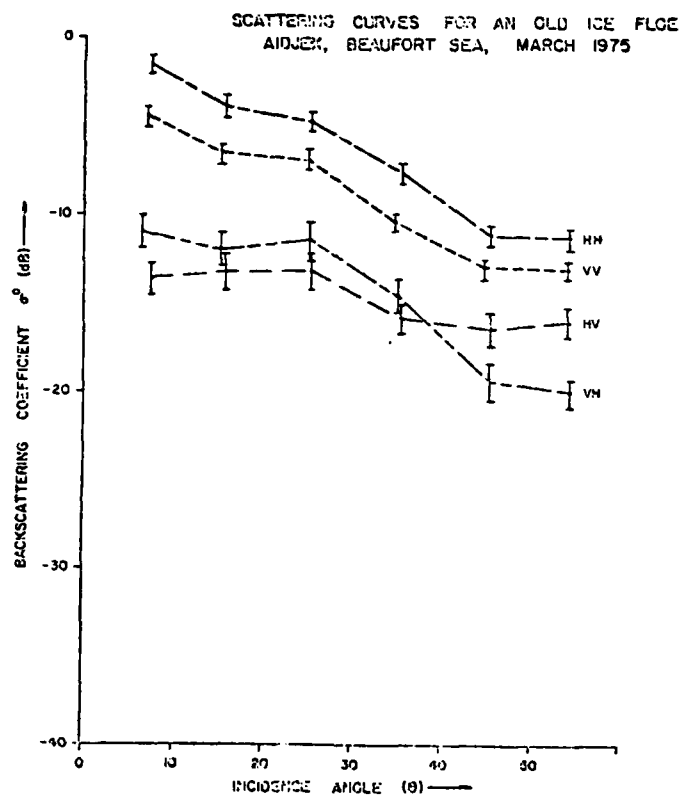


Figure 1.2-17. Graph illustrating the four backscattering curves as a function of incidence angle for relatively smooth, ridge-free old ice (Gray, Ramseier, and Campbell, 1977).

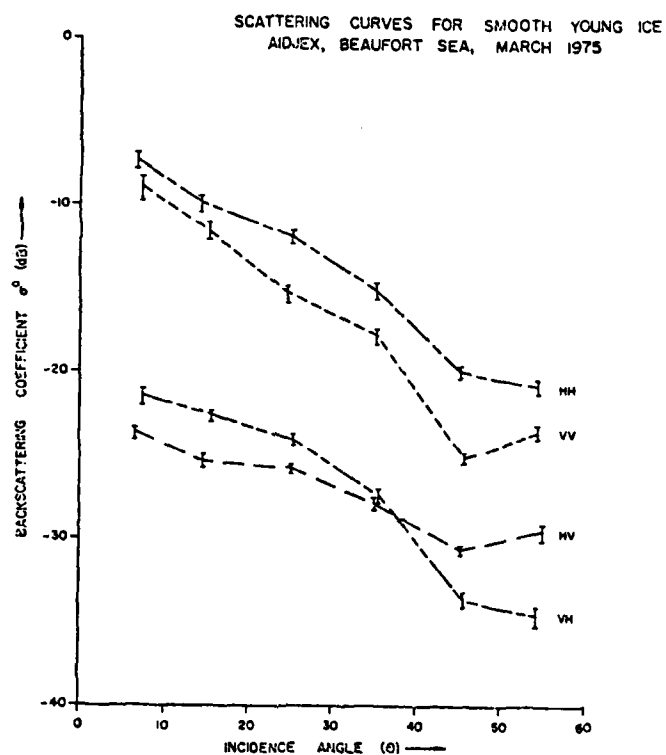


Figure 1.2-18. Graph illustrating the four backscattering curves as a function of incidence angle for an area of smooth young ice (Gray, Ramseier, and Campbell, 1977).

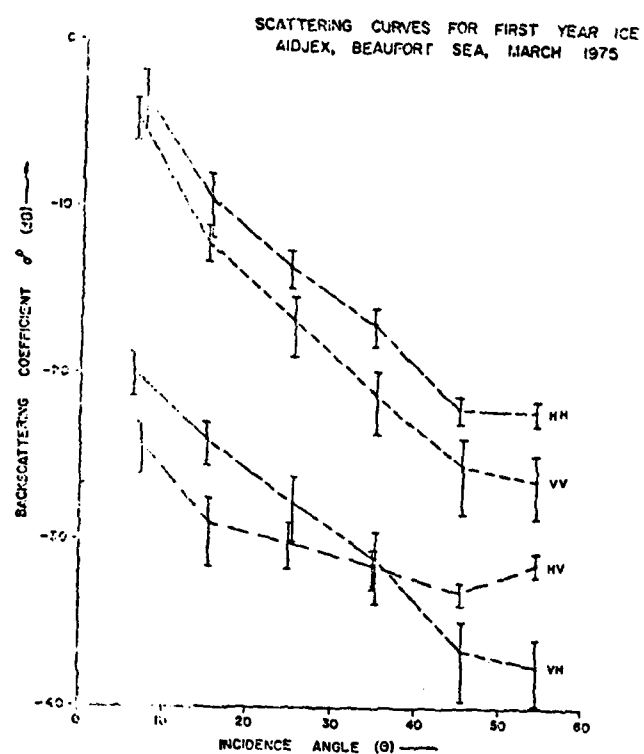


Figure 1.2-19. Graph illustrating the four backscattering curves as a function of incidence angle for an area of first-year ice (Gray, Ramseier, and Campbell, 1977).

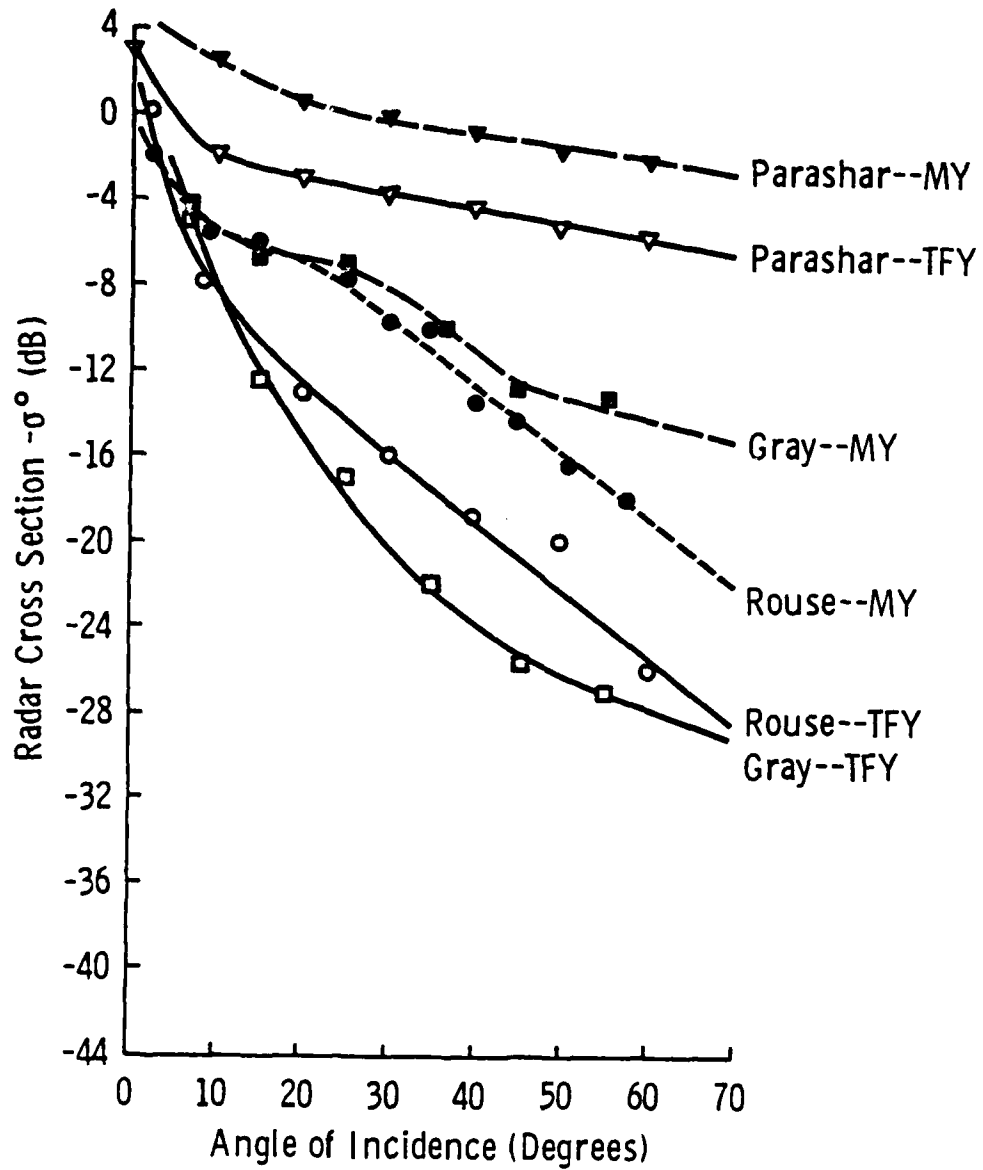


Figure 1.2-20. Comparison of multiyear and thick first-year ice scattering cross-sections according to Rouse (1968), Parashar, et al. (1974), and Gray, et al. (1977).

arise due to two problem areas that are common to airborne scatterometer systems. First, there is the problem of accurately describing the illumination on the ground. To do this properly a gain pattern of the antenna must be measured with the antenna attached to a very good replica of the fuselage of the airborne platform. Only in this way is it really known for certain how the gain distribution characteristics are shaped by the multicurved shape of the airborne-ground plane. Second unless extreme care and precision is taken with the calibration of the airborne sensor with a known standard radar target, and is done periodically, variations in the absolute level in calibration may occur.

TABLE 1.2-1

COMPARISON OF THE RADAR CROSS-SECTION  $\sigma^0$  (IN dB) RESULTS  
ROUSE (1968), PARASHAR (1974), AND GRAY (1977) FOR  
MULTIYEAR AND THICK FIRST-YEAR SEA ICE RADAR CROSS-SECTIONS

	MULTIYEAR			THICK FIRST-YEAR		
	20°	40°	60°	20°	40°	60°
Rouse	-7.0	-13.5	-19.0	-13.0	-19.0	-26.0
Parahsar	+ .5	- 1.0	-12.5	- 3.5	- 4.5	- 6.0
Gray	-7.0	-11.5	-13.5	-15.0	-24.0	-27.5

## 2.0 CHARACTERISTICS OF SEA ICE

### 2.1 Formation

Sea ice forms due to freezing of sea water. Sea ice consists of fresh water ice and very small liquid inclusions of brine, referred to as brine pockets, entrapped in the ice matrix during the process of freezing. Fresh water ice forms at temperatures below the initial freezing point temperature, at which ice is in equilibrium with the sea water of given salinity. The impurities present in the sea water are rejected during the formation of pure ice, enriching the neighboring liquids. This is why the salinity of sea ice at all stages of development is less than the original sea water from which it was formed.

Many factors influence the formation of sea ice. These include wind, sea state, currents, cooling rate, distribution, and salinity of the sea water, surface temperature, and depth of water. As has been found, the combination of these factors lead to variation in the vertical and horizontal properties throughout the ice sheet. Also, under conditions of wind, current, waves, and pressure, ice fields may break up into floes and drift. This redistribution may cause pressure effects which may cause ice to pile up as ridges and hummocks or the overriding of one sheet of ice over another, which is called rafting.

Sea ice may be classified according to its age, the way it was formed, or by concentration. A widely used system of classification is the World Meteorological Organization "Glossary of Ice Terms" [19].

## 2.2 Physical Properties

The ability to distinguish between open water, thin ice, first-year ice, and multiyear ice is of prime importance. For example, thickness and physical properties differ greatly between first-year and multiyear ice. In general, a first-year ice floe is smooth-surfaced with angular floe edges. Multiyear ice has generally a rolling rough surface while the edges of the floe are rounded. These changes occur due to the melt conditions that take place in the summer which modify surface features and the grinding action that takes place between floes tend to round off the corners. The melt process not only modifies the surface features, but extensively changes the material properties of the ice. Typical examples of the salinity, density, and temperature profiles of first-year and multiyear ice are illustrated in Figure 2.2-1. In first-year ice the salinity is usually high, both near the air-ice interface and at the ice-water interface. The density may be slightly lower near the air-ice interface, but is constant throughout the remainder of the ice sheet. The temperature profile is very often almost linear during most of the year. If the ice is not covered by a layer of snow, the surface temperature of the ice is close to the air temperature. Because the thermal conductivity of snow is much lower than that of ice, a layer of snow upon the ice keeps the surface temperature of ice closer to the melting point. Bare sea ice temperatures track fairly well with rapidly changing air temperatures. Snow cover tends to keep the temperature of the ice constant with changes of  $10^{\circ}\text{C}$  in air temperature needed to change the temperature of the ice surface by  $5^{\circ}\text{C}$  with these temperature fluctuations effecting the top 25 cms or so. In multiyear ice

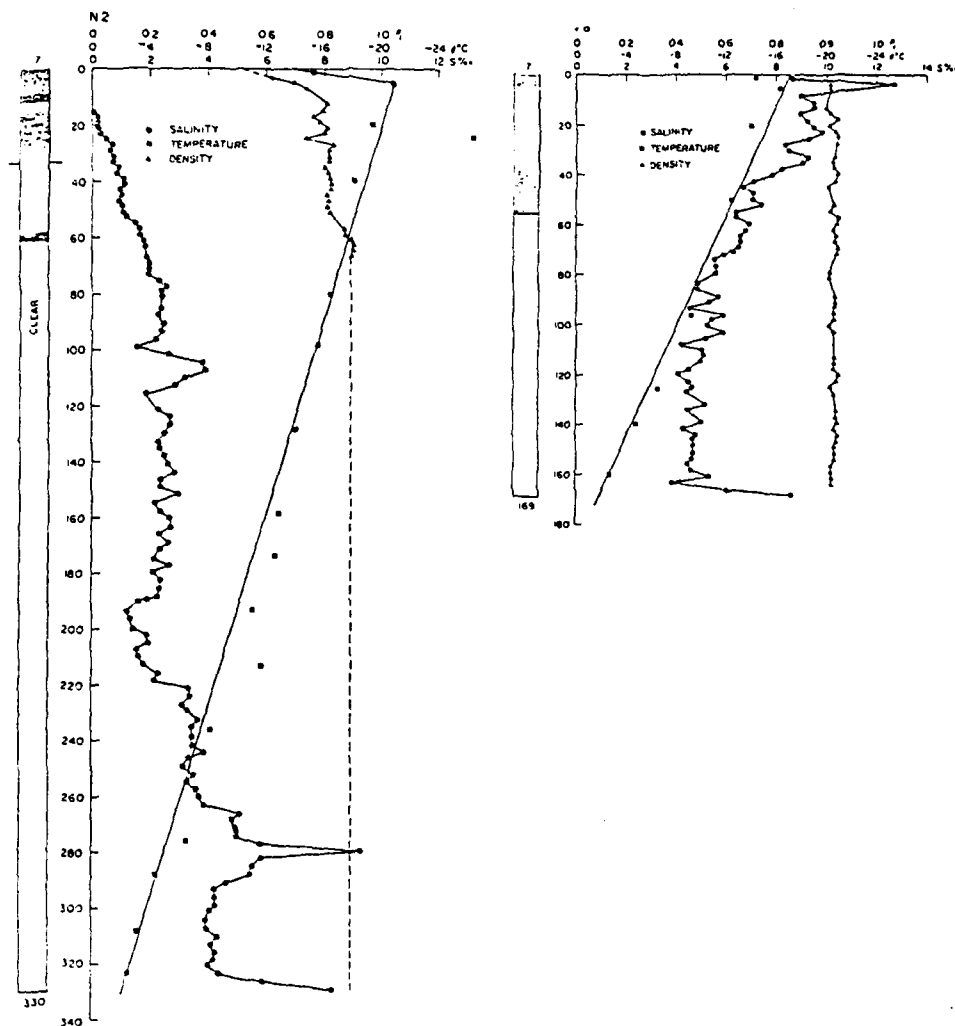


Figure 2.2-1. Depth profiles of salinity, density, and temperature for first-year and multiyear ice obtained during April 1975 at the AIDJEX camp. The schematic of the core is shown on the left hand side of the profiles indicating the structural changes in the ice cover (Campbell et al., 1975).

the salinity starts near zero and increases with depth. Density is lower in the top part of the cover. The temperature profile follows in the same fashion as in first-year ice.

The phase diagram for standard sea ice may be used to describe some of the physical properties of sea ice (see Figure 2.2-2). The amount of brine present may be found from the diagram. As the temperature is lowered, the brine concentration increases as the volume of brine decreases. As shown by the phase diagram, sea ice at equilibrium at a given temperature consists of fresh water ice and brine of a specific composition. The first salt to precipitate is  $\text{NaSO}_4 \cdot 10 \text{H}_2\text{O}$ , which begins to crystallize at  $-8.2^\circ \text{C}$ . Brine concentration continues until  $-22.9^\circ \text{C}$  when  $\text{NaCl} \cdot 2 \text{H}_2\text{O}$  starts to precipitate.  $\text{NaCl}$ , being the principal salt in the brine liquid, causes a rapid decrease in brine volume near  $-23^\circ \text{C}$ . Brine liquid exists at temperatures below  $-50^\circ \text{C}$ .

The relative volume of brine in sea ice is proportional to the salinity of the ice and may be computed from the numerical formulas as given by Frankenstein and Garner [26] in parts per thousand:

$$\begin{aligned} V_b &= S(-52.56/T - 2.28) & -0.5^\circ \geq T \geq -2.06^\circ \text{C} \\ V_b &= S(-45.917/T + .930) & -2.06^\circ \geq T \geq -8.2^\circ \text{C} \\ V_b &= S(-43.795/T + 1.189) & -8.2^\circ \geq T \geq -22.9^\circ \text{C} \end{aligned} \quad (2-1)$$

For temperatures close to the melting point an equation was obtained from the data given in Assur (1960):

$$V_b = S(1.0028/T^2 - 48.6837/T + 4.09201) \quad -0.1^\circ \geq T \geq -0.5^\circ \text{C} \quad (2-2)$$

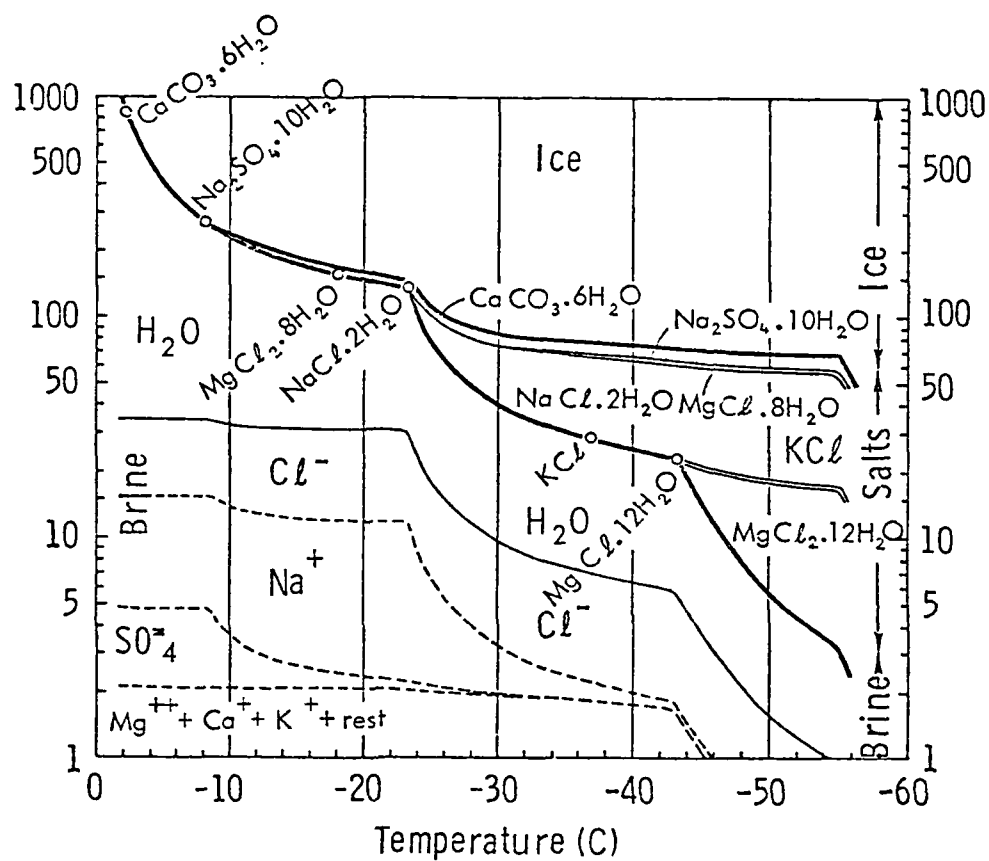


Figure 2.2-2. Standard sea ice phase diagram (Assur, 1960).

The temperature dependence of the relative volume of brine liquid is shown in Figure 2.2-3. At temperatures above  $-23^{\circ}\text{C}$  sea ice consists primarily of fresh water ice and brine liquid. For example, at  $-10^{\circ}\text{C}$   $1^{\circ}/\text{‰}^*$  sea ice contains 993.4 grams of fresh water ice and 6.6 grams of brine liquid. At  $-2^{\circ}\text{C}$  the brine liquid content has risen to 26.6 grams.

An empirical equation for the freezing temperature of sea water is given by Kester [24]:

$$T_f = -0.137 - .05199 S_{sw} - .00007225 S_{sw}^2 \quad (2-3)$$

The freezing point is important in the calculation of the temperature of the ice at the ice-water interface.

### 2.3 Electrical Properties

The electrical properties of sea ice are an important link, along with surface roughness and internal structure of the medium, in the understanding of the scattering of radar from it. To completely describe the radar backscatter properties of sea ice, at least a four-layer model may be necessary in the description (see Figure 2.3-1). The inclusion of the snow layer may be especially important during the warmer summer months. The electrical properties of sea ice are directly linked to its physical properties. It is then evident that as the physical properties change with time and age, the electrical properties are also evolving.

---

\* $^{\circ}/\text{‰}$  = parts per thousand.

THIS PAGE IS BEST QUALITY PRACTICABLE  
FROM COPY FURNISHED TO LDC

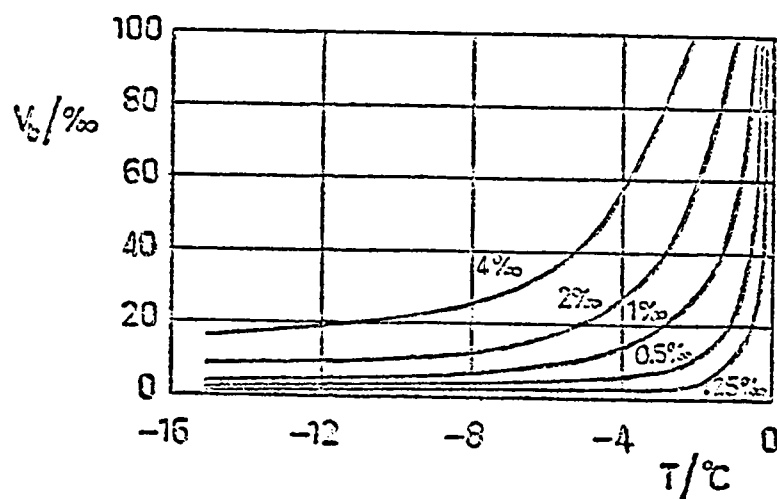


Figure 2.2-3. Temperature dependence of the relative volume of brine liquid in sea ice.

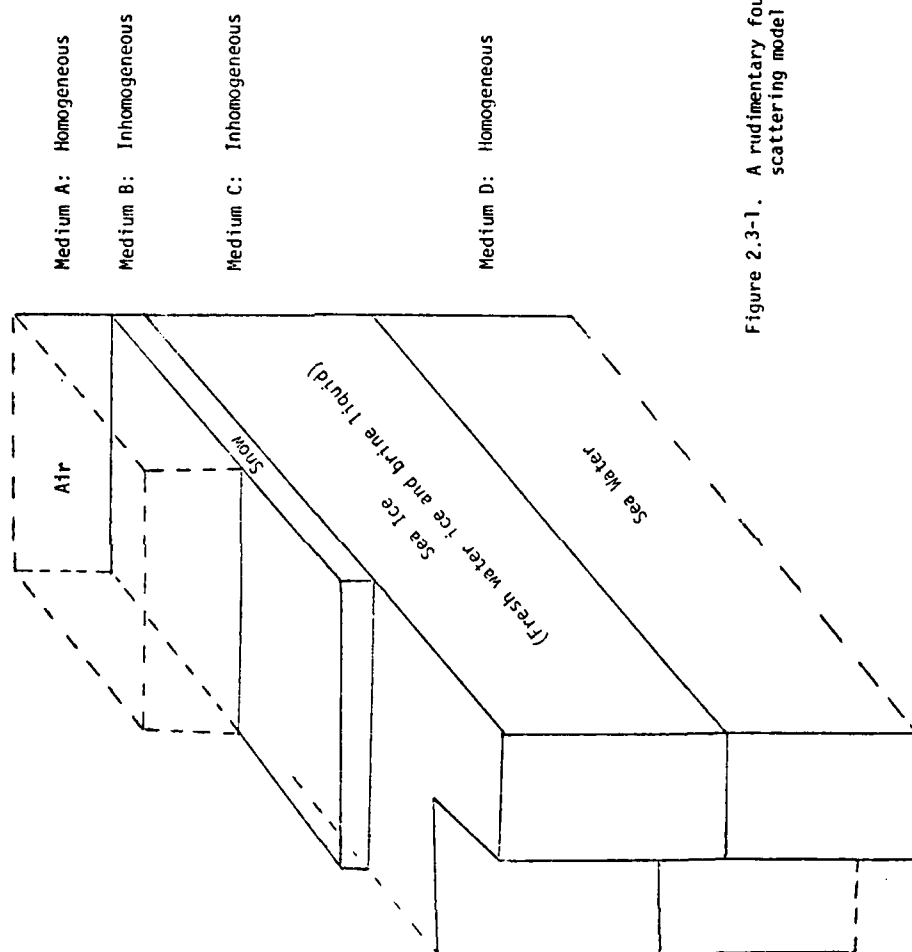


Figure 2.3-1. A rudimentary four-layer scattering model of sea ice.

The model which describes the entire sea ice medium includes a snow layer, fresh water ice, brine liquid, and sea water. The dielectric properties at microwave frequencies of each of these will be reviewed.

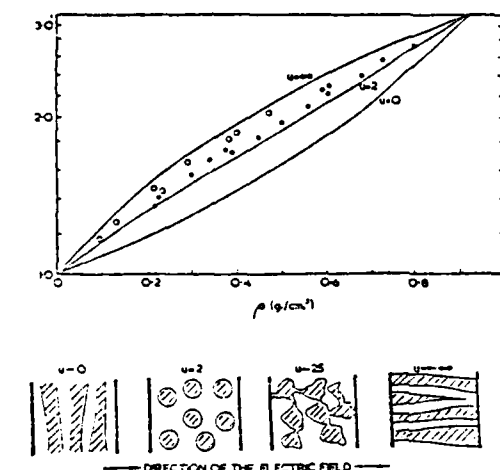
#### 2.3.1 Snow

In most cases it has been found that when the relatively shallow Arctic snow layer is dry it is transparent to microwave radiation. Preliminary results obtained during the AIDJEX 1975 experiment indicate that vertically polarized microwave measurements are nearly independent of the amount of dry snowpack (at  $-18^{\circ}\text{C}$ ) encountered. Horizontally polarized microwave measurements were found to be strongly effected. The effect of liquid water in the snow layer has a strong effect on the microwave emission from the snowpack.

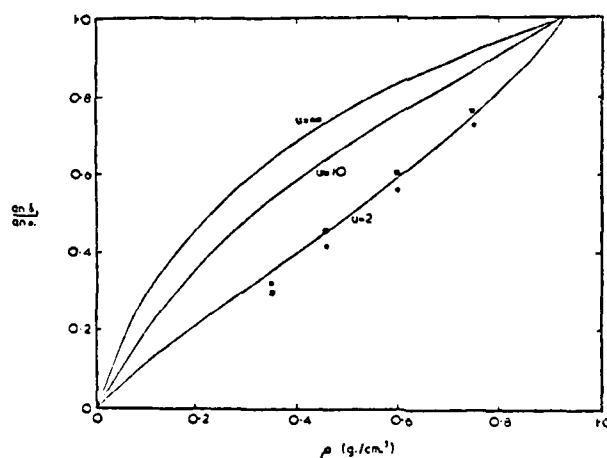
The dielectric constant of dry snow may be described by the Weiner theory for mixtures [25], which relates the dielectric constant to the density of the dry snow. The relationship between dielectric constant and loss tangent of snow to snow density is illustrated in Figure 2.3-2 by Evans [26] for the data obtained from several experimenters. Cummings [27] found that the real part of the dielectric constant for dry snow was temperature independent with the loss tangent sensitive to temperature as described in Figure 2.3-3. Skin depths calculated from dielectric constant information, both experimental and theoretical, as reported in the literature are shown in Table 2.3-1.

#### 2.3.2 Fresh Water Ice

Sea ice consists of fresh water ice and small brine inclusions. The complex permittivity of sea ice can be calculated by considering the



Relative permittivity of snow (ordinates) versus density (abscissa). The upper curves are computed as explained in section 1.2 for snow particles having the characteristic Formzahl values  $u = 0, 2, 10$  and  $\infty$  in Weiner's formula and taking the relative permittivity of solid ice to be 90 at low frequencies. The lower curves are for the limiting value of the permittivity at high frequencies, taken to be 3.2 for solid ice. Measured values: 0 due to Kuroiwa (1956) at frequencies less than 1 MHz and at 3 MHz due to Cumming (1952) at 9.375 MHz. The sketches beneath the graphs show how snow structure is related to the Formzahl.



Loss tangent of snow versus density (abscissa). The quantity plotted vertically is the ratio of the loss tangent of the ice/air mixture forming snow to that of the solid ice. Smooth curves are plotted for different values of the Formzahl in Weiner's formula assuming that  $\tan \delta$  is much less than unity for the solid ice considered. Measured values are due to Cumming (1952) at 9.375 MHz at 0°C, at -8°C.

FIGURE 2.3-2 Dielectric properties of dry snow (Evan, 1965)

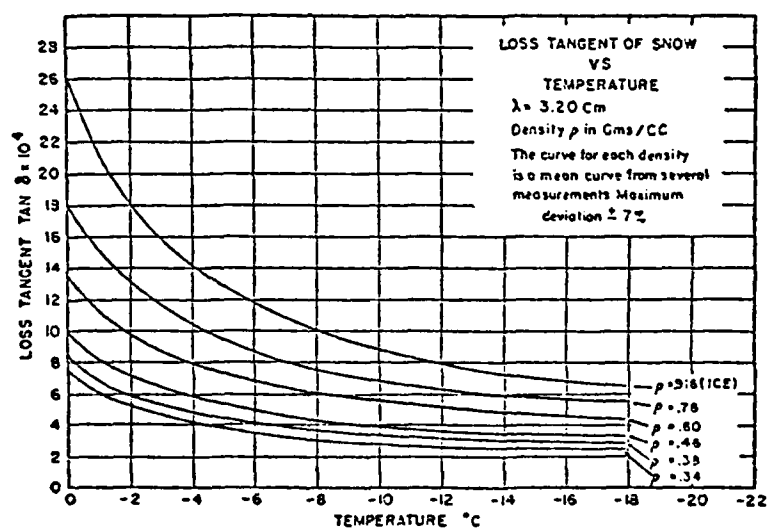


Figure 2.3-3. Variation of loss tangent of snow with temperature (Cumming, 1965).

TABLE 2.3-1  
SKIN DEPTH FOR SNOW AND ICE

DESCRIPTION	FREQUENCY (GHz)	K'	K''	$\tan \delta$	SKIN DEPTH	TYPE	SOURCE
Dry snow	37	1.9	.05	-----	7 cm	experimental	Edgerton, 1971
Dry snow	13.6	2.76	.03	-----	38.8 cm	experimental	Edgerton, 1971
Wet snow	1.0	1.5	-----	$10^{-1}$	78 cm	theoretical	Linlor, 1972
Wet snow	8.0	1.5	-----	$10^{-1}$	9.7 cm	theoretical	Linlor, 1972
Dry snow	1.0	1.32	.0002	-----	548 m	experimental	Evans, 1965
Dry snow	8.0	1.32	.0002	-----	68 m	experimental	Evans, 1965
Foam 8.5% H <sub>2</sub> O	1.83	-----	-----	-----	43 cm	experimental	Linlor, 1975
Foam 8.5% H <sub>2</sub> O	8.0	-----	-----	-----	3 cm	experimental	Linlor, 1975
Saturated snow	10.0	-----	-----	-----	.9 cm	theoretical	Linlor, 1975
Fresh snow	3.0	1.2	-----	.00029	100 m	experimental	Vickers, 1972
Fresh snow	10.0	1.26	-----	.00042	20.2 m	experimental	Vickers, 1972
Hard packed snow	3.0	1.5	-----	.0009	28.9 m	experimental	Vickers, 1972
Ice	3.0	3.2	-----	.0009	19.8 m	experimental	Vickers, 1972
Ice	35.3	1.91	.114	-----	1.5 cm	experimental	Perry, 1972
Ice	94.5	1.88	.064	-----	.75 cm	experimental	Perry, 1972

effects of each of these constituents separately. Much work has gone into the investigation of the dielectric properties of pure and fresh water ice [26, 27, 29, 30, 31]. At frequencies below 300 MHz the permittivity follows closely the Debye dielectric equation for polar molecules and single relaxation time [26]:

$$\epsilon_p = \epsilon_p' - j\epsilon_p'' = \epsilon_{p\infty} = \epsilon_{p\infty} + (\epsilon_{ps} - \epsilon_{p\infty})/(1 + jw\tau_p) \quad (2-4)$$

where:

- $\epsilon_p$  = permittivity of pure ice
- $\epsilon_p'$  = dielectric constant of pure ice
- $\epsilon_p''$  = loss factor of pure ice
- $\epsilon_{p\infty}$  = high frequency dielectric constant of pure ice
- $\epsilon_{ps}$  = static dielectric constant of pure ice
- $\tau_p$  = relaxation time of pure ice
- $w$  = angular frequency

The high frequency dielectric constant has been observed at microwave frequencies. It is found to be on the order of 3.15 and independent of temperature. The loss factor is mildly temperature sensitive, as shown in Figure 2.3-4.

### 2.3.3 Brine Liquid

Brine liquid is a concentrated form of sea water. There are more than 44 elements with 6 major ions (sodium, magnesium, potassium, calcium, sulphate, and chloride) in its composition. Salts increase the dielectric loss of water by adding free charge carriers. The loss factor of sea water includes an additional term due to the dc conductivity. The dielectric properties of sea water follows a modified Debye equation [32]:

$$\epsilon_{SW} = \epsilon_{S\infty} + (\epsilon_{SWS} - \epsilon_{S\infty}) / (1 + j\omega\tau_{SW}) - j\sigma_{SW} / \epsilon_0\omega \quad (2-5)$$

where:

- $\epsilon_{SW}$  = permittivity of sea water
- $\epsilon_{S\infty}$  = high frequency dielectric constant of sea water
- $\epsilon_{SWS}$  = static dielectric constant of sea water
- $\tau_{SW}$  = relaxation time of sea water
- $\sigma_{SW}$  = dc conductivity of sea water
- $\epsilon_0$  = dielectric constant of free space

The parameters of the modified Debye equation can be represented as functions of temperature only as illustrated in Figures 2.3-5 to 2.3-9.

#### 2.3.4 Sea Ice

Measurements of the dielectric properties of sea ice and NaCl ice at microwave frequencies have been reported in the literature. Hoekstra and Cappillino [33] measure the loss factor of ice samples obtained by flash freezing sea water at 400 MHz, 9.8 GHz, and 23 GHz. Salinities ranged from 4 ‰ to 12 ‰ and temperatures ranging from -60° C to -30° C up to about -5° C. Byrd [34] reported measurements at 26-40 GHz at 2 perpendicular directions. Temperatures ranged from -7° C to -32° C and salinities ranged from 2.85 ‰ to 7.2 ‰. Bogorodsky and Khokhlov [35] made measurements of the Bering Sea ice at 10 GHz. Salinities ranged from 2.5 ‰ to 7.5 ‰ and temperatures from -13° C to -10° C.

Hoekstra and Cappillino [33], Vant et al. [36], and Hallikainen [37] made measurements investigating the permittivity and loss factor

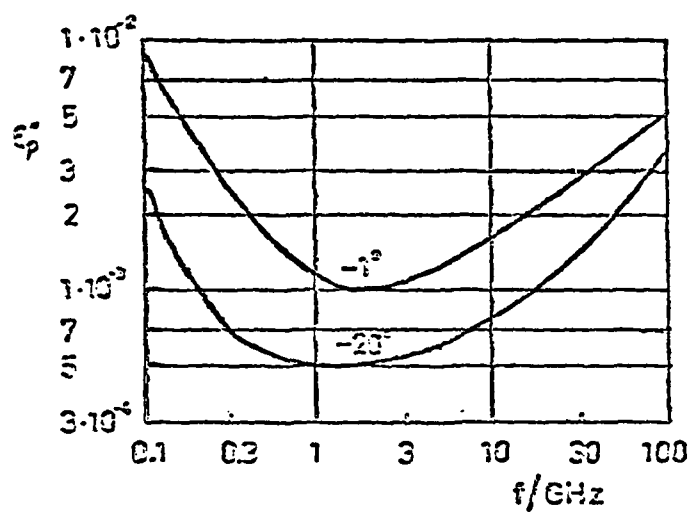


Figure 2.3-4. Loss factor of fresh water ice as a function of frequency.

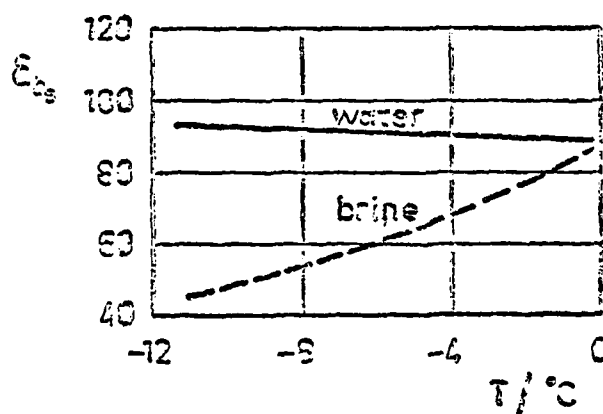


Figure 2.3-5. Static dielectric constant of brine and water as a function of temperature.

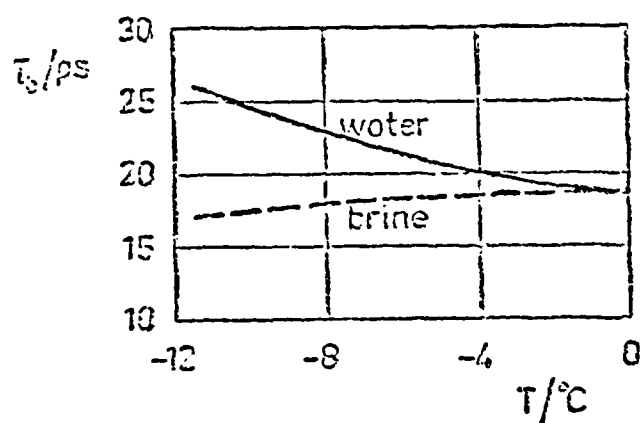


Figure 2.3-6. Relaxation time of brine and water as a function of temperature.

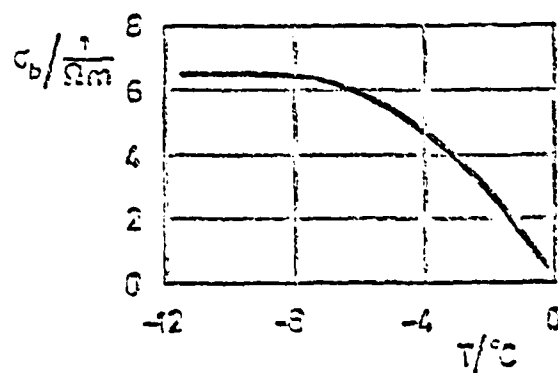


Figure 2.3-7. Conductivity of brine as a function of temperature.

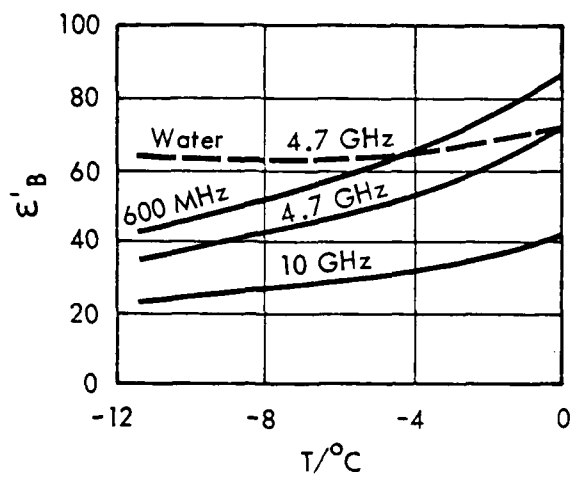


Figure 2.3-8. Dielectric constant of brine and water as a function of temperature.

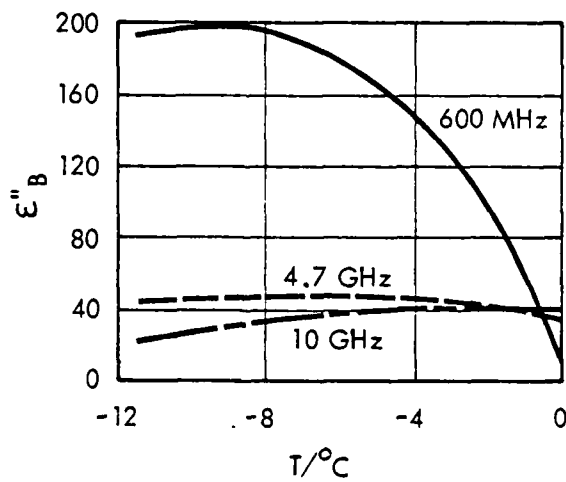


Figure 2.3-9. Loss factor of brine as a function of temperature.

of NaCl ice at microwave frequencies over a variety of salinities and temperature ranges.

Hoekstra and Cappillino [33] obtained the following loss factor for sea ice as a function of temperature (see Figure 2.3-10) and a function of frequency (see Figure 2.3-11). It is compared with the theoretical loss factor calculated using a random oriented elongated brine pocket model [38]:

$$\epsilon_{si}/\epsilon_p = (\epsilon'_{si} + j\epsilon''_{si})/\epsilon_p = 1 - \frac{1}{3} V_{br} [1 - \epsilon_b/\epsilon_p] \cdot [1 + 4\epsilon_{si}/(\epsilon_{si} + \epsilon_b)] \quad (2-6)$$

where:

- $\epsilon_{si}$  = permittivity of sea ice
- $\epsilon_p$  = permittivity of pure ice
- $\epsilon_b$  = permittivity of brine liquid
- $V_{br}$  = relative volume of brine liquid in sea ice

as a function of brine volume in ice has been studied by Hoekstra and Cappillino [33]. They measured the dielectric constant over a wide range of salinities and temperature at 9.8 GHz. Their results, as shown in Figure 2.3-13, draw the conclusion that dielectric constant is closely related to brine volume.

The theoretical loss factor using the random orientation model at 4.7 GHz is shown in Figure 2.3-14 as a function of temperature and salinity. The theoretical dielectric constant of sea ice is shown as a function of temperature and salinity in Figure 2.3-15. Figure 2.3-16 shows the theoretical attenuation factor of sea ice at 4.7 GHz.

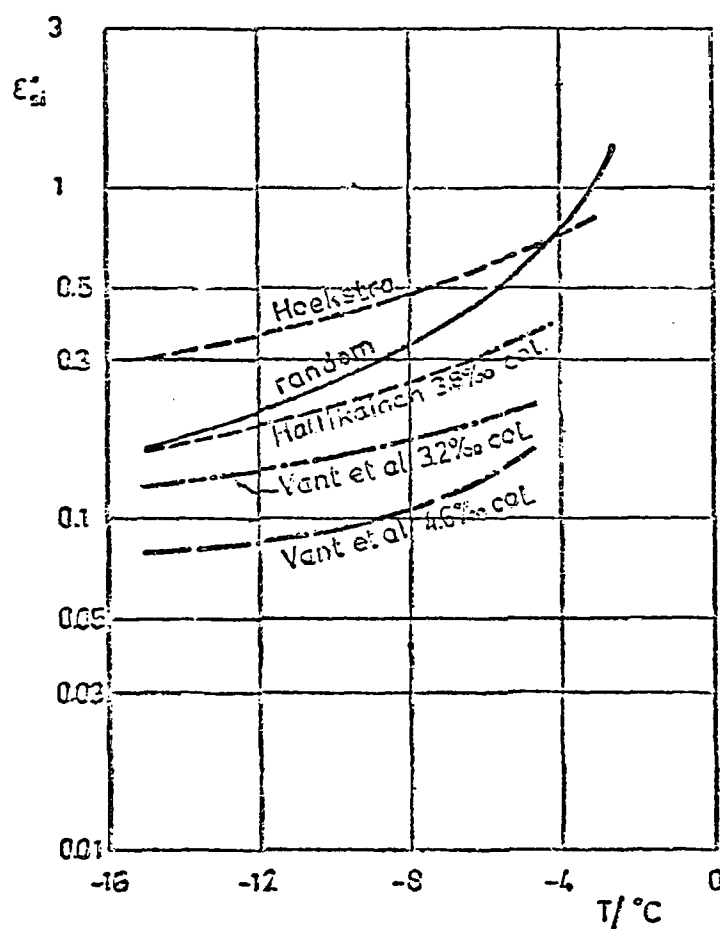


Figure 2.3-10. Theoretical loss factor of sea ice compared to experimental data. The frequency used by Hoekstra and Cappillino (1971) was 9.86 GHz, in Hallikainen (1977), 16 GHz, and in Vant et al. (1974), 10 GHz.

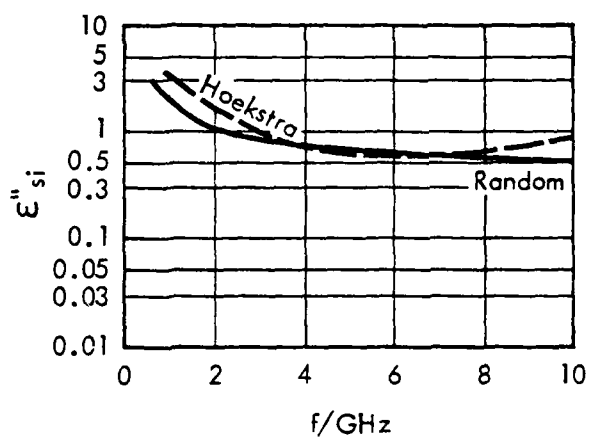


Figure 2.3-11. Theoretical loss factor of sea ice as a function of frequency. The salinity is 8 ‰ and temperature is -10°C.

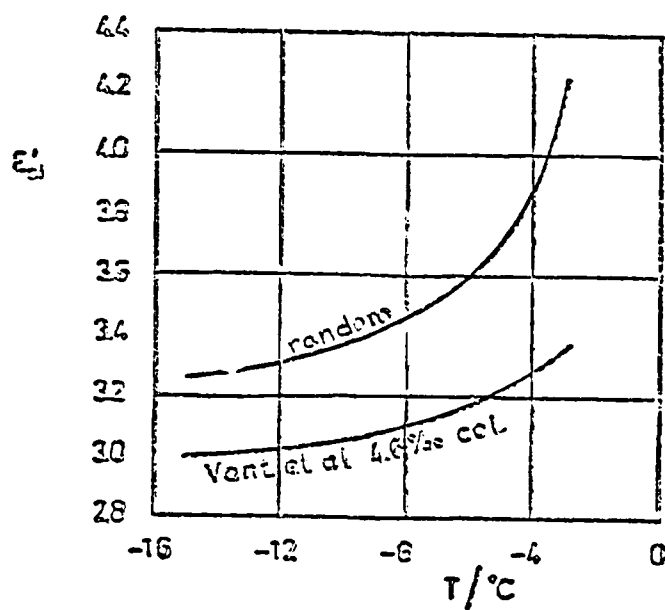


Figure 2.3-12. Theoretical dielectric constant of sea ice compared to experimental results by Vant et al. (1974). The frequency is 10 GHz.

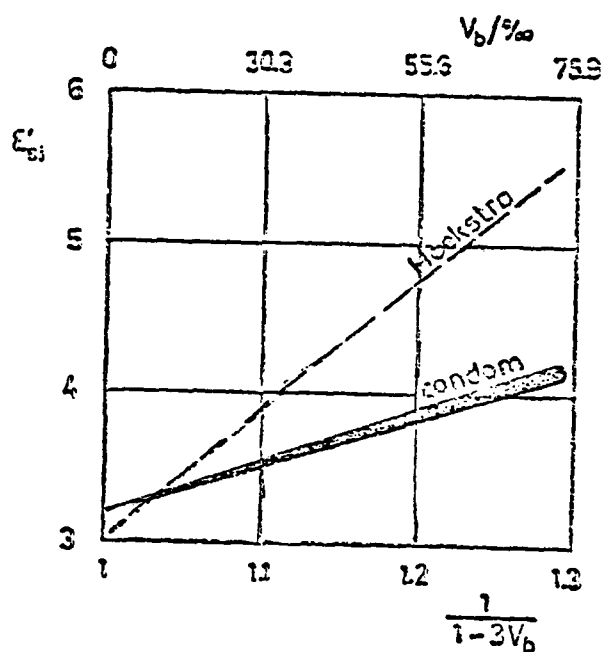


Figure 2.3-13. Dielectric constant of sea ice as a function of brine volume at 9.8 GHz. The theoretical results were obtained by using salinities from 4 ‰ to 8 ‰ and temperatures from  $-3^{\circ}\text{C}$  to  $-16^{\circ}\text{C}$ .

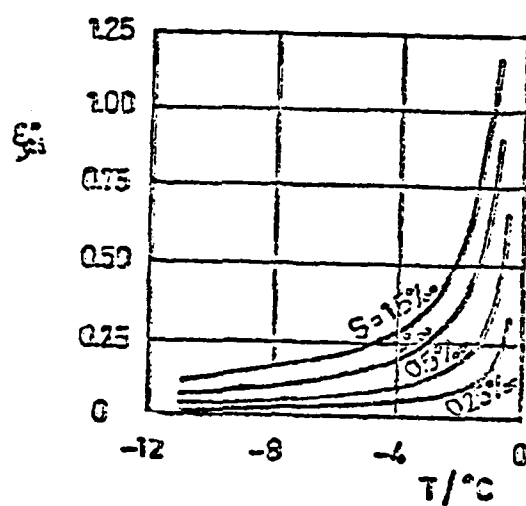


Figure 2.3-14. Theoretical loss factor of sea ice at 4.7 GHz as a function of temperature and salinity (random orientation model).

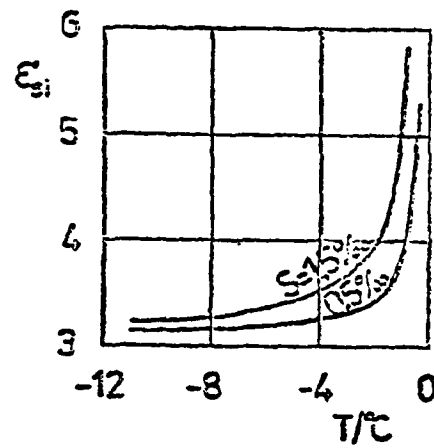


Figure 2.3-15. Theoretical dielectric constant of sea ice at 4.7 GHz as a function of temperature and salinity (random orientation model).

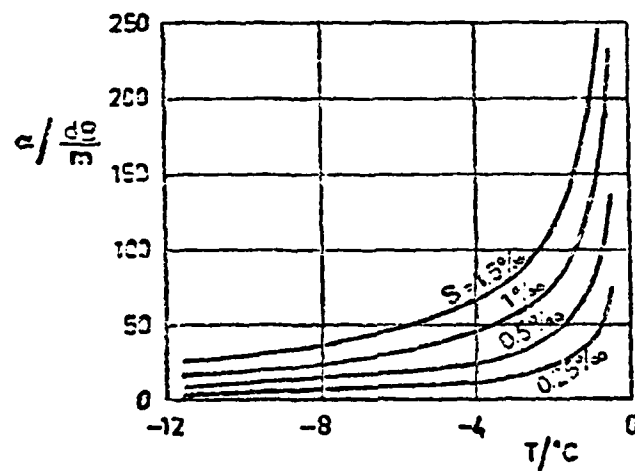


Figure 2.3-16. Theoretical attenuation factor of sea ice at 4.7 GHz as a function of temperature and salinity (random orientation model).

### 3.0 INVESTIGATION OF SEA ICE

#### 3.1 Introduction

Previous programs to measure radar backscatter from sea ice have involved radar scatterometers flown in aircraft, with support from sparse surface-based ice measurements. Numerous imaging-radar flights have also been made, but all of the systems were uncalibrated. The aircraft systems used have been those that were available for use which severely restricted attempts to determine optimum frequency and polarization. For these reasons, surface-based scatterometer experiments were proposed by the University of Kansas to provide well-controlled systematic studies to relate radar backscatter return to sea ice and to pin down some of the uncertainties associated with the results from the various airborne experiments.

#### 3.2 May 1977 and April 1978 Surface-Based Missions

The need to design an optimum ice reconnaissance radar system has been well-documented by both civilian and military users. To do this the effects of polarization, frequency, incidence angle, and resolution must be described in terms of their contribution in the ability to use radar to discriminate among types of sea ice and to measure other properties of the ice. During the months of May 1977 and April 1978, missions were conducted to contribute to this description [40, 41]. Active-microwave backscatter measurements were made on shorefast sea ice off the coast of Point Barrow, Alaska, and on two frozen fresh-water lakes near the coast. The objectives of these measurement programs were to study the available categories of sea ice, using in the study the radar parameters of frequency, transmit-receive polarization, and

incidence angle, with simultaneous collection of ground-truth parameters. Backscatter measurements were conducted using a four-antenna frequency-modulated continuous-wave 1-2 GHz and 8-18 GHz microwave active spectrometer/scatterometer mounted on a transportable surface-based support structure which placed the antennas at fixed ranges from the ice.

### 3.2.1 Microwave Remote Sensor -- TRAMAS

The microwave active spectrometer (MAS) used was a transportable surface-based wide-band FM-CW radar. The assembled system is shown prepared for operation in Figure 3.2-1. The L-band (1-2 GHz) radar is located at the apex of the inverted vee. The horn antenna transmits and the dish antenna receives. The Ku-X-band (8-18 GHz) parabolic dish antennas are located at the base of the structure and are aimed at a flat plate reflector which directs the radar signal to a focal point in the intersection of the plane of the inverted vee and the ground plane. Nominal system specifications are detailed in Table 3.2-1 and a system block diagram is given in Figure 3.2-2.

The L-band radar was swept from 1.1 to 1.9 GHz for VV and VH polarizations. Ku-X-band frequencies were centered at 9.0, 10.0, ..., 17.0 GHz and swept  $\pm .5$  GHz. Transmit-receive configurations were HH, HV, VH, and VV.

Calibration of the scatterometer was achieved by frequently passing the signal through a delay line of known attenuation and by less frequently observing a standard radar target of known radar cross-section. A corner reflector was used in the calibration of the L-band radar and a Luneberg-lens reflector in the calibration of the Ku-X-band radar.

Reduction in the fading effects of constructive and destructive interference of the signal components of the scattering elements within

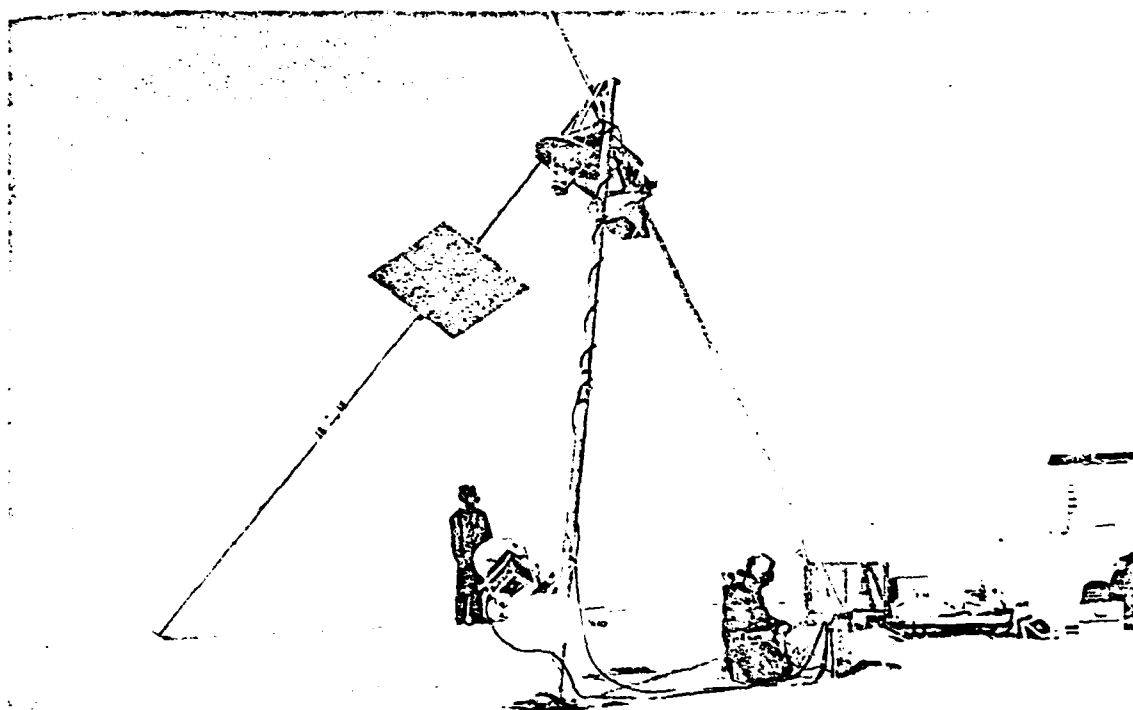


Figure 3.2-1. The assembled transportable microwave active spectrometer (TRAMAS)

TABLE 3.2-1  
NOMINAL SYSTEM SPECIFICATIONS

	<u>Ku-X-band</u>	<u>L-band</u>
Type	FM-CW	FM-CW
Frequency Range	8-18 GHz	1.5 GHz
Modulating Waveform	Triangular	Triangular
FM Sweep: $\Delta f$	1 GHz	800 MHz
Transmitter Power	14-19 dBm	19 dBm
Intermediate Frequency	50 kHz	50 kHz
IF Bandwidth	10 kHz	10 kHz
Antennas		
Receive Type	46 cm. Reflector	91 cm. Reflector
Transmit Type	31 cm. Reflector	Standard Gain Horn
Feeds	Dual Ridge Horn	Log Periodic
Polarization Capabilities	HH, HV, VV, VH	VV, VH
Target Distance	10.7 meters	6.1 meters
Transmit Beamwidth	8.2° at 8 GHz 4.0° at 17.7 GHz	27°
Receive Beamwidth	5.3° at 8 GHz 2.3° at 17.8 GHz	9.5°
Incidence Angle Range	10° - 70°	10° - 70°
Calibration		
Internal	Signal Injection (delay line)	Signal Injection (shorted delay line)
External	Luneberg Sphere Reflector	Square Trihedral Corner Reflector
Operating Temperature Range	-50°C to +50°C	-50°C to +50°C

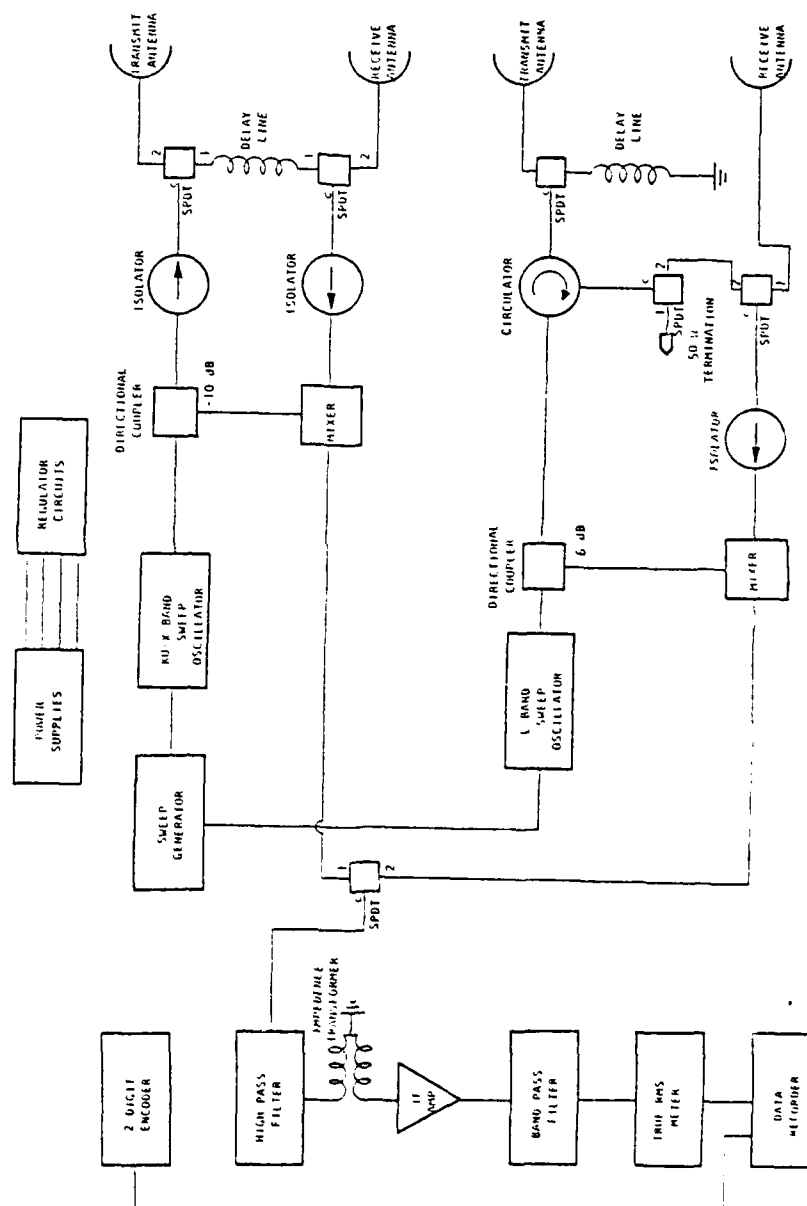


Figure 3.2-2. Block diagram of TRAMAS system.

the resolution cell was accomplished by increasing the number of independent samples through frequency, volume, and spatial averaging [42, 43]. A single measurement of the backscatter from a particular target is almost meaningless. Several samples, preferably a relatively large number, must be measured and the results averaged together to reduce the effects of the fading. The precision of the radar scattering coefficient measurement with a scatterometer is limited by these fading effects. Frequency averaging consisted of sweeping with bandwidth in excess of that required for resolution [44]. Additional independent looks were obtained through physically repositioning the structure.

### 3.2.2 Experiment Description

The experiment team was ground-based out of the Naval Arctic Research Laboratory (NARL) located outside of Point Barrow. This facility provided for messing, billeting, laboratory space, and logistics support. Backscatter measurements were made in the shorefast ice off the coast near NARL. Measurements were also made of two inland fresh-water lakes located near the camp. The TRAMAS system and support equipment were transported to ice sites by snowmobile and sled or by truck.

In 1977 the selection of ice sites was done with the aid of Dr. W.F. Weeks, of U.S. Army Cold Regions Research and Engineering Laboratory (CRREL), by both ground and air visual inspection of the off-shore coastal area near NARL. Ice categories such as multiyear and thick first-year, and pressure ridges, were located in the shorefast ice zone. Inland ice sites within reach included fresh-water lakes with scientifically interesting ice structures. Representative samples of the available types of ice that were accessible by snowmobile were selected.

Ice conditions in April 1978 fell short of the ideal conditions found in May of the previous year. Much of the shorefast ice zone was composed of heavily deformed thick first-year ice. The site that was selected for the investigation was a large, very smooth thick first-year ice area which formed due to the refreezing of a lead. This site received much attention from the numerous experimenters based at NARL.

### 3.3 Ground Truth Information

The task of the ground-truth phase of the experiment was to make measurements at the time of the backscatter measurements that would describe snow and ice conditions in the area of the radar footprint. The following parameters were used in the description of the snow pack: depth; density; snow surface temperature; a general description of grain size, shape, and texture; and surface roughness. In describing the nature of the sea ice being studied, the following parameters were used: ice type, thickness, surface roughness (both small and large scale), small-scale horizontal inhomogeneities (based on thin sections from ice cores), ice surface temperature, ice salinity profile, and vertical inhomogeneities (based on a visual core examination). At two sites statistical studies were also made of the degree of preferred crystal orientation at various levels in the ice sheet.

#### 4.0 DATA ANALYSIS

##### 4.1 Introduction

The normalized measure of backscatter return is described by a scattering coefficient (scattering cross-section per unit area or also called the differential scattering cross-section)  $\sigma^0$ . This is a measure of the strength of the observed signal which evolves due to the scattering properties of the observed region [11]. A discussion of the scattering equation may be found in the following section. The angular and frequency responses of the measured ice categories are also presented and discussed. Comparisons are made to describe the ability of radar to discriminate among ice types. The effects of snow depth, temperature, and anisotropic properties are also considered. The results of the 1-2 GHz measurements are described in Section 4.4 and the 8-18 GHz measurements are described in Section 4.5. The frequency response of the differential scattering cross-sections ( $\sigma^0$ ) in the 1-2 and 8-18 GHz frequency regions is discussed in Section 4.6. Application to ice type/thickness identification is found in Section 4.7.

##### 4.2 Scatterometer Equation

The scattering coefficient,  $\sigma^0$ , is used to describe the backscatter return because it is independent of the geometric radar parameters (factors which shape the illuminated area). This representation assumes the incoherent collection of signals from a very large number of separate scatterers and that locations of these scatterers are sufficiently random in the resolution cell that the received power from each may be added to the power from all the others without consideration

for phase [45]. When it is applied in ground-sensing a target where the radar parameters remain essentially unchanged from one part of the resolution cell to the other, the radar equation is given by the following [46]:

$$P_R = \frac{P_t G_t G_r \lambda^2 \sigma^0 A_{ILL}}{(4\pi)^3 R_t^4} \quad (4-1)$$

where

- $P_R$  = average power returned
- $P_t$  = transmitted power
- $G_t$  = transmit antenna gain
- $G_r$  = receive antenna gain
- $\lambda$  = wavelength
- $\sigma^0$  = differential scattering cross-section
- $A_{ILL}$  = illuminated area
- $R_t$  = range to target

Looking at the average return power on a single scatterer basis, we have for a region which contains  $n$  scattering elements and which is illuminated at one instant of time by a radar the following equation:

$$P_R = \sum_i^n \frac{P_{ti} G_{ti} \lambda^2 \sigma_{\Delta}^0 A_{ILLi}}{(4\pi)^3 R_{ti}^4} \quad (4-2)$$

Using the modified radar equation (4-1), we may express the differential scattering cross-section  $\sigma^0$  as:

$$\sigma^0 = \frac{P_R (4\pi)^3 P_t^4}{P_t G_t G_r \lambda^2 A_{ILL}}$$

(4-3)

The TRAMAS system uses square-law detection to measure the return power. To calibrate the system, the returns from a standard target of known radar cross-section are measured. Immediately before and after recording the return from the target of interest, a coaxial delay line of known loss is switched in place of the antenna paths to provide an instantaneous measure of calibration. Using both the frequent delay-line calibrations and the less-frequent standard radar target calibrations, the absolute value of the radar cross-section may be determined [47].

Numerous return-power measurements of each ice category are made. These measurements are then used in the overall description of the ice category. An average is made of the  $n$  measurements of power (not dB). That is, the  $n$  measured output voltages ( $v_1, v_2, v_3, \dots, v_n$ ) are averaged and the mean  $\sigma^0$  is given (in dB) by:

$$\sigma_{\theta}^0 \text{ (dB)} = 20 \log_{10} \left[ \frac{1}{n} \sum_{i=1}^n v_{\theta i} \right]$$

(4-4)

where  $v_i(\theta)$  is the  $i$ th output voltage for angle of incidence  $\theta$ .

#### 4.3 Surface Truth

The TRAMAS surface-based scatterometer is very attractive because it permits easy measurement of "surface truth" for the target of interest. The TRAMAS system maintains a fixed range to target at all angles of incidence; therefore, only the size of the resolution cell changes with change in incidence angle, not both the location of the cell and the size of the cell.

The purpose of the surface-truth task is to describe the conditions of the target at the time of measurement. This information allows for the correlation of changes in the physical properties of the medium with changes in backscatter response. The surface truth may give insight on the backscatter mechanisms and is very important if one compares the backscatter responses from similar situations in the same experiment, responses from similar ice types from experiment to experiment, or the results from other experiment groups. There is more to surface truth than the mere classification of the ice type, and it is hoped that this section vividly demonstrates this point to future experimenters.

##### 4.3.1 The May 1977 Barrow-Experiment Surface Truth Measurement.

Four categories of ice were investigated in May of 1977. These included two thick first-year shorefast sea-ice sites, two fragments of multiyear sea ice, one small pressure-ridged sea-ice site, one fresh-water inland lake with an underlying layer of water, and one fresh-water inland lake frozen to its mud bottom. The sea ice sites were located off the Alaskan coast near Point Barrow and the Naval Arctic Research Laboratory (see Figure 4.3-1). The lake ice sites were also located in this

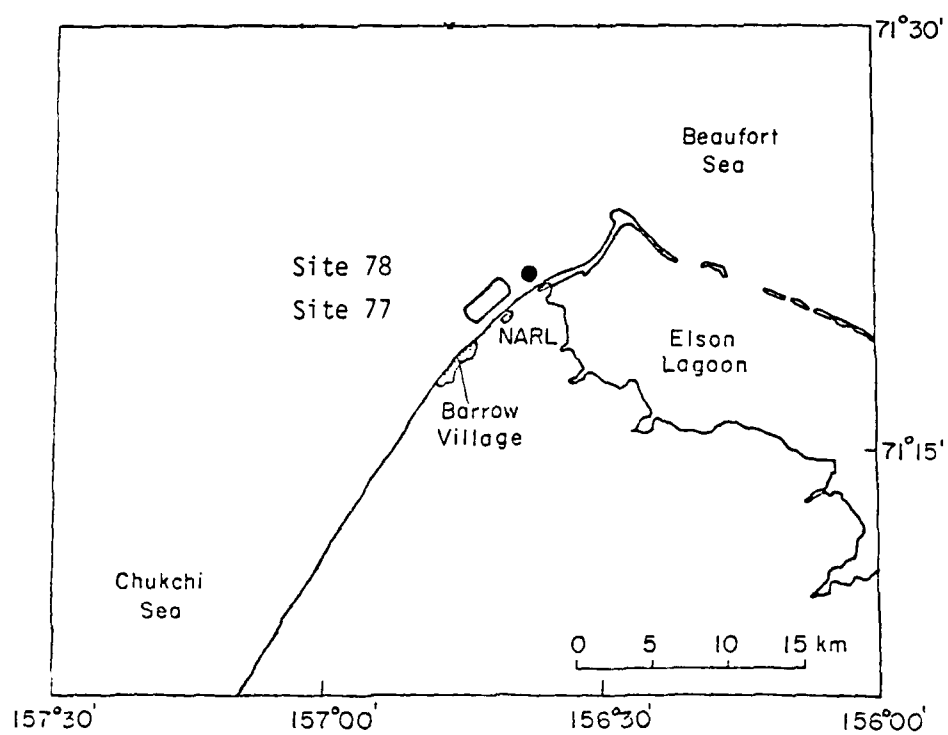


FIGURE 4.3-1 Offshore Ice Experiment Locations Near Barrow, Alaska, in the Chukchi Sea.

vicinity. Brief descriptions of these ice sites may be found in Table

4.3.1. More elaborate descriptions on a site-by-site basis follow.

4.3.1.1 Site #1: Thick First-Year Shorefast Sea Ice. The ice was 1.65 meter thick and had approximately 10 cm of snow cover. The surface was composed of 2-3 m diameter pans. In general, the topography was flat except for 4-cm-high vertical steps at the edges of the pancakes. Five sets of spatially-independent backscatter measurements were made. This was possible because the antenna support structure was located at each of several positions about the site. The air and snow-ice interface temperatures for this site and the other sites may be found in Figure 4.3-2. Snow densities for this site and the other sites may be found in Table 4.3-2.

This site had a 24 cm fine-grain slush-like layer. The c-axis orientation of these crystals was apparently random. The top 10 cm had a dense bubble distribution, the next 15 cm had a moderately-dense bubble distribution, and the remainder was congelation ice with a less-dense distribution of bubbles (see Figures 4.3-3 and 4.3-4). From the horizontal thin section made at 10 cm depth, Figures 4.3-5 and 4.3-6, it is seen that the bubble distribution is random and that the bubbles are very small in diameter. The horizontal thin section, when viewed through a polarizing filter, demonstrates the random nature of the ice crystals and that they are small in size. The horizontal thin section made at 51 cm depth (see Figures 4.3-7 and 4.3-8) contains tiny brine inclusions. These are systematically distributed and show a preferred crystal orientation. When this section is viewed through a polarizing filter, it is seen that the ice-crystal platelets at this level have grown in a preferred direction and that they are much larger than those in the upper parts of the ice sheet.

TABLE 4.3.1

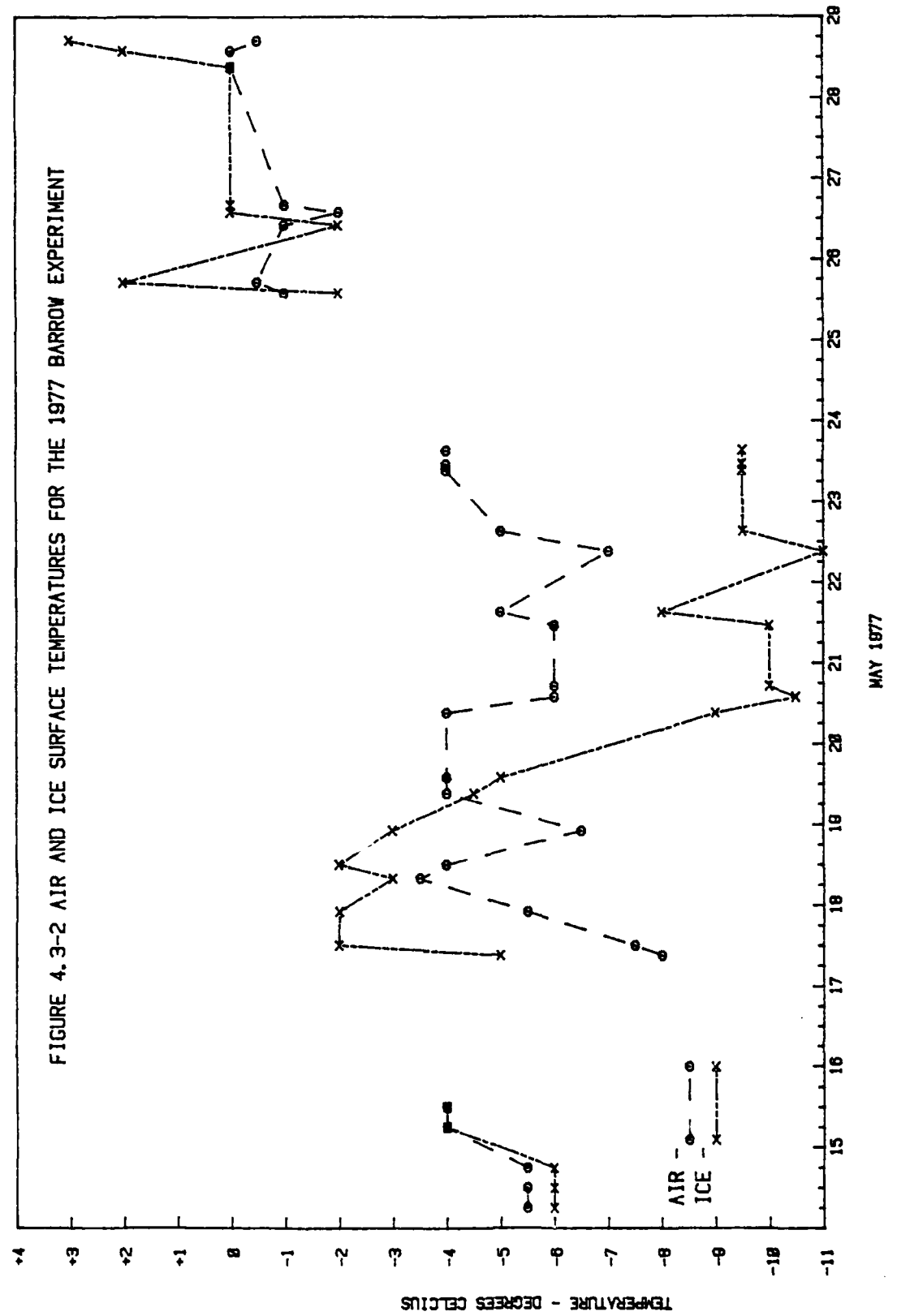
## SITE DESCRIPTIONS

THIS TABLE IS A SUMMARY OF THE INFORMATION  
FROM OUR 1968-1969 FIELD STUDY

ICE TYPE (Thickness)	SNOW		ICE		Temperature (°C)		Brine Volume of Top 0.10 Meters (0/00)	SITE DESCRIPTION
	Thickness (m)	Mean Density (g/cm <sup>3</sup> )	Thickness (m)	Salinity (0/00)	Air	Ice Surface		
1 First-year (1.65 m)	0.10 (0.06-0.14)	312 (280-316)	1.65	7.7	-4.2 to -7.0	-4.0 to -5.8	99 39	Ice surface composed of pancakes 2-3 m in diameter. General topography is flat except for 4 cm high vertical steps at the edges of the pancakes. Upper 24 cm of core is frozen slush. Scrapings of top 1 m of ice have salinity of 13 0/00.
2 Multiyear (2.3 m)	0.10 (0.01-0.19)	322 (240-304)	2.3	0.7	-2.0 to -3.0	-2.0 to -8.0	18 4	Measurements made on a 50 cm high melt hummock that was ca. 3 m in diameter. Small scale roughness on hummock was usually 4 cm, although occasional 1 cm high roughness elements occur. Upper 3 cm of ice is granular with grain size of ca. 1 mm and a salinity of 3.2 0/00. Top 55 cm of core contains spherical bubbles up to 4 mm in diameter, below 55 cm structure is compaction ice.
3 First-year (1.33 m)	0.02 (0.01-0.03)	---	1.37	7.0	-5.0 to -10.5	-3.5 to -6.0	102 61	Very flat, uniform unrafted ice. Scrapings of upper ice surface have salinity of 12 0/00. Strong preferred horizontal c-axis alignment is present in ice 15 cm below upper surface (mean c-axis direction 350 true).
4 First-year (2.3 m)	0.16 (0.00-0.43)	346 (322-356)	1.40	8.5	-8.0 to -11.0	-5.0 to -7.0	81 64	Small first-year pressure-ridge. Ice block composition ridge are 10 cm thick (ridge formed in fall when ice was thin). Width of the base of the ridge sail is 2 m, sail height approximately 0.9 m. Surrounding undeformed first-year ice is 1.3 m thick.
5 Multiyear (2.3 m)	nfl	---	2.3	0.7	-1.0 to -6.0	-4.0 to -5.0	9 7	Ice surface is flat on large-scale. Pronounced small scale melt produced roughness with a height of 0.5 to 1.0 cm. Upper 130 cm of core showed layered bubbly structure, below 130 cm ice is normal compaction ice.
6 Ice core (2.06 m)	nfl	---	2.10	0.1	+2.0 to -2.0	-0.5 to -2.0	N/A	Ice core below 90 cm was wet (water appears in drill hole). The ice was not frozen to the lake bed.
7 Ice core (1.76 m)	0.18	414 (410-440)	0.74	0.6	+4.0 to +1.0	0.0 to -0.5	N/A	Upper ice surface is very smooth and snow covered. The ice was frozen completely to the bottom of the lake.

TABLE 4.3-2  
 SNOW DENSITIES TAKEN AT  
 SITES 77-1, 77-2, 77-4, AND 77-7

SITE NUMBER	LOOK NUMBER	DEPTH BELOW SNOW SURFACE	SNOW DENSITY (gm/cm <sup>3</sup> )	COMMENTS
77-1	1	4	312	on ice surface
		7	276	
	2	4	376	on ice surface depth hoar
		11	296	
	3	3	288	
	4	3	348	on ice surface
		7.5	308	
77-2	1	3	352	on ice surface
		8	344	
		12	384	
		16	344	
	2	7	280	
77-4	--	8	332	
		20	356	
77-7	--	3	416	on ice surface
		9	448	
		14	448	
		15	424	



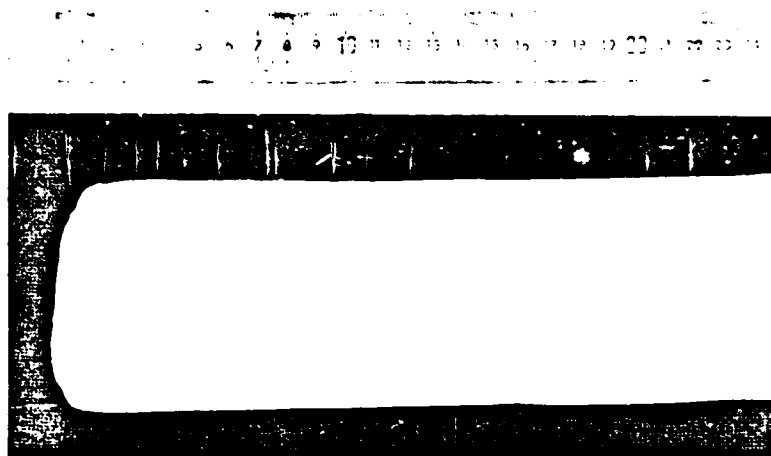


Figure 4.3-3. 0-24 cm section of Site 77-1 ice core.

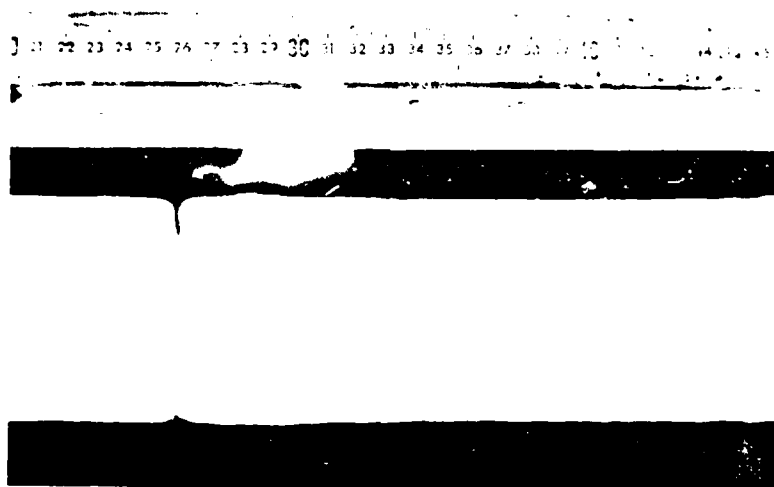


Figure 4.3-4. 20-45 cm section of Site 77-1 ice core.

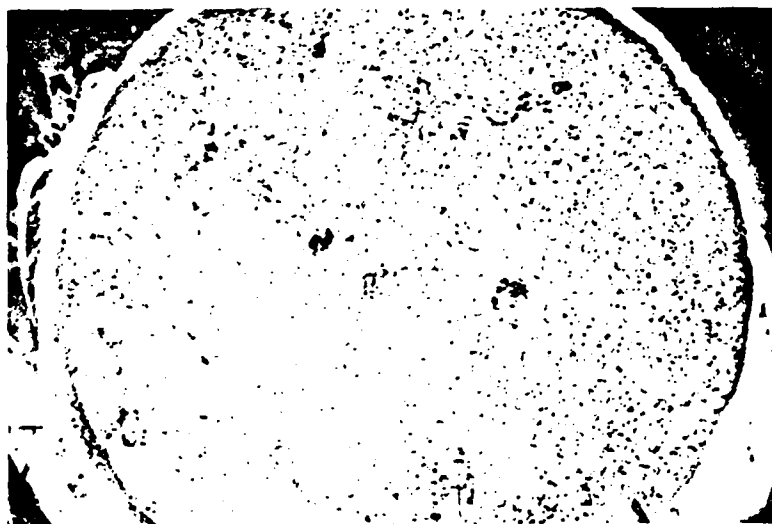


Figure 4.3-5. Horizontal thin section of Site 77-1 taken at depth 10 cm.

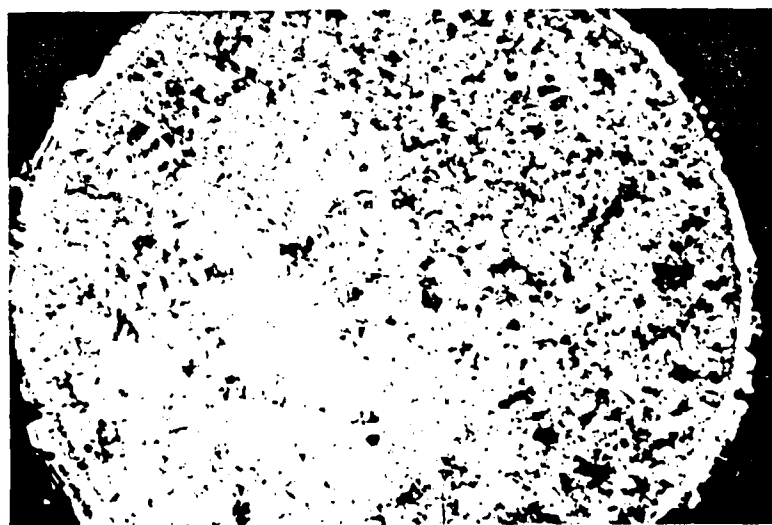


Figure 4.3-6. Horizontal thin section of Site 77-1 taken at 10 cm depth as viewed through polarizing filter.

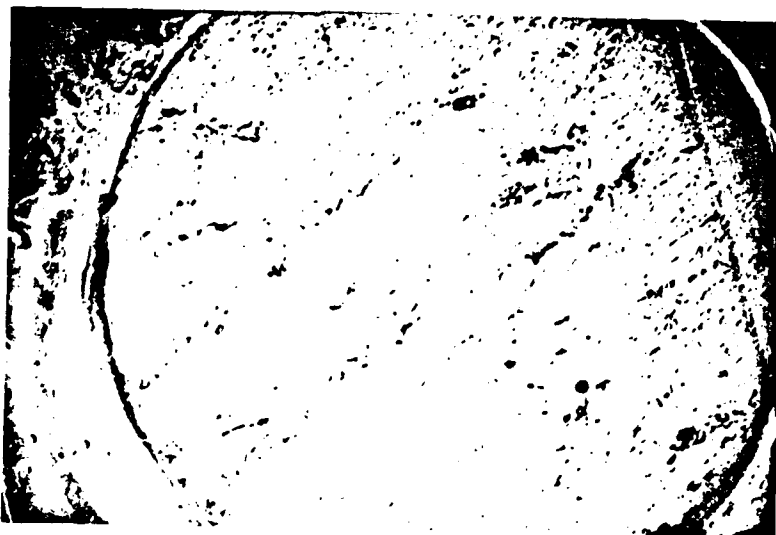


Figure 4.3-7. Horizontal thin section of Site 77-1 taken at 51 cm depth.



Figure 4.3-8. Horizontal thin section of Site 77-1 taken at 51 cm depth as viewed through polarizing filter.

Profiles of the parameters most important in controlling the "state" of the ice (temperature and salinity) are shown in Figures 4.3-9 and 4.3-10. The salinity profile is a typical irregular c-shaped curve characteristic of first-year ice [48,49]. The temperature profile is nearly linear, again a situation that is common in first-year ice when there have not been recent major air temperature changes. The temperature gradient was  $.76^{\circ}\text{C}$  per m. The brine-volume profile, which is determined by both the temperature and the salinity profiles (see equation 2-1), is shown in Figure 4.3-9. The calculated profile is characteristic of many other first-year brine-volume profiles that have been observed in that a slight increase in brine volume occurs near the surface, a minimum occurs at some intermediate depth (in this case 15 cm), and a drastic increase occurs near the bottom of the ice sheet. This latter increase, of course, is the result of the increase in salinity near the interface with sea water and near melting temperatures.

4.3.1.2 Site #2: Multiyear Sea Ice. This fragment of multiyear sea ice was greater than three meters thick with a snow cover of 1-19 cm. Six spatially-independent backscatter measurements were made on a 50-cm-high melt hummock of ridge origin which was about 3 meters in diameter. The small-scale roughness on the hummock was usually 4 mm, although occasional 1-cm-high roughness elements occur. The upper 3 cm of ice was granular with grain size of 1 mm (see Figures 4.3-12 and 4.3-18). The top 55 cm of the cores made both at the base of the hummock (meltpond) and at the top of the hummock contained spherical bubbles up to 4 mm in diameter (see Figures 4.3-11 to 4.3-14 and 4.3-18 to 4.3-20). Below 55 cm the surface was that of more typical congealed ice (see Figures 4.3-14 to 4.3-16 and 4.3-20 to 4.3-22).

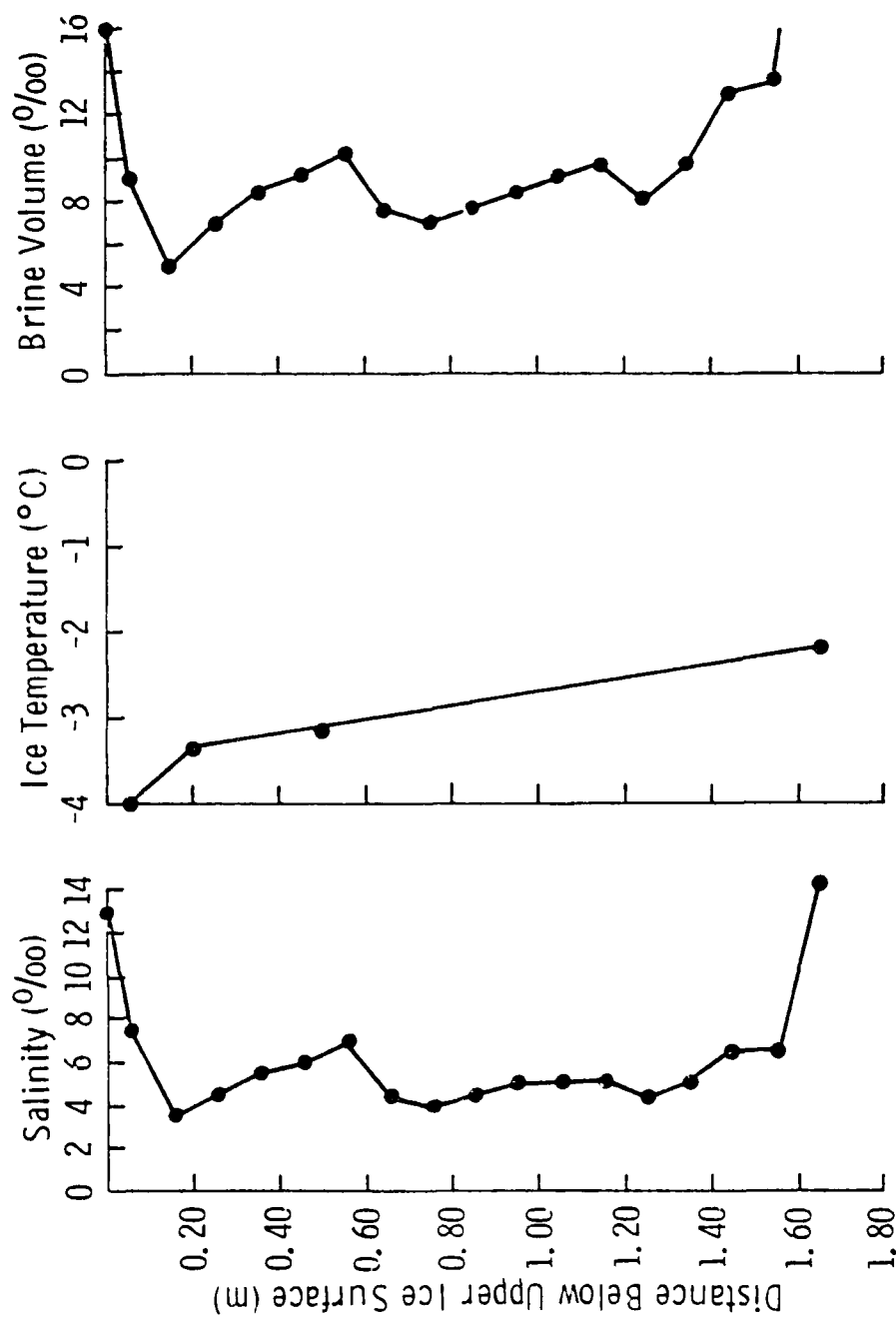


Figure 4.3-9. The salinity, ice temperature and brine volume profiles for the sea ice from Site 77-1 on May 14, 1977.

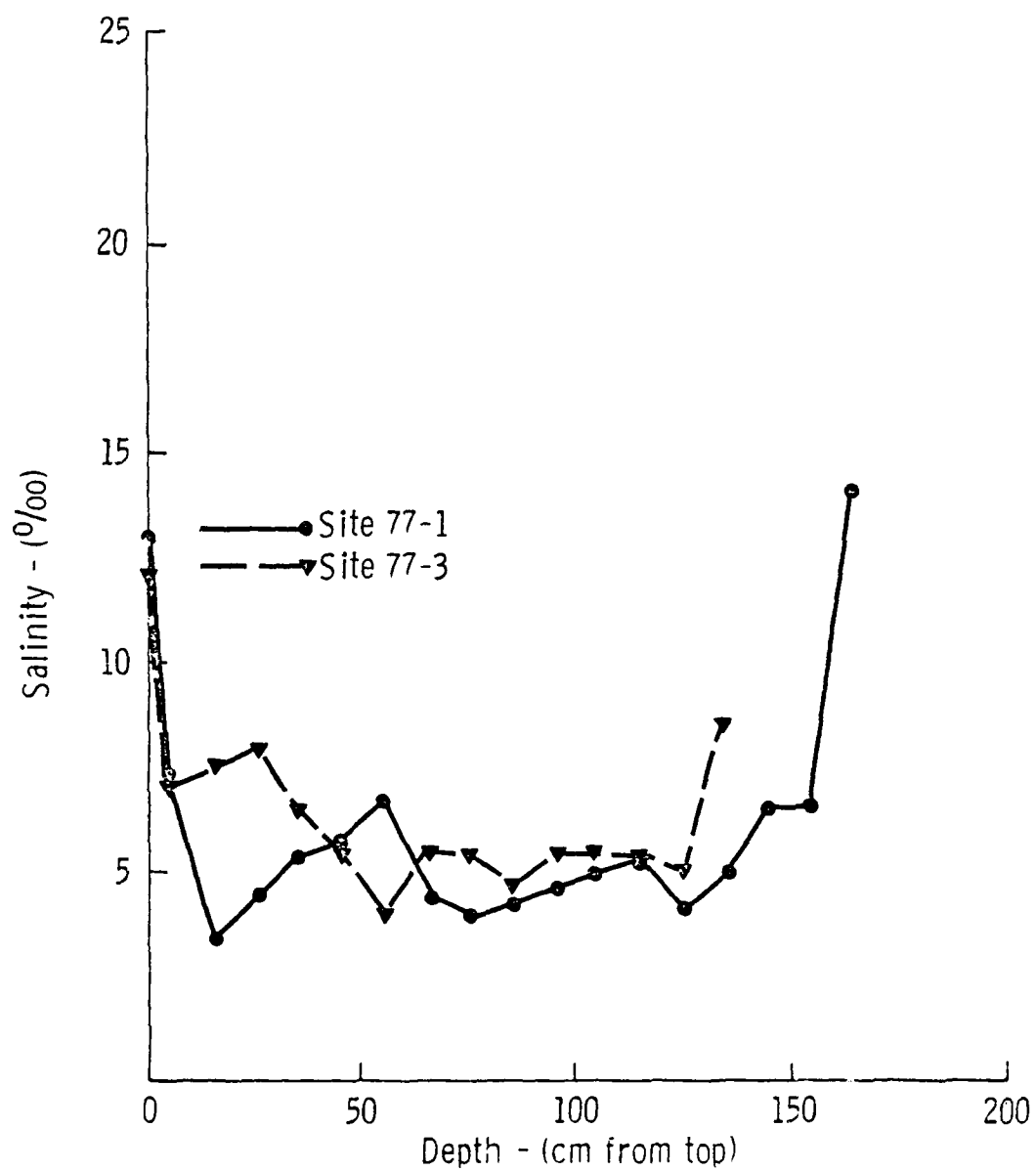


Figure 4.3-10. Salinity profile for Sites 77-1 and 77-3, thick first-year shore fast sea ice.

AD-A087 032

KANSAS UNIV/CENTER FOR RESEARCH INC LAWRENCE REMOTE --ETC F/6 17/9

RADAR BACKSCATTER STUDY OF SEA ICE.(U)

FEB 80 R G ONSTOTT, G J DOME, C V DELKER

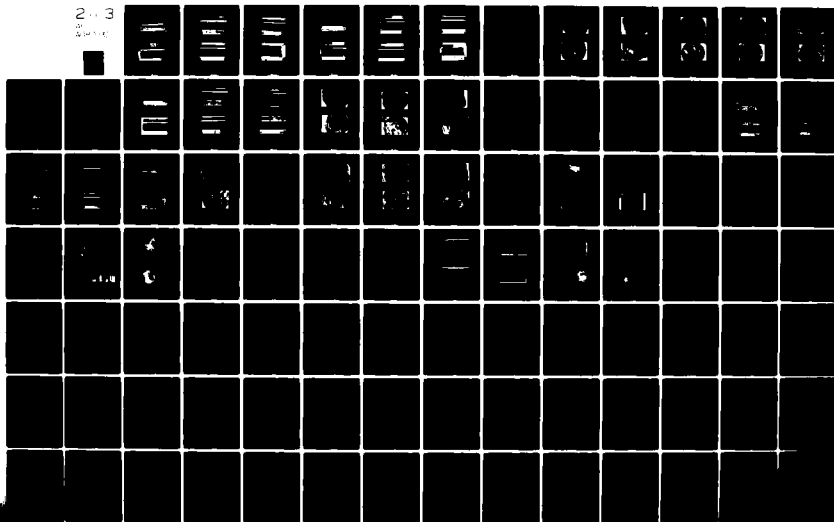
N00014-76-C-1105

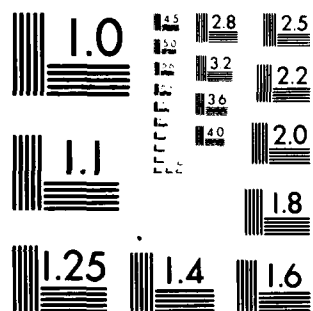
UNCLASSIFIED

CRINC/RSL-TR-331-14

NL

2-3  
of 3





MICROCOPY RESOLUTION TEST CHART  
NATIONAL BUREAU OF STANDARDS-1963-A

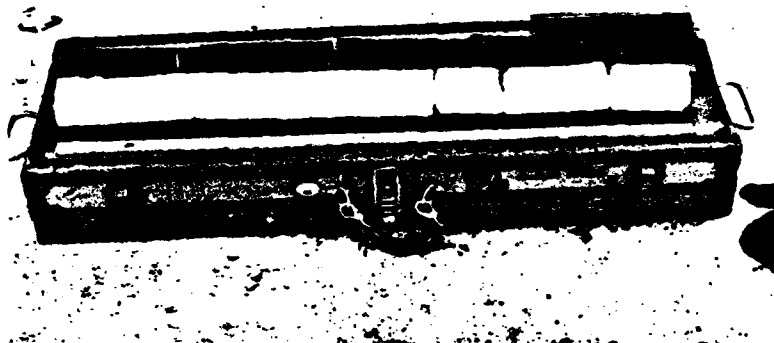


Figure 4.3-11. Complete ice core of Site 77-2 (meltpond).

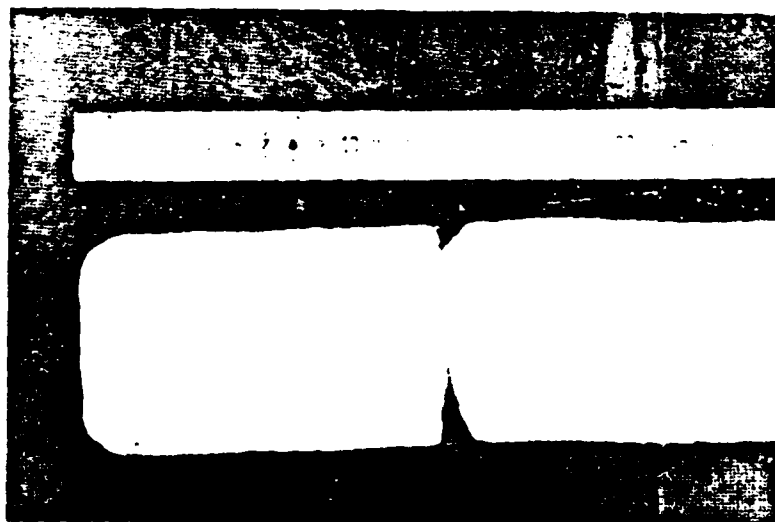


Figure 4.3-12. 0-25 cm section of Site 77-2 (meltpond).

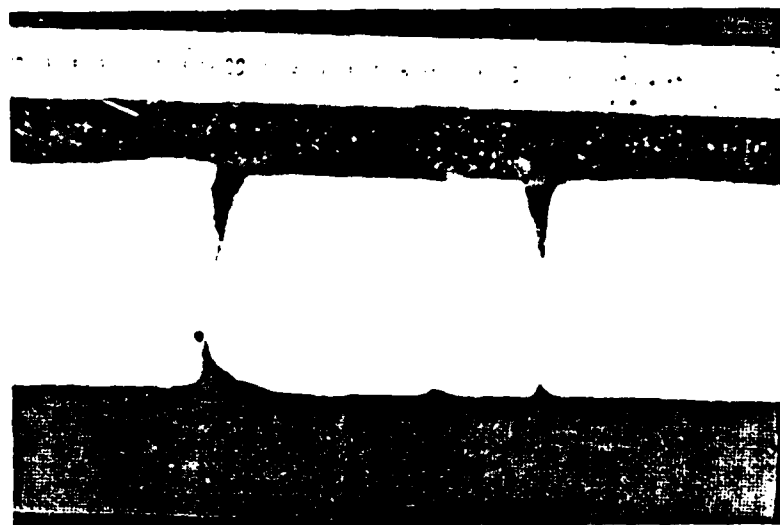


Figure 4.3-13. 21-48 cm section of Site 77-2 (meltpond).

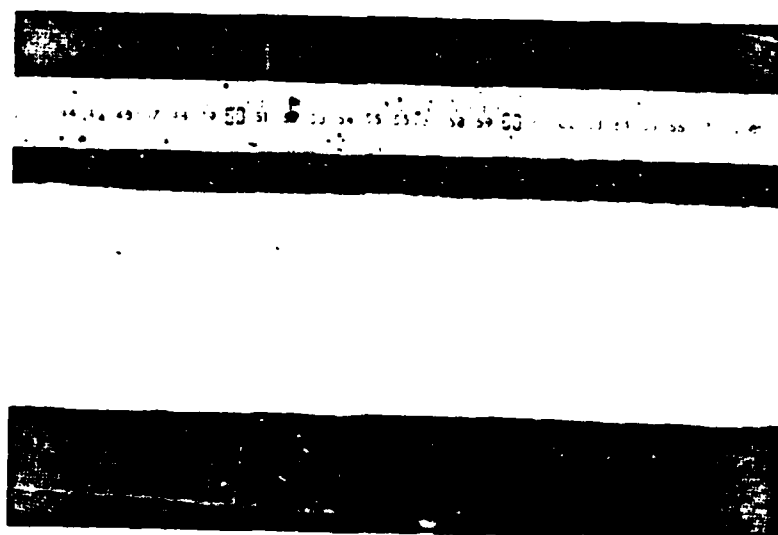


Figure 4.3-14. 42-68 cm section of Site 77-2 (meltpond).

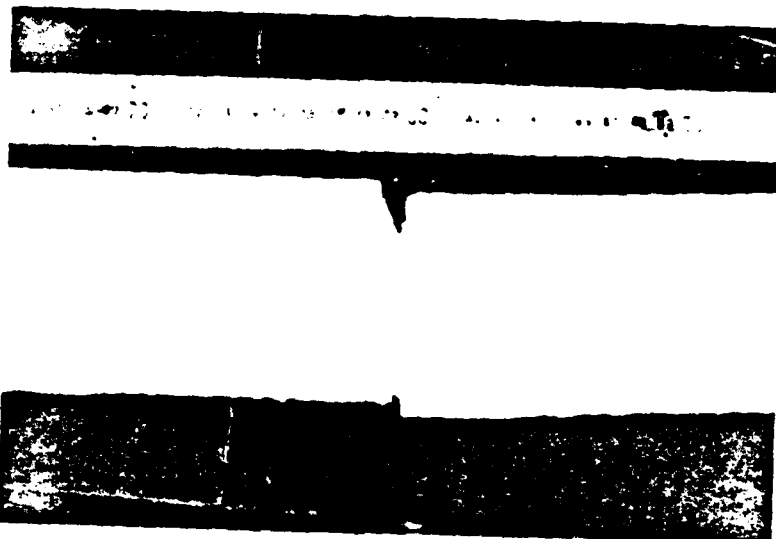


Figure 4.3-15. 64-91 cm section of Site 77-2 (meltpond).

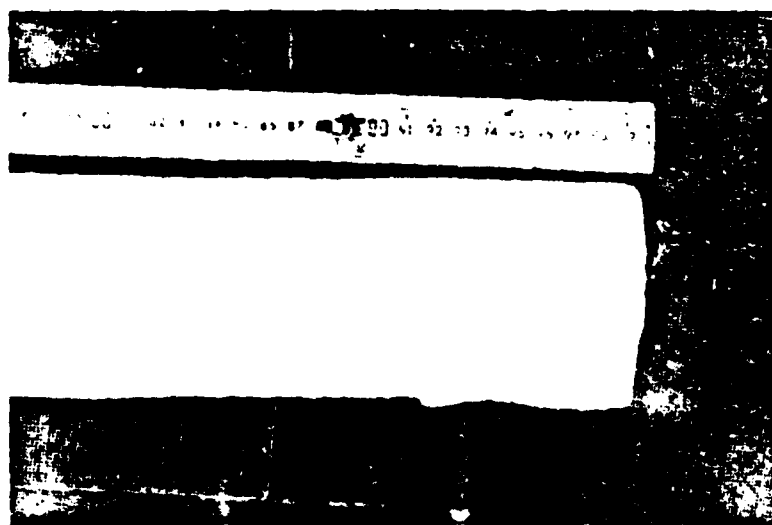


Figure 4.3-16. 78-100 cm section of Site 77-2 (meltpond).

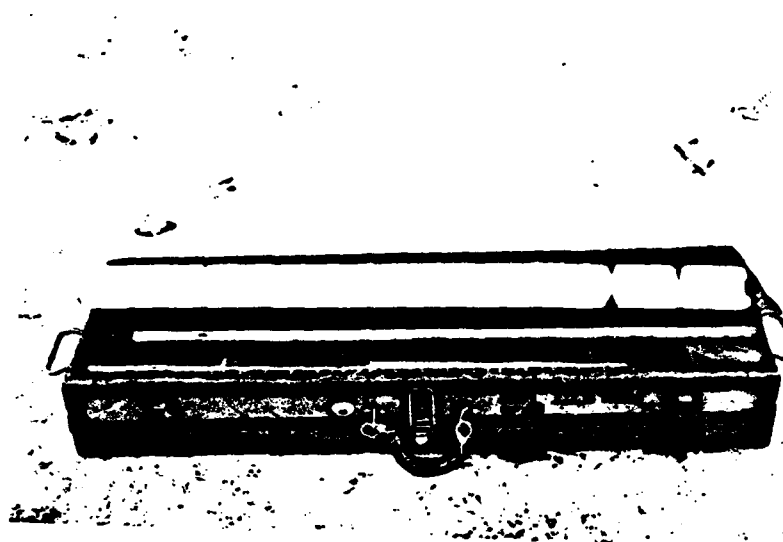


Figure 4.3-17. Complete ice core of Site 77-2 (hummock).

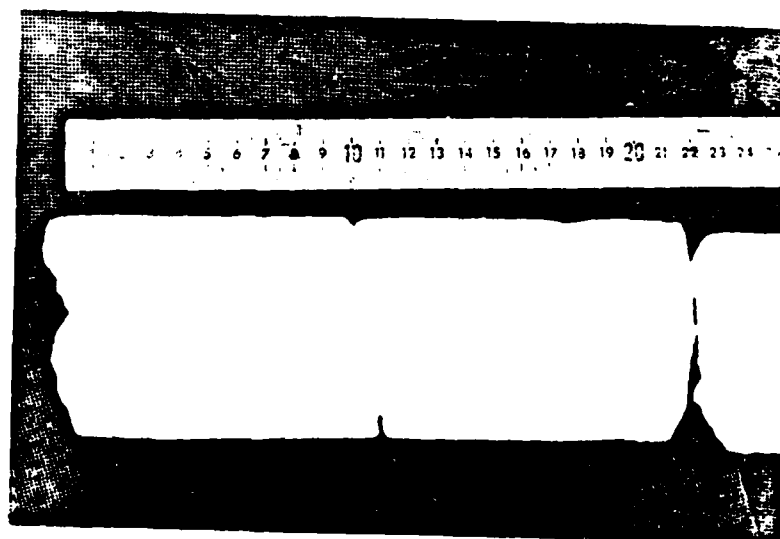


Figure 4.3-18. 0-24 cm section of Site 77-2 (hummock).

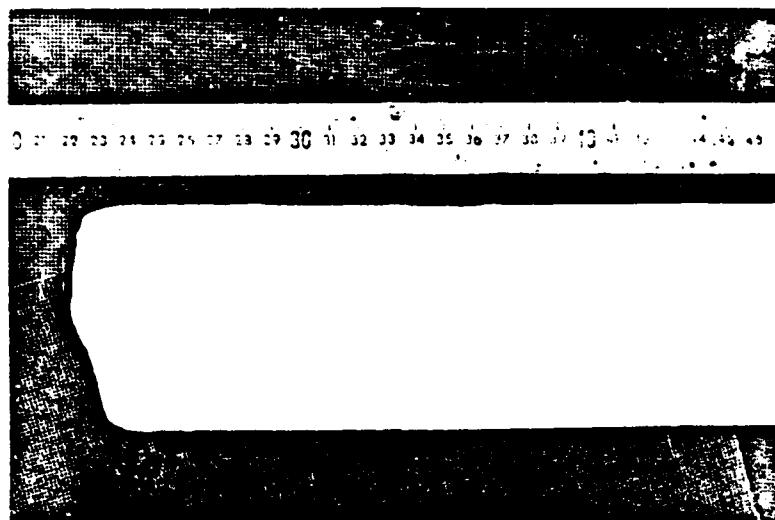


Figure 4.3-19. 20-46 cm section of Site 77-2 (hummock).

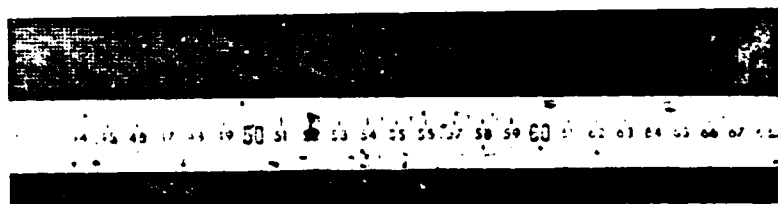


Figure 4.3-20. 41-67 cm section of Site 77-2 (hummock).

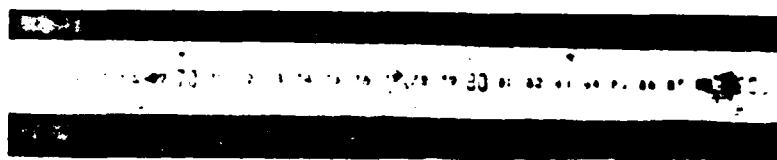


Figure 4.3-21. 64-90 cm section of Site 77-2 (hummock).

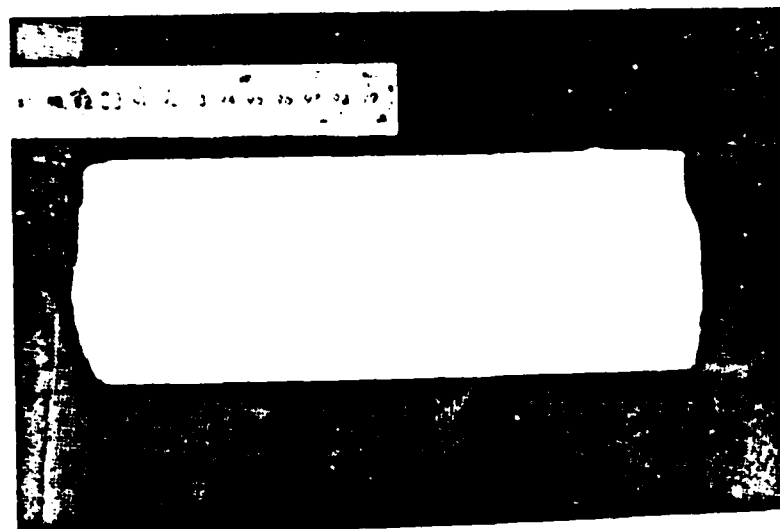


Figure 4.3-22. 89-110 cm section of Site 77-2 (hummock).

The horizontal thin section shown in Figure 4.3-23 shows the size, distribution, and shape of the bubbles in the upper 10 cm of the ice core taken at the base of the hummock.

The horizontal thin section made at 10 cm depth at the base of the hummock is shown in Figures 4.3-23 and 4.3-24. The large-diameter bubbles are found to be randomly distributed. Bubble shapes vary from near-perfect spheres to globular globs. When the section is viewed through a polarizing filter, it is seen that the ice crystals at this depth are moderate in size. A vertical thin section made at 78 cm depth (see Figures 4.3-25 and 4.3-26) shows a moderately dense distribution of bubbles and pockets. These are, in general, smaller than those found in the upper layers, with sizes ranging to the microscopic. This section contains many ellipsoidal shapes, along with many smaller spherical shapes. Again, this distribution appears to be random. This section, when viewed through a polarizing filter, shows a large columnar vertical crystal growth very much characteristic of sea ice. A horizontal thin section made at 99 cm depth (see Figure 4.3-28) contains moderate crystal sizes. A horizontal thin section at 5 cm depth made from the ice core taken from the top of the hummock, contains less smaller sized bubbles than the thin section made from the core taken at the base of the hummock. When it is viewed through a polarizing filter, large horizontal crystals are observed to occur. A horizontal thin section at 140 cm depth (see Figures 4.3-31 and 4.3-32) contains a well-distributed, moderately-dense irregularly-sized population of pockets and brine drainage tubes. Crystal growths are also larger in size.

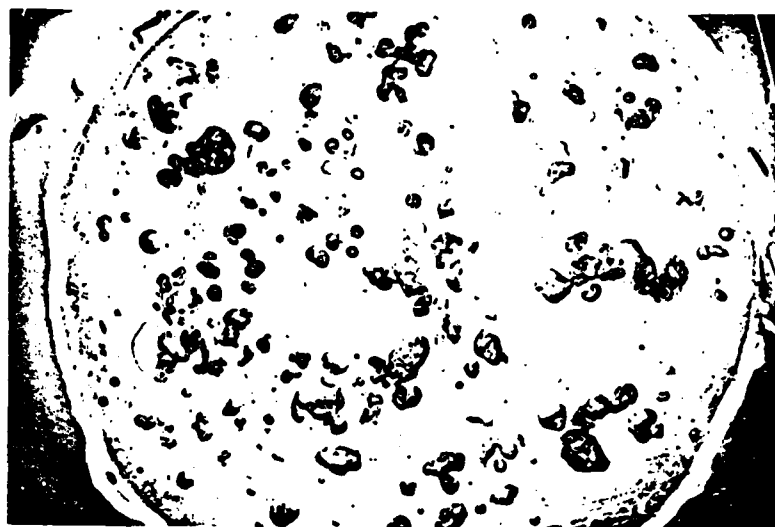


Figure 4.3-23. Horizontal thin section of Site 77-2 (meltpond) at 10 cm depth.

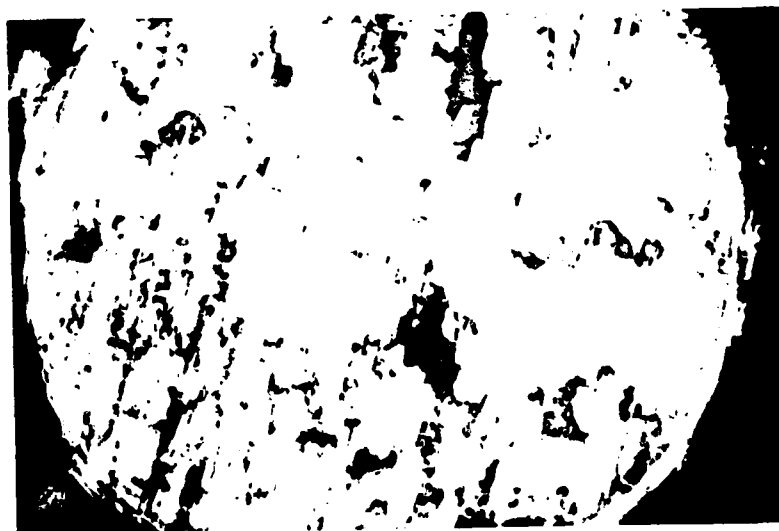


Figure 4.3-24. Horizontal thin section of Site 77-2 (meltpond) at 10 cm depth as viewed through polarizing filter.



Figure 4.3-25. Vertical thin section of Site 77-2 (meltpond) at 78 cm depth.

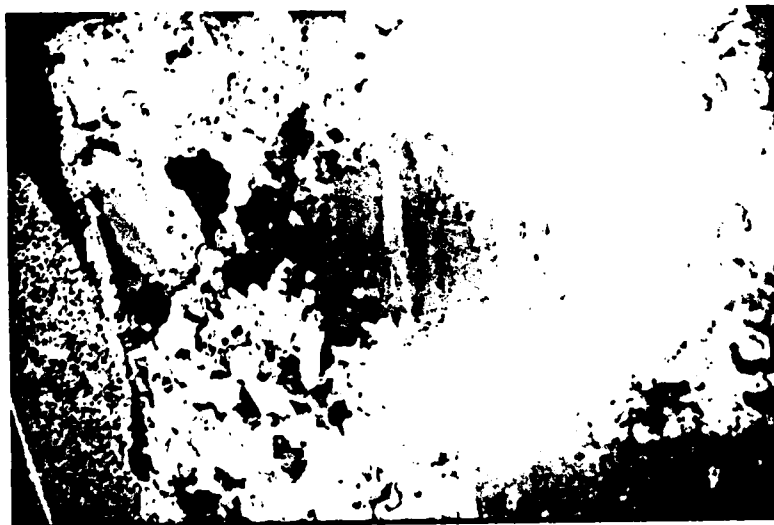


Figure 4.3-26. Vertical thin section of Site 77-2 (meltpond) at 78 cm depth as viewed through polarizing filter.

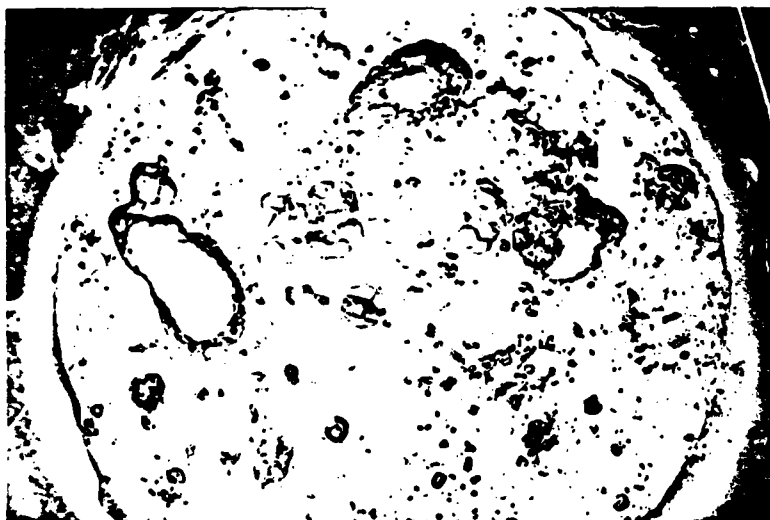


Figure 4.3-27. Horizontal thin section of Site 77-2 (meltpond) at 99 cm depth.

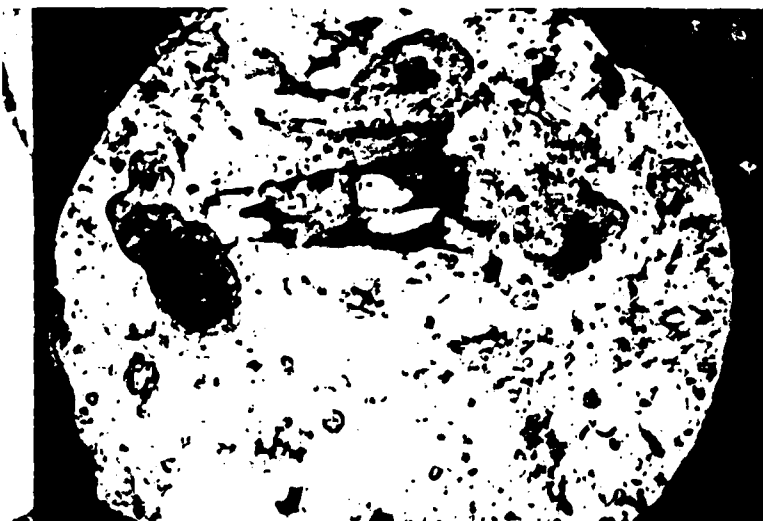


Figure 4.3-28. Horizontal thin section of Site 77-2 (meltpond) at 99 cm depth as viewed through polarizing filter.

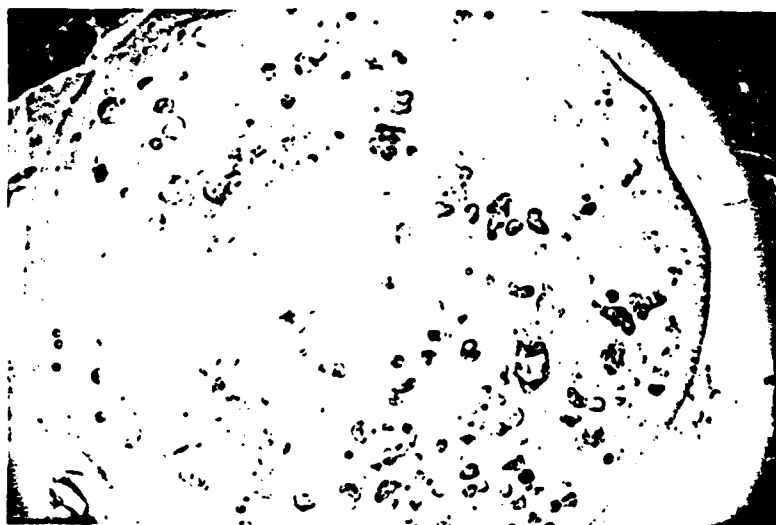


Figure 4.3-29. Horizontal thin section of Site 77-2 (hummock) at 5 cm depth.

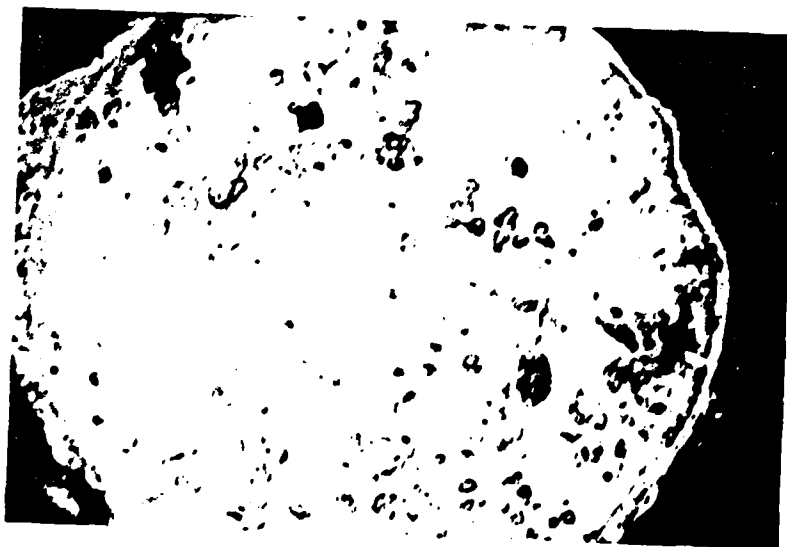


Figure 4.3-30. Horizontal thin section of Site 77-2 (hummock) at 5 cm depth as viewed through polarizing filter.

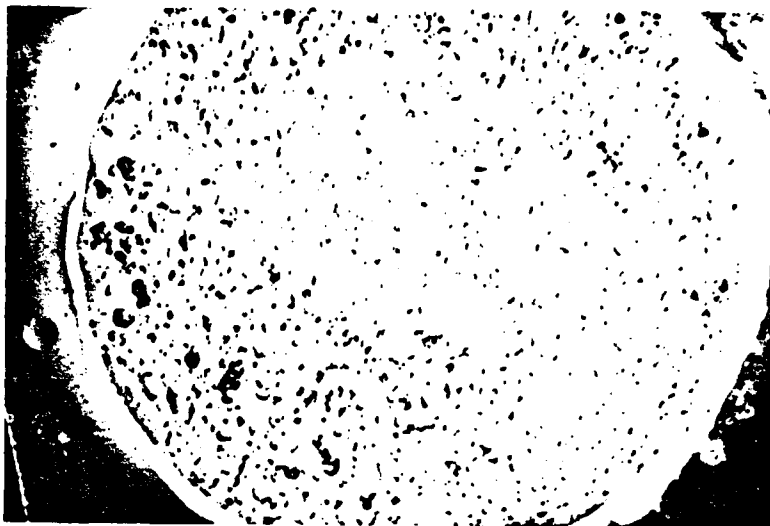


Figure 4.3-31. Horizontal thin section of Site 77-2 (hummock) at 140 cm depth.

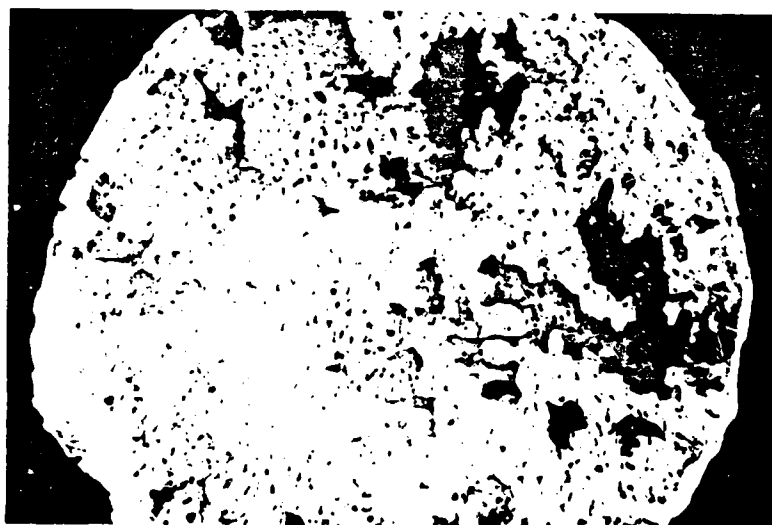


Figure 4.3-32. Horizontal thin section of Site 77-2 (hummock) viewed through polarizing filter.

Salinity profiles of cores taken at the base of the hummock, on top of the hummock, and down the side of the hummock are shown in Figure 4.3-33. These figures show profiles characteristic of multiyear sea ice where salinities start near zero and increase with depth.

4.3.1.3 Site #3: Thick First-Year Shorefast Sea Ice. This thick first-year sea ice site was 1.37 m thick with a uniform 2 cm snow cover. The ice was very smooth, uniform, and unrafted (see Figures 4.3-34 to 4.3-39). Six spatially-independent backscatter measurements were made. The salinity profile, which is very characteristic of first-year ice, is shown in Figure 4.3-10.

The upper 2 cm of the ice sheet (see Figure 4.3-35) was a snow-ice crust layer. A horizontal thin section at 15 cm depth (see Figures 4.3-38 and 4.3-39) shows a light distribution of moderate-sized channels and pockets with a heavy, almost uniform, distribution of microscopic brine inclusions, which show the possibility of a preferred growth direction of the moderate-sized crystals. A horizontal thin section at 130 cm depth (see Figures 4.3-40 and 4.3-41) shows a heavy population of tiny brine inclusions; the crystals are large in size, and they exhibit a preferred growth direction. A vertical thin section at 122 cm depth (see Figures 4.3-44 and 4.3-45) also shows the existence of a dense population of brine inclusions and a pronounced crystal elongation parallel to the direction of heat flow, a strong crystal orientation, and an increase in crystal size, as measured in the sheet which is characteristic of the columnar zone of sea ice [48].

Figure 4.3-46 contains fabric diagrams from two different levels (15 and 130 cm). Even at the 15 cm level, there was a pronounced crystal orientation within the horizontal plane, and at the 130 cm depth

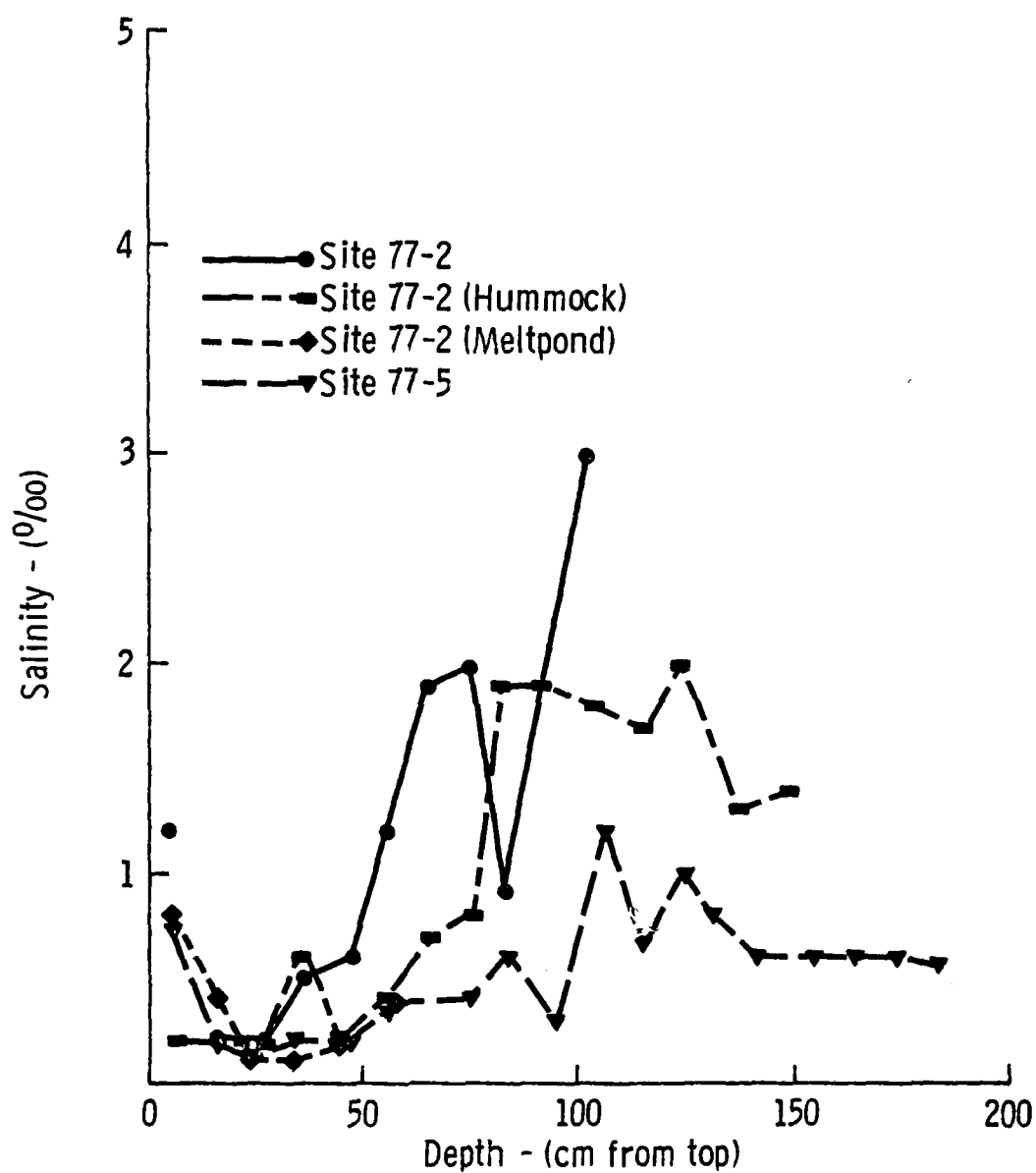


Figure 4.3-33. Salinity profile for Site 77-2 and Site 77-5, multiyear sea ice.

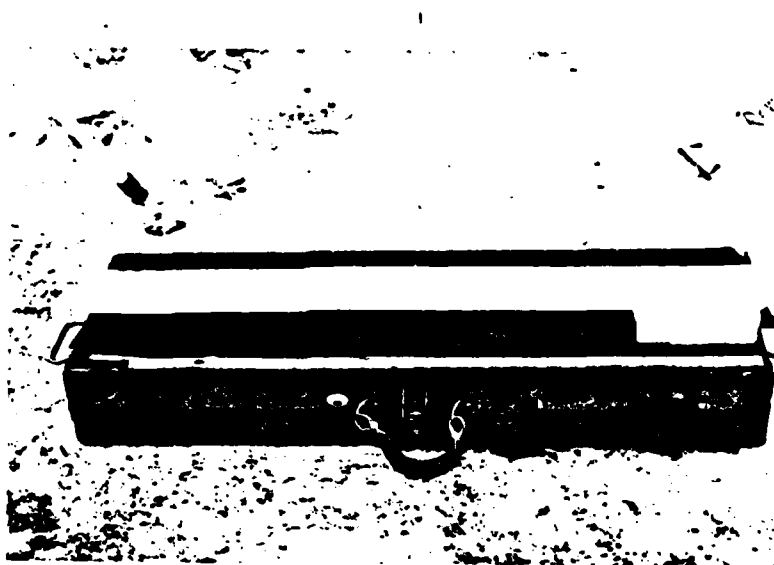


Figure 4.3-34. Complete ice core of Site 77-3.

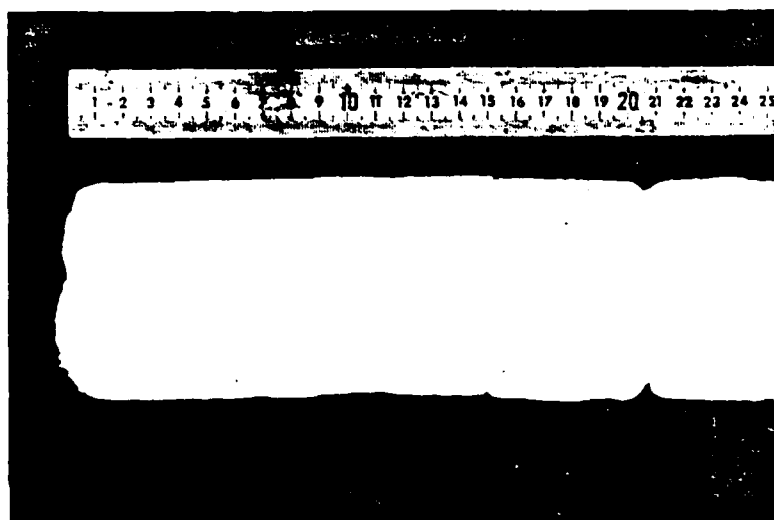


Figure 4.3-35. 0-25 cm section of Site 77-3 ice core.

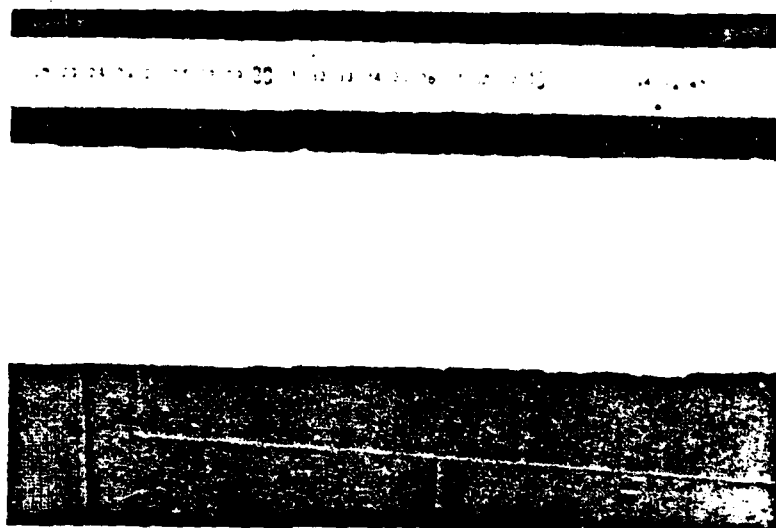


Figure 4.3-36. 21-47 cm section of Site 77-3 ice core.

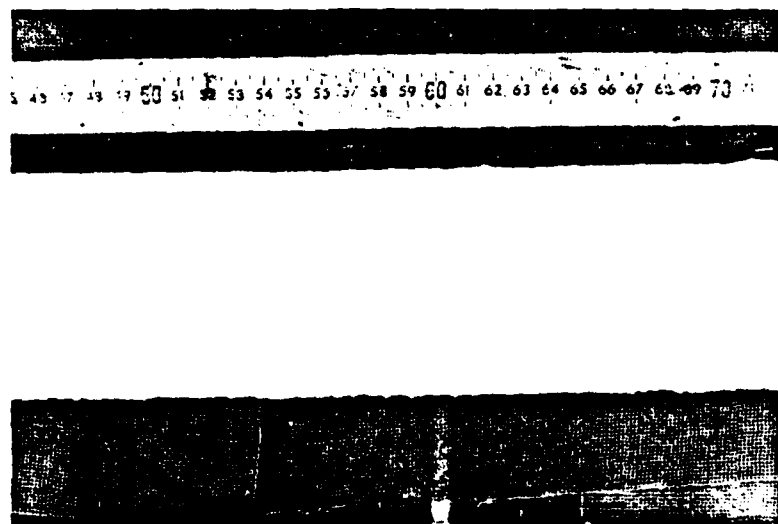


Figure 4.3-37. 46-71 cm section of Site 77-3 ice core.

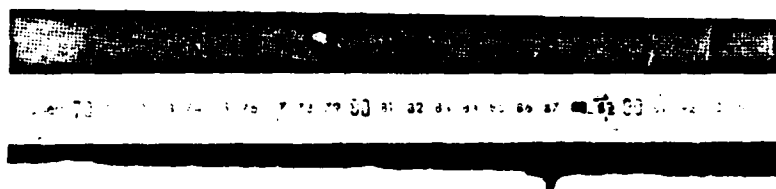


Figure 4.3-38. 67-94 cm section of Site 77-3 ice core.



Figure 4.3-39. 91 to 117 cm section of Site 77-3 ice core.



Figure 4.3-40. Horizontal thin section of Site 77-3 at 15 cm depth.

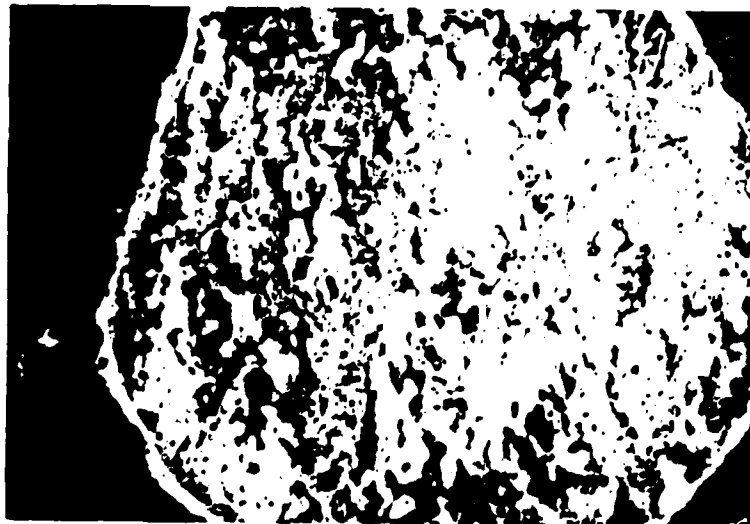


Figure 4.3-41. Horizontal thin section of Site 77-3 at 15 cm depth as viewed through polarizing filter.



Figure 4.3-42. Horizontal thin section of Site 77-3 at 130 cm depth.

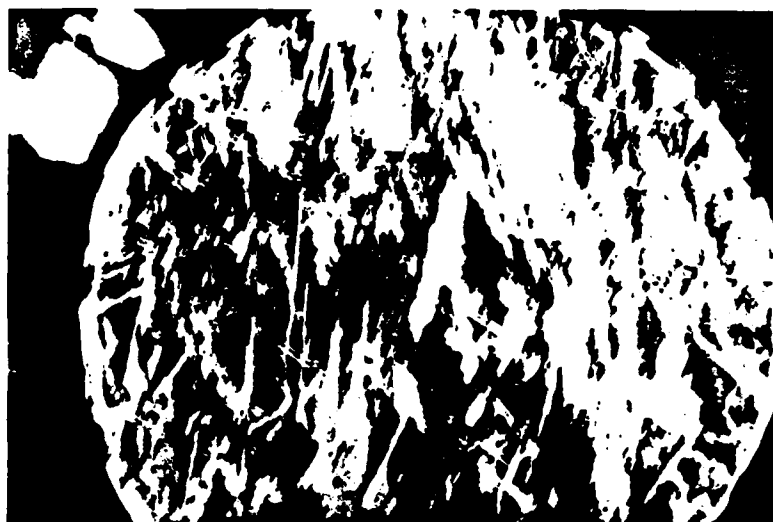


Figure 4.3-43. Horizontal thin section of Site 77-3 as viewed through polarizing filter.

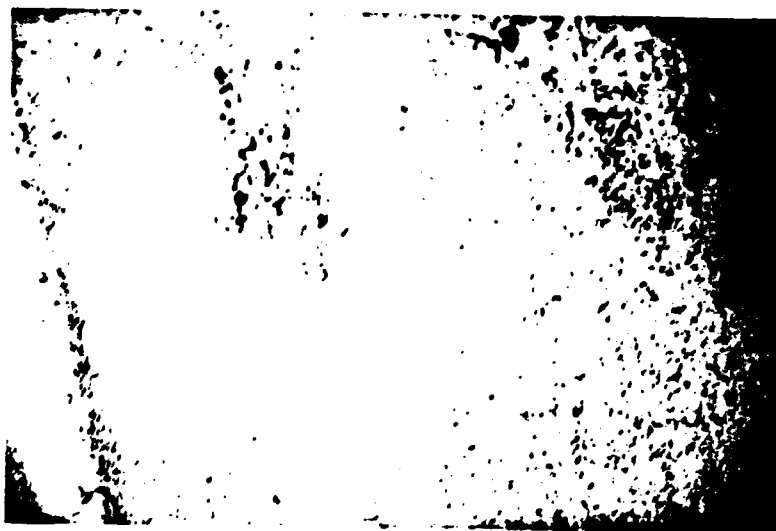


Figure 4.3-44. Vertical thin section of Site 77-3 at 122 cm depth.



Figure 4.3-45. Vertical thin section of Site 77-3 at 122 cm depth as viewed through polarizing filter.

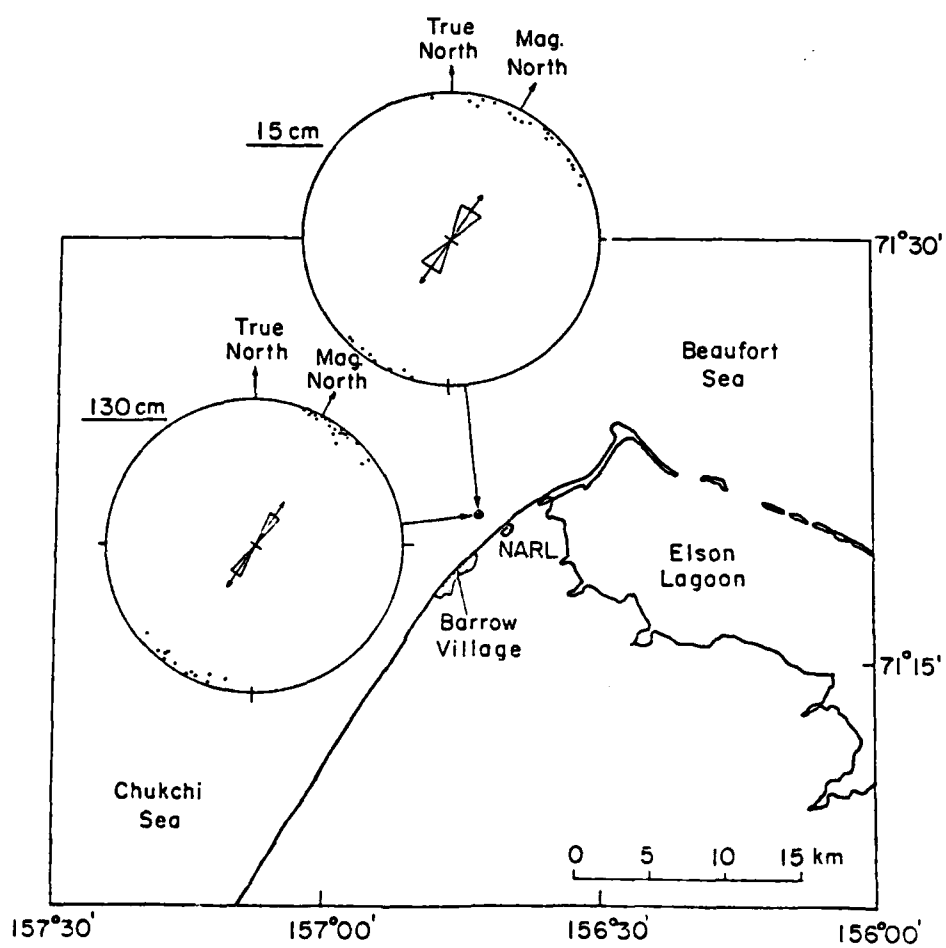


FIGURE 4.3-46 C-axis Orientations Measured Offshore from Barrow, Alaska, in the Chukchi Sea (Weeks and Gow, 1978).

the preferred orientation was well developed (circular standard deviation,  $s_0 = 9.7^\circ$ ). The orientation direction was almost exactly the same at both levels, with the c-axis aligned parallel to the coastline [50]. This orientation was in excellent agreement with oceanographic observations, which indicate a strong northeasterly current parallel to the Chukchi Sea coast in the vicinity of Barrow [51,52].

4.3.1.4 Site #4: First-Year Pressure-Ridged Sea Ice. This site was a small 2.3-meter-high pressure ridge formed in the fall when the ice was thin. Ice blocks composing the ridge are 10 cm thick. The width of the base of the ridge sail is 2 m, with a sail depth of 90 cm. Surrounding undeformed first-year ice is 1.3 to 1.8 m thick. Two sets of spatially-independent backscatter measurements were made diagonal to the ridge. A cross-section of the pressure ridge showing the variation in ice depth and snow cover in the vicinity of the ridge is shown in Figure 4.3-47. The salinity profile of a core from the center of the ridge is shown in Figure 4.3-48.

4.3.1.5 Site #5: Fragment of Multiyear Ice. This fragment of multiyear sea ice was greater than 3 meters thick and had very little snow covering. The ice surface was flat on large scale (in terms of a few meters) with pronounced small scale melt-produced roughness with height of .5 to 1.0 cm. The upper 130 cm of core had a layered bubble structure (see Figures 4.3-49 to 4.3-55) and below 130 cm ice was normal congealed ice (see Figures 4.3-56 to 4.3-58). A horizontal thin section taken at 5 cm depth (see Figures 4.3-59 and 4.3-60) shows a moderately-dense randomly-distributed population of bubbles of moderate size and of odd shapes. Crystal diameters ranged in size from small to medium. At 100 cm depth the horizontal thin section

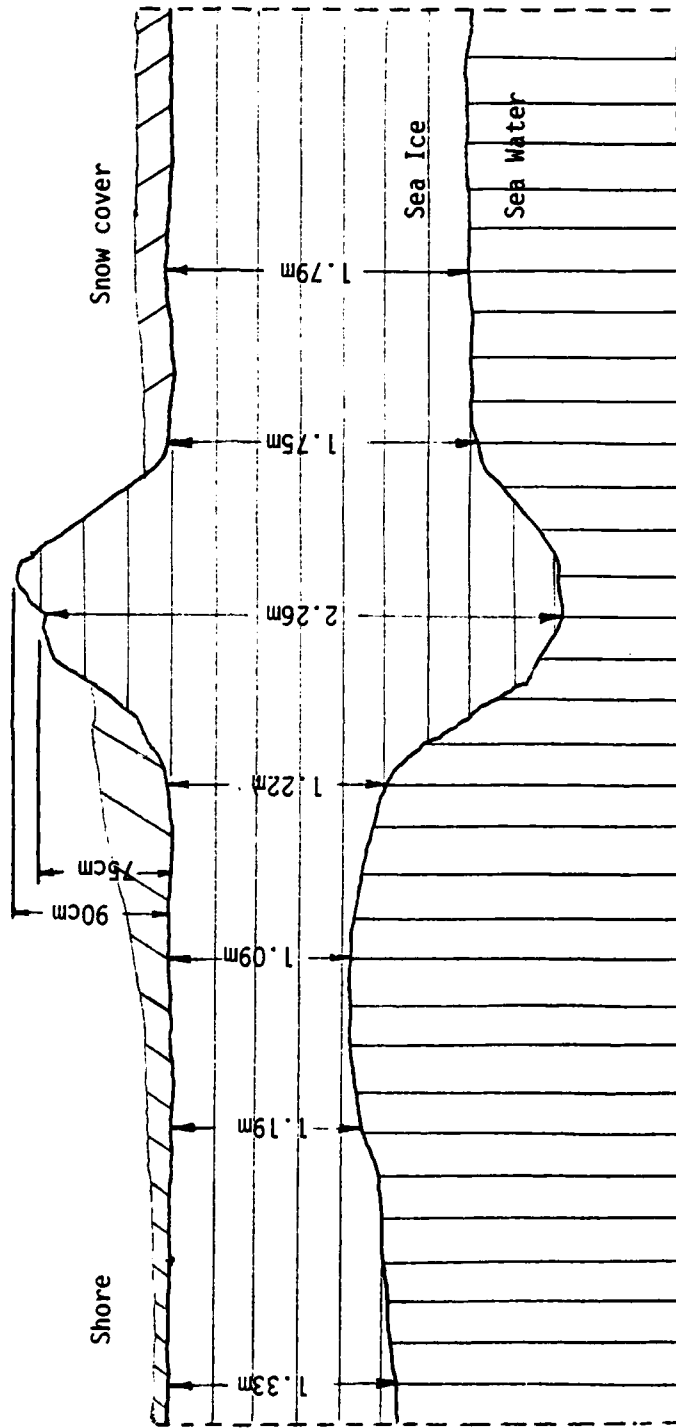


Figure 4.3-47. Cross section of a small first-year sea ice pressure ridge, Site 77-4.

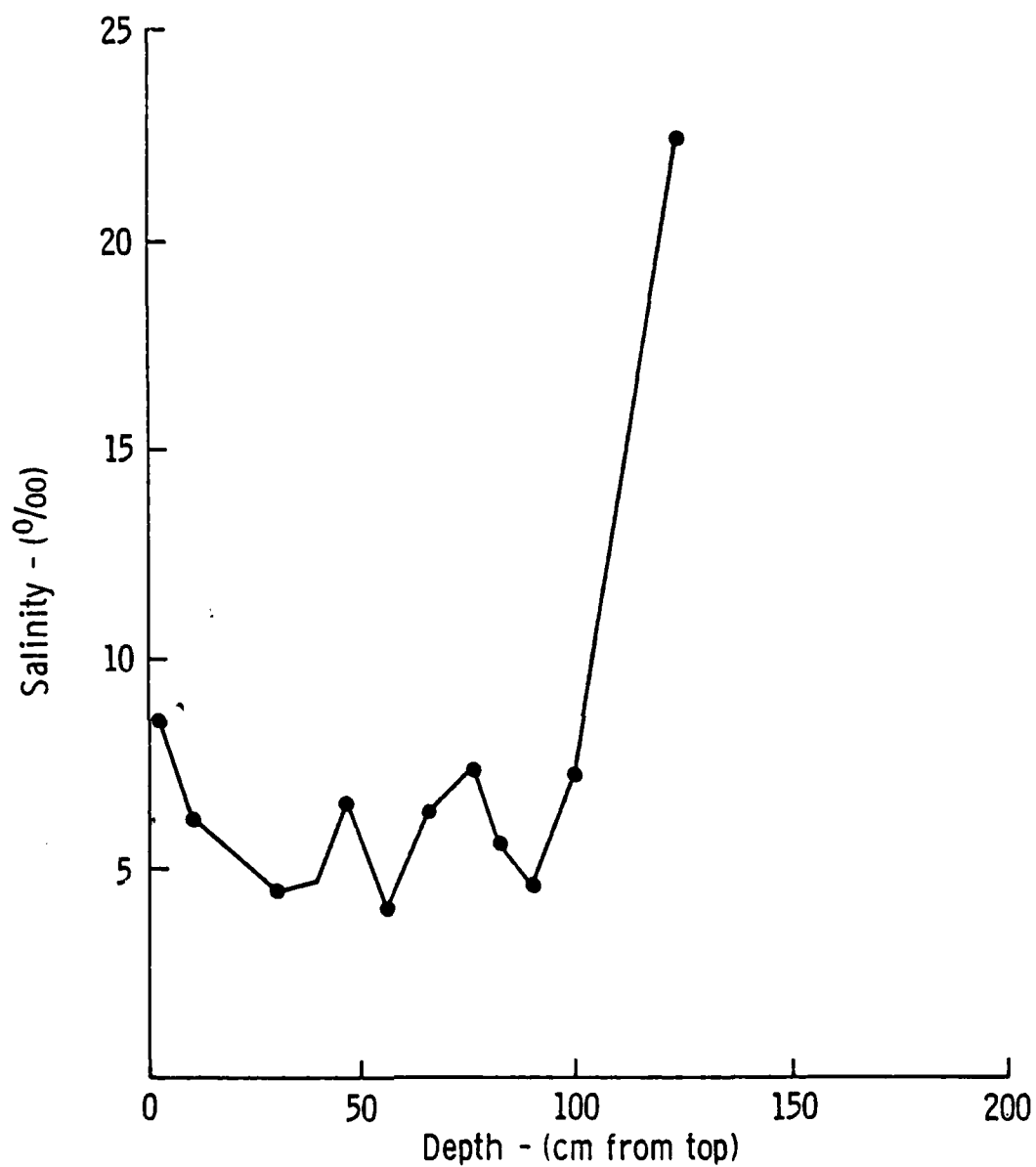


Figure 4.3-48. Salinity profile of Site 77-4, first-year pressure-ridged sea ice.

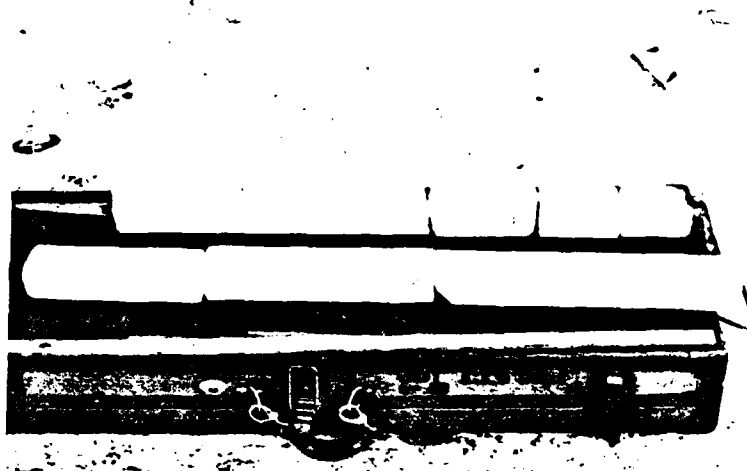


Figure 4.3-49. Complete core of Site 77-5.

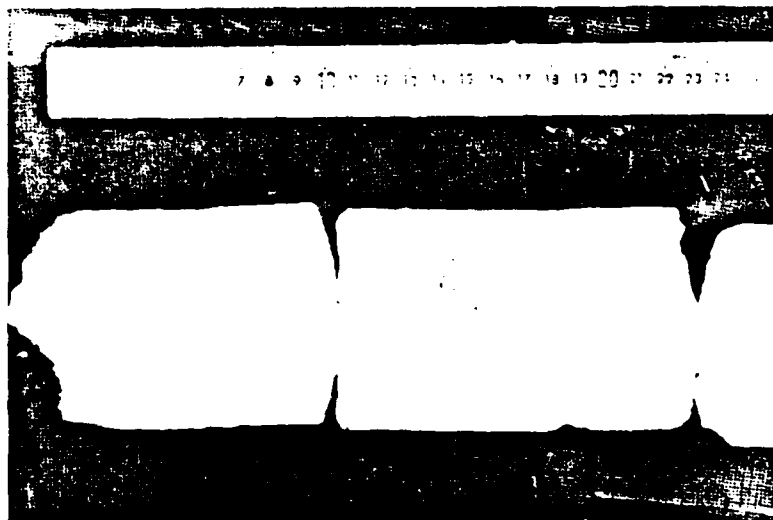


Figure 4.3-50. 0-26 cm section of Site 77-5 ice core.

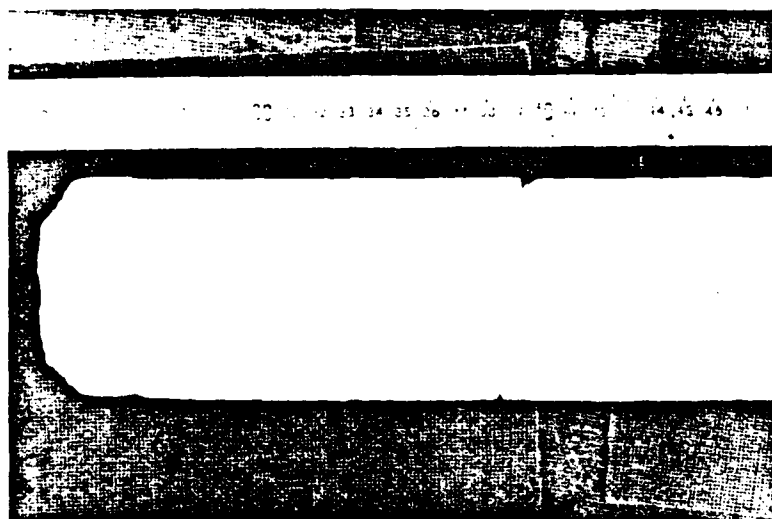


Figure 4.3-51. 21-47 cm section of Site 77-5 ice core.

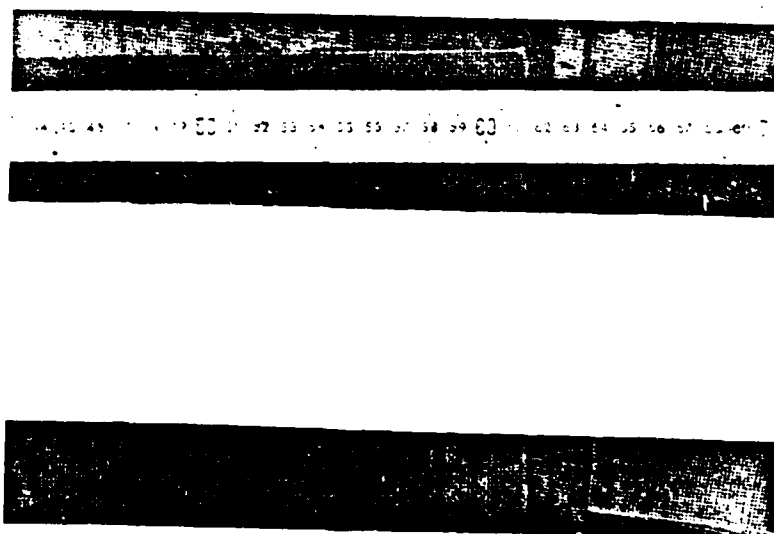


Figure 4.3-52. 44-70 cm section of Site 77-5 ice core.

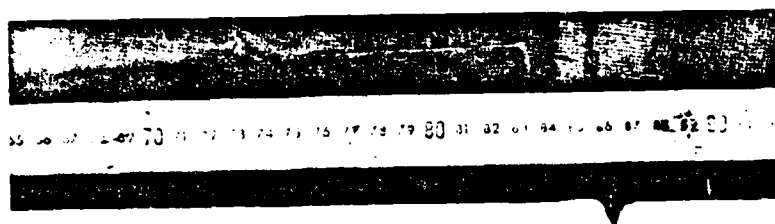


Figure 4.3-53. 65-91 cm section of Site 77-5 ice core.

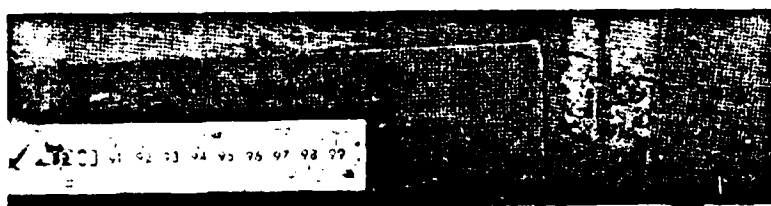


Figure 4.3-54. 89-115 cm section of Site 77-5 ice core.

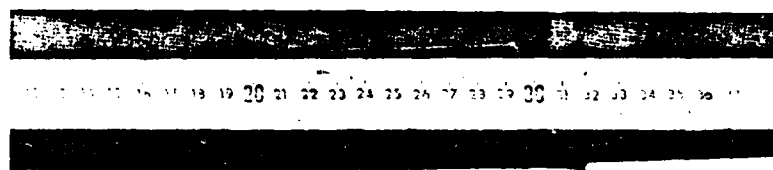


Figure 4.3-55. 111-138 cm section of Site 77-5 ice core.

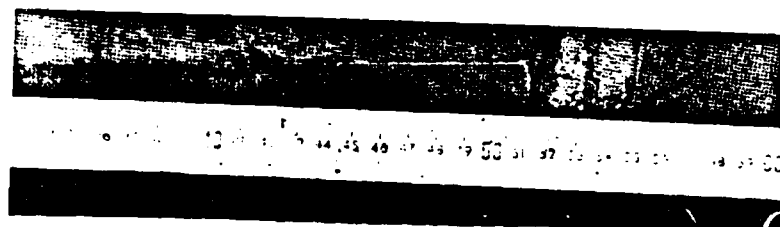


Figure 4.3-56. 132-158 cm section of Site 77-5 ice core.

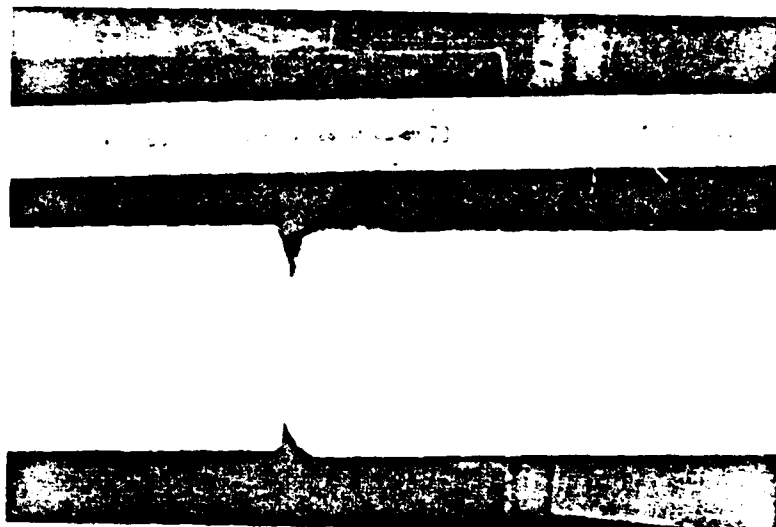


Figure 4.3-57. 155-180 cm section of Site 77-5 ice core.

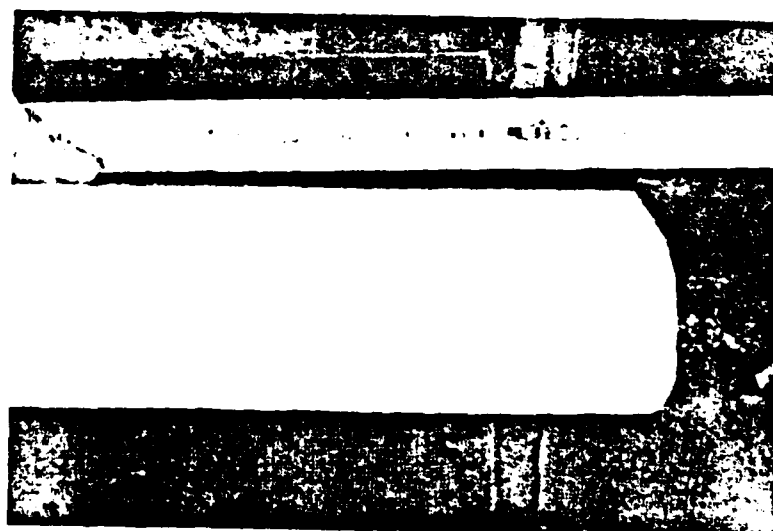


Figure 4.3-58. 172-193 cm section of Site 77-5 ice core.

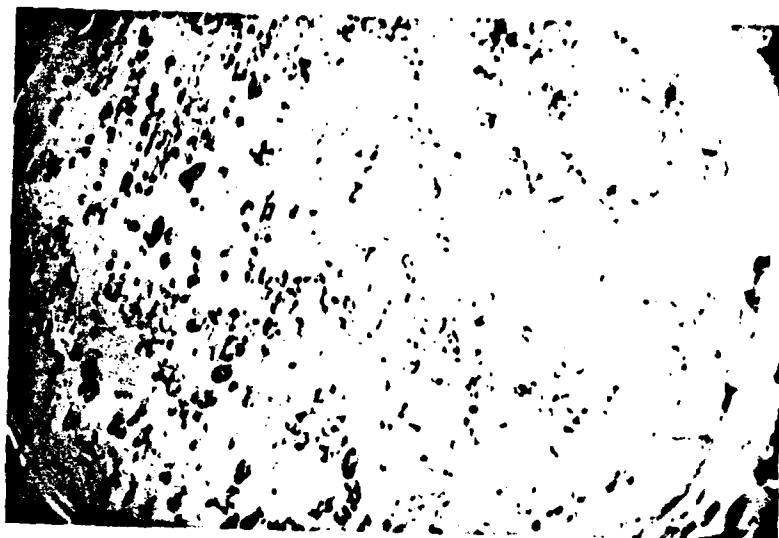


Figure 4.3-59. Horizontal thin section of Site 77-5 taken at 5 cm depth.

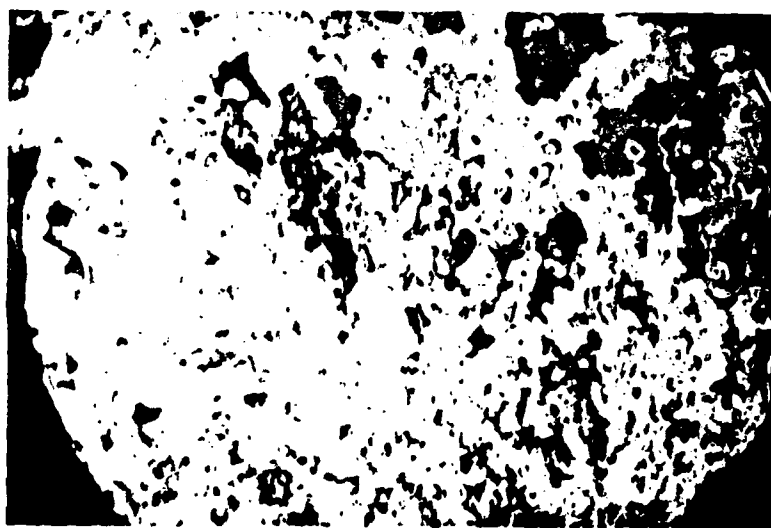


Figure 4.3-60. Horizontal thin section of Site 77-5 viewed through polarizing filter.

(see Figures 4.3-61 and 4.3-62) contains a lighter population of randomly-distributed bubbles and brine shafts with sizes ranging from very small (microscopic) to moderately large (in mm's). Ice crystal sizes were noticeably increased. At the 170 cm depth only a moderately-dense population of microscopic brine inclusions could be seen in the horizontal thin section (see Figures 4.3-63 and 4.3-64). At this depth, ice crystals were found to have grown much larger than at levels closer to the air-ice interface.

A vertical thin section was also made at this depth (see Figures 4.3-65 and 4.3-66). In it the ice crystals were extremely elongated and parallel to the vertical (the direction of heat flow) a characteristic of the columnar zone of sea ice. Brine drainage tubes were also found, which made themselves apparent through vertical strings of small crystals.

The salinity profile obtained for this site (see Figure 4.3-33) had the trend characteristic of multiyear ice; that is, low salinity near the air-ice interface, and an increase with depth. Five spatially-independent backscatter measurements were made at this site.

4.3.1.6 Site #6: Lake Ice with Ice-Water Interface. This lake-ice site, Emikpuk Lake, had an ice surface that was flat in the large scale and in the small scale had an upper surface that was very smooth and free of snow cover. This lake ice was 2.06 m in depth and had an underlying water layer. Below 90 cm the ice core hole filled with water. Air and ice temperatures at time of the six spatially-independent backscatter measurements are shown in Figure 4.3-2. The upper layer of ice was found to be very brittle, which is characteristic of low-salinity ice, and thus a large part of the core was badly disced. The complete core is

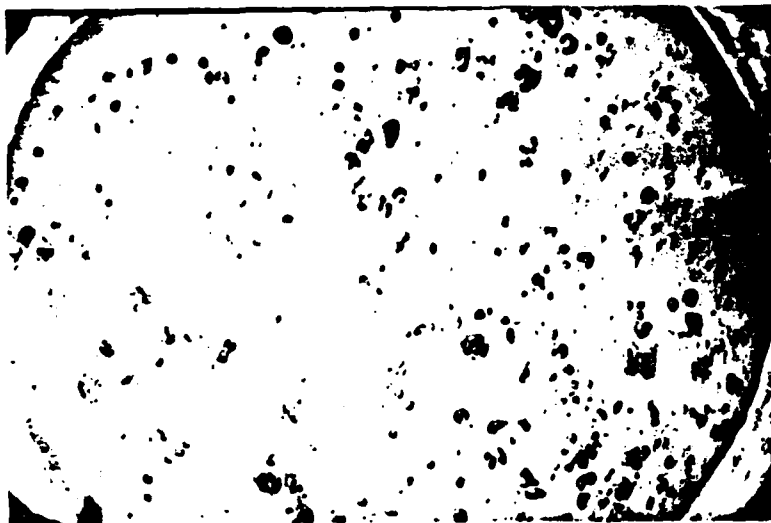


Figure 4.3-61. Horizontal thin section of Site 77-5 taken at 100 cm depth.

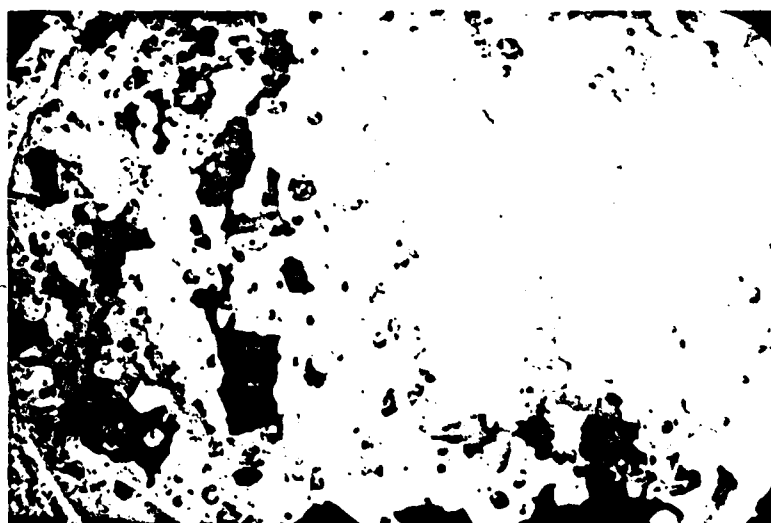


Figure 4.3-62. Horizontal thin section of Site 77-5 viewed through polarizing filter.



Figure 4.3-63. Horizontal thin section of site 77-5 taken at 170 cm depth.



Figure 4.3-64. Horizontal thin section of Site 77-5 viewed through polarizing filter.



Figure 4.3-65. Vertical thin section of Site 77-5 taken at 170 cm depth.



Figure 4.3-66. Vertical thin section of Site 77-5 viewed through polarizing filter.

shown in Figure 4.3-67. The upper 9 cm of the ice sheet (see Figure 4.3-68) had a heavy population of moderate-sized bubbles. Below 9 cm to about 134 cm the population of bubbles was very light and appeared free of anything but the smallest microscopic features. This purity was also apparent in the thin section made at the 20 cm depth (see Figures 4.3-71 and 4.3-72). Crystals were moderate to small in size. At depths between 134 and 205 cm large drainage tubes became quite prominent (see Figure 4.3-70). The ice at these levels was similar to the ice at the upper levels except for the drain tubes. This is apparent in the horizontal thin section obtained at the 198 cm depth (see Figures 4.3-73 and 4.3-74). The ice crystals here are found to be very large in size.

The salinity profile, which showed very low salinity near the surface and increases with increasing depth, is shown in Figure 4.3-75.

4.3.1.7 Site #7: Lake Ice Frozen to Its Mud Bottom. This fresh water lake ice site, South Meadow Lake, was .74 meters in depth and had a snow cover of 18 cm. The upper ice surface was very smooth and the ice sheet extended to its mud bottom. This lake was found to be very pure; its salinity profile is shown in Figure 4.3-75. An attempt was made to obtain ice cores, but because of the very low salinity of the ice, cores were badly disced. Three spatially-independent backscatter measurements were made at this site.

#### 4.3.2 The April 1978 Barrow Experiment Surface Truth

The site of the 1978 surface-based experiment, Site 78, was located approximately 200 m off the coast of the Chukchi Sea (near the southwest end of the NARL runway). This site was selected (also was limited to)

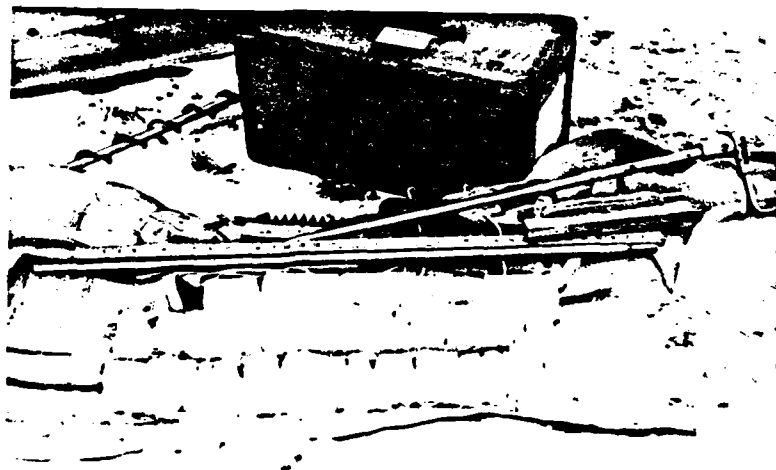


Figure 4.3-67. Complete ice core of site 77-6.

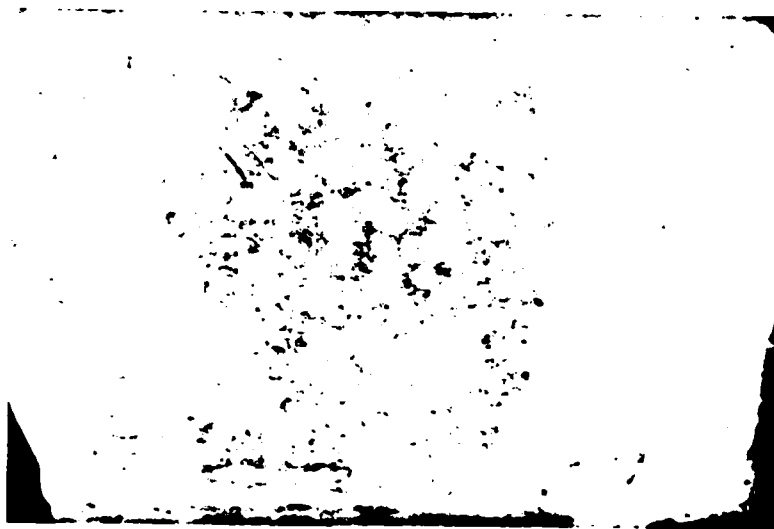


Figure 4.3-68. 0-9 cm section of Site 77-6 ice core.



Figure 4.3-69. Section representative of 9-134 cm depths at Site 77-6.

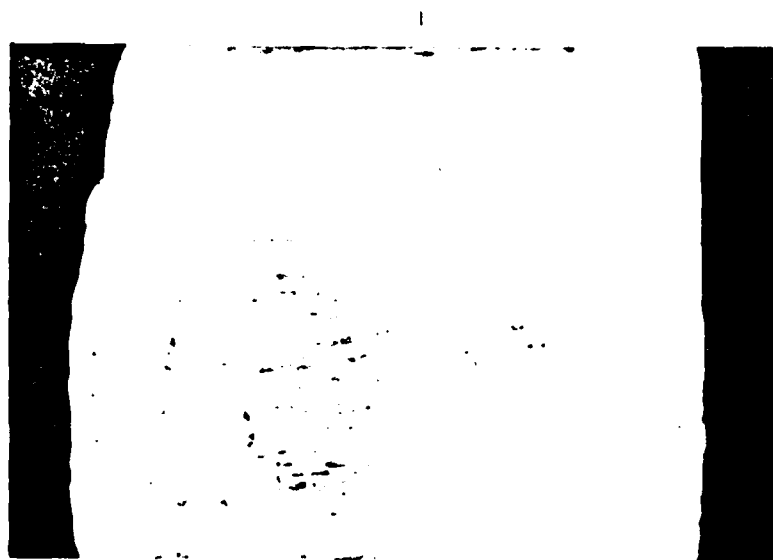


Figure 4.3-70. Section representative of 134-205 cm depths at Site 77-6.



FIGURE 4.3-71 Horizontal Thin Section of Site 77-6 Taken at 20 cm Depth.



FIGURE 4.3-72 Horizontal Thin Section of Site 77-6 Taken at 20 cm Depth Viewed Through Polarizing Filter.

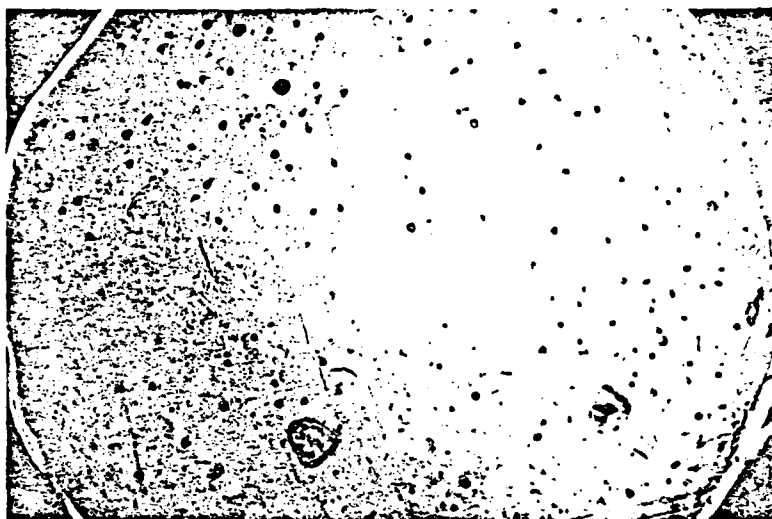


FIGURE 4.3-73 Horizontal Thin Section of Site 77-6 Taken at 198 cm Depth.



FIGURE 4.3-74 Horizontal Thin Section of Site 77-6 Taken at 198 cm Depth Viewed Through Polarizing Filter.

due to the fact that the ice along the Chukchi coast was well broken up, no other ice categories of interest were available in the area, and there was an area approximately 300 m in diameter of apparently uniform, undeformed fast ice. The level upper surface was found to be very uniform and clean (no visible silt or sand). The upper portion of the ice sheet was composed of a fine-grain slush-like layer that varied slightly in thickness from location to location. Vertical thin sections of this sea ice are shown in Figure 4.3-76. As can be seen, the slush layer here was 4 cm thick. Below 4 cm the crystals immediately elongate parallel to the vertical (the direction of heat flow) and the elongated brine inclusions characteristic of sea ice are evident. The other three vertical thin sections show extreme crystal elongation which is characteristic of the columnar zone of sea ice. Elongated brine pockets are particularly evident in section c (76 to 85 cm) as are brine drainage tubes which show themselves through vertical strings of small crystals visible on the right hand side of the same section and in two places in section d (153 to 167 cm).

Horizontal thin sections and fabric diagrams from the same block of ice are shown in Figure 4.3-77. Below the slush layer no strong systematic variations in mean grain size appear with depth. At all levels the platy substructure of sea ice that is revealed by the systematic distribution of brine inclusions is strongly developed (see particularly the thin section from 130 cm depth). Even at 25 cm there is clearly an identifiable preferred crystal orientation in the horizontal plane. The degree of crystal alignment becomes increasingly strongly developed with increasing depth in the ice sheet, and approximately parallel to the coast. This is demonstrated by the systematic decrease with depth in the ice of the

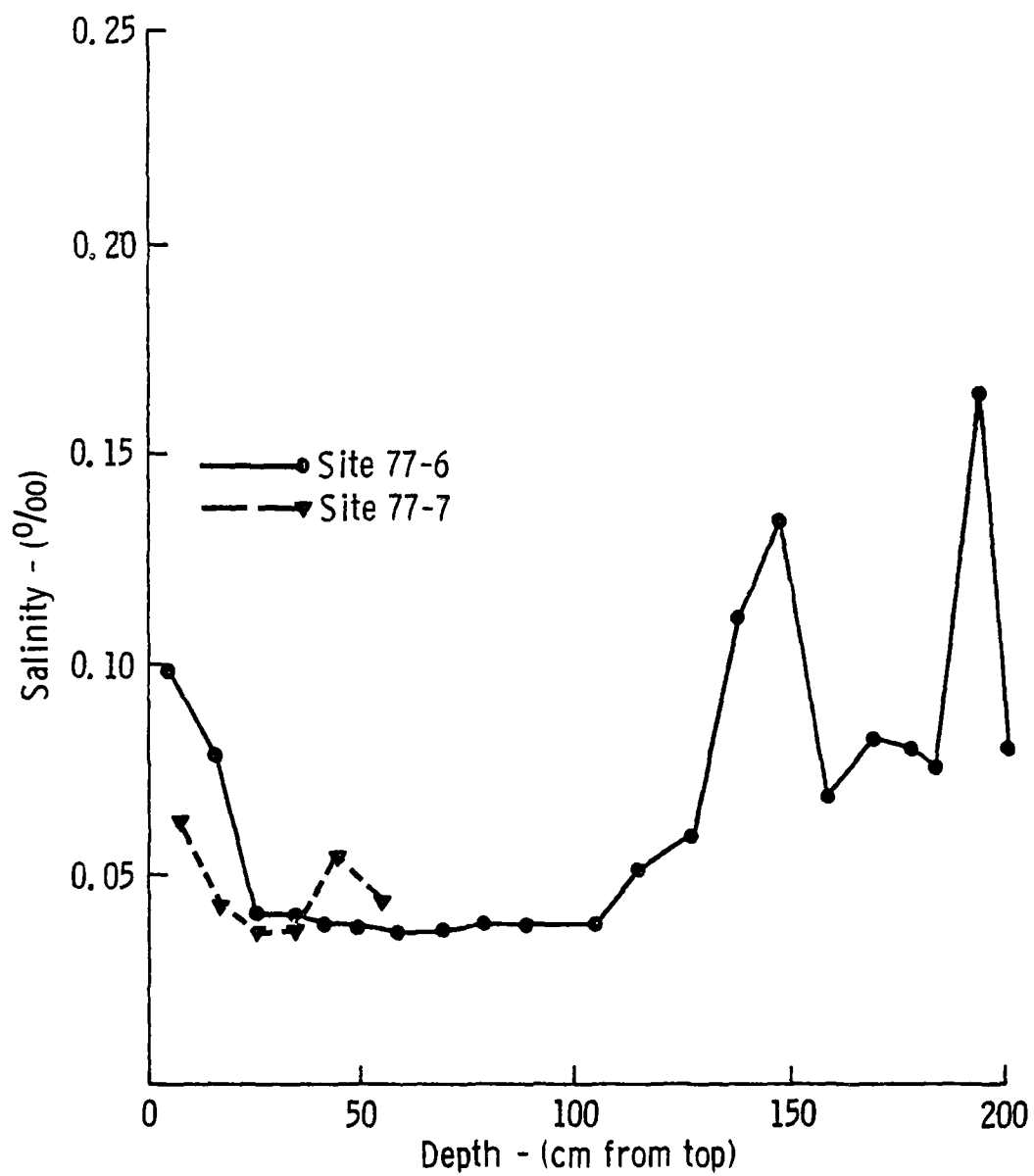


Figure 4.3-75. Salinity profile of Site 77-6, lake ice with an underlying layer of water, and Site 77-7, lake ice that is frozen to its mud bottom.

## SITE 78-17, BARROW



(a) 0-8.5 cm



(c) 76-85 cm



(b) 34-43 cm



(d) 153.5-162 cm

FIGURE 4.3-76 Vertical Thin Sections of Sea Ice from the Chukchi Sea Near Barrow, Alaska (Site 78-17). Sections of centimeter graph paper are shown for scale on sections (c) and (d). Photographs made using crossed polaroids.

THIS PAGE IS NOT TO BE REPRODUCED  
FROM ANY SOURCE OTHER THAN THE  
ORIGINAL DOCUMENT

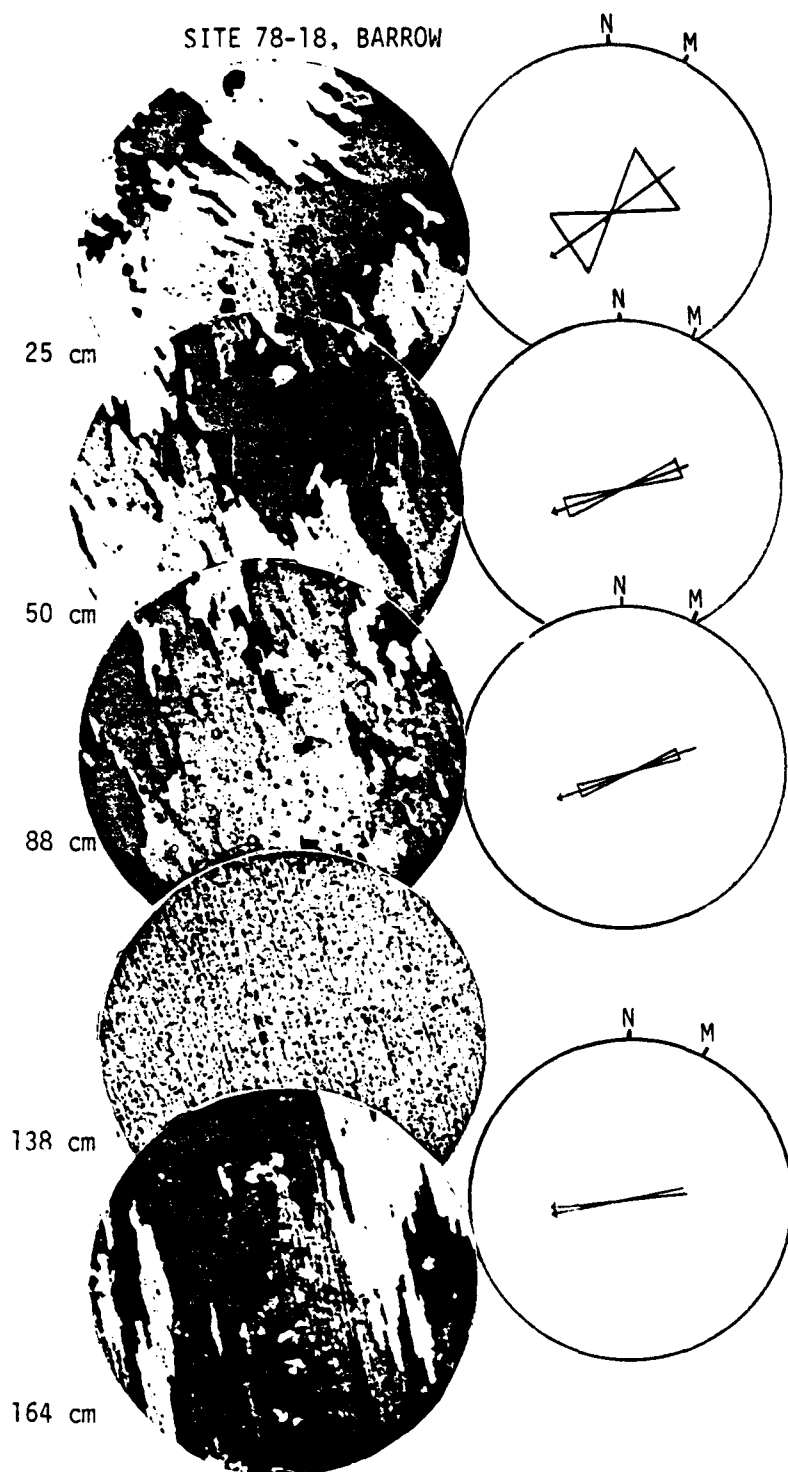


FIGURE 4.3-77

Crystal Textures and Fabrics of Sea Ice From the Chukchi Sea Near Barrow, Alaska. The fabric data are placed on equal area nets. N and M indicate true north and magnetic north respectively. The diameter of the thin sections is 6.7 cm. The two headed arrow indicates the circular mean and the "bow tie" indicates  $\pm$  a standard deviation.

standard deviation of the c-axis orientations about the mean (measured in the horizontal plane; see Figure 4.3-78). Also, the mean c-axis orientation at 25 cm is  $57^\circ$  (True) and in general gradually increases to  $84^\circ$  near the bottom of the ice sheet.

Profiles of the two parameters most important in controlling the "state" of the ice (temperature and salinity) are shown in Figure 4.3-79. The salinity profile is a typical irregular c-shaped curve which is characteristic of first-year ice. The temperature profile is nearly linear, a common situation in first-year ice when there have not been recent major air temperature changes. The temperature gradient was  $10.7^\circ \text{C}$  per meter. The ice is not cold enough for  $\text{NaCl} \cdot 2\text{H}_2\text{O}$  to precipitate. However, the solid salt  $\text{Na}_2\text{SO}_4 \cdot 10\text{H}_2\text{O}$  should be present in the ice colder than  $-8.7^\circ \text{C}$  (in the ice above 104 cm).

The brine volume profile, shown in Figure 4.3-79, was also determined by the temperature and salinity profiles. The calculated profile is characteristic of many other first-year brine profiles that have been observed in that a slight increase in brine volume occurs near the top of the ice sheet, a minimum occurs at some intermediate depth (in this case 65 cm), and a drastic increase occurs near the bottom of the ice sheet where both an increase in salinity and near melting temperatures are found.

Additional salinity profiles for Site 78 are shown in Figure 4.3-80. Photographs of sections of an ice core taken at Site 78 are shown in Figures 4.3-81 to 4.3-87. The top 13 cm of the ice sheet is shown in Figure 4.3-81. Twelve to 36 cm ice is represented in Figure 4.3-82, 36 to 85 cm ice is represented in Figures 4.3-83 and 4.3-84, 86 to 146 cm

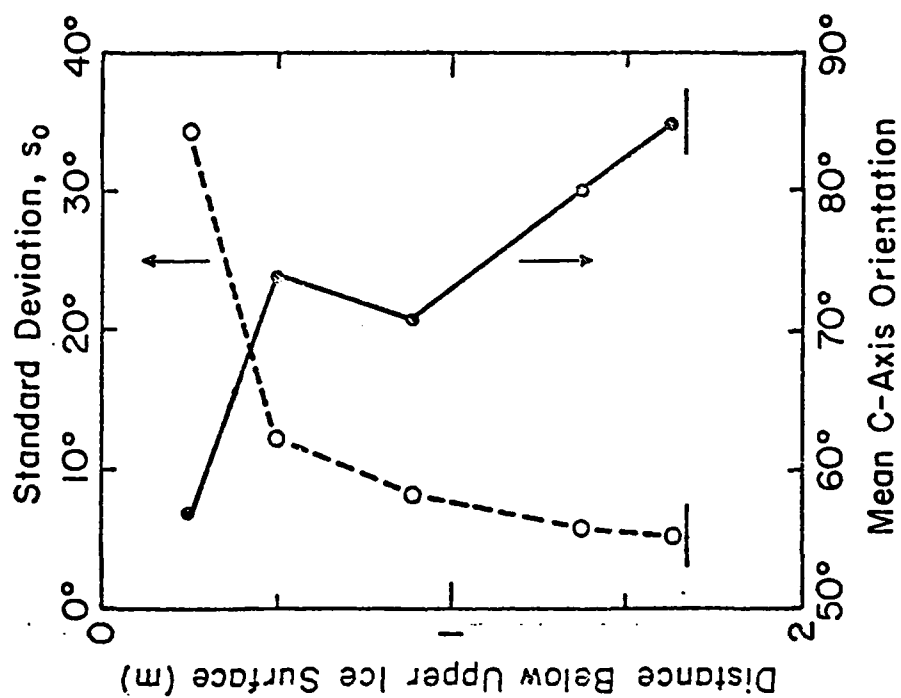


FIGURE 4.3-78

Mean C-Axis Orientation in the Horizontal Plane and the Standard Deviation of the C-Axes (As Measured in the Horizontal) as a Function of the Vertical Distance Measured from the Upper Surface of the Sea Ice.

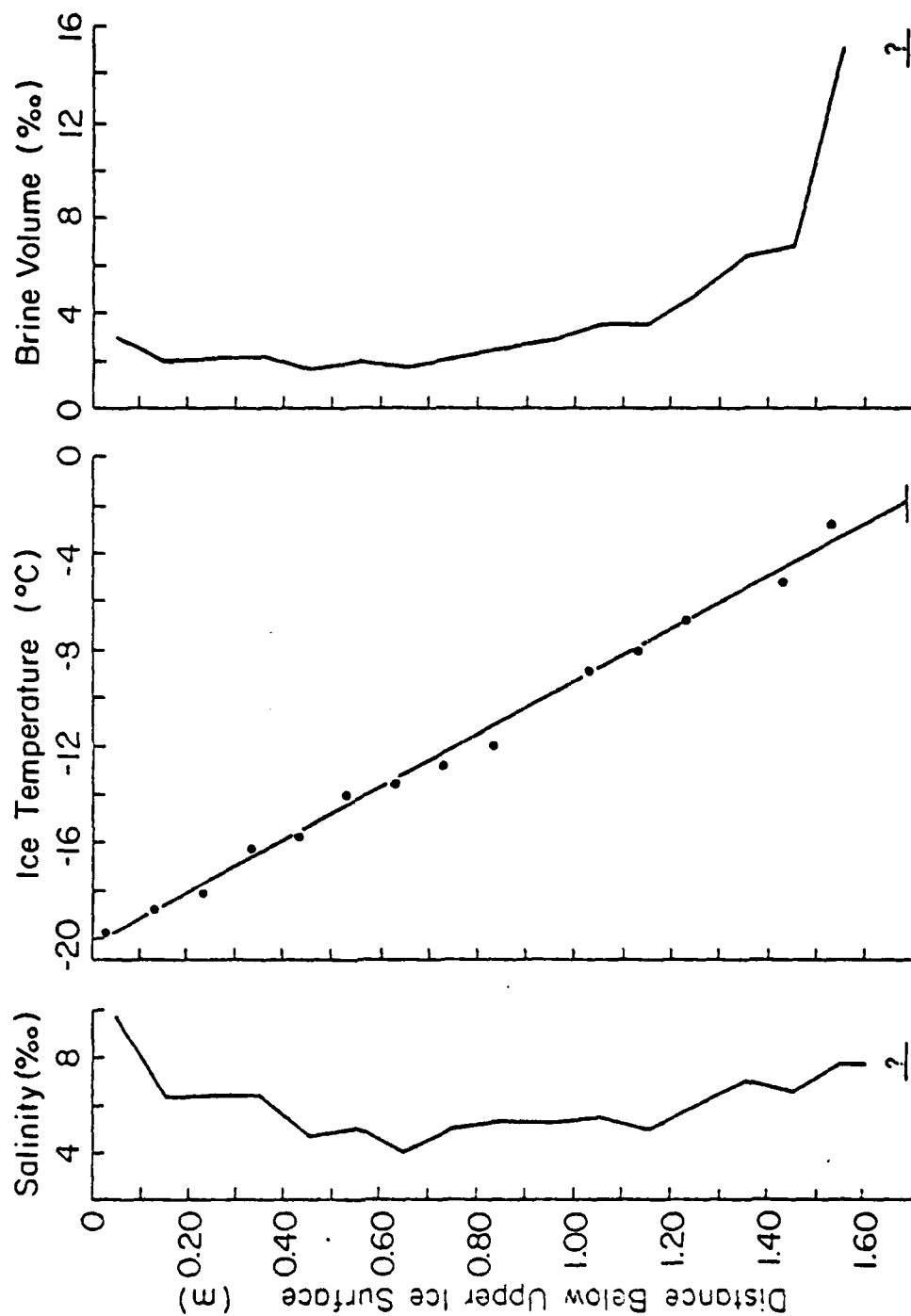


FIGURE 4.3-79 The Salinity, Ice Temperature and Brine Volume Profiles for the Sea Ice from Site 78-17 on 8 April 1978.

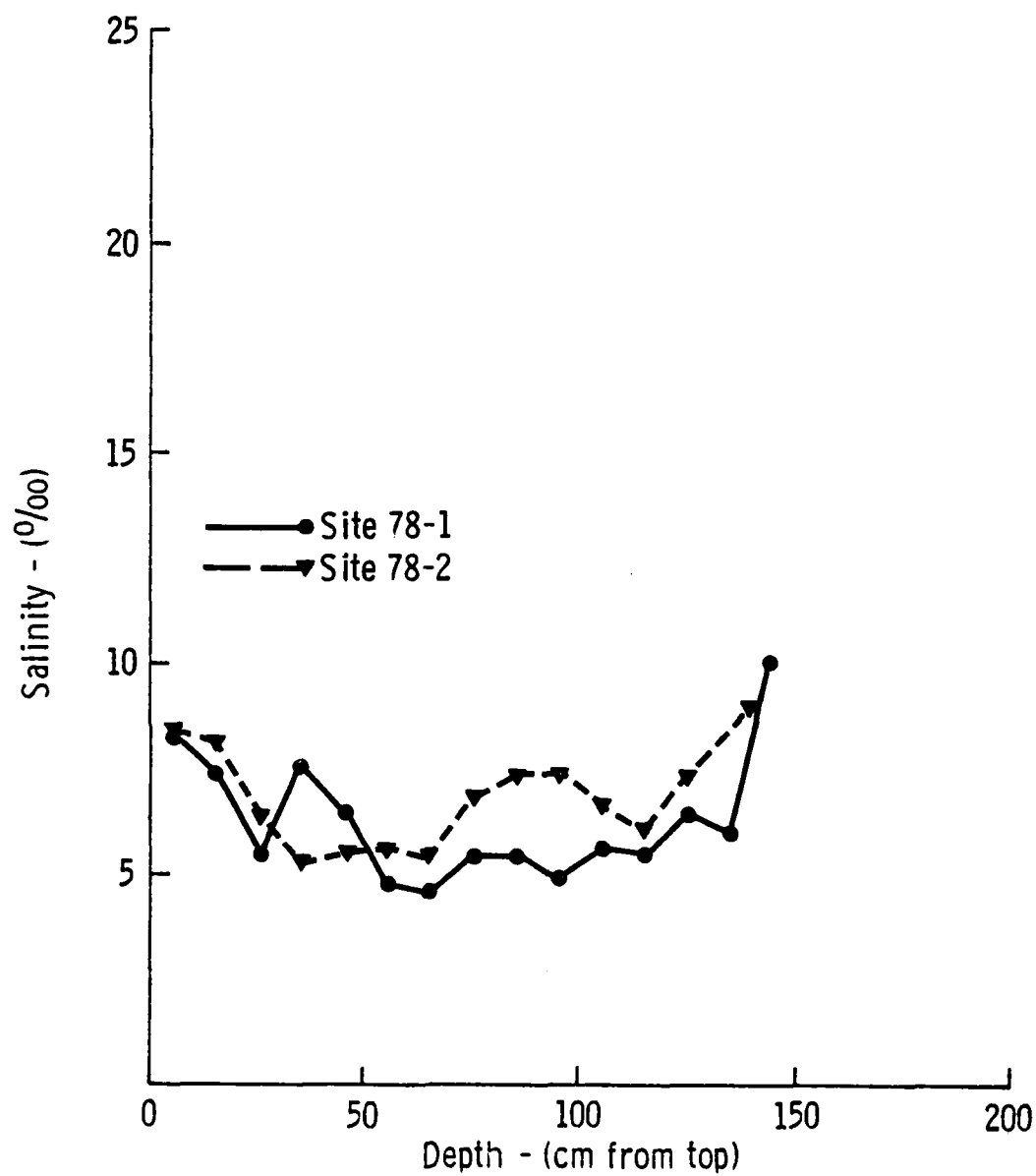


Figure 4.3-80. Salinity profiles for Site 78-1 and 78-2, thick first-year shorefast sea ice.

THIS PAGE IS BEST QUALITY PRACTICABLE  
FROM COPY POINT TO BDC

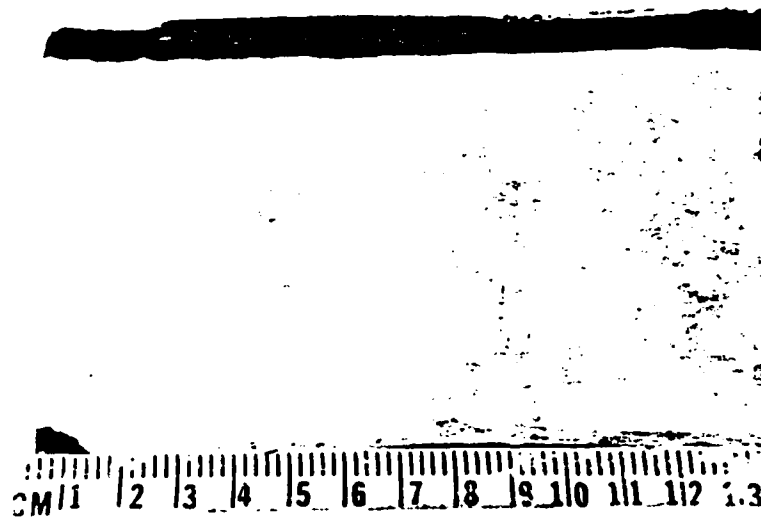


Figure 4.3-81. 0 to 13 cm section of Site 78 ice core.

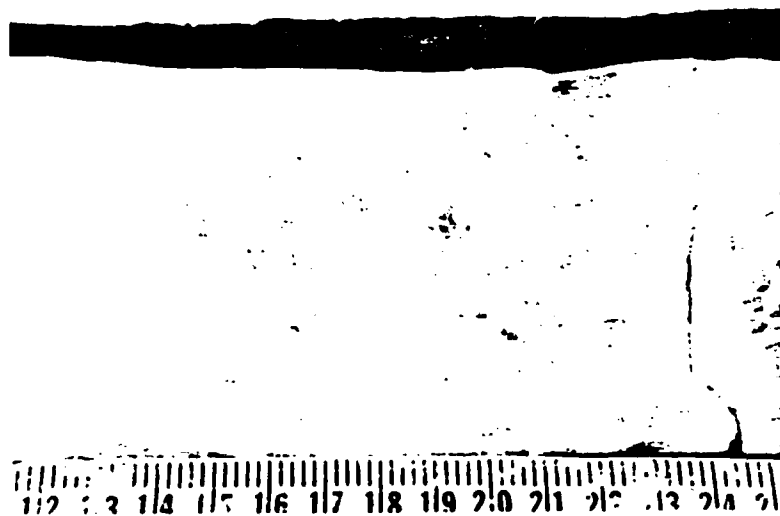


Figure 4.3-82. 12 to 25 cm section of Site 78 ice core.

THIS IS A PHOTOGRAPH OF THE  
FROM CORE SECTION TO 200



Figure 4.3-83. 60 to 73 cm section of Site 78 ice core.

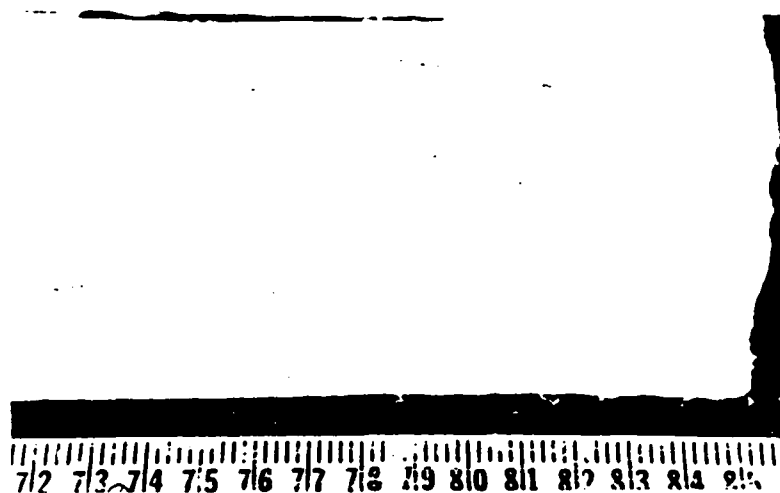


Figure 4.3-84. 72 to 85 cm section of Site 78 ice core.

THIS IS A PHOTOGRAPH OF THE  
FROM CORE SECTION TO 200

THIS PAGE IS BEST QUALITY PRACTICABLE  
FROM COPY FURNISHED TO EDC

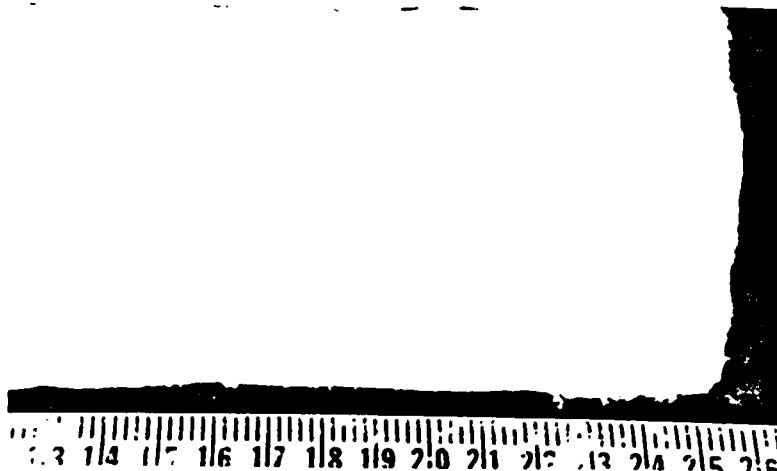


Figure 4.3-85. 113 to 125 cm section of Site 78 ice core.



Figure 4.3-86. 166 to 175 cm section of Site 78 ice core.

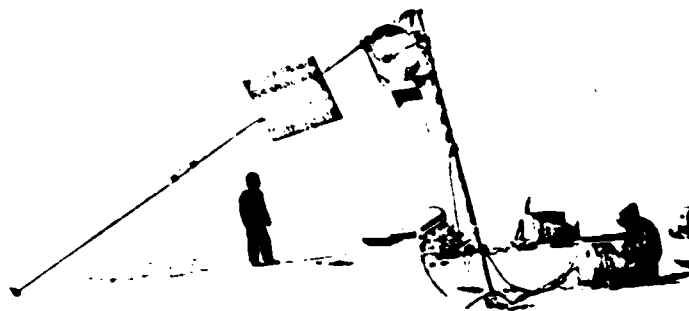


Figure 4.3-87. A bare ice surface is shown under study by the TRAMAS system.

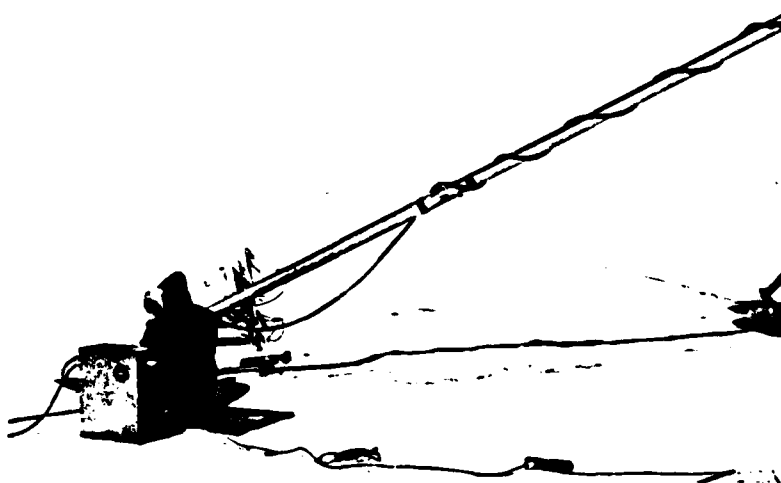


Figure 4.3-88. Ice with an 8 cm manmade snow cover is shown under study by the TRAMAS system.

ice is represented in Figure 4.3-85 and 146 to 175 cm ice is represented in Figure 4.3-86. The TRAMAS system is shown studying bare, shorefast ice in Figure 4.3-87 and shorefast ice with a heavy manmade snow cover in Figure 4.3-88.

#### 4.4 L-Band Data Analysis

##### 4.4.1 Results

4.4.1.1 Thick First-Year Ice. We initially believed that the returns from apparently-featureless thick first-year ice should yield simple returns. However, as is shown in Figures 4.4-1 and 4.4-2, this was not the case in 1977. We actually observed a pronounced clustering of the observed returns into families. This separation is most apparent at large incidence angles. Like-polarized returns at  $70^\circ$  for the two groups at Site 77-1 and Site 77-3 were separated by 12 dB and 8 dB, respectively.

The scattering coefficient of thick first-year ice with a 2 cm snow cover is shown in Figure 4.4-3. These returns were found to be nicely behaved with the mean return falling to within 1-2 dB of a linear angular response. When returns were compared, Site 77-1, Site 77-3, and Site 77-8 were found to fall into three apparent families (see Figure 4.4-4). Returns from Site 78 fall into the family with the lowest return with Site 77-3 (3,4,5,6) and they follow very similar trends, from angles of  $20^\circ$  and greater. Cross-polarization returns (see Figure 4.4-5) have a less defined grouping into families, but may be said to group into two general categories.

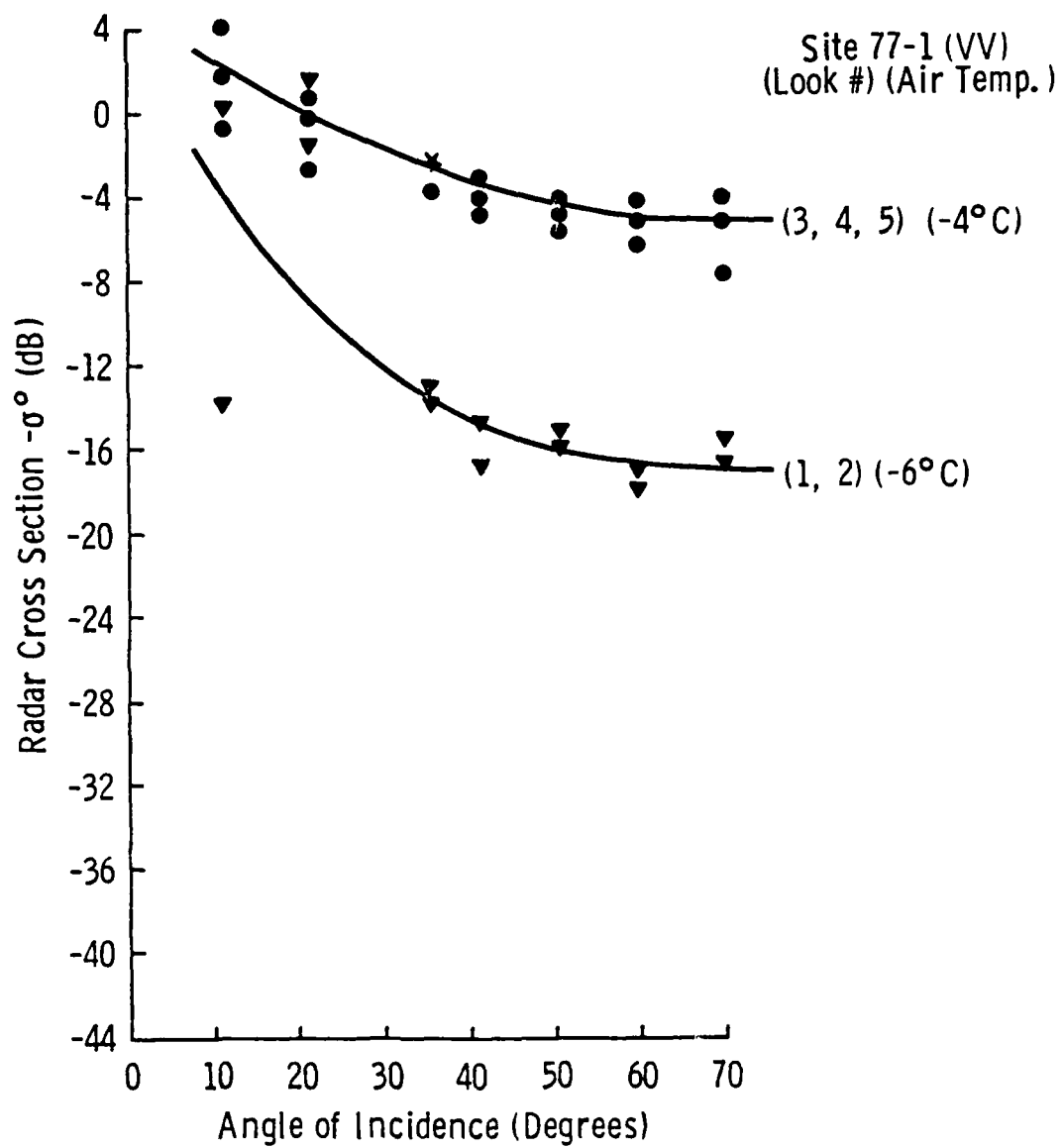


Figure 4.4-1. Scattering coefficient of thick first-year ice, Site 77-1, at 1-2 GHz, VV.

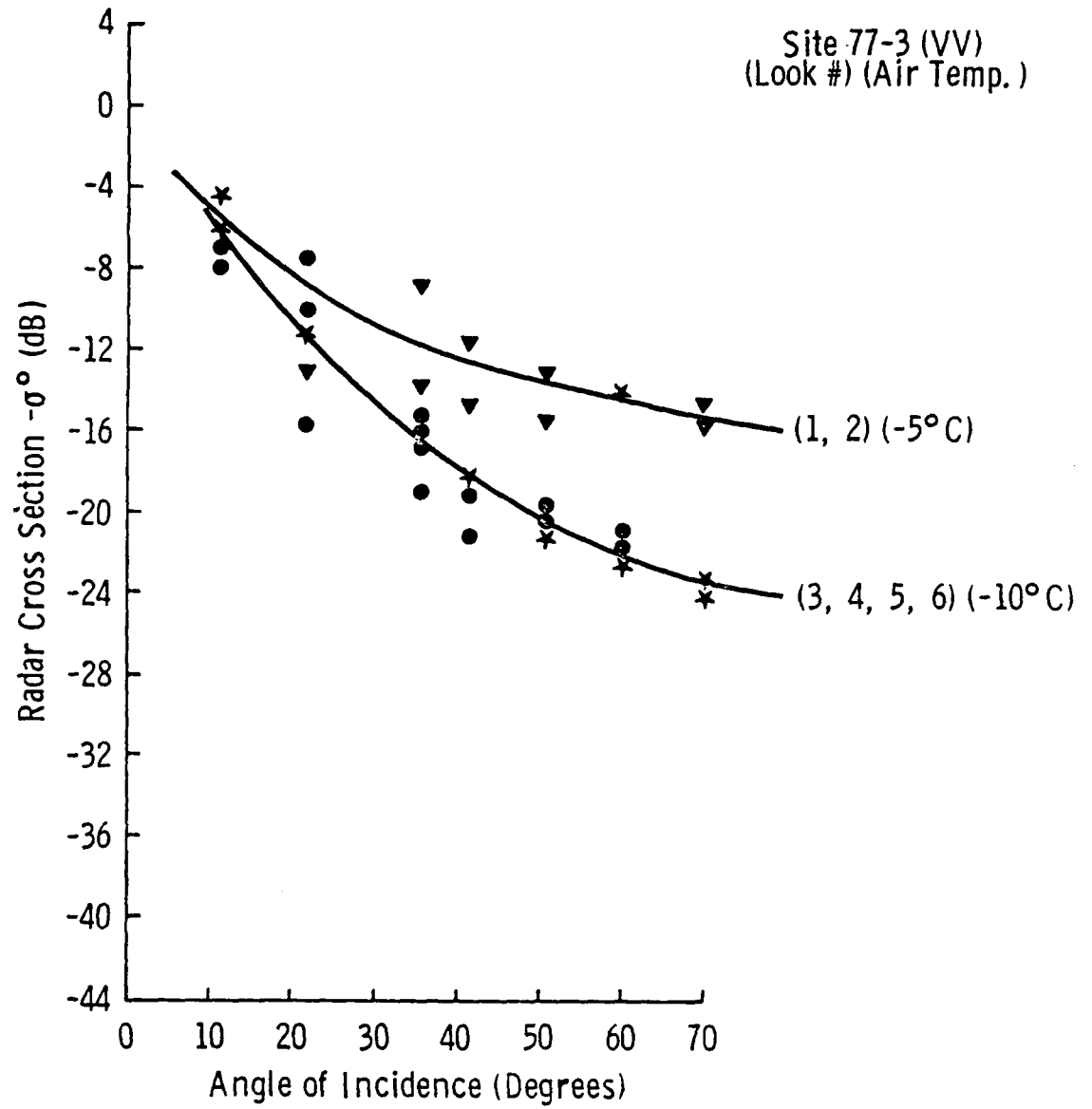


Figure 4.4-2. Scattering coefficient of thick first-year ice, Site 77-3, at 1-2 GHz, VV.

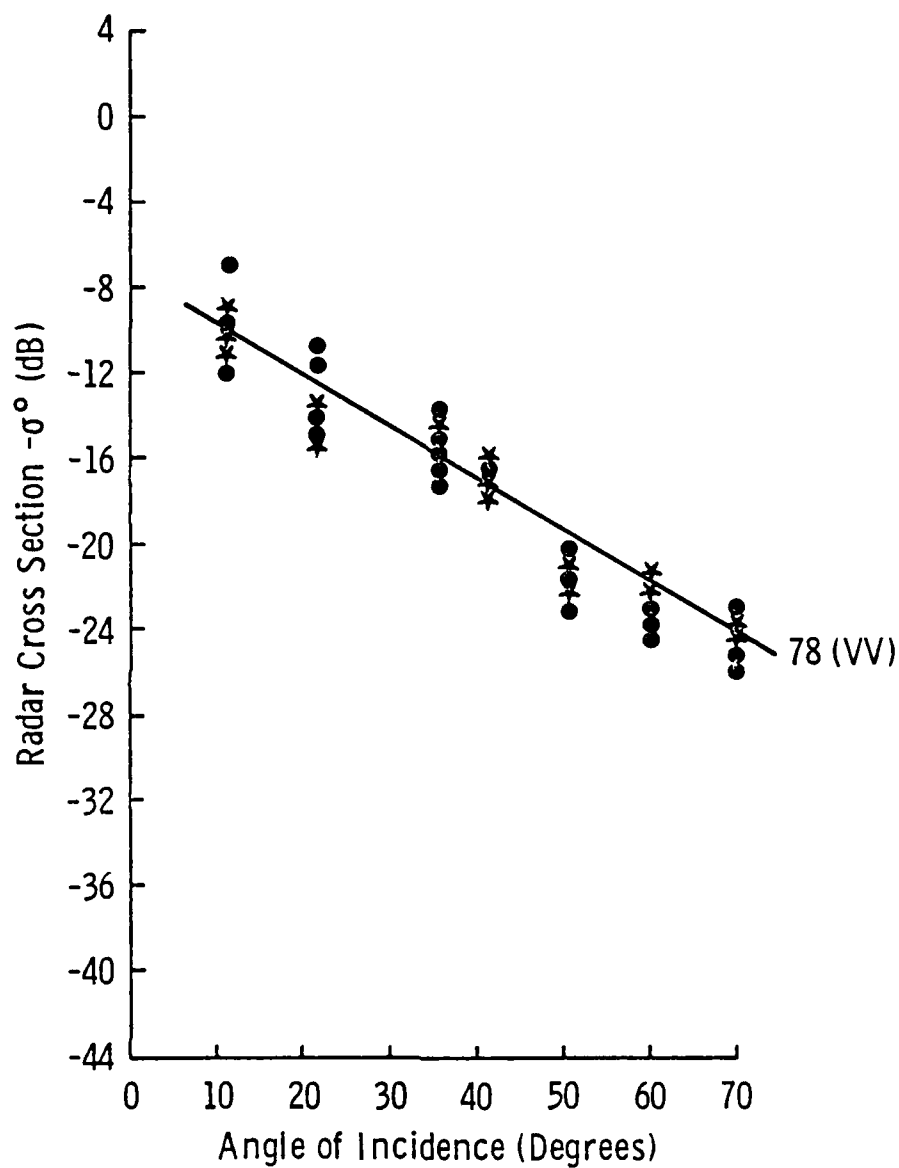


Figure 4.4-3. Scattering coefficient of thick first-year ice, Site 78, at 1-2 GHz, VV. Measurements with 2-4 cm snow cover were selected (9 looks).

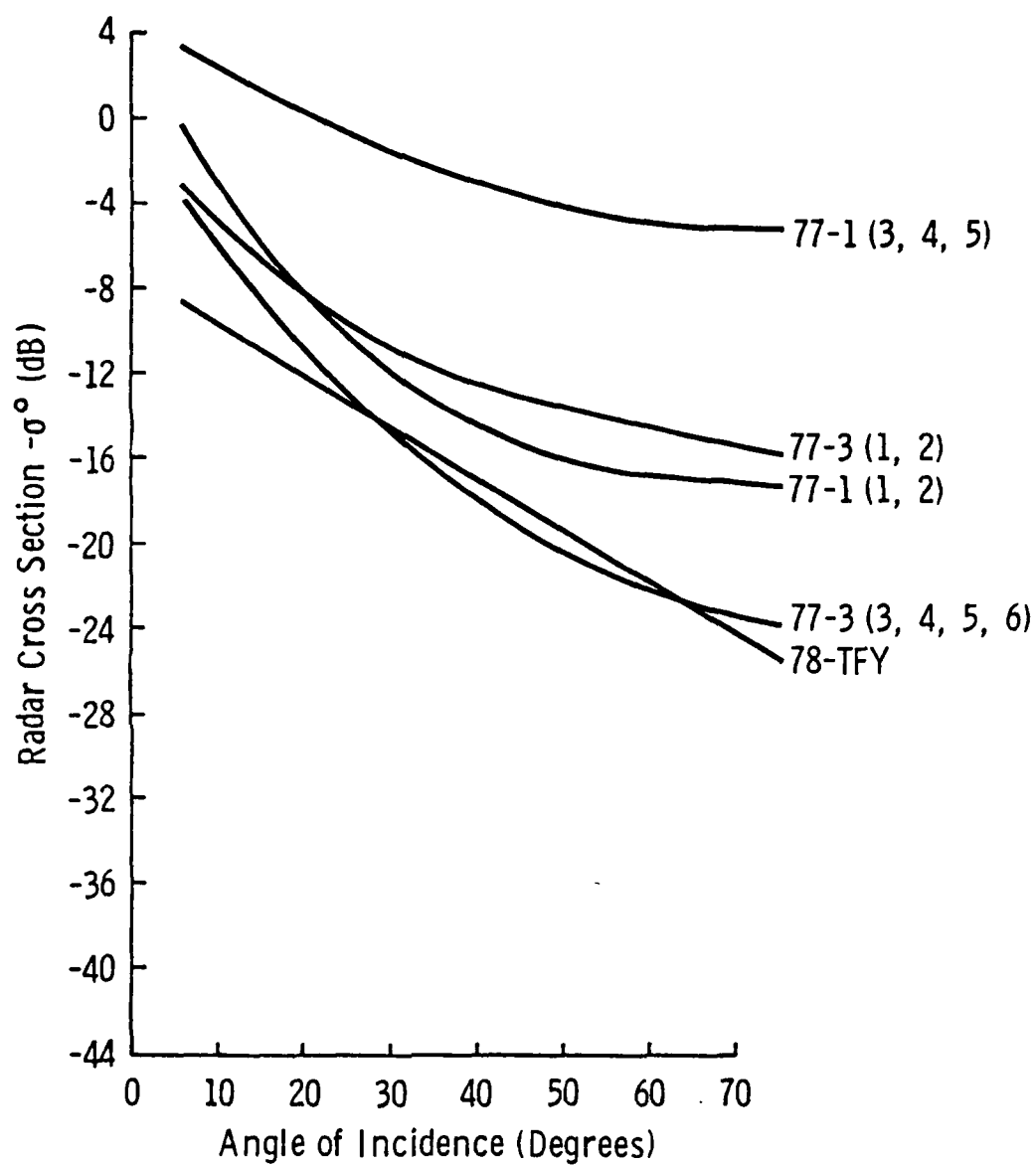


Figure 4.4-4. Scattering coefficient of thick first-year ice; Site 77-1, Site 77-3, and Site 78; at 1-2 GHz, VV.

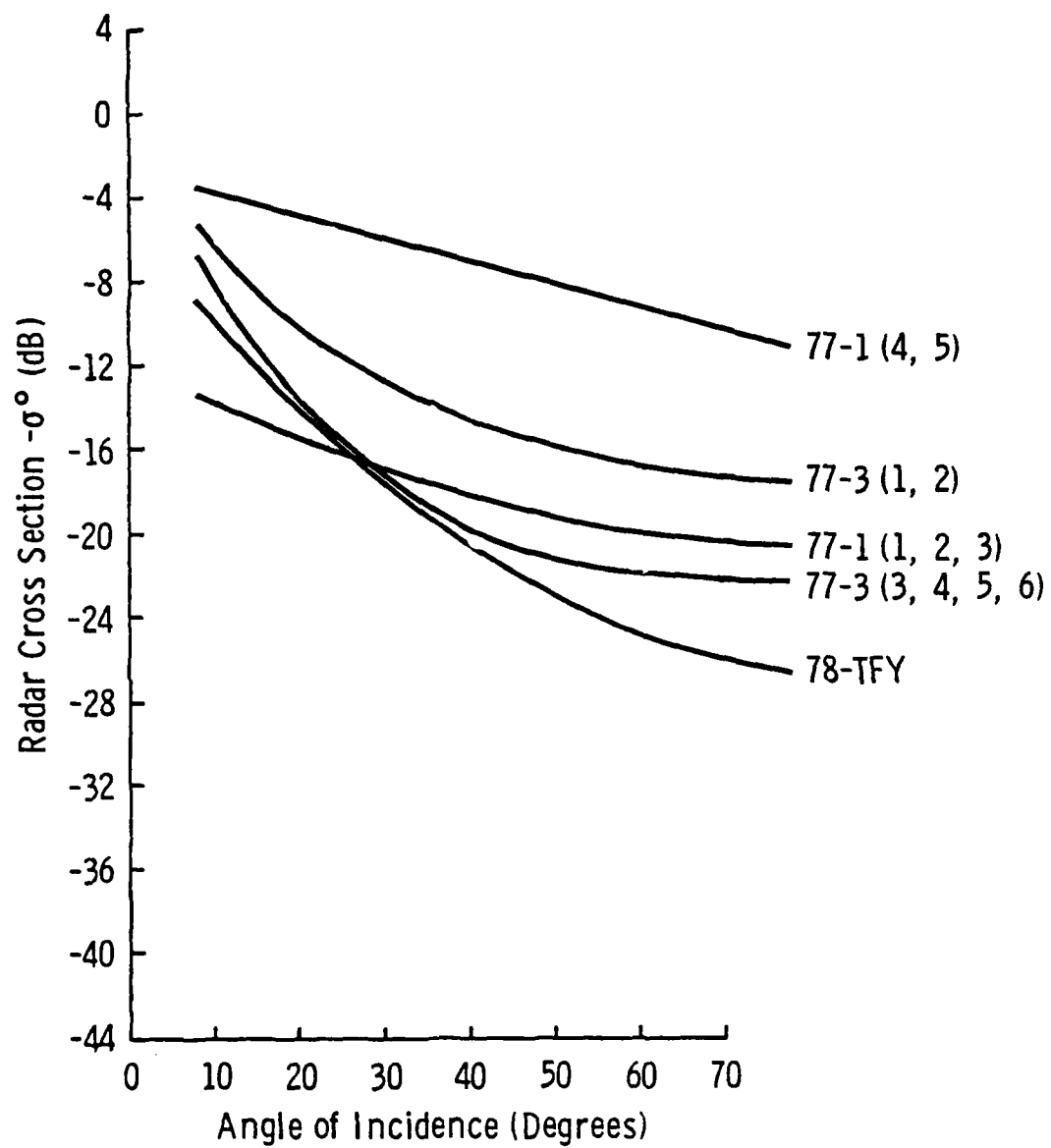


Figure 4.4-5. Scattering coefficient of thick first-year ice; Site 77-1, Site 77-2, and Site 78; at 1-2 GHz, VH.

An average of the lower two families of the 1977 sites was made (using  $\sigma^0$  but reporting result as  $\sigma_{dB}^0$ ); it is used to represent thick first-year ice for a composite 1977 site, Site 77-TFY. A comparison of the average scattering coefficient for Site 77-TFY and Site 78-TFY is shown in Figure 4.4-6. The average angular responses have slightly different trends. Scattering from Site 77-TFY has an exponential response with a slope that changes from very large (10-45°) to slight (45-70°), while Site 78-TFY has a rapidly-decaying linear response.

4.4.1.2 Multiyear Ice. Analysis of multiyear ice was expected to be difficult using data collected by a surface-based system because of the characteristically non-uniform upper surface of such ice. The scattering coefficients of multiyear ice are shown in Figures 4.4-7 and 4.4-8. The data did not exhibit the expected wide variation between independent looks and was found to cluster more tightly than would be expected from surface scatter alone. This is especially apparent in the returns from Site 77-5. A comparison of multiyear ice sites shows similar angular response trends with absolute levels falling within 2 dB.

4.4.1.3 Small Thick First-Year Pressure Ridge. The scattering coefficient of a small first-year pressure ridge is shown in Figure 4.4-10. Large returns were measured throughout all angles of incidence. Returns at angles less than 40° were almost constant, while returns at angles greater than 40° decayed much more rapidly.

4.4.1.4 Lake Ice. The scattering coefficients of lake ice with an underlying layer of water and of lake ice that was frozen to its mud bottom are shown in Figures 4.4-11 and 4.4-12, respectively. Both

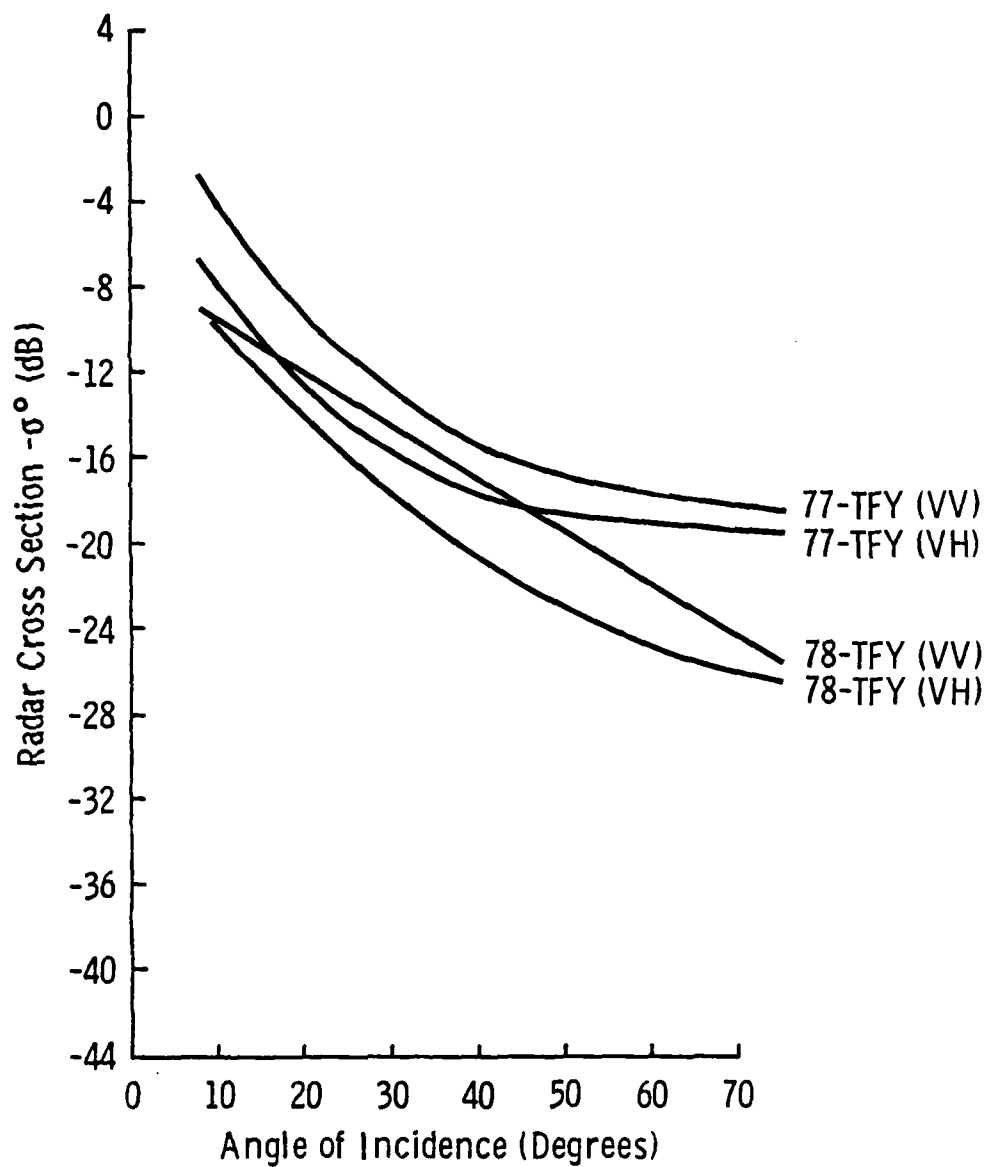


Figure 4.4-6. Comparison of average scattering coefficients for Site 77 - (1 + 3) and Site 78 at 1-2 GHz, VV and VH.

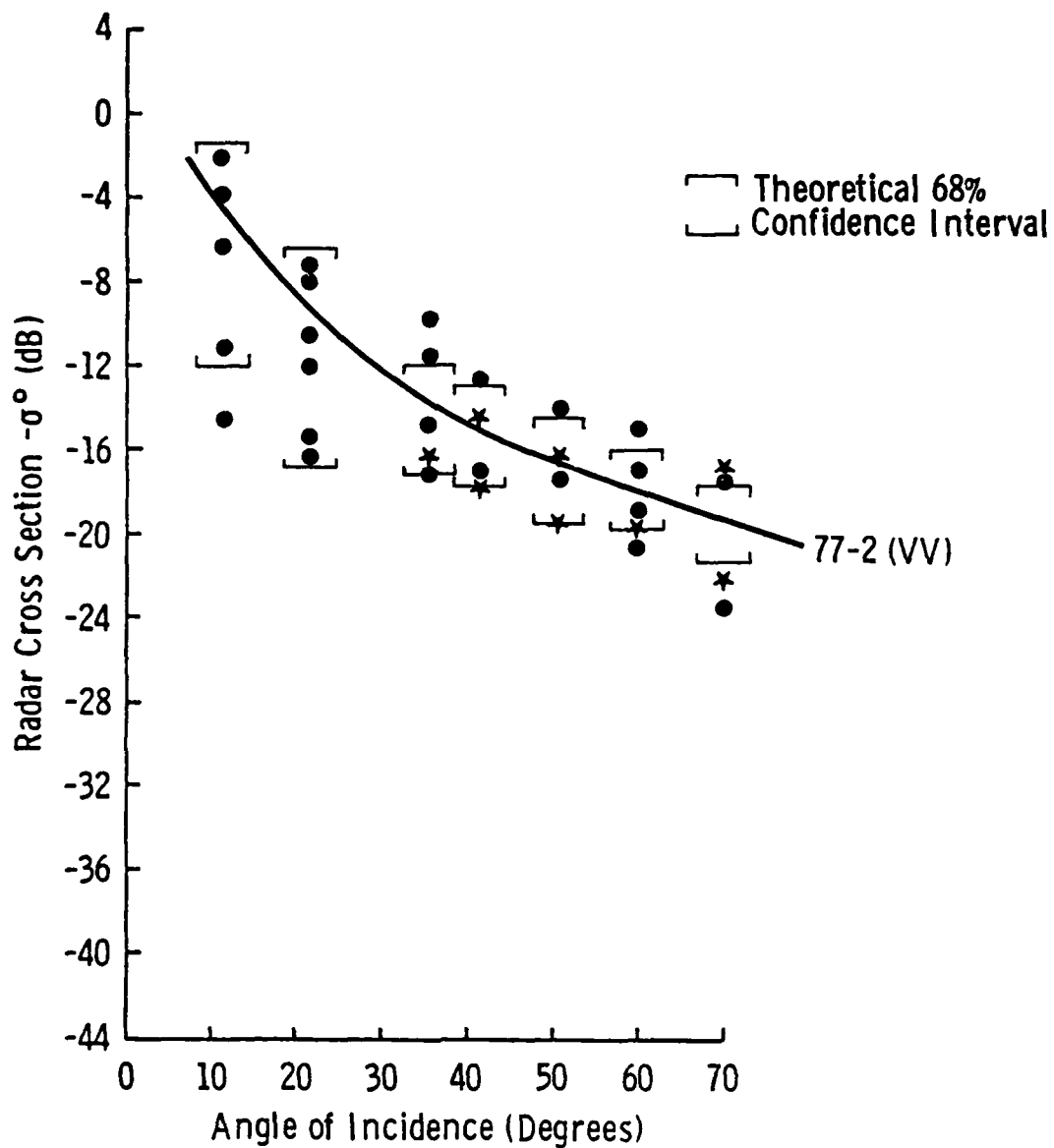


Figure 4.4-7. Scattering coefficient of multiyear ice, Site 77-2, at 1-2 GHz, VV.

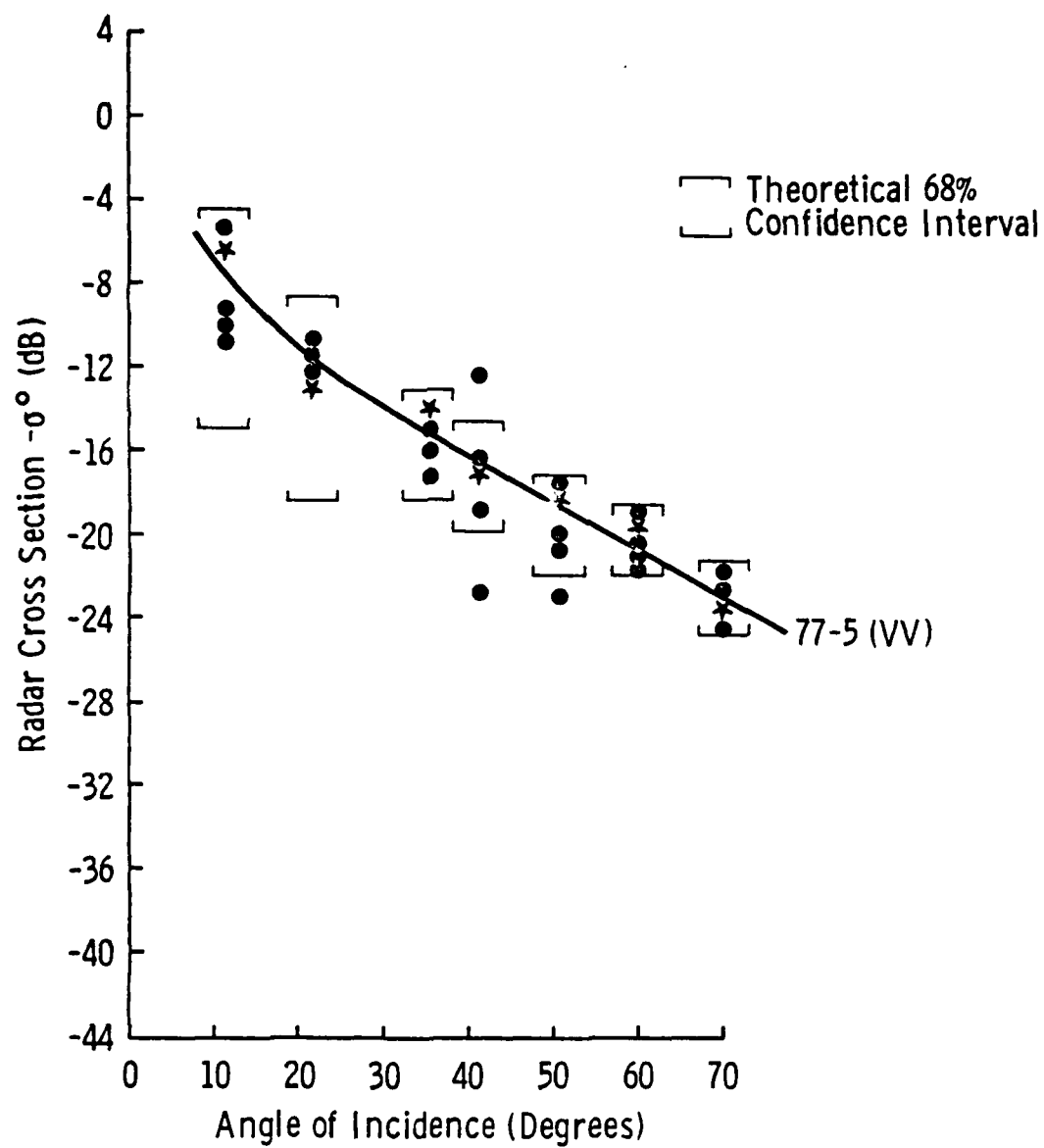


Figure 4.4-8. Scattering coefficient of multiyear ice, Site 77-5, at 1-2 GHz, VV.

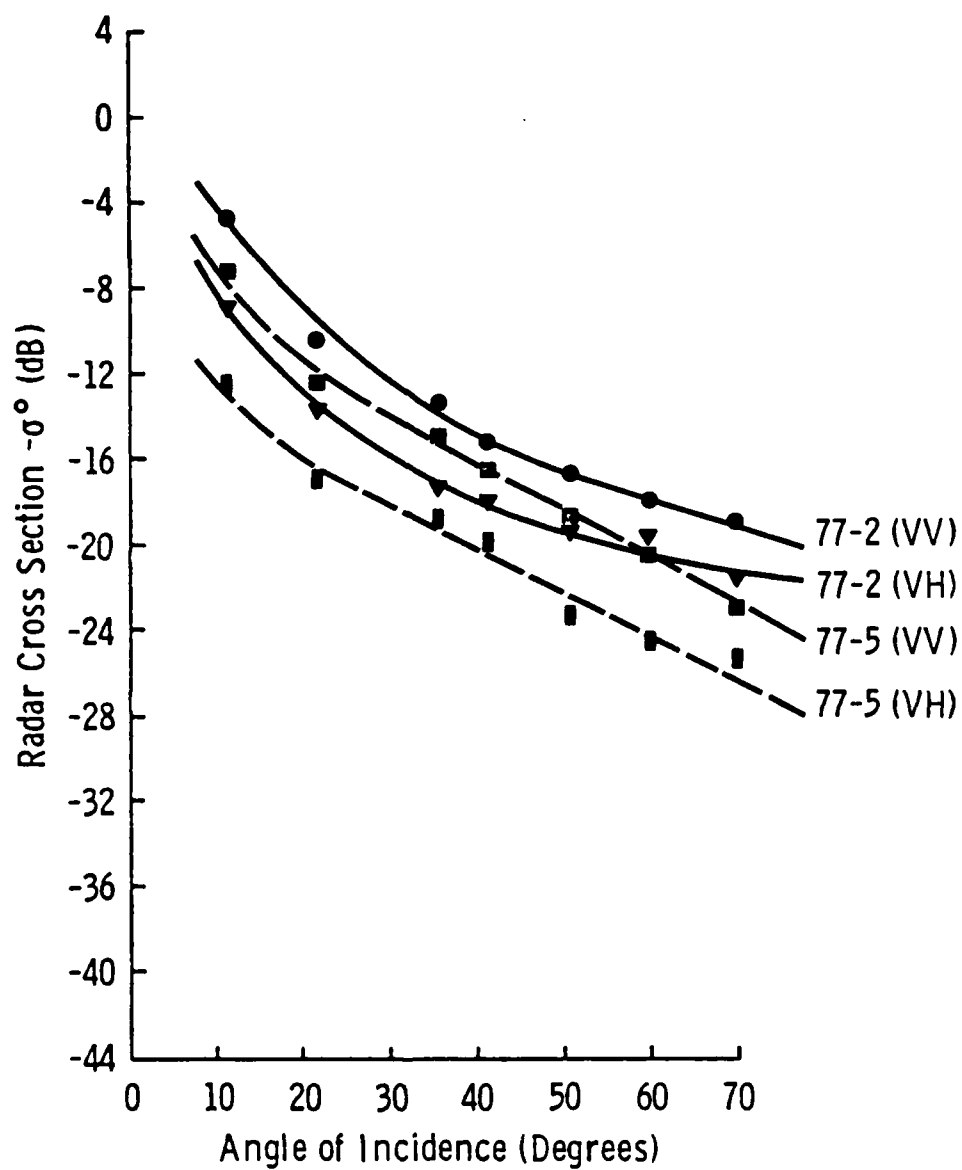


Figure 4.4-9. Scattering coefficient of multiyear ice, Site 77-2 and Site 77-5, at 1-2 GHz, VV and VH.

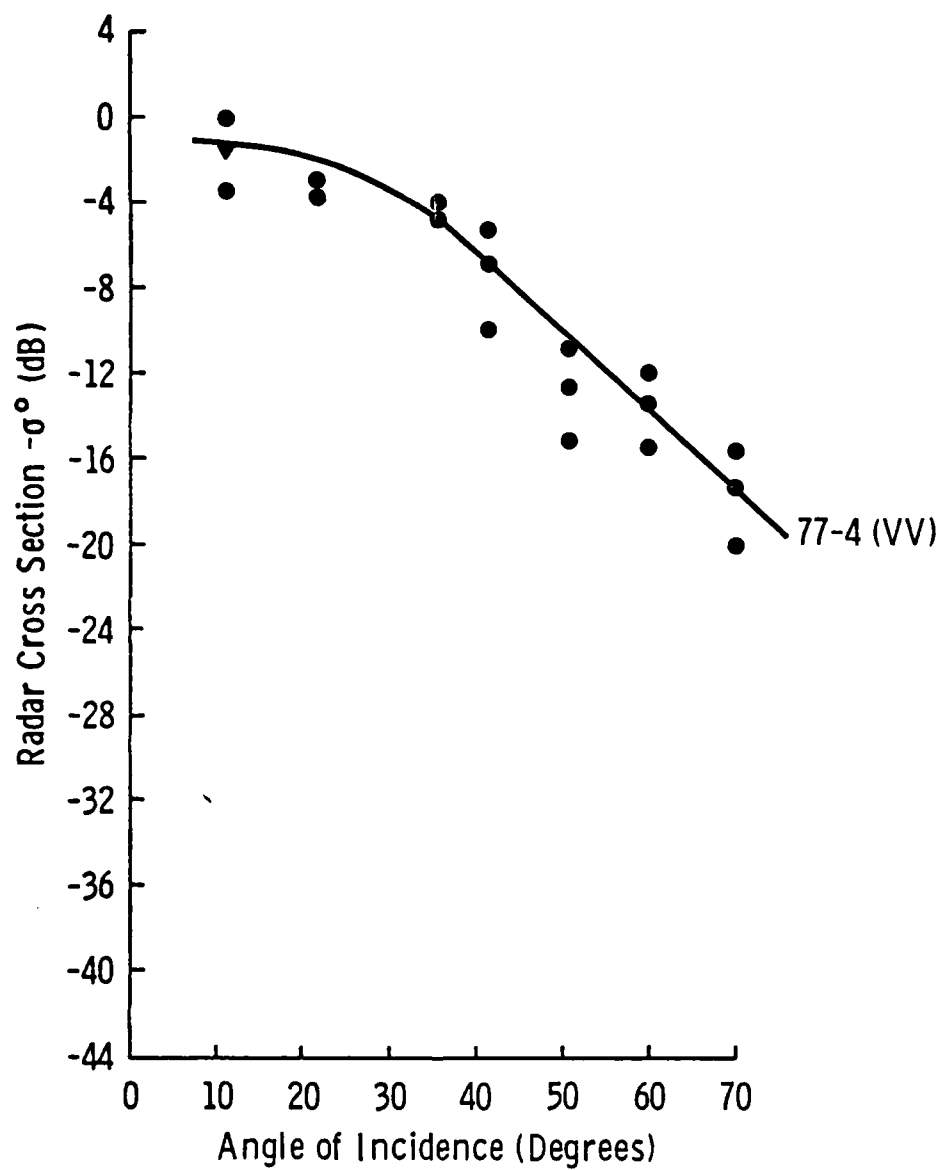


Figure 4.4-10. Scattering coefficient of a small thick first-year pressure ridge, Site 77-4, at 1-2 GHz, VV.

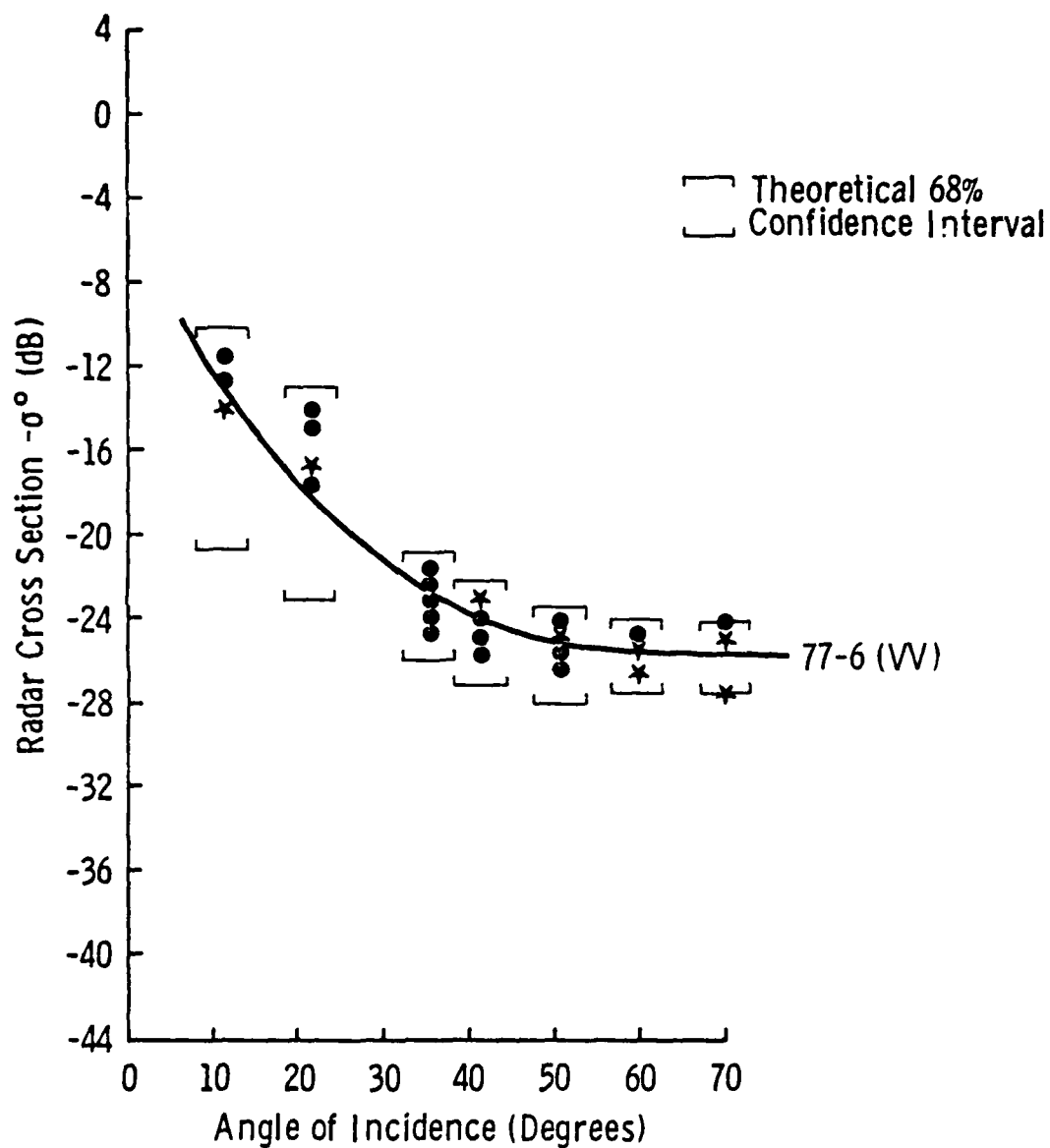


Figure 4.4-11. Scattering coefficient of lake ice with underlying layer of water, Site 77-6, at 1-2 GHz, VV.

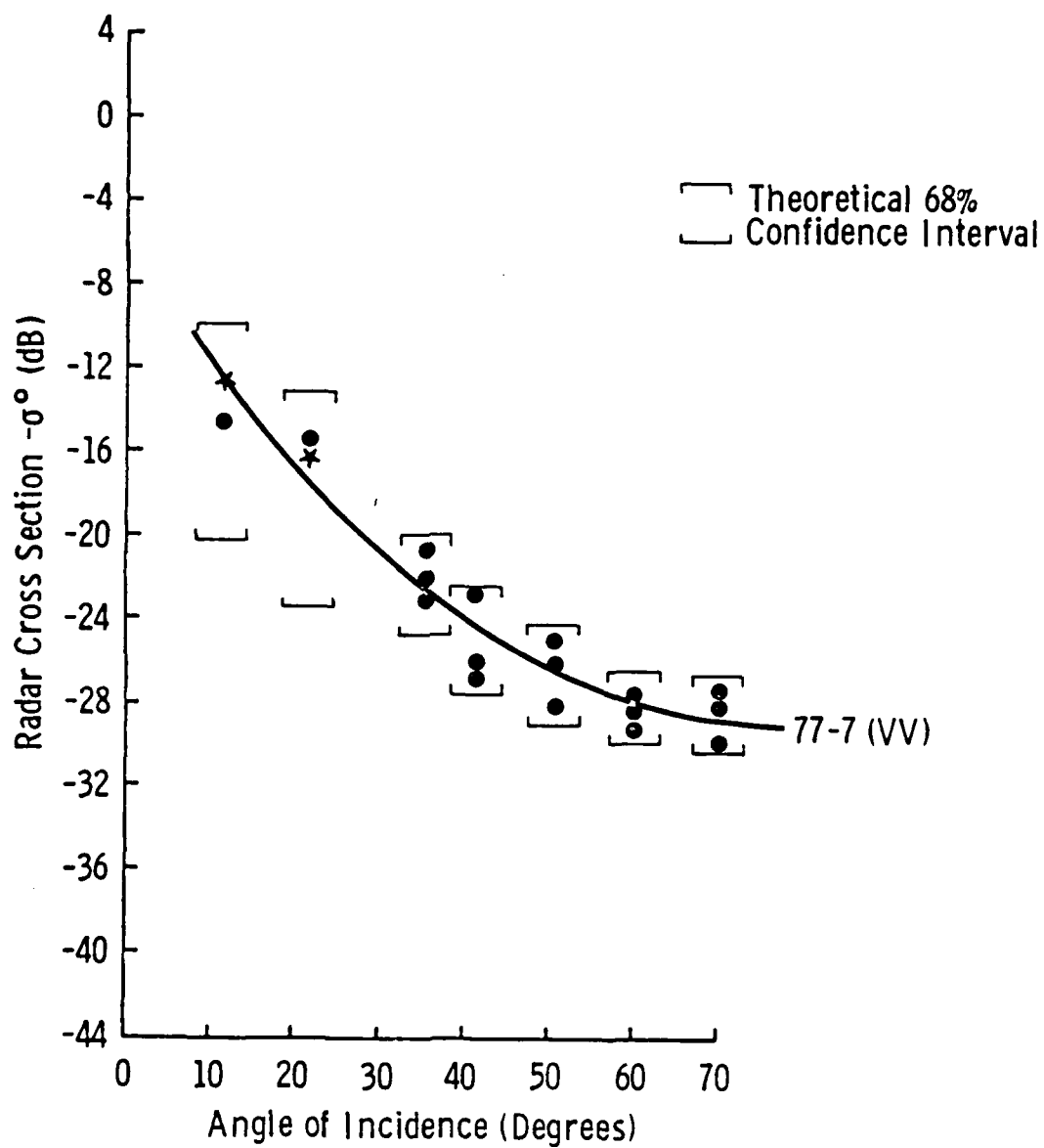


Figure 4.4-12. Scattering coefficient of lake ice frozen to its mud bottom, Site 77-7, at 1-2 GHz, VV.

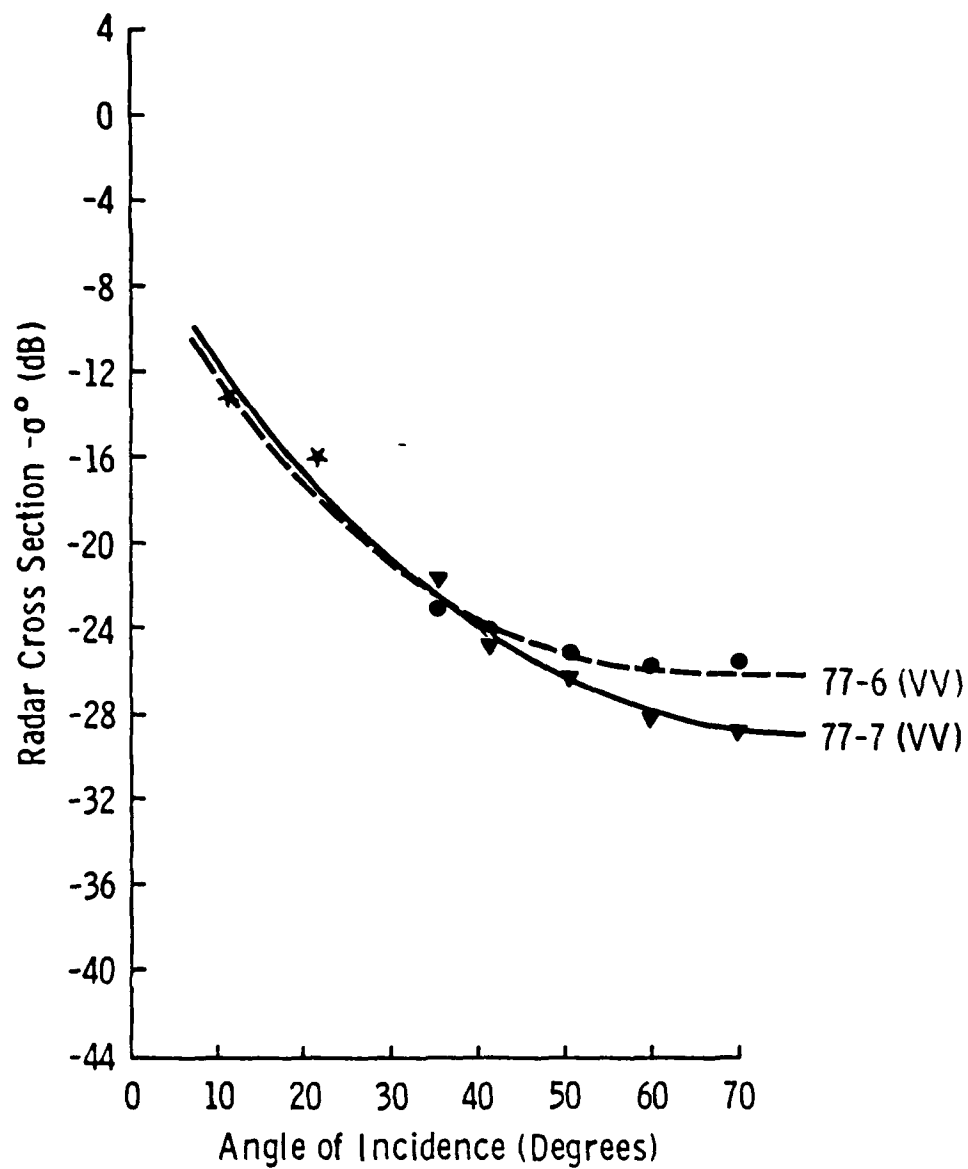


Figure 4.4-13. Scattering coefficient of lake ice, Site 77-6 and Site 77-7, at 1-2 GHz, VV.

# Scattering Coefficient of Thick First-Year and Multiyear Ice at 1-2 GHz

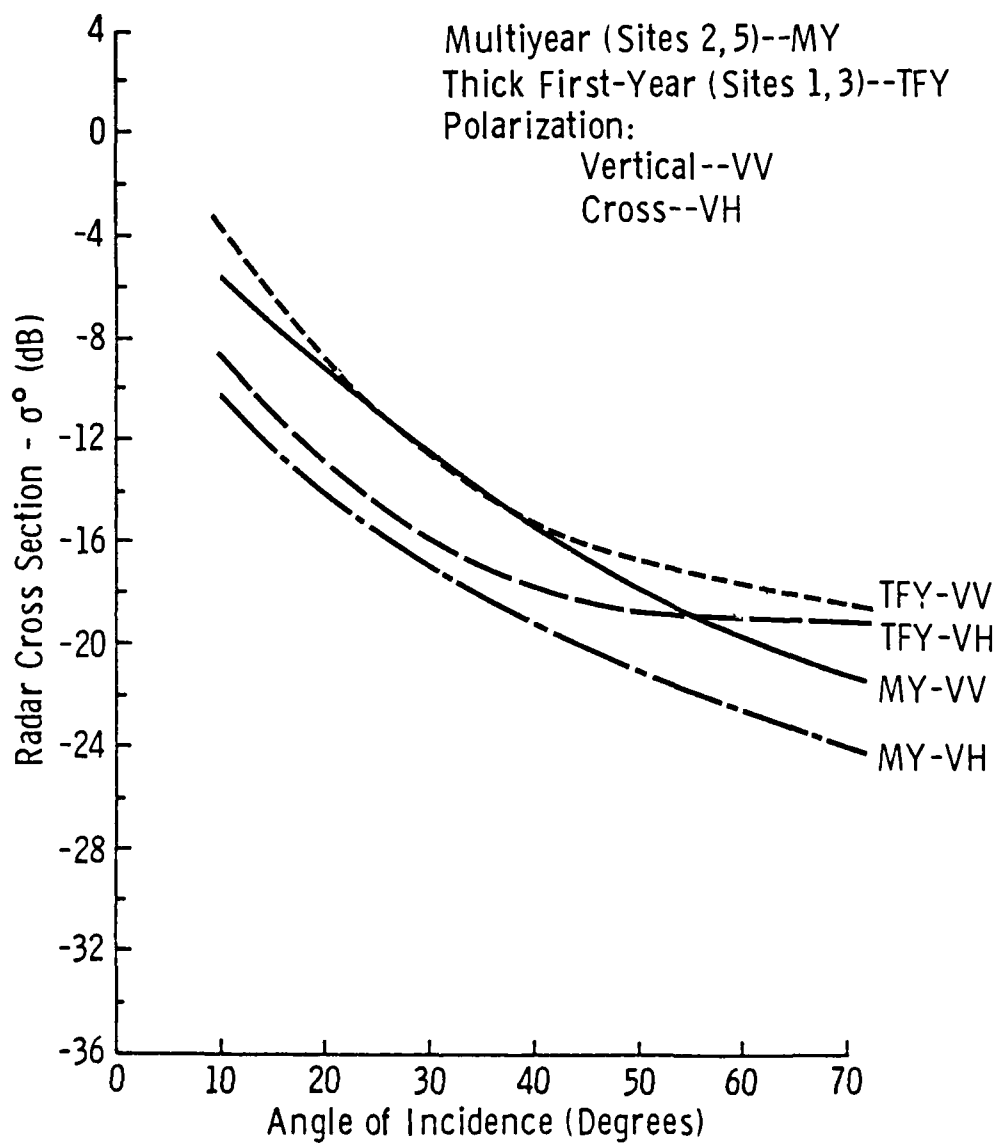


FIGURE 4.4-14 Scattering Coefficient of Thick First-Year  
and Multiyear Ice at 1-2 GHz.

# Scattering Coefficient of Thick First-Year, Multiyear, Fresh Water Lake, and Pressure Ridge Ice at 1-2 GHz

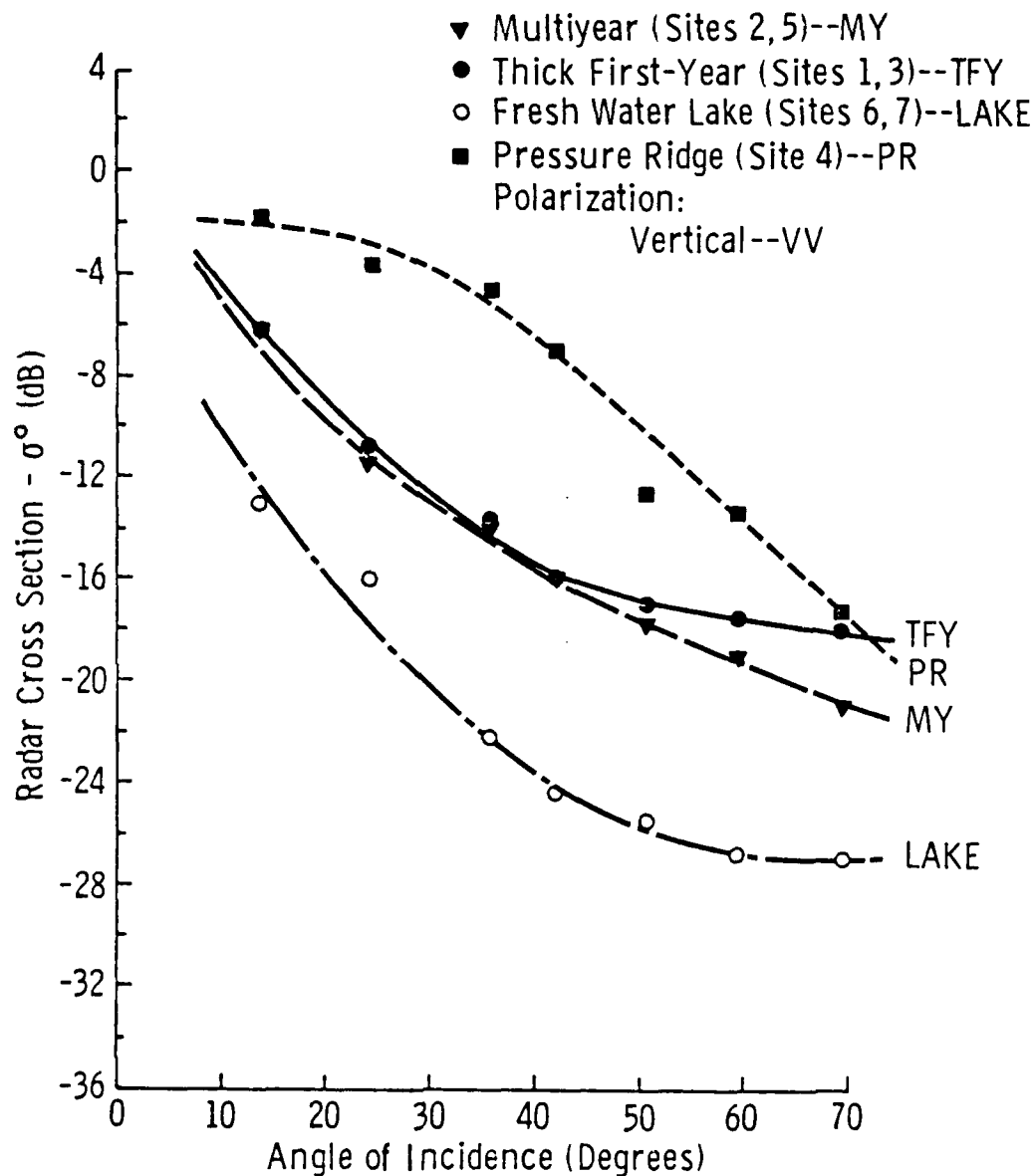


FIGURE 4.4-15 Scattering Coefficient of Thick First-Year, Multiyear  
Fresh Water Lake, and Pressure Ridge Ice at 1-2 GHz.

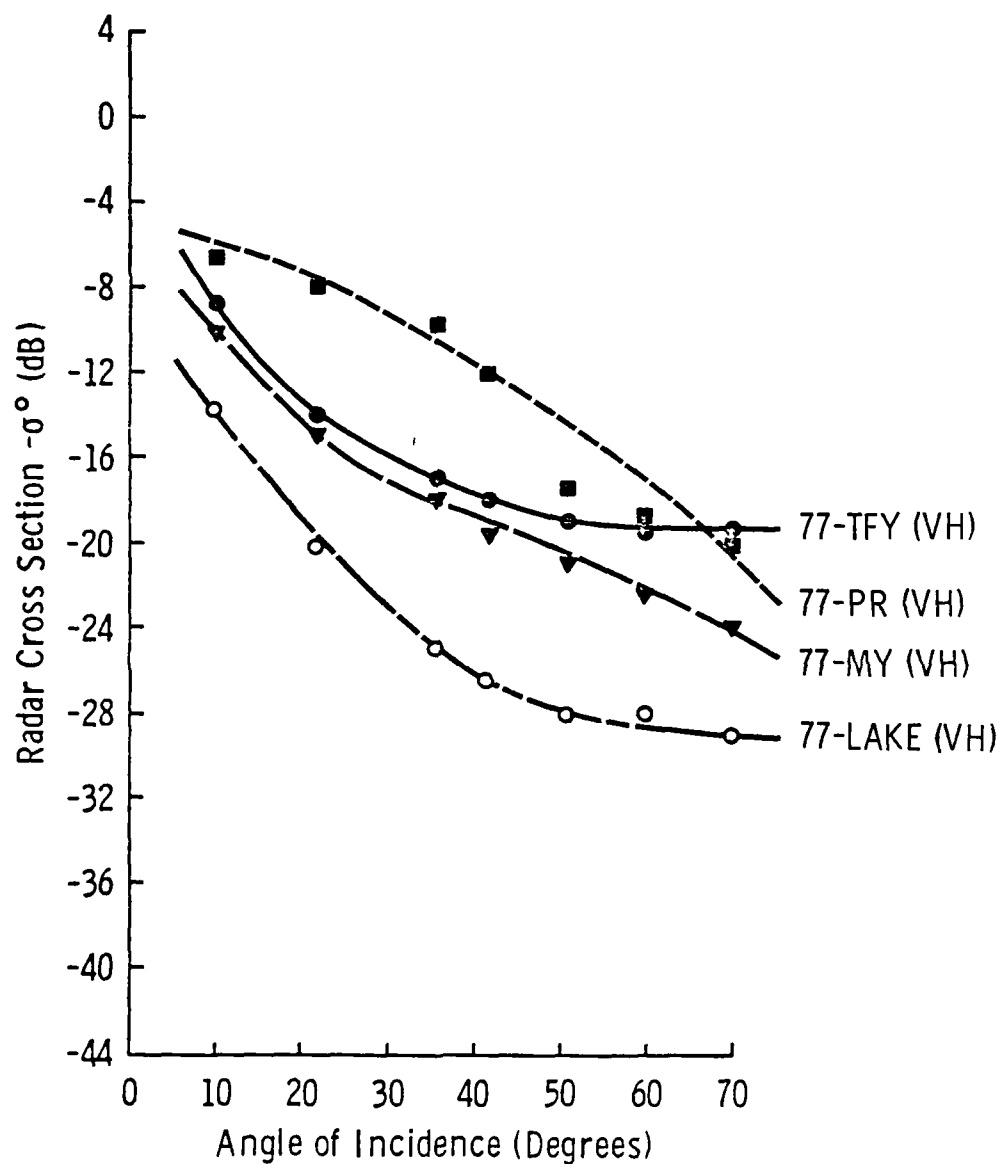


Figure 4.4-16. Average scattering coefficient of thick first-year, multiyear, fresh water lake, and pressure ridge ice at 1-2 GHz, VH.

sites had scattering that was low in absolute level and decayed exponentially. These returns, like the returns from multiyear ice, did not exhibit the expected wide variation between independent looks; they were found to cluster significantly more tightly than would be expected from surface scatter alone. This is especially evident at the near-vertical angles. The scattering from the two lake ice sites was almost identical from  $10^\circ$  to  $40^\circ$ . However, after  $40^\circ$  the returns from the ice that was frozen to its mud bottom continue to fall off, while the returns from the ice with an underlying layer of water show a leveling-off effect (see Figure 4.4-13).

#### 4.4.2 Comparison of Scattering Coefficients.

At large angles of incidence, multiyear ice returns decayed more rapidly than those of thick first-year ice (see Figure 4.4-14). The ability to discriminate between thick first-year ice, multiyear ice, pressure ridged ice, and lake ice is illustrated in Figures 4.4-15 and 4.4-16. Multiyear and thick first-year ice were not found to be discriminable between  $10^\circ$  and  $60^\circ$ . Cross-polarization provided the greatest discriminatory capability and may be useable at higher angles. Sharply-cornered pressure-ridged ice and the flat smooth-surfaced ice of the pack could easily be distinguished from each other at all but the highest angle of incidence. Also, lake ice had a significantly lower return (6 dB) than the sea ice types that were studied.

#### 4.4.3 The Effect of Snow Depth on Backscatter Return.

The effect on snow depth on the backscatter return from sea ice was investigated in the 1978 shorefast ice experiments. Natural snow depths were found to vary from 2-4 cm. Depths of 8 and 14 cm were artificially

generated. Experiments were also performed where the snow layer was removed, and a bare ice surface remained. The scattering coefficients for the 5 sites (a site indicates the positioning of the ground-based structure at a unique location in the selected ice area) in 1978 were averaged into two categories: ice with a snow layer and ice with a bare surface. In Figure 4.4-17 returns at 1-2 GHz frequencies from thick first-year shorefast sea ice with 2-4 cm snow covers and temperatures ranging from  $-3^{\circ}\text{C}$  to  $-10^{\circ}\text{C}$  is shown to be insensitive to snow cover. However, when examined on a look-by-look basis, results are more interesting and even confusing. In Figure 4.4-18 are shown the returns measured at Site 78-1 for ice of the same temperature and 0, 2, and 8 cm snow layers. The bare surface produced the lowest returns while the thickest layer of snow produced the greatest return. Large differences are found at near-vertical angles. Returns from ice with the bare surface are about 2 dB lower than returns from ice with a 2 cm snow cover and 1.5-7.0 dB below the returns from ice with an 8 cm snow cover. Two looks were made at Site 78-2 at the same temperature, but differing by one having a bare surface and the other having 4 cm of snow cover. Their returns are nearly identical (see Figure 4.4-19), as are the returns from ice with a bare surface and ice with 14 cm of snow cover at Site 78-3 (see Figure 4.4-20), returns from ice with a bare surface and ice with 2 cm of snow cover in Site 78-4 (see Figure 4.4-21), and returns from ice with a bare surface and ice with 4 cm of snow cover in Site 78-5 (see Figure 4.4-22). Two things, however, stand out about the responses of Sites 78-2, 78-4, and 78-5. Returns near nadir are higher for ice with a bare surface, and ice with a bare surface has a greater deviation in return about the average response.

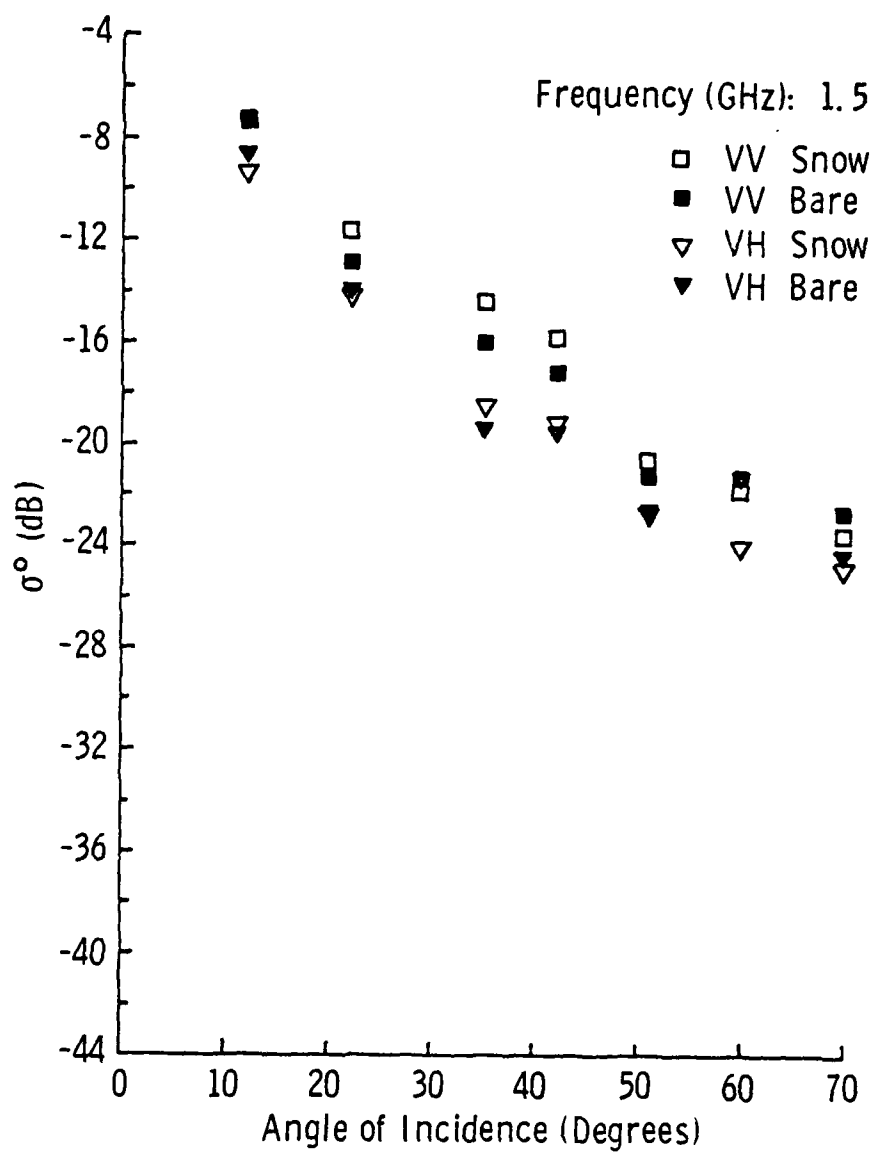


Figure 4.4-17. Average  $\sigma^0$  versus angle of incidence ( $\theta$ ) curve for bare-ice and snow-covered ice, 1.5 GHz.

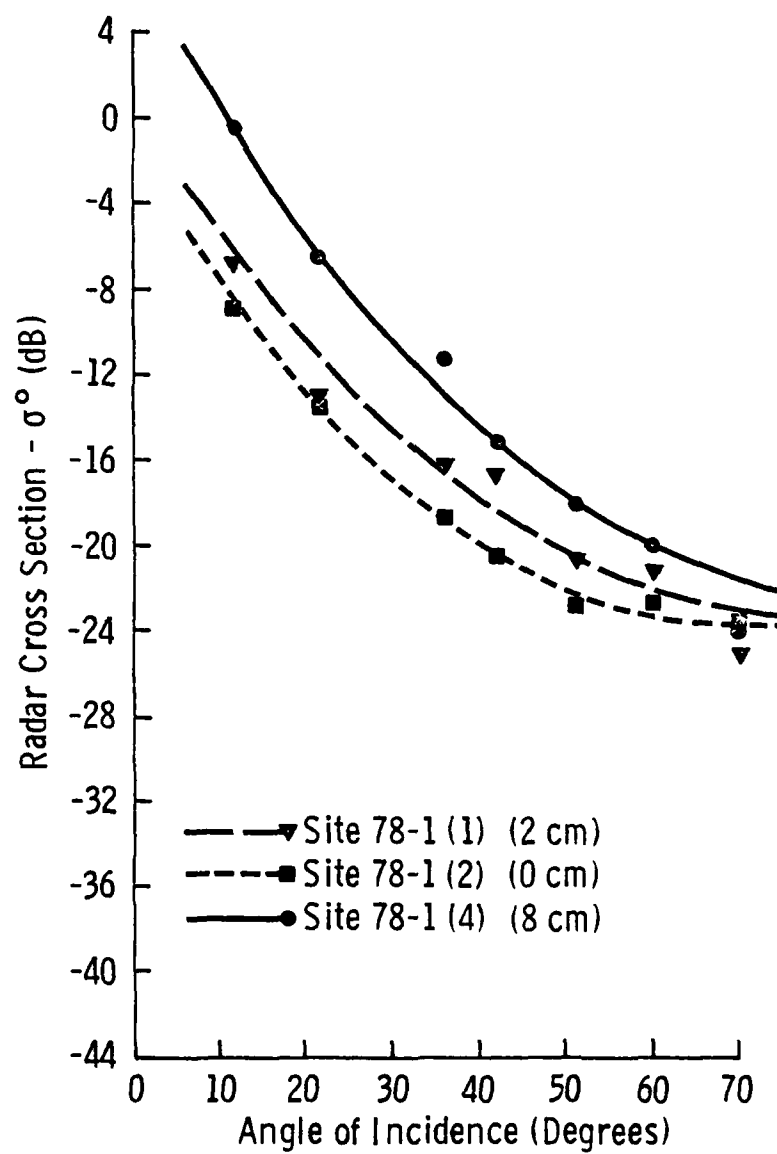


Figure 4.4-18. Scattering coefficients of thick first-year ice, Site 78-1, with a 0, 2, and 8 cm snow layer at 1-2 GHz, VV.

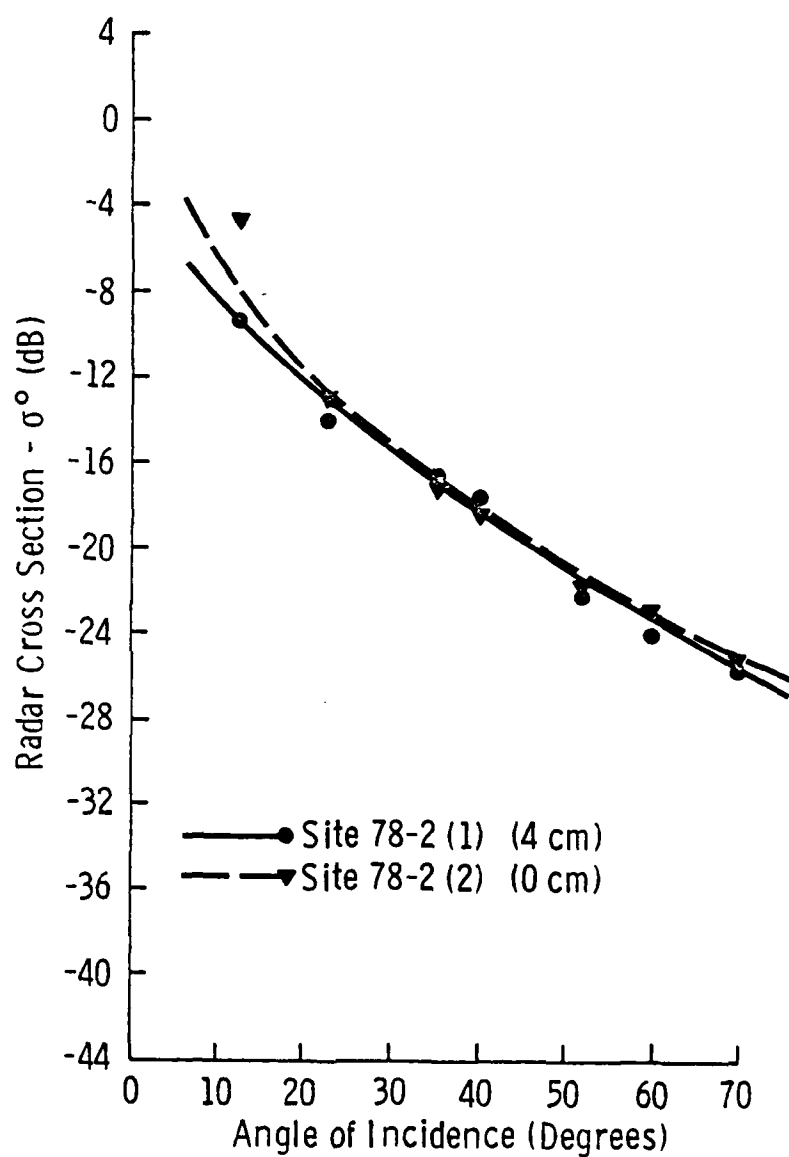


Figure 4.4-19. Scattering coefficient of thick first-year ice, Site 78-2, with a 0 and 4 cm snow layer at 1-2 GHz, VV.

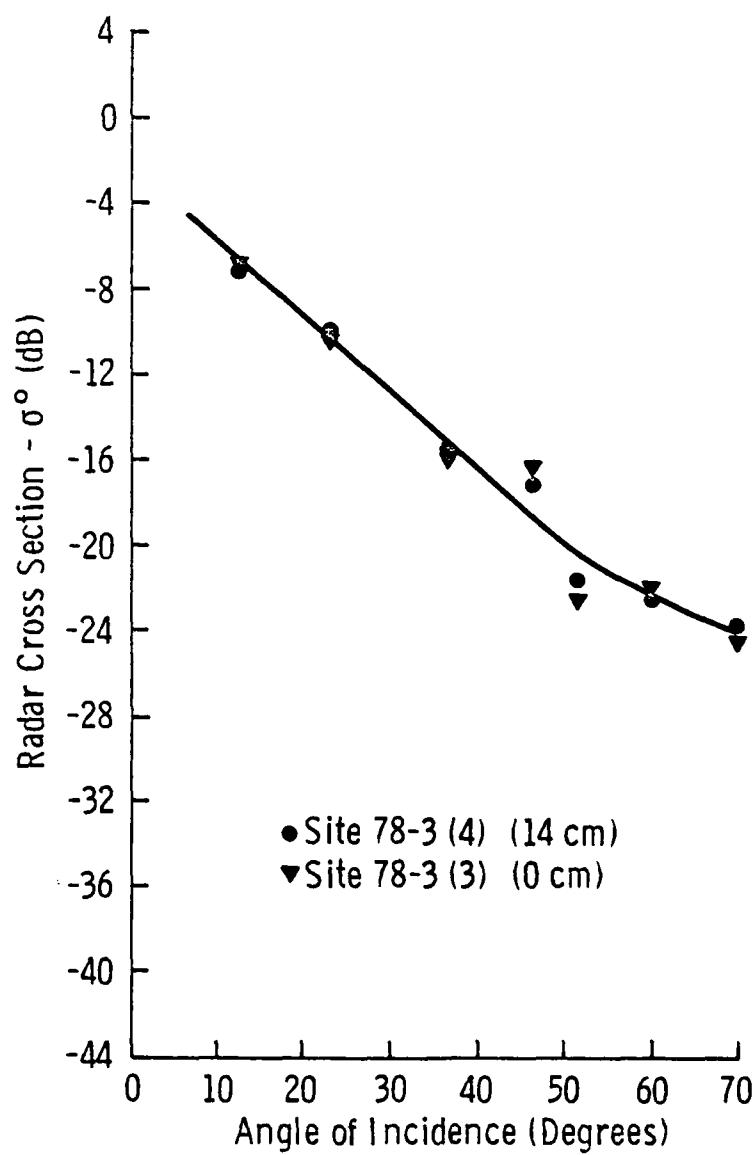


Figure 4.4-20. Scattering coefficient of thick first-year ice, Site 78-3, with 0 and 14 cm snow cover at 1-2 GHz, VV.

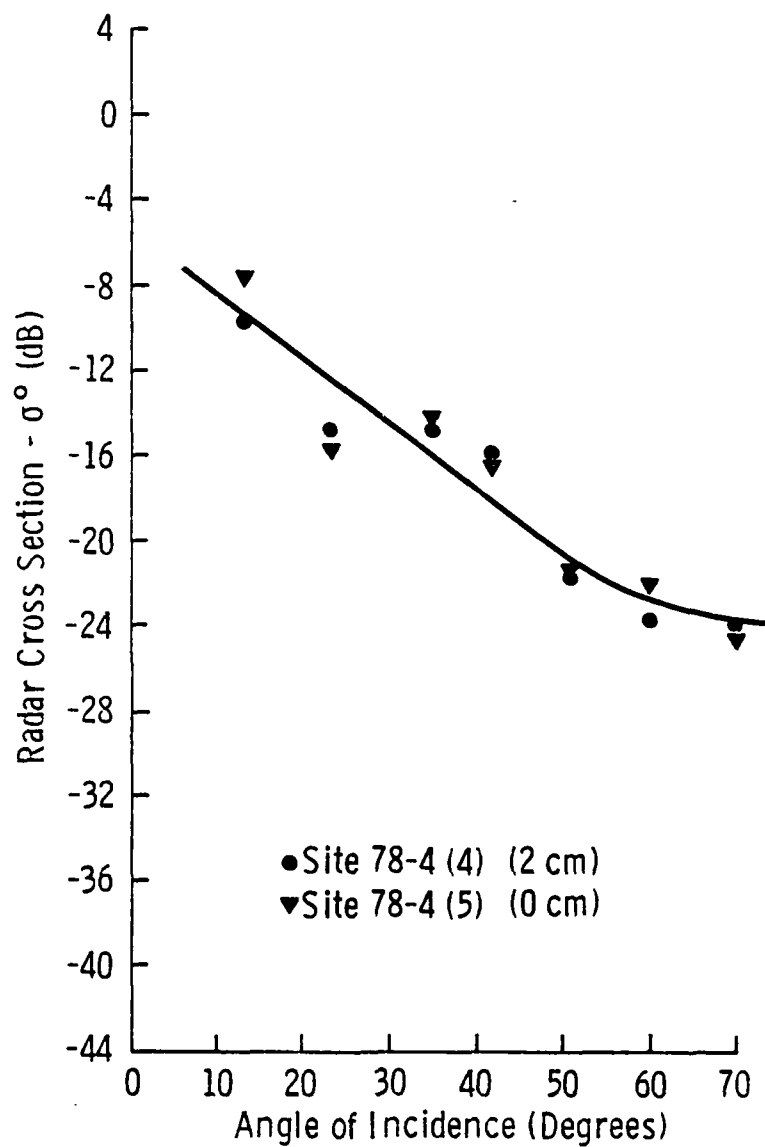


Figure 4.4-21. Scattering coefficient of thick first-year ice, Site 78-4, with 0 and 2 cm snow cover at 1-2 GHz, VV.

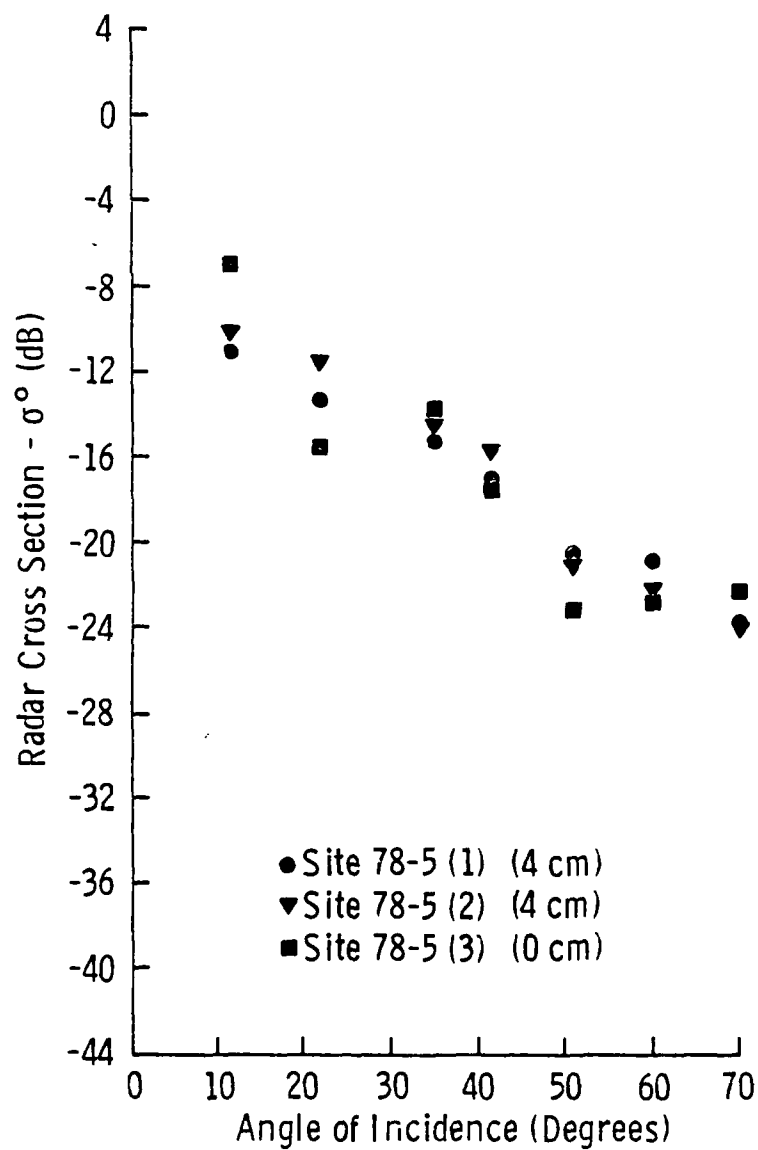


Figure 4.4-22. Scattering coefficient of thick first-year ice, Site 78-5, with 0 and 4 cm snow cover at 1-2 GHz, VV.

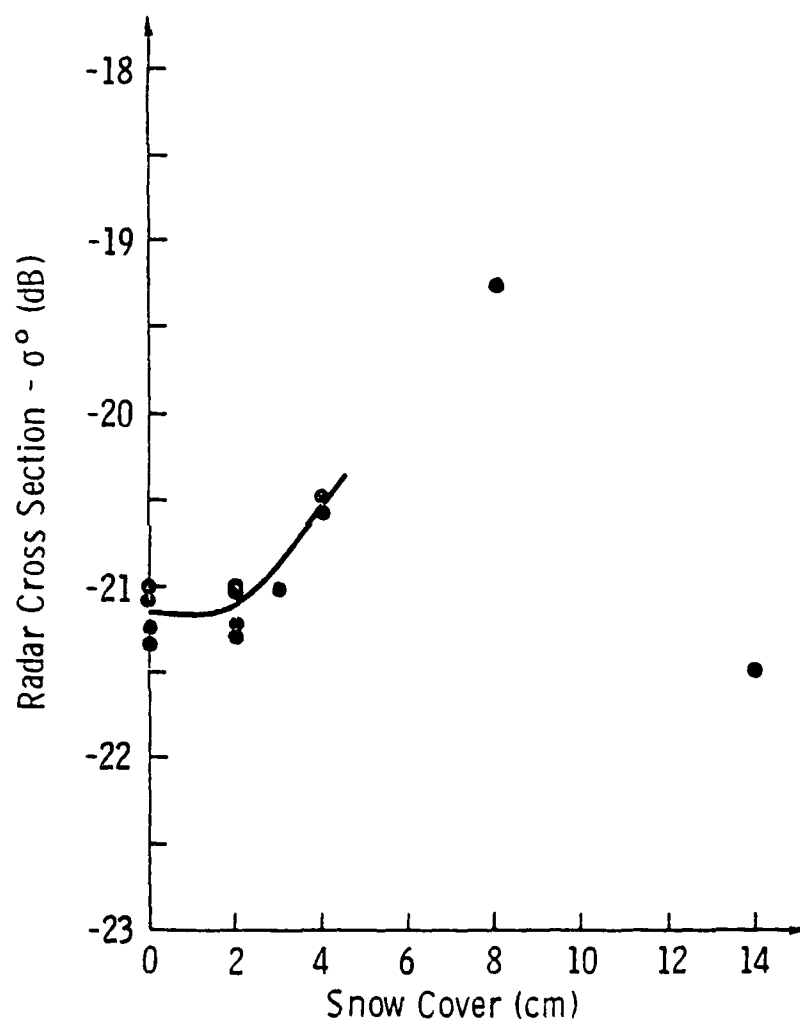


Figure 4.4-23. To illustrate the overall effect of snow depth on radar return at 1-2 GHz, VV, the average dB return for 42, 51, 60, and 70 degree angles is plotted versus snow depth.

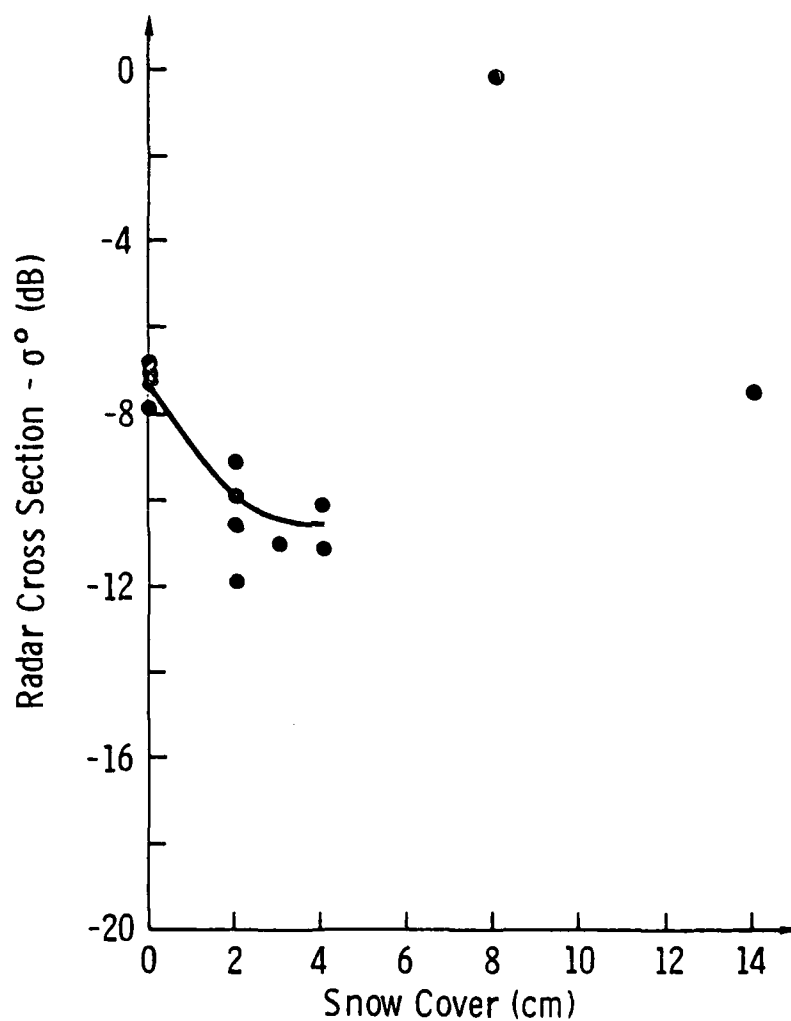


Figure 4.4-24. To illustrate the overall effect of snow depth on radar return at 1-2 GHz, VV, the average dB return for  $12^\circ$  is plotted versus snow depth.

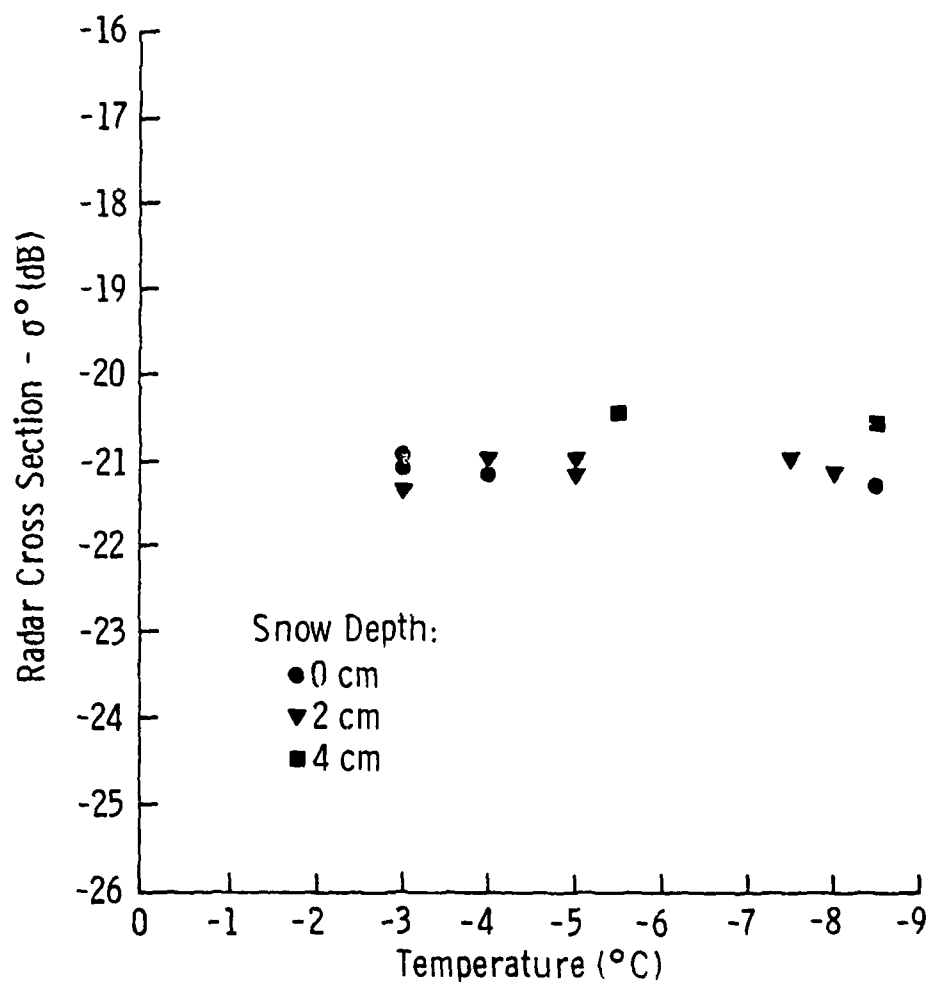


Figure 4.4-25. The effect of ice temperature on the backscatter return from thick first-year shore fast sea ice at 1-2 GHz, VV, for 42, 51, 60, and 70 degree angles is shown.

The overall effect of snow depth on radar return at 1-2 GHz is illustrated in Figure 4.4-23 where the return (average of  $\sigma_{dB}^0$ ) for 42, 51, 60, and 70 degree angles is plotted versus snow depth. In general, little difference is detected in return from ice with a bare surface and ice with up to 3 cm of snow cover. Ice with snow covers of 4 cm and 8 cm yielded higher returns than ice with 0-3 cm snow covers. Ice with a 14 cm snow cover gave lower return than ice with 0-3 cm, contrary to the apparent trend. The effect of snow depth on radar return at near-nadir angles is illustrated in Figure 4.4-24 where the return at  $12^\circ$  is plotted versus snow depth. It is seen that, for ice with snow covers from 0-4 cm, the largest returns came from ice with a bare surface and lowest returns from ice with a 4 cm snow cover. Returns from 8 cm and 14 cm snow covered ice do not continue this apparent trend.

Backscatter studies of snow-covered ground also illustrate a behavior that is similar to that found for snow-covered sea ice [56]. Scattering coefficients at angles away from nadir were found to increase with increasing snow cover. However, at depths approaching 2 m, returns did not increase significantly with increasing depth.

#### 4.4.4 The Effect of Temperature on Backscatter Return.

The effect of ice surface temperature on the backscatter return from thick first-year shorefast sea ice at 1-2 GHz with varying degrees of snow cover (0, 2, and 4 cms) is illustrated in Figure 4.4-25. It is seen that backscatter is not greatly effected by changes in ice surface temperature of  $-3^\circ\text{C}$  to  $-9^\circ\text{C}$ . The scattering cross-section of snow-covered ground has also been found to be unaffected by changes of snow temperature in this range [56].

#### 4.4.5 Relation Between Backscatter and Crystal Orientation.

Radar anisotropy of landfast sea ice has been demonstrated to exist by Kovacs and Morey using the results of a linearly-polarized 100 MHz impulse radar [53]. They observed strong bottom reflections when the antenna E-field was oriented parallel with the c-axis of the ice crystals and no detectable bottom reflection when the antenna E-field was oriented perpendicular to the c-axis.

Results of the University of Kansas wide-band scatterometry experiments and the study of crystal alignments in the fast ice performed by Weeks and Gow in 1977 (1978) [50] and in 1978 (1979) [54] indicate that microwave frequencies of 1-2 GHz were possibly sensitive to the anisotropy of the preferred crystal orientation in the fast ice, but that these effects are smaller than 1 dB. Since short wavelengths do not penetrate to the depths in the landfast ice where strong orientation effects are observed, the 8.5 - 17.5 GHz microwave frequencies were found to lack any strong correlation between azimuthal orientation and strength of radar return.

Study of c-axis alignments in 1978 indicated that the mean c-axis orientation was  $57^\circ$  (true) at 25 cm depths and in general gradually increased to  $84^\circ$  near the bottom of the ice sheet. As a reference, and also in consideration of the penetration capability of the 1 - 2 GHz radar,  $60^\circ$  was selected as the axis running parallel to the mean c-axis. Study of c-axis alignments in 1977 indicated that the mean c-axis orientation was  $35^\circ$ . Table 4.4-1 presents a summary of site information that was considered in the discussion of the preferred c-axis orientation effect on radar backscatter return. The table includes snow depth, ice surface temperature, the azimuthal orientation

TABLE 4.4-1  
SUMMARY OF SITE INFORMATION USED IN THE DISCUSSION OF C-AXIS  
EFFECTS ON RADAR BACKSCATTER RETURN

YEAR OF EXPERIMENT	SITE NUMBER	SHOT NUMBER	SNOW DEPTH (cm)	ICE SURFACE TEMPERATURE (° C)	ANTENNA E-FIELD ORIENTATION (° TRUE)	MEAN C-AXIS ORIENTATION (° TRUE)	E-FIELD ORIENTATION WRT C-AXIS (°)	AVERAGE SCATTERING CROSS-SECTION (dB)	SLOPE FROM LINEAR REGRESSION dB/degree
1978	1	1	2	- 6	15	60	45	-21.00	- .0130 - (.0108)**
	2	1	4	- 3	0		60	-22.21*	
	3	1	3	- 6	290		50	-21.04	
	4	1	2	- 4	350		70	-20.97	
		2		- 7				-21.21	
		3		-10				-21.13	
		4		- 3				-21.30	
	5	1	4	- 7	48	35	12	-20.45	
		2		- 8				-20.59	
		1		---	345		50	-14.35	
1977		2		- 4	20		15	-14.22	
		3		- 5	75		40	-21.74	
	3	4	2	---	120		85	-21.55	
		5		-10	35		0	-21.52	
		6		- 6	250		35	-20.66	

\* Data point which is an outlyier on regressed line.

\*\* Slope resulting when outlying data point is not included in regression.

of the antenna E-field with respect to true north, the mean c-axis orientation with respect to true north, the orientation of the antenna E-field with respect to the c-axis of the landfast ice, the average radar scattering cross-section at 40°, 50°, 60°, and 70° incidence angles, and the slope of the linear regression which was used to demonstrate the radar anisotropy trend. The average of the  $\sigma_{dB}^0$  from different incidence angles was taken to provide for a quantitative description of the angular response of the sea ice. The 40°, 50°, 60°, and 70° angles were chosen, since their return resulted from the greatest number of independent samples of measurement due to the large illuminated area of the radar footprint at these angles and the effect of having swept in frequency with excess bandwidth.

The results of the 1977 experiment are shown in Figure 4.4-26. In this experiment returns were found to cluster into two families. Within each family trends indicate that antenna E-field orientations near the c-axis of the landfast sea ice result in only a slightly higher backscatter return than orthogonal orientations. The slopes of these trends were -.0037 and -.0025.

The results of the 1978 experiments (see Figure 4.4-27) illustrate the apparent radar response trend with azimuthal orientation better than those for the 1977 data. This may be due to the greater number of measurements made in 1978. These returns were from 9 looks with 5 orientations. Snow cover ranged from 2 to 4 cm and temperatures ranged from -3° to -10° C. These data were linearly regressed, and a negative slope of -.0130 dB/° resulted.

The sample correlation coefficient was 0.623. To test the hypothesis that there is zero correlation between the scattering cross-

section strength and orientation with c-axis, a significance test at the 5 percent level was performed. The critical value of this test was 0.666. This hypothesis was not rejected at the 5 percent level, but may be at a slightly greater level. The standard error of estimates,  $s_{y/x}$ , which is due to the scatter of the  $\sigma^0$  about the regression line, was 0.175 dB. If it is assumed that for  $\sigma^0$ 's various orientations have normal distributions about the true regression line with common standard deviation  $\sigma_{y/x}$ , then 68 percent of the combined populations lie within a  $\pm \sigma_{y/x}$  of the true regression line and 95 percent within a  $\pm 2 \sigma_{y/x}$ . With large samples we could expect to approximate this situation.

The data point corresponding with Site 78-2 is an apparent outlier. If it is considered a bad point and is not included in the regression, the sample correlation coefficient is .926, the standard error of estimate is .0146 dB, and the slope is -.0108 dB/°. The significance test for this condition has a critical value of .707 for the 5 percent level and a value of .834 for the 1 percent level. Therefore, in this case the hypothesis that there is zero correlation between scattering cross-section strength and c-axis orientation is clearly rejected.

The slope of the regressed data with the outlier data point included would indicate that a 1.17 dB difference would exist between aximuthal look directions along the c-axis and perpendicular to the c-axis. The slope of the regressed data with the outlier data point excluded would indicate that a .972 dB difference would exist between the above orthogonal looks.

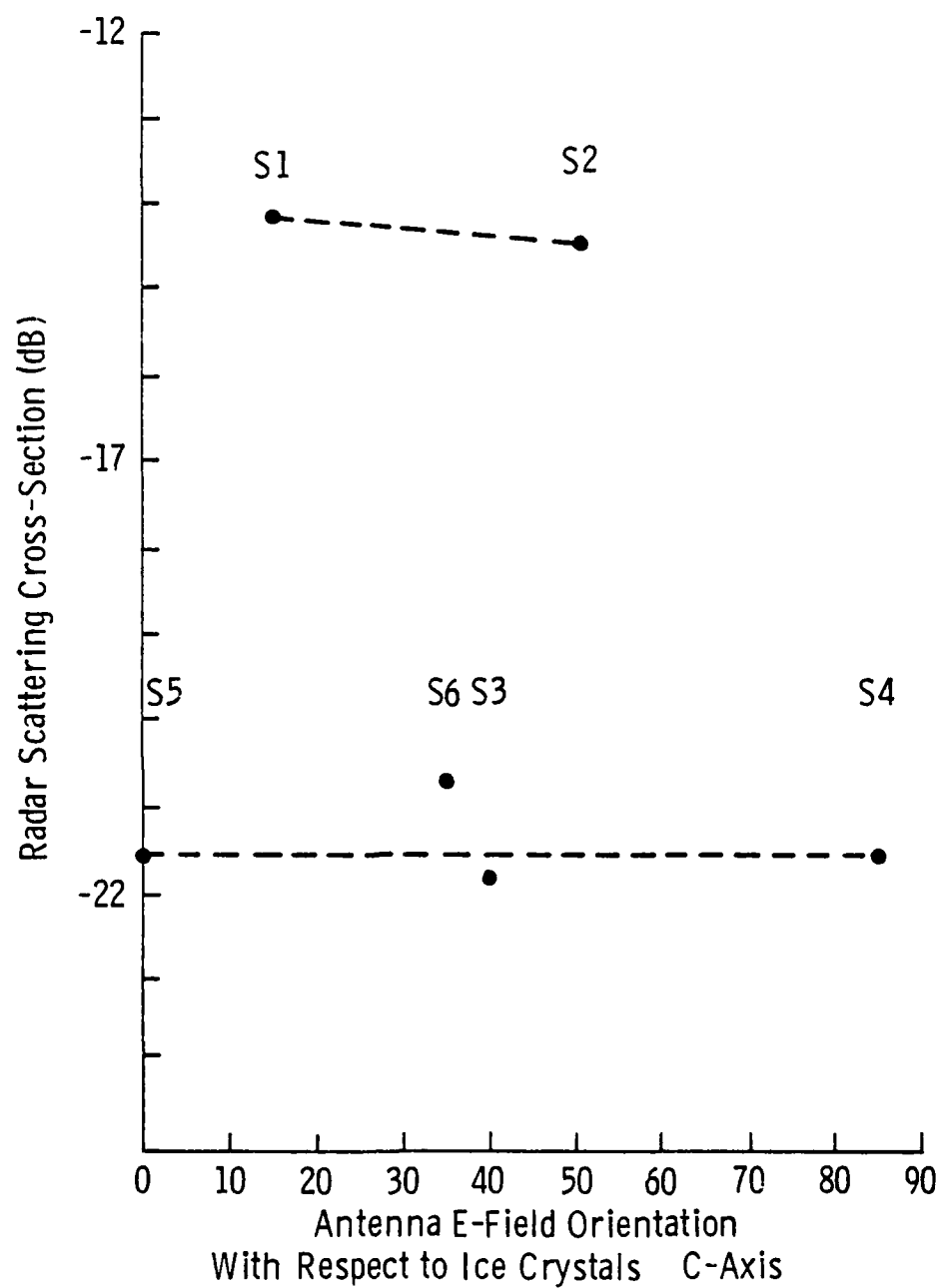
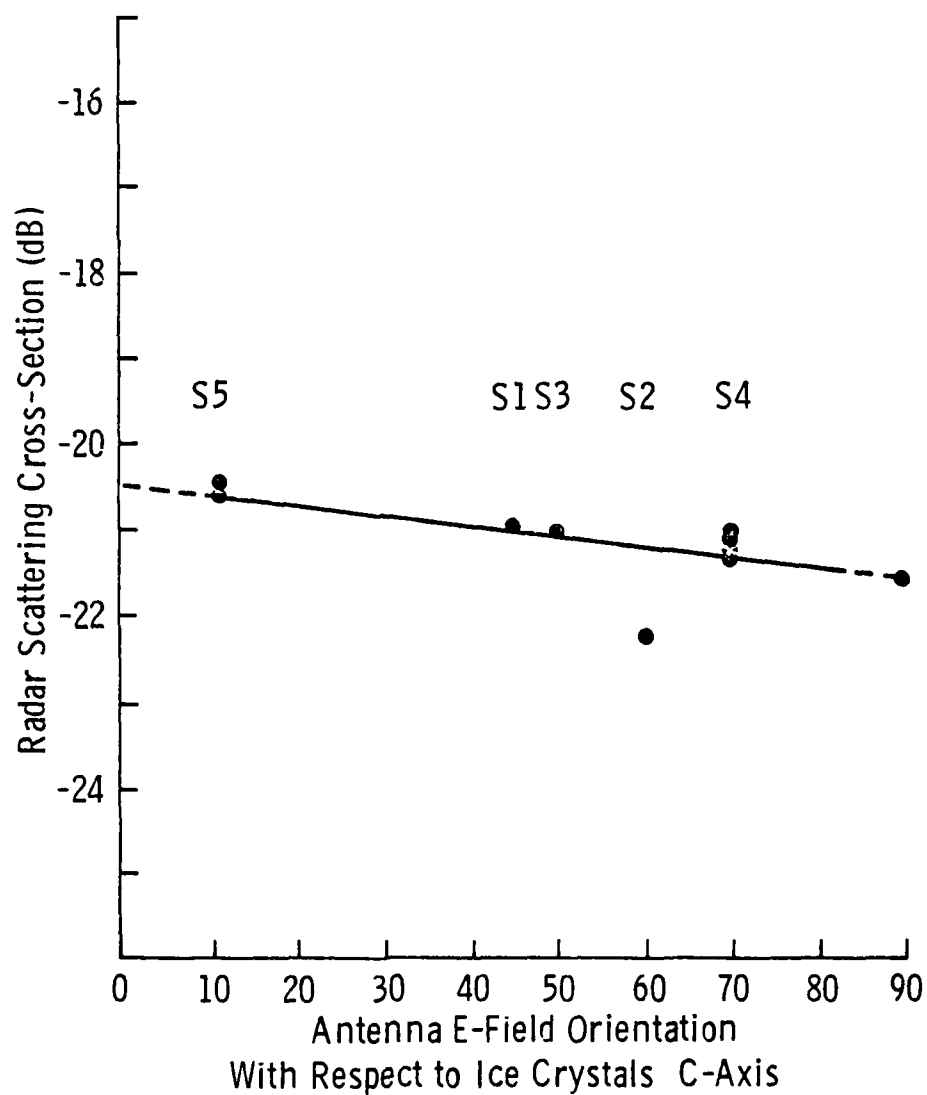


Figure 4.4-26. Results of the 1977 experiment demonstrating the effects of a preferred ice crystal orientation on 1-2 GHz like-polarized (VV) radar backscatter return.



#### 4.4.6 Discussion of L-Band Results

Dielectric properties of sea ice are primarily a function of brine volume in the ice, which in turn is controlled by ice temperature and salinity. Because the salinity profiles of thick first-year ice and Sites 77-1 and 77-3 were similar, ice temperature was a definite index of brine volume. Temperature effects on radar return were demonstrated as shifts in return trends for thick first-year ice. Each level was directly relatable to air or ice temperature at time of backscatter measurement. The largest returns were observed when air and ice temperatures were the highest. Correspondingly weak returns were observed when temperatures were at their lowest. It should be noted, however, that the data set over which the temperature effect is described is small and may be due to coincidence. These sites also have different histories of ice formation. Site 77-1 was formed from pancake ice (raised edges occurred above the normally flat surface), had an average of 11 cm of snow cover, and measurements of looks 3, 4, and 5 were taken with reasonably high air temperatures (higher air temperatures increase the free water content of the snow layer) which may account for the wider separation between its families, whereas Site 77-3 is very smooth unrafted ice with a 2 cm snow cover.

Average backscatter response ( $\sigma^\circ$  dB) of thick first-year ice was found to decay exponentially with incidence angle in 1977 and linearly in 1978. Average returns at  $35^\circ$  to  $42^\circ$  were very similar in absolute level.

For multiyear ice, for the pressure ridge, and for lake ice, the individual looks clustered more tightly than would have been expected

from fading produced by surface scatter alone; hence we conclude that volume scatter plays a major role in the scattering process, thereby allowing the wide sweep width to give non-coherent averaging of numerous independent samples for each look.

A firm conclusion as to the ability to detect where a fresh water inland lake is frozen to its mud bottom may not be possible from the backscatter responses obtained from Site 77-6 and 77-7. Other conditions were significantly different that strong comparisons may not be valid. These other conditions were as follows for sites 77-6 and 77-7: ice temperatures were  $-2^{\circ}$  to  $-0.5^{\circ}$  C and  $-0.5^{\circ}$  to  $0^{\circ}$  C, air temperatures were  $-2^{\circ}$  to  $+2^{\circ}$  C and  $0^{\circ}$  to  $+4^{\circ}$  C, thickness of snow cover was 0 and 18 cm, respectively. The heavy wet snow cover of Site 77-7 along with high temperatures may have masked a more characteristic backscatter return.

#### 4.5 KU-X-Band Data Analysis

##### 4.5.1 Results

4.5.1.1 Thick First-Year Ice. The backscatter from what appeared at the time of measurement to be featureless thick first-year shorefast sea ice was found to be much as expected for frequencies in the 8 to 18 GHz frequency range. As the scatter plots of the angular response of the radar cross-section indicate for the 9, 13, and 17 GHz microwave frequencies (VV) (see Figures 4.5-1 to 4.5-3), the overall angular response was toward a common microwave signature. As discussed in Section 4.4.1.1, this was not the case for backscatter measured at L-Band frequency. At this lower frequency there was an apparent breaking of the microwave signature into separate families. The effect of fading was also demonstrated in the fluctuation in the scatter

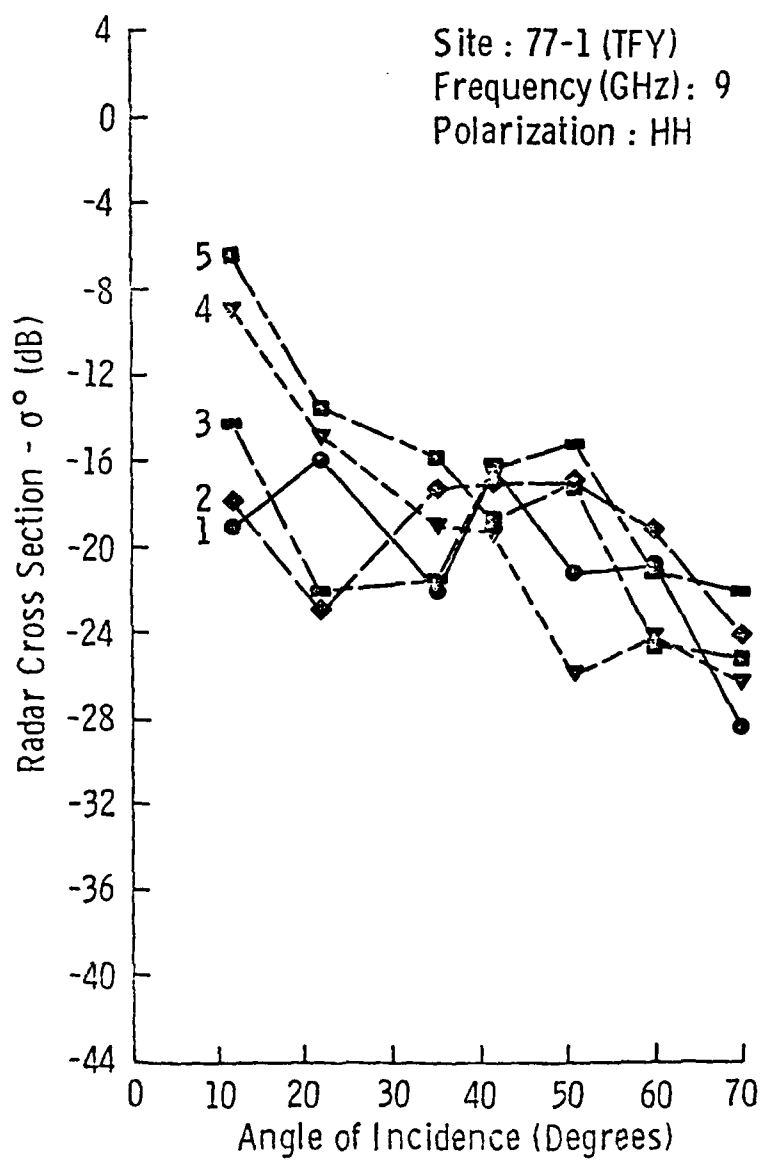


FIGURE 4.5-1 Scatter Plot of the Angular Response of the Radar Cross-Section of Thick First-Year Ice, Site 77-1, at 9 GHz, HH.

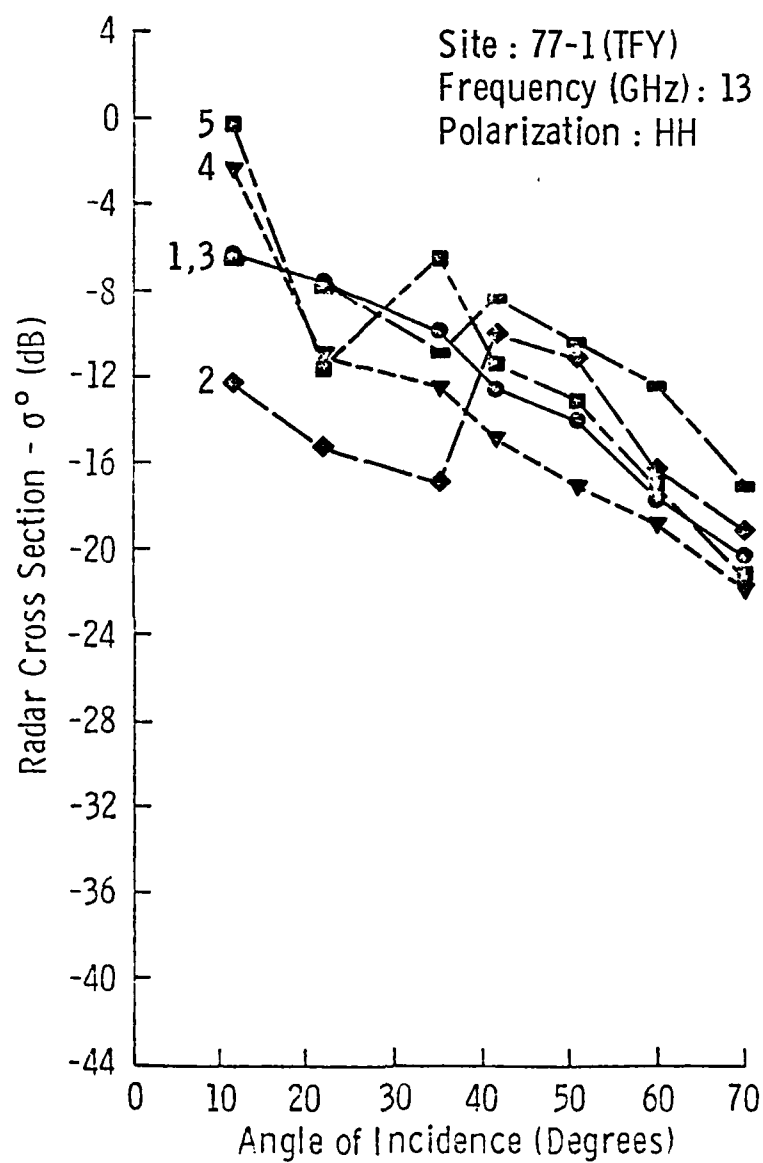


FIGURE 4.5-2 Scatter Plot of the Angular Response of the Radar Cross-Section of Thick First-Year Ice, Site 77-1, at 13 GHz, HH.

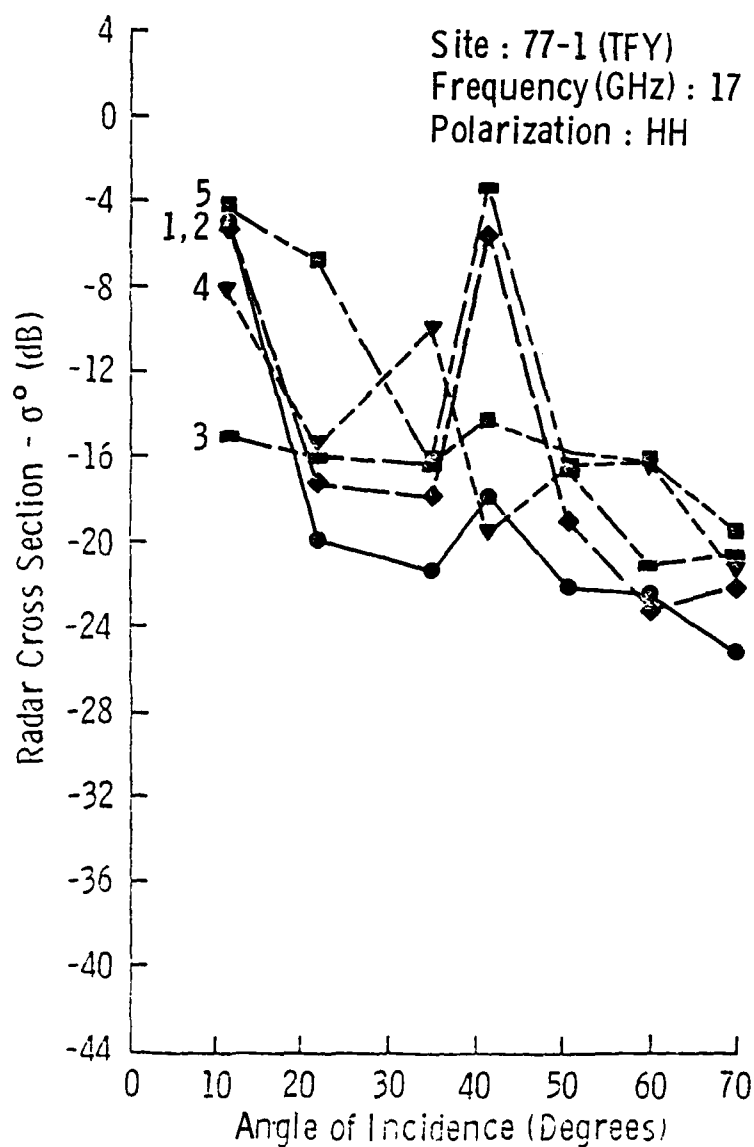


FIGURE 4.5-3 Scatter Plot of the Angular Response of the Radar Cross-Section of Thick First-Year Ice, Site 77-1, at 17 GHz, HH.

between individual looks at the same site. This was illustrated in Figures 4.5-1 to 4.5-3 by linking the individual data points of a given look (orientation of antenna structure). The scatter plots serve to demonstrate the need to obtain numerous independent samples to describe accurately the radar backscatter characteristics of a target, and that a single independent sample is of little value in the description of backscatter properties.

In Site 77-1 an interesting feature does generate some curiosity. At 9 GHz and 17 GHz there is a noticeable increase (2.5 and 8 dB, respectively) in the scattering cross-section at 50° and 40°, respectively. This increase may be explained by the action of the edges of the pancake ice that compose the top few cm of the ice sheet; those may act as corner reflectors, due to the discontinuous surface and the short wavelengths.

Comparisons of the angular response of the average radar scattering cross-section (see equation 4-4 for definition of average  $\sigma^\circ$  response) for HH and VV like-polarizations and an average of the HV and VH cross-polarizations are shown in Figures 4.5-4 to 4.5-6. These average radar cross-sections were also linearly regressed against angle of incidence (outliers were not included in the regression) and the regression line was included in the figures. Results indicate that VV and HH scattering coefficients were very much the same in absolute level and that the linear fit applied well over most of the range of angle of incidence. However, at 17 GHz, scatter for the two like-polarizations (HH and VV) was separated by 4 dB, although the slopes of the straight line fits were nearly identical. It should be noted that small slope differences have very little, if any, significance. For example, in this case, the

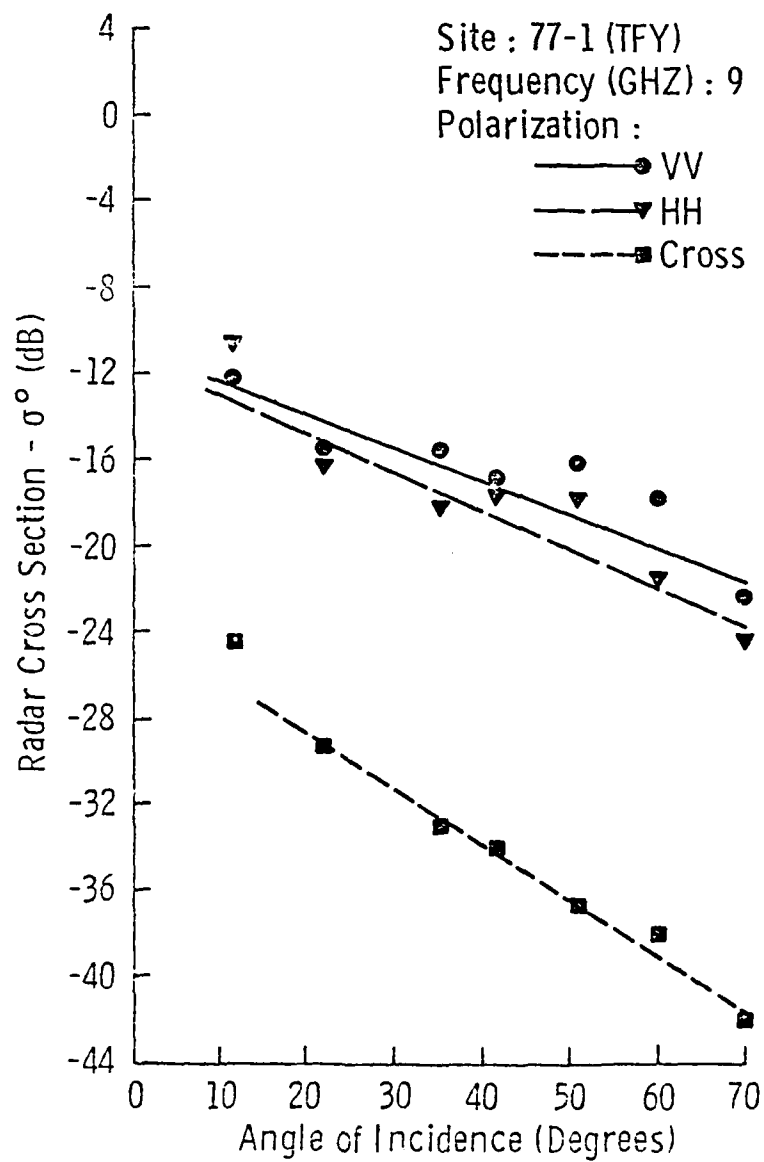


FIGURE 4.5-4 Scattering Coefficient of Thick First-Year Ice, Site 77-1, at 9 GHz.

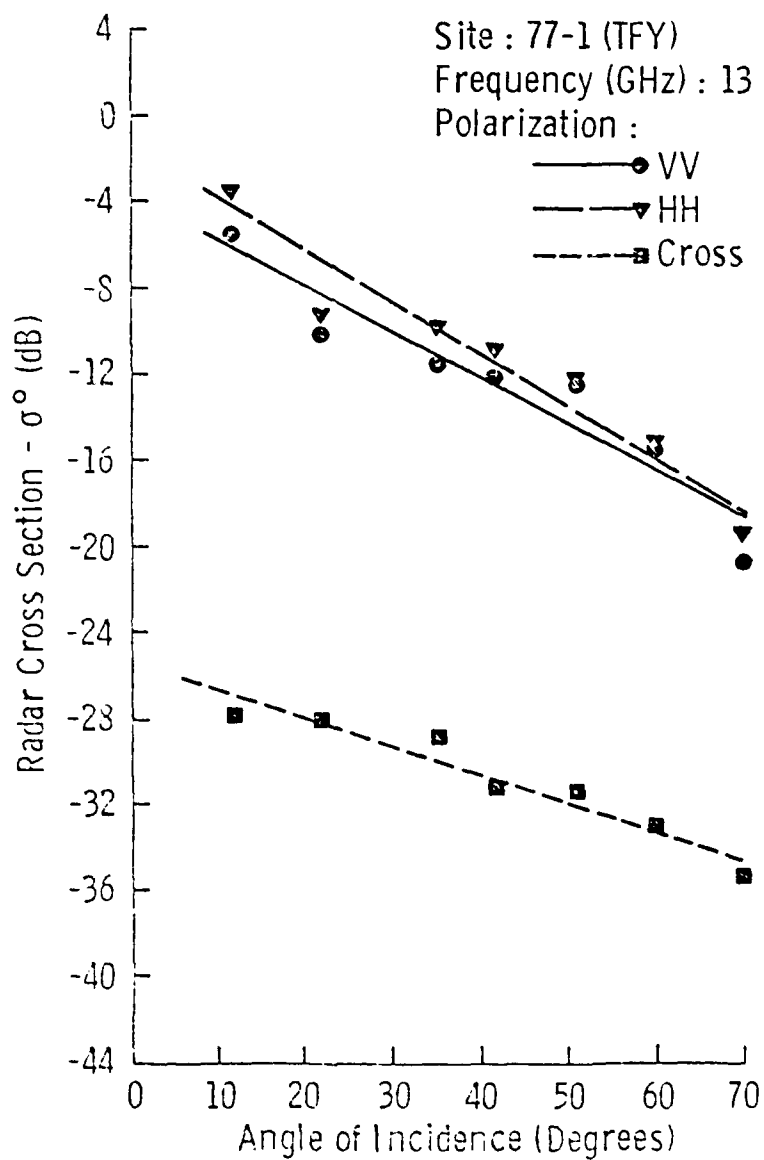


FIGURE 4.5-5 Scattering Coefficient of Thick First-Year Ice, Site 77-1, at 13 GHz.

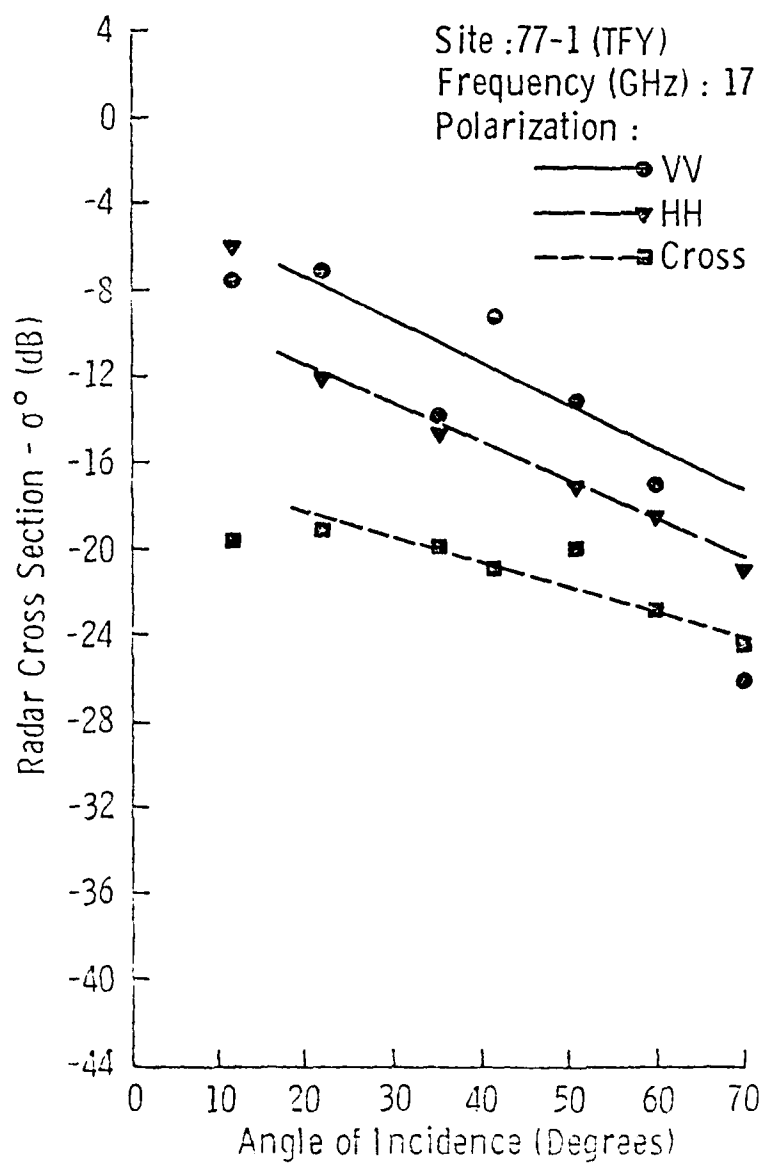


FIGURE 4.5-6 Scattering Coefficient of Thick First-Year Ice, Site 77-1, at 17 GHz.

AD-A007 032

KANSAS UNIV/CENTER FOR RESEARCH INC LAWRENCE REMOTE --ETC F/6 17/9

RADAR BACKSCATTER STUDY OF SEA ICE.(U)

FEB 80 R 6 ONSTOTT, G J DOME, C V DELKER

N00014-76-C-1105

UNCLASSIFIED

CRINC/RSL-TR-331-14

NL

3 OF 3

SLA 14

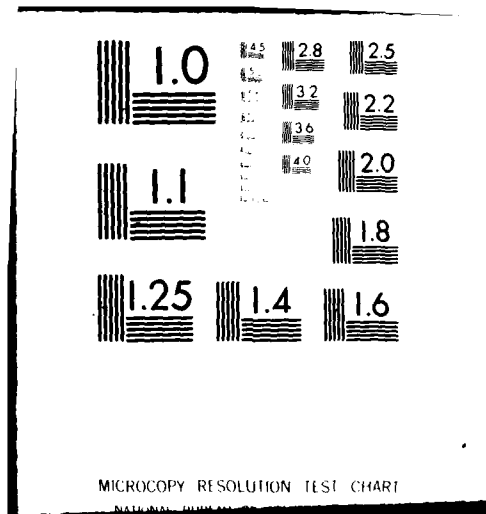


END

DATE

FILED

DTIC



slopes and corresponding intervals of 95% confidence for VV and HH polarizations were  $0.131 \pm .041$  and  $0.196 \pm .086$ , respectively. The scattering coefficient for cross-polarization was found to be very much lower in absolute level than those for like-polarizations. This separation of level was 16, 14 and 7 dB at  $40^\circ$  for 9, 13, and 17 GHz, respectively. This may indicate that, as frequency increased, the depolarizing mechanism of the medium becomes more significant.

Like-polarization (HH and VV) and averaged cross-polarization returns for Site 77-3 are shown in Figures 4.5-7 to 4.5-9. Interval bars are also included to show the maximum deviation about the average VV return. Deviations from the average for HH and cross-polarizations were found to behave very much the same as the deviations found in the VV case. The angular response was again found to be well-fitted with a straight line between the angles of  $20^\circ$  and  $70^\circ$ .

Scatter for the two like-polarizations followed very much the same angular response, but exhibited differences in absolute levels of 2 to 3 dB between VV and HH. Scatter for cross-polarization was found to be well-separated from the like-polarization scatter - by 13, 13.5, and 10 dB at  $40^\circ$  for 9, 13, and 17 GHz, respectively. The cross-polarization angular response also showed a slope that was consistently less than the slope of the like-polarization response.

The radar scattering cross-sections of shorefast thick first-year sea ice with natural snow cover measured at the one major site in 1978, Site 78, are shown in Figures 4.5-10 to 4.5-12. The angular response of the scatter was found to be reasonably well fit with a straight line. This fit was usually found to be good from  $20^\circ$  to  $70^\circ$ , but in many instances it was a very good fit in to  $12^\circ$  (9 GHz, 13 GHz-VV, 9 GHz-

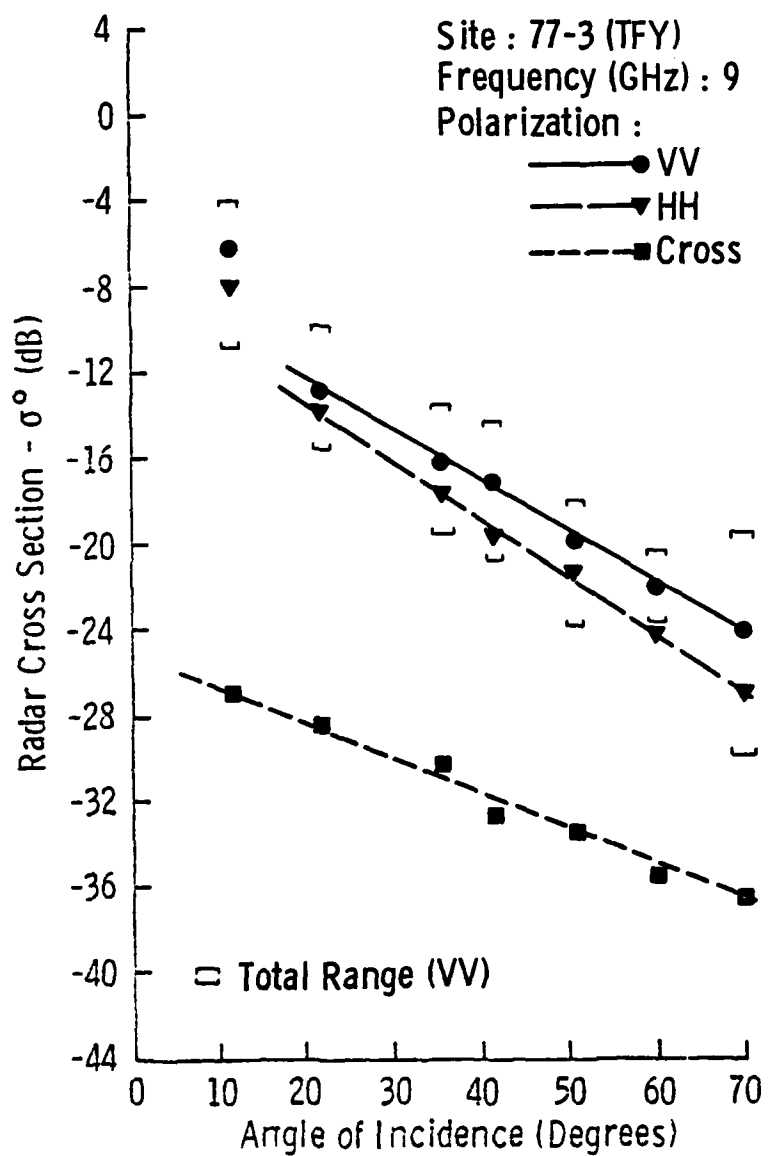


FIGURE 4.5-7 Scattering Coefficient of Thick First-Year Ice, Site 77-3, at 9 GHz.

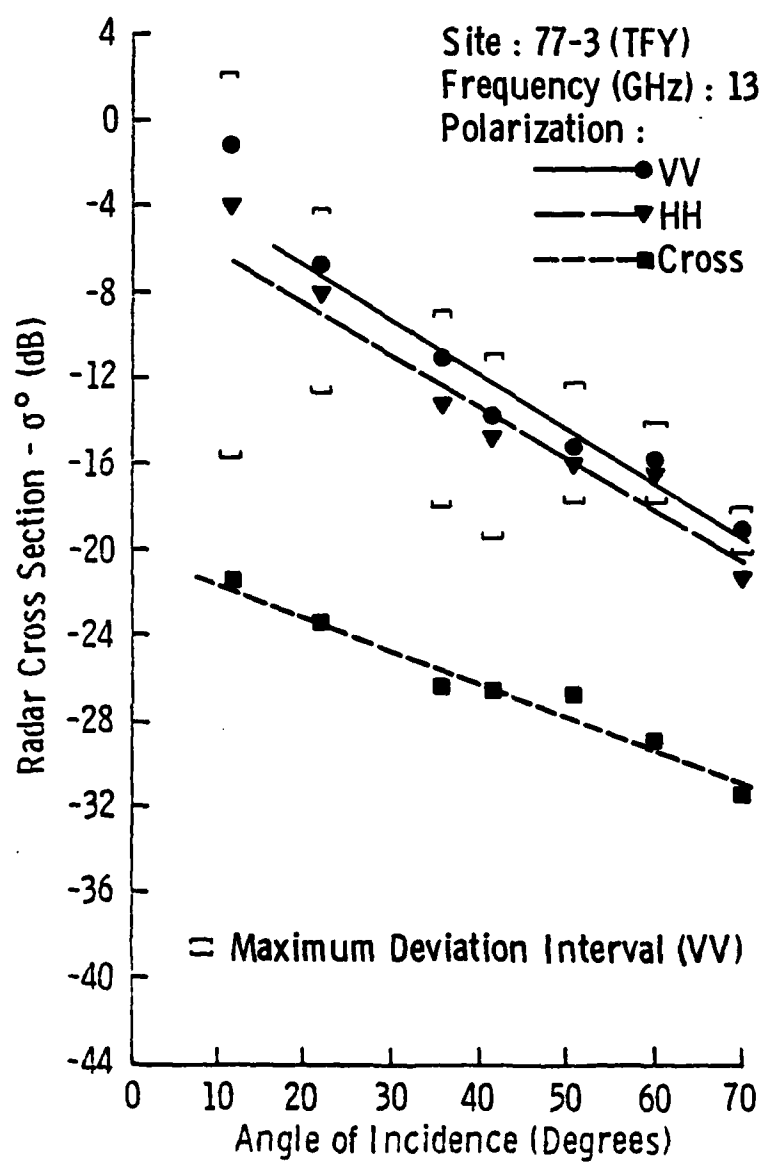


FIGURE 4.5-8 Scattering Coefficient of Thick First-Year Ice, Site 77-3, at 13 GHz.

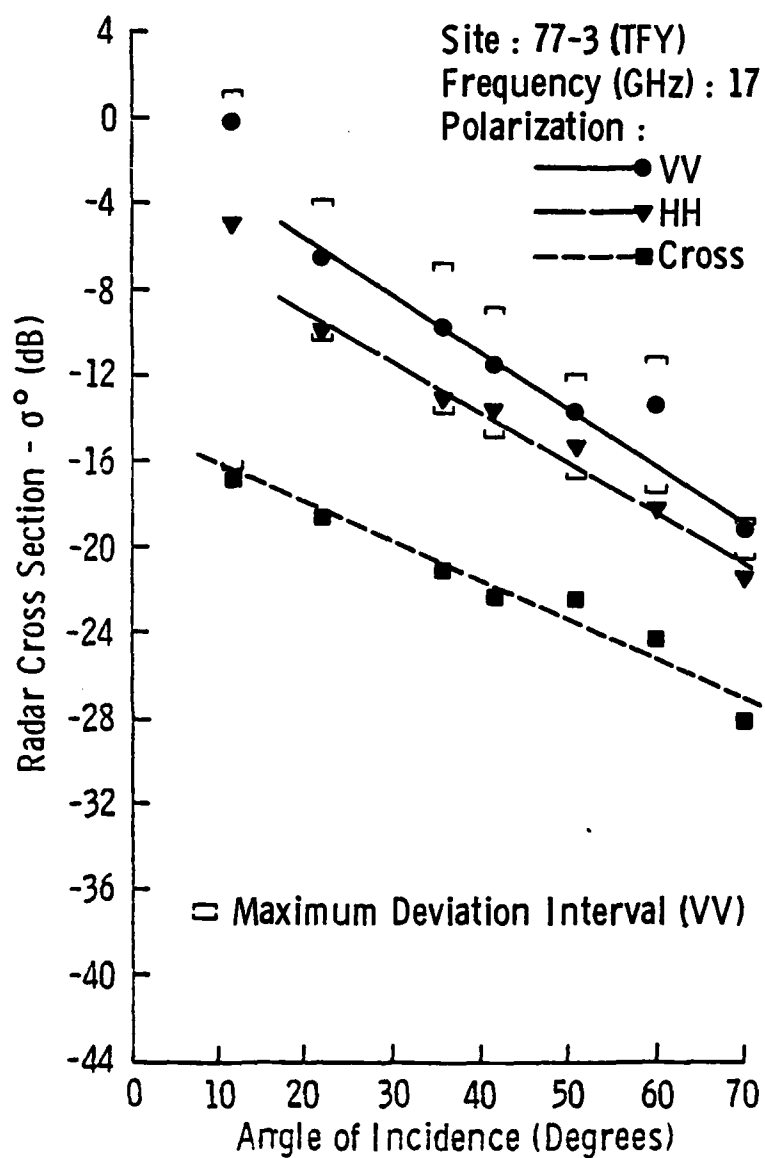


FIGURE 4.5-9 Scattering Coefficient of Thick First-Year Ice, Site 77-3, at 17 GHz.

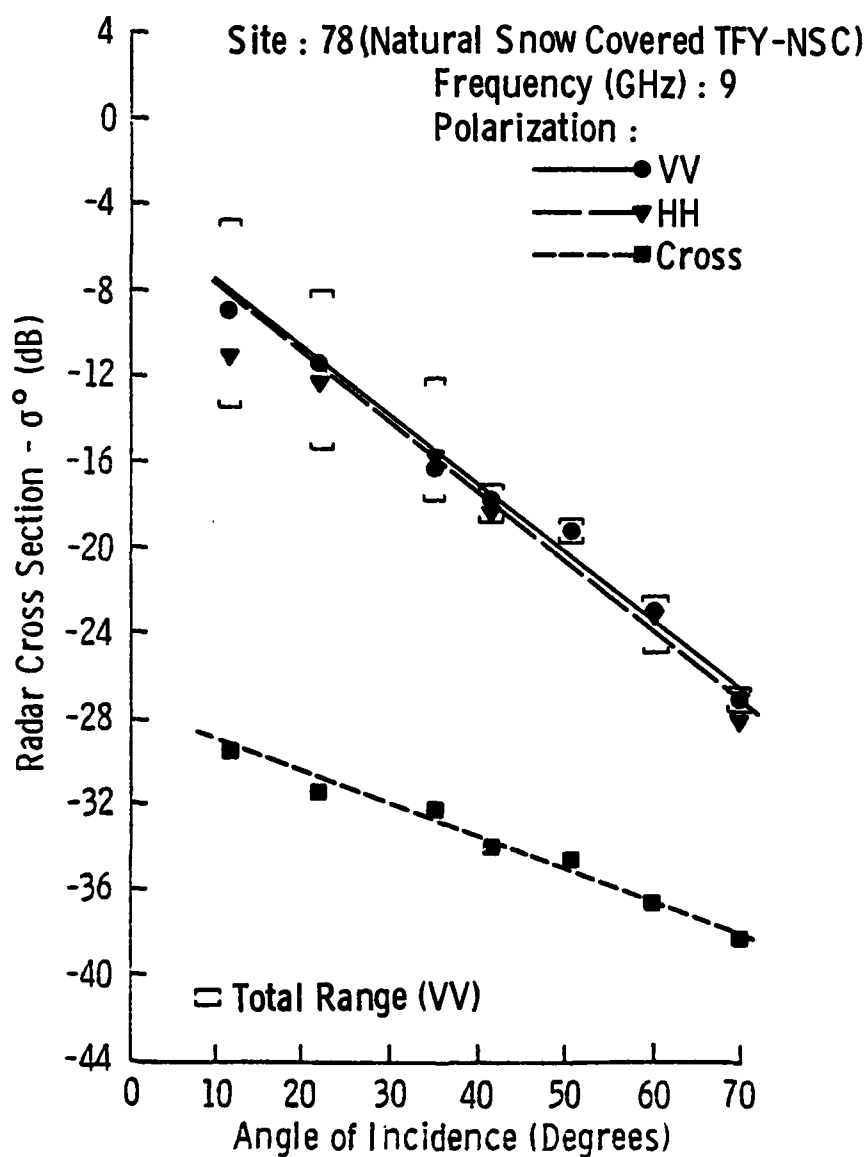


FIGURE 4.5-10 Scattering Coefficient of Thick First-Year Ice with Natural Snow Cover, Site 7, at 9 GHz.

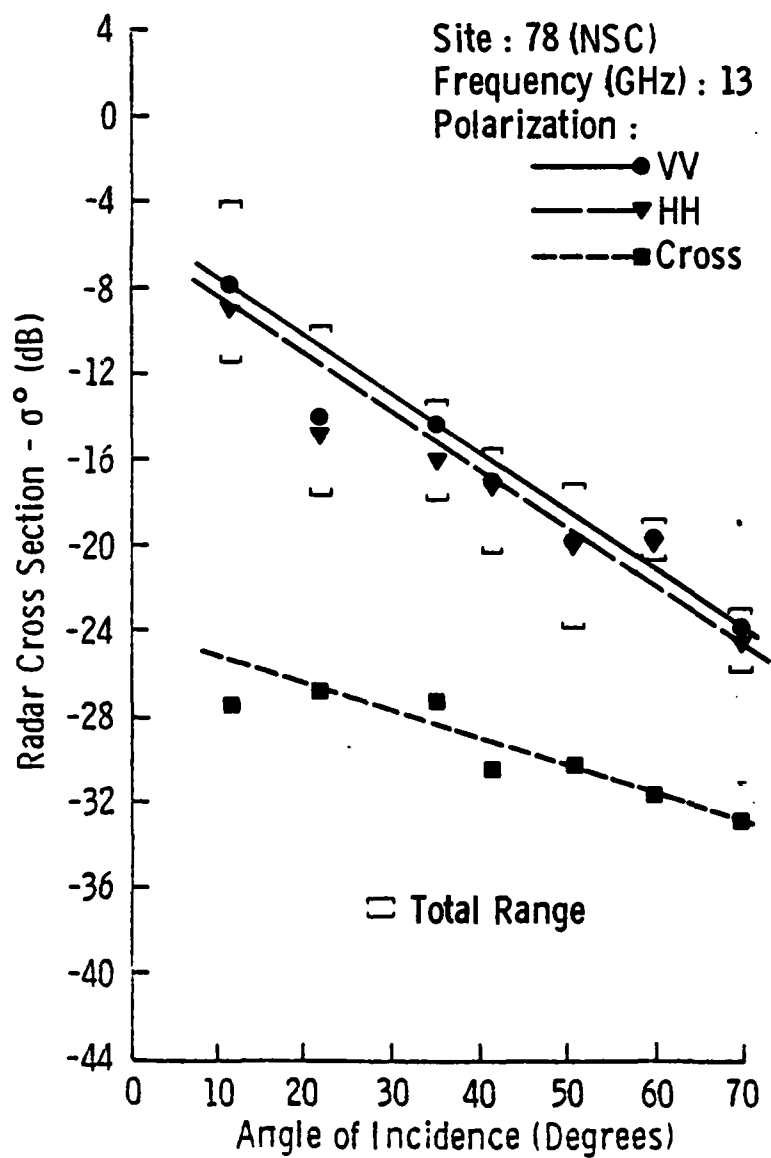


FIGURE 4.5-11 Scattering Coefficient of Thick First-Year Ice with Natural Snow Cover, Site 78, at 13 GHz.

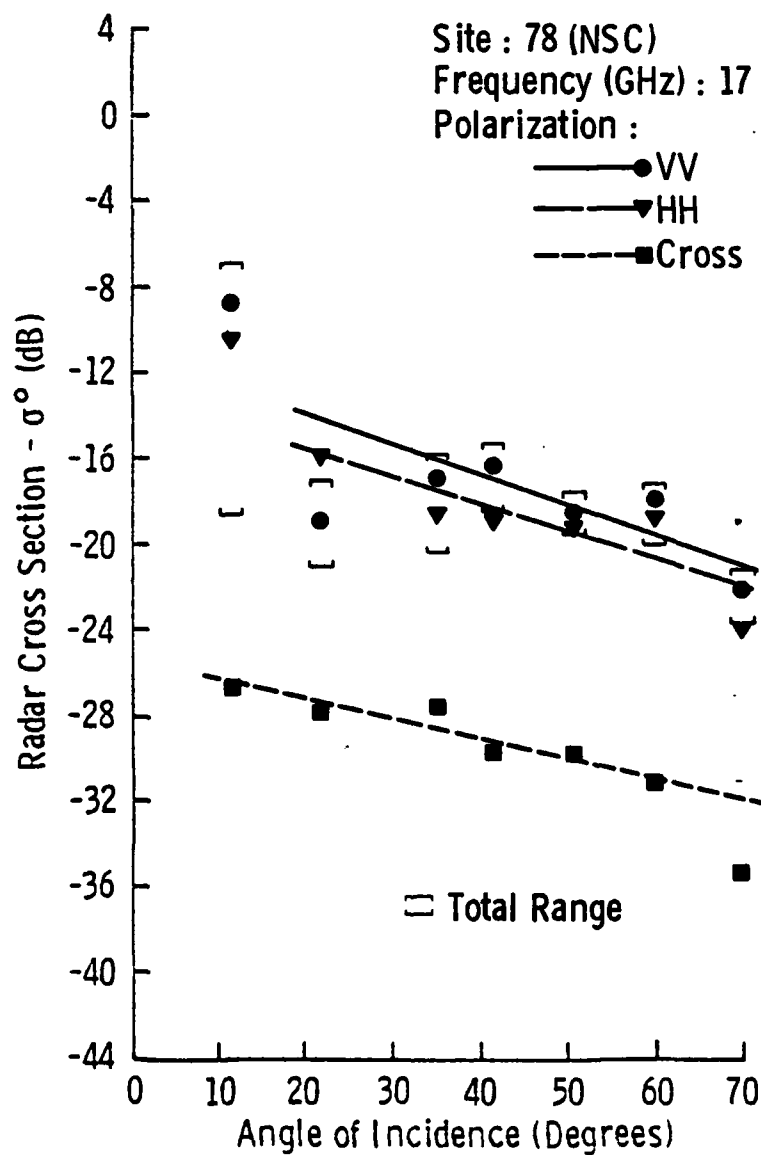


FIGURE 4.5-12 Scattering Coefficient of Thick First-Year Ice with Natural Snow Cover, Site 78, at 17 GHz.

Cross, 13 GHz-HH, and 17 GHz-Cross). The like-polarization angular response of VV and HH had nearly the same slopes, but differed in absolute level (0.5, 1.5, and 2.0 dB for 9, 13 and 17 GHz, respectively). Again, cross-polarization scatter exhibited slopes that were slightly less steep than the slopes of like-polarization. Separations between like (HH) and cross-polarization (HV) were found to be 16, 12, and 11 dB at 40° for 9, 13, and 17 GHz, respectively.

Comparisons of Site 77-1, Site 77-3, and Site 78 at 9, 13, and 17 GHz (HH) are shown in Figures 4.5-13 to 4.5-15. The overall comparison of the three angular responses for the three thick first-year sea ice sites of slightly different origins shows similar absolute levels and similar slopes. Site 78 was found to have an absolute level that was consistently lower than the levels found in the other two sites. It had an angular response that was fairly well-behaved (with respect to the regressed straight line). The angular response of Site 77-3 was also well-behaved, but the angular response of Site 77-1 varied greatly about its straight line fit.

4.5.1.2 Small Thick First-Year Pressure Ridge. The angular response of the radar cross-section (HH, VV, and Cross) at 13 GHz is shown in Figure 4.5-16. Responses for HH and VV like-polarizations were very much the same with nearly identical slopes, although separated in absolute level by 3 dB. Returns at 70° were much lower than the returns at all other angles and fell significantly away from the trend line. This response may possibly be peculiar to the geometry of the measurement scheme and the pressure ridge itself.

4.5.1.3 Multiyear Ice. The average angular response (with deviations) of the radar backscatter cross-section of multiyear ice, Site

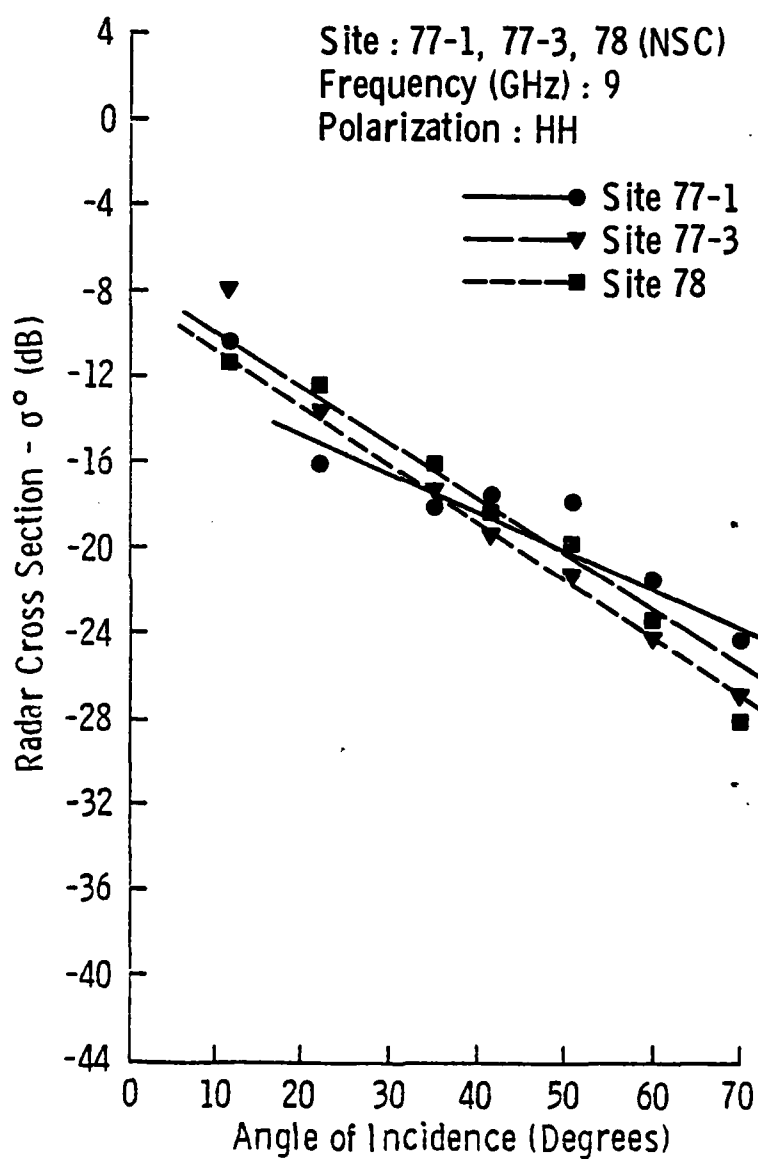


FIGURE 4.5-13 A Comparison of the Scattering Coefficients of Thick First-Year Sea Ice for Sites 77-1, 77-3, and 78 at 9 GHz, HH.

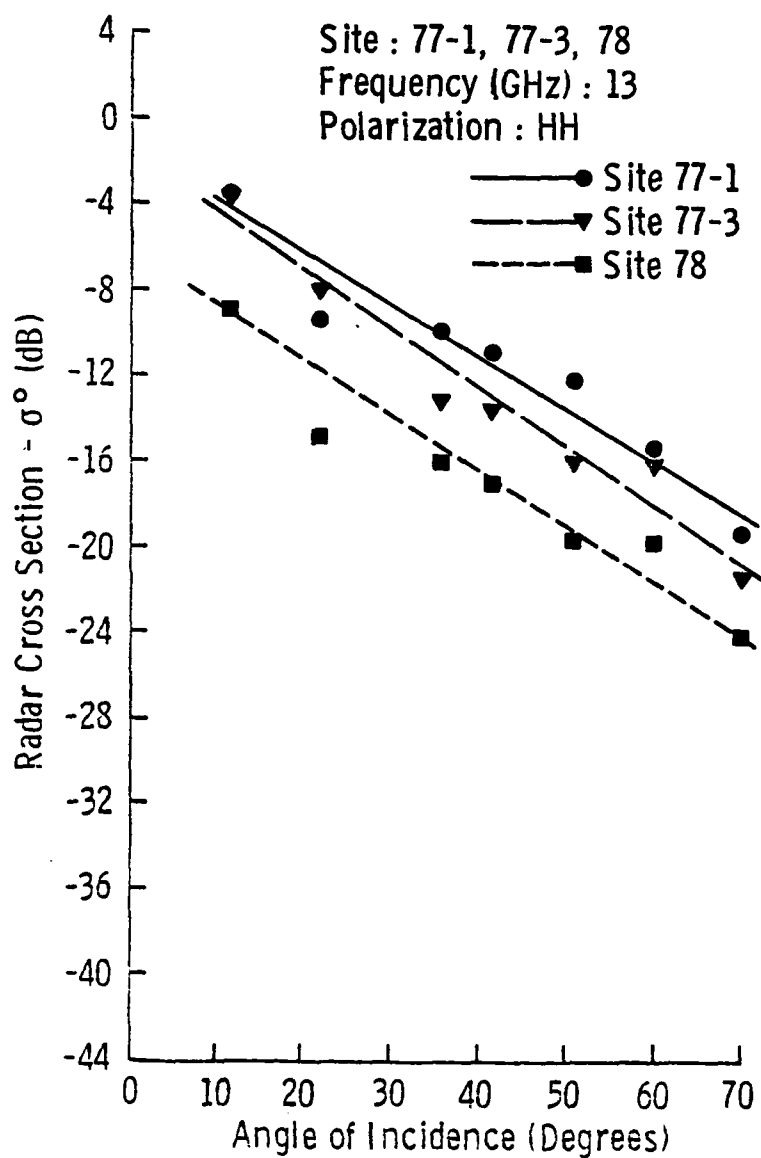


FIGURE 4.5-14 A Comparison of the Scattering Coefficients of Thick First-Year Sea Ice for Sites 77-1, 77-3, and 78 at 13 GHz, HH.

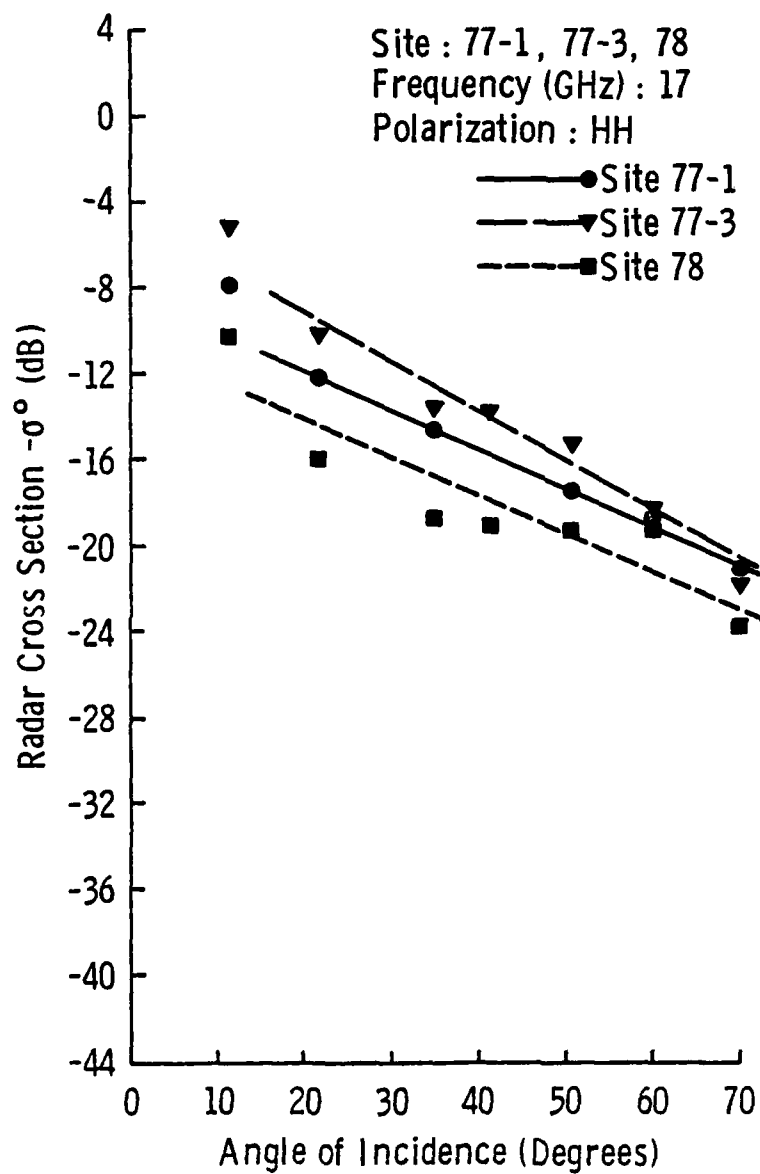


FIGURE 4.5-15 A comparison of the scattering coefficients of thick first-year sea ice for Sites 77-1, 77-3, 78 at 17 GHz, HH.

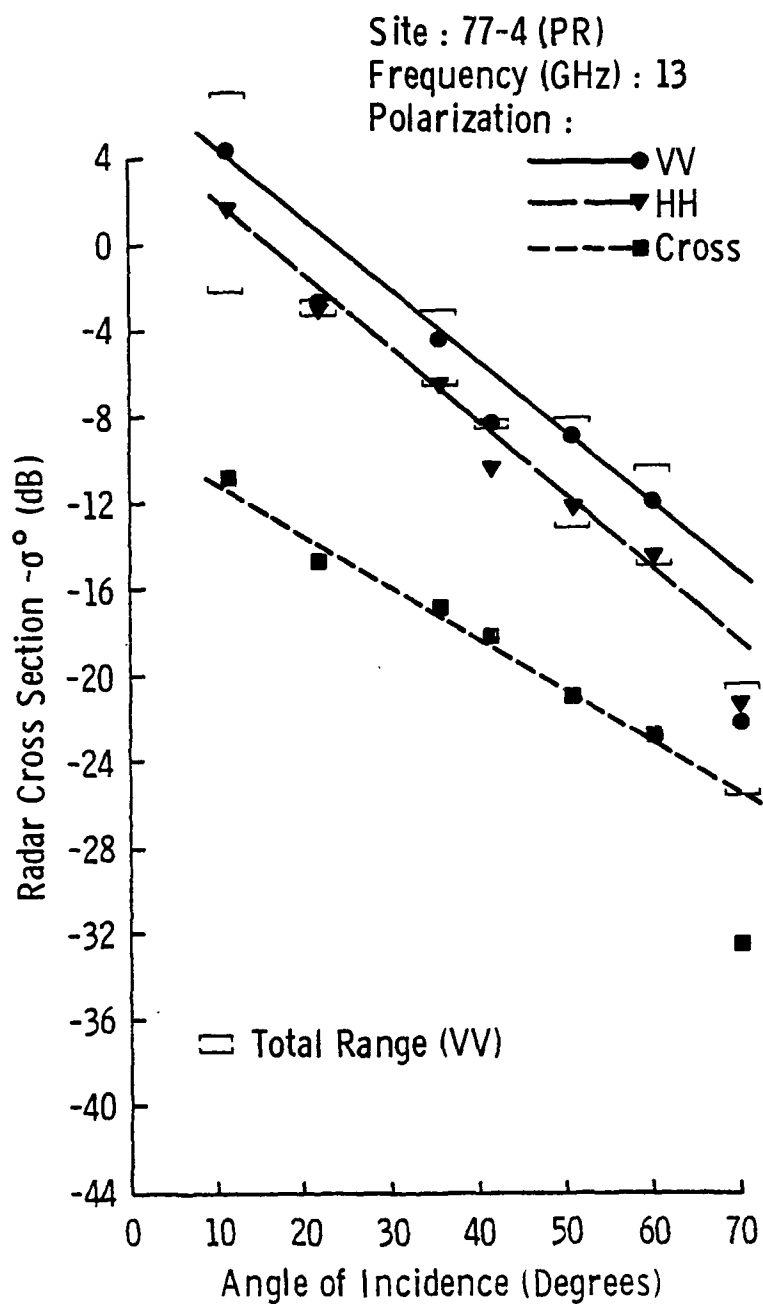


FIGURE 4.5-16 Scattering coefficient of a small thick first-year pressure ridge, Site 77-4, at 13 GHz.

77-2 and Site 77-5, is shown for 9, 13, and 17 GHz (HH) in Figures 4.5-17 to 4.5-19.

The scattering coefficients from the two fragments of multiyear ice overlap reasonably well. This is interesting because these two sites were examples of two different kinds of surface roughness that may occur in multiyear ice. Site 77-2 was of a large hummock formation (a large amplitude and prominent rolling feature) while Site 77-5 would be described as having rolling features of small amplitude. The higher the frequencies the greater was the spread between the average microwave signatures (1.5, 2, and 4 dB at 40° and 9, 13, and 17 GHz, respectively).

4.5.1.4 Lake Ice. Average scatter for lake ice with an underlying layer of water, Site 77-6, is shown in Figures 4.5-20 to 4.5-22. Results were fit with a linear regression of all or selected data points. Both like-polarizations exhibited almost identical slopes, but they showed separations in absolute level of 2.5, 1.5, and 3.2 dB at 9, 13, and 17 GHz, respectively. Again, the cross-polarization response showed a smaller slope than the like-polarization responses, and they were separated in absolute level at 40° by 8, 11, and 6 dB for 9, 13, and 17 GHz, respectively. Interestingly, there was a significant drop in return strength for all polarizations at 70° (1, 3, and 2 dB at 9, 13, and 17 GHz, respectively).

Scatter for lake ice which was frozen to its mud bottom, Site 77-7, is shown in Figures 4.5-23 to 4.5-25. The angular responses were linear in shape, this being especially true at angles of incidence from 35° to 70°. HH and VV responses were nearly identical, with separation in absolute level being less than one dB throughout the frequency range.

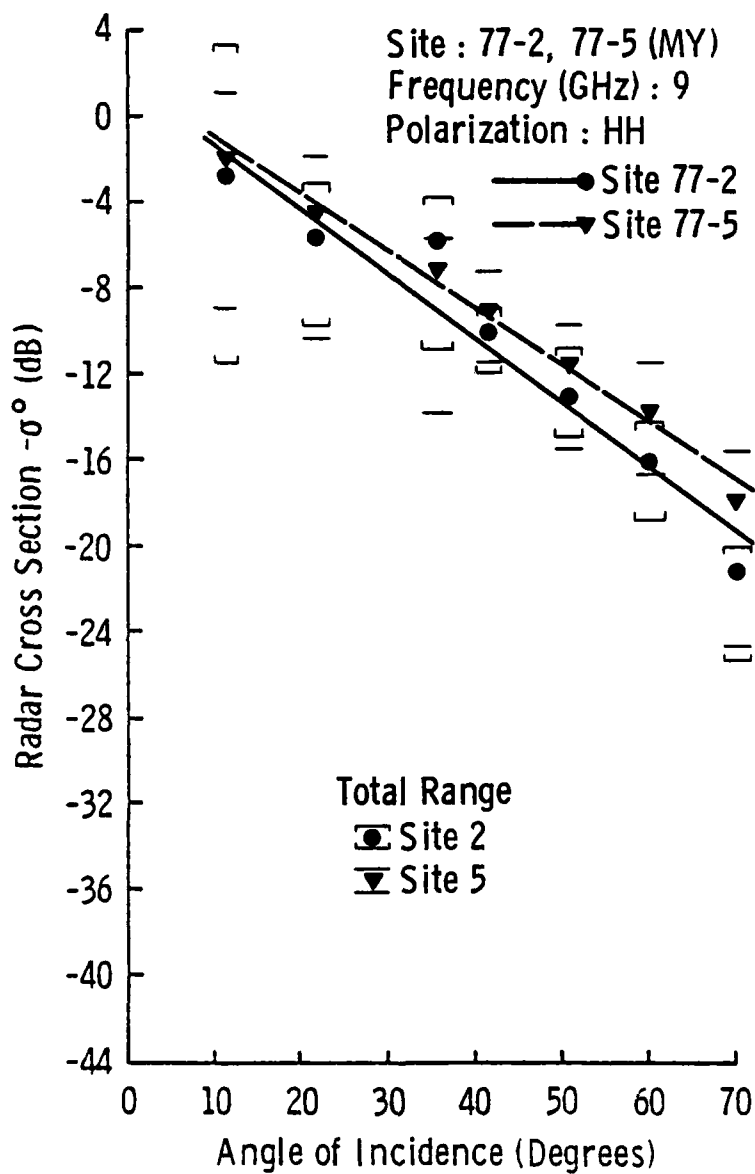


FIGURE 4.5-17 Scattering Coefficient Of Multiyear Ice, Site 77-2 and Site 77-5, at 9 GHz, HH.

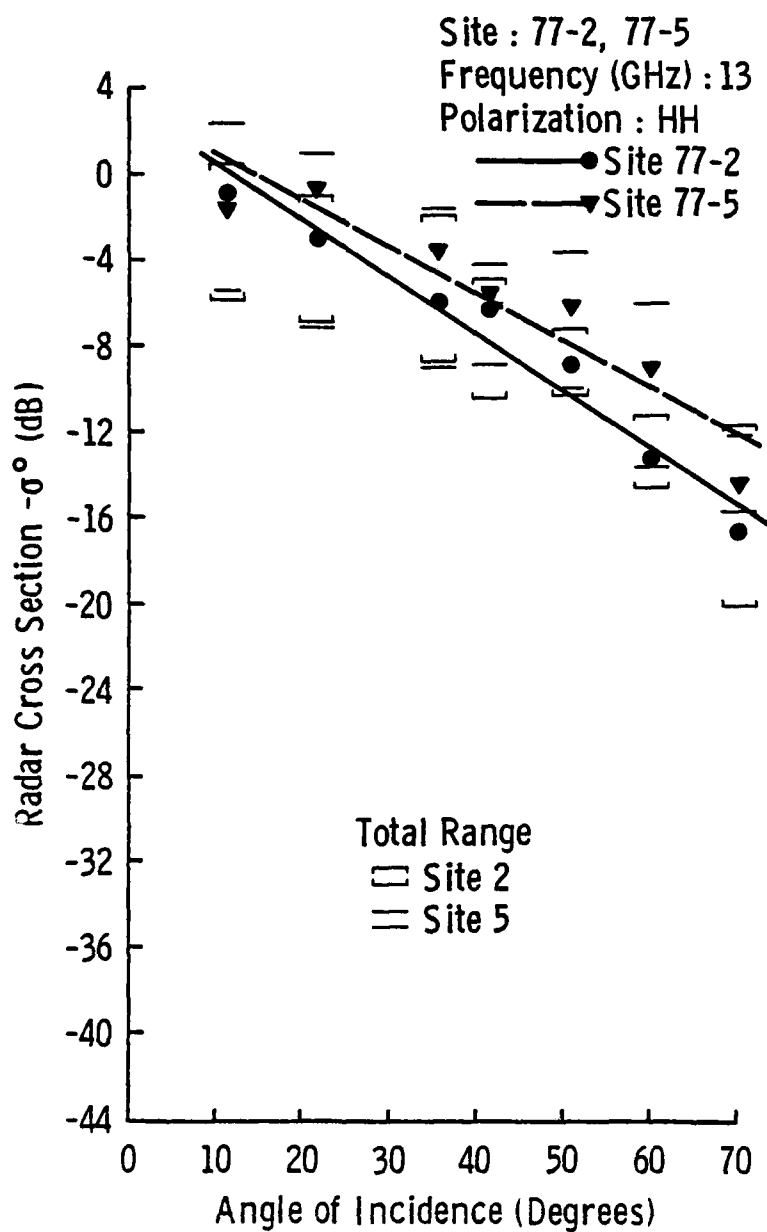


FIGURE 4.5-18 Scattering coefficient of multiyear ice, Site 77-2 and Site 77-5, at 13 GHz, HH.

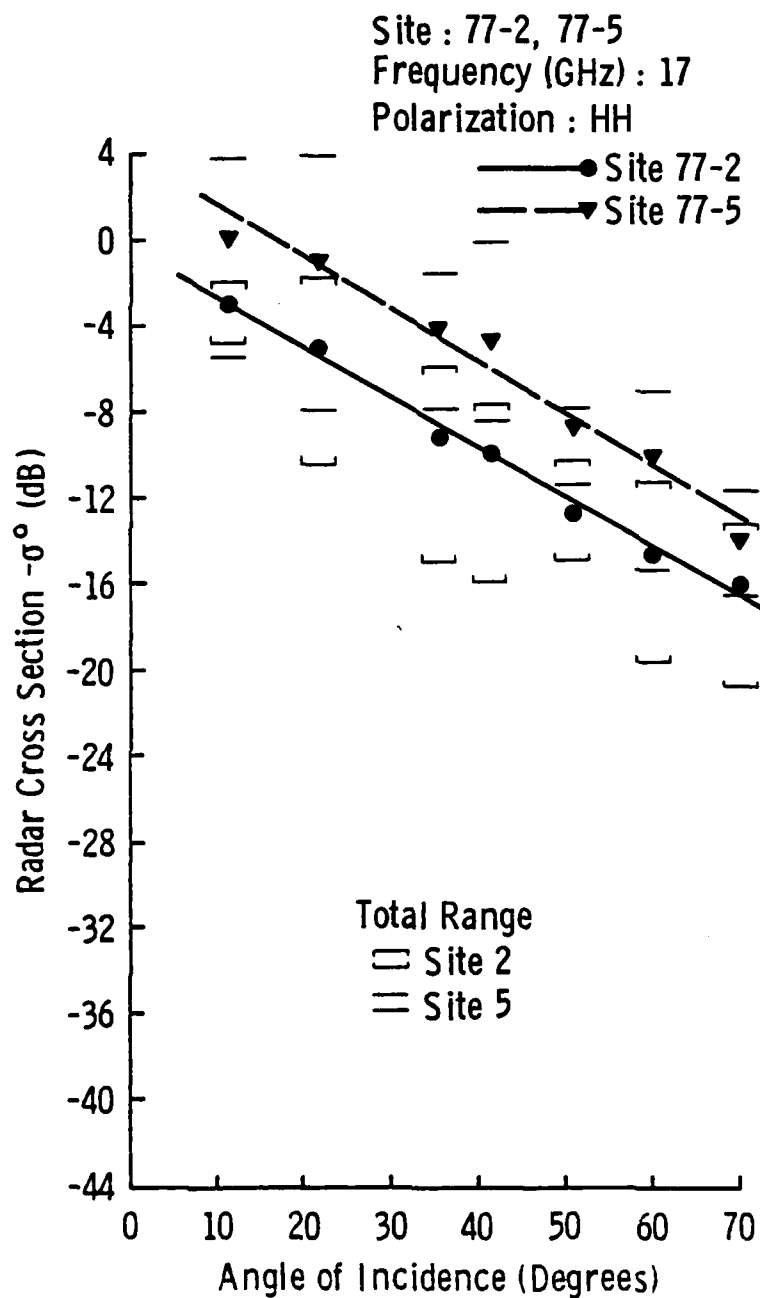


FIGURE 4.5-19 Scattering coefficient of multiyear ice, Site 77-2 and 77-5, at 17 GHz.

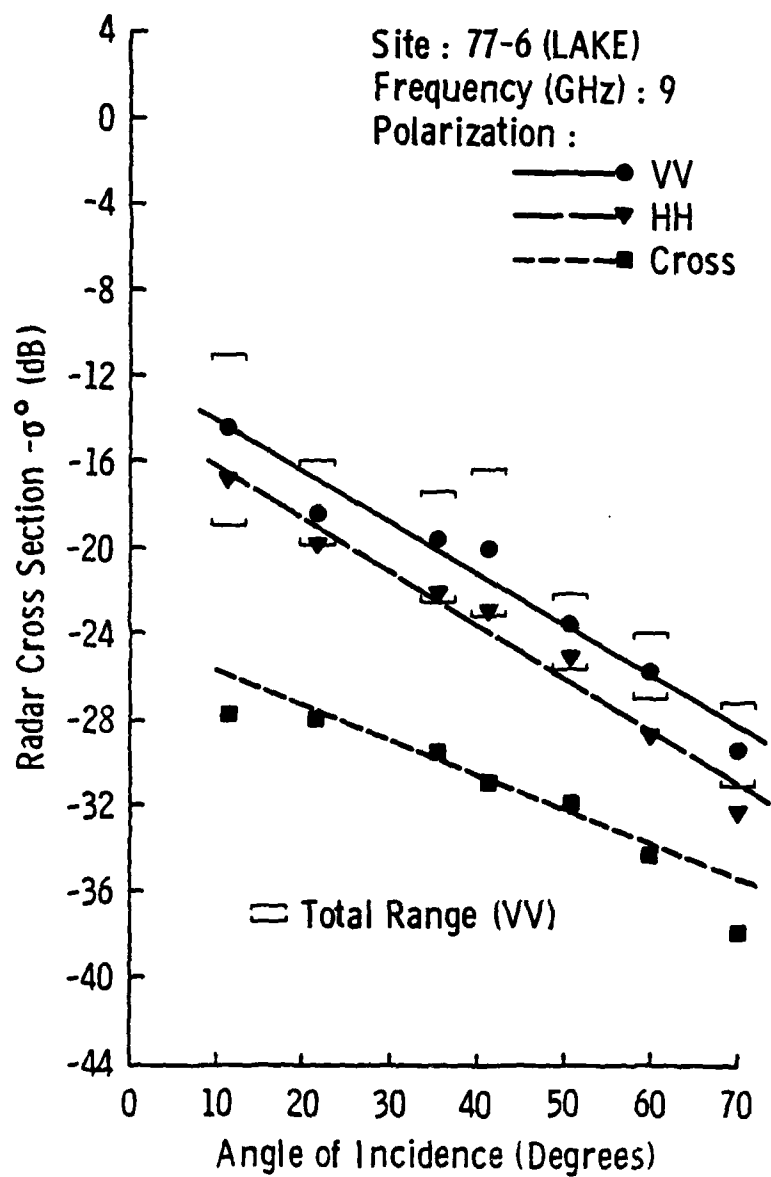


FIGURE 4.5-20 Scattering coefficient of lake ice with underlying layer of water, Site 77-6, at 9 GHz.

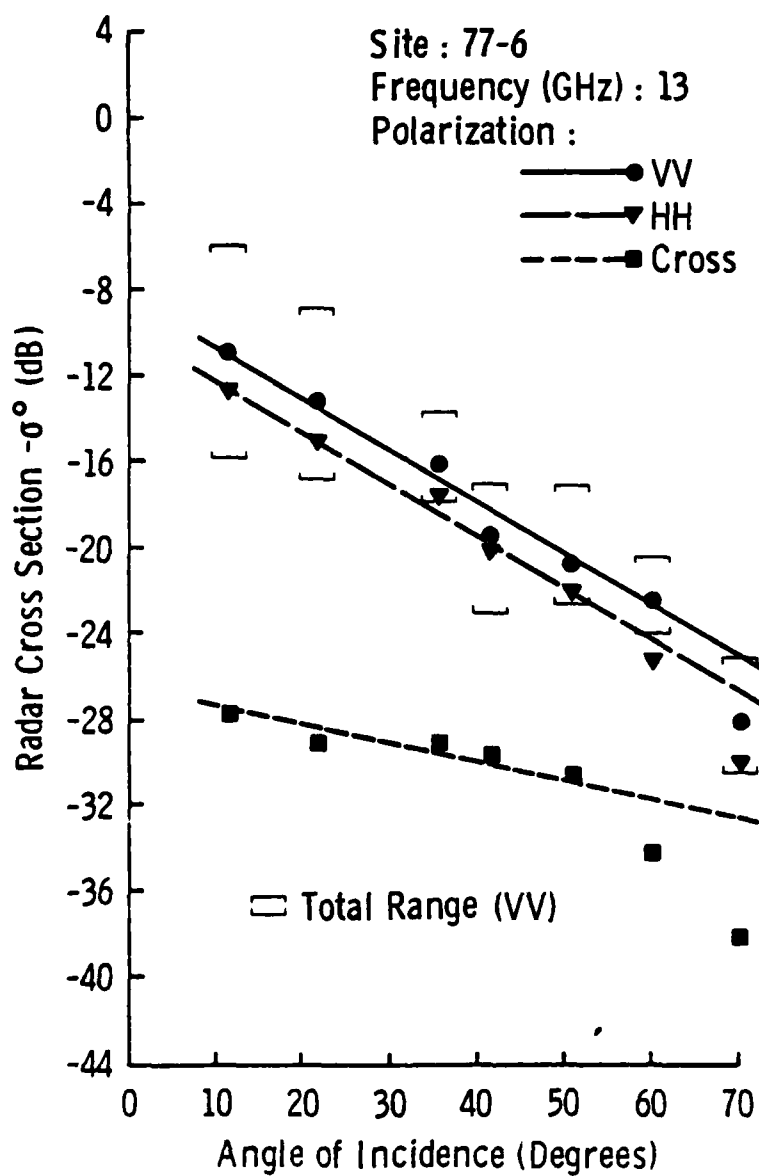


FIGURE 4.5-21 Scattering coefficient of lake ice with underlying layer of water, Site 77-6, at 13 GHz.

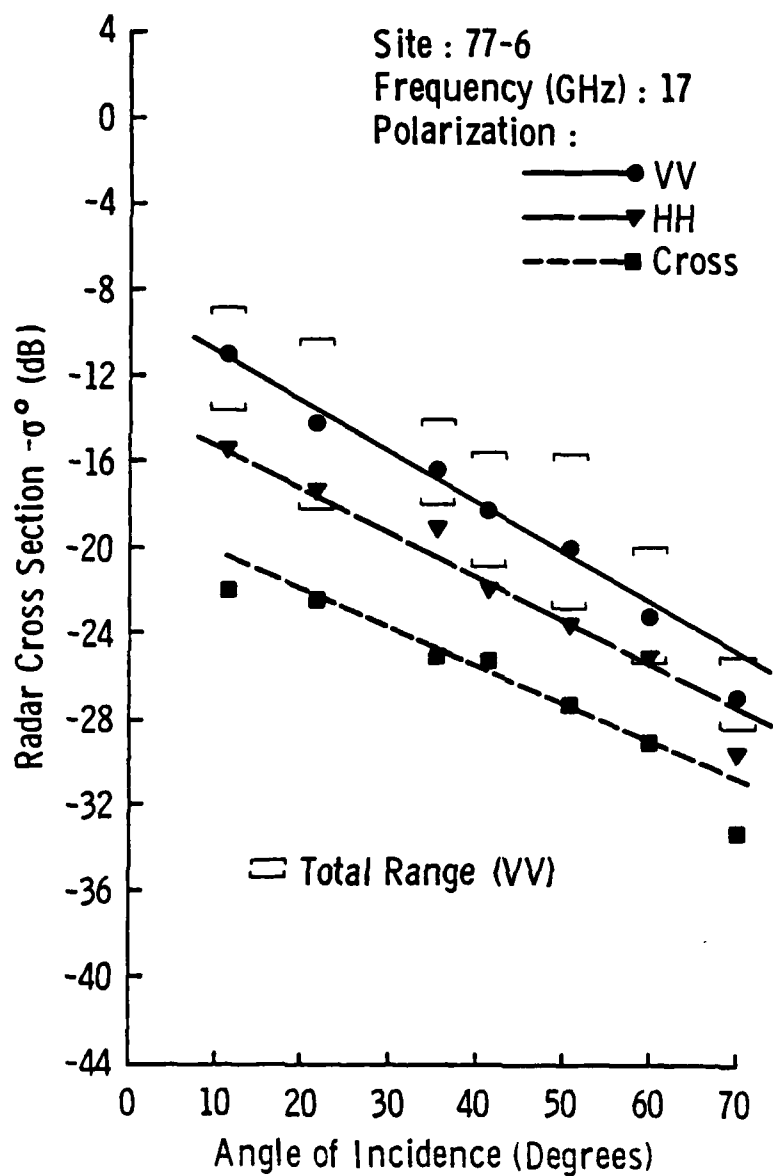


FIGURE 4.5-22 Scattering coefficient of lake ice with underlying layer of water, Site 77-6, at 17 GHz.

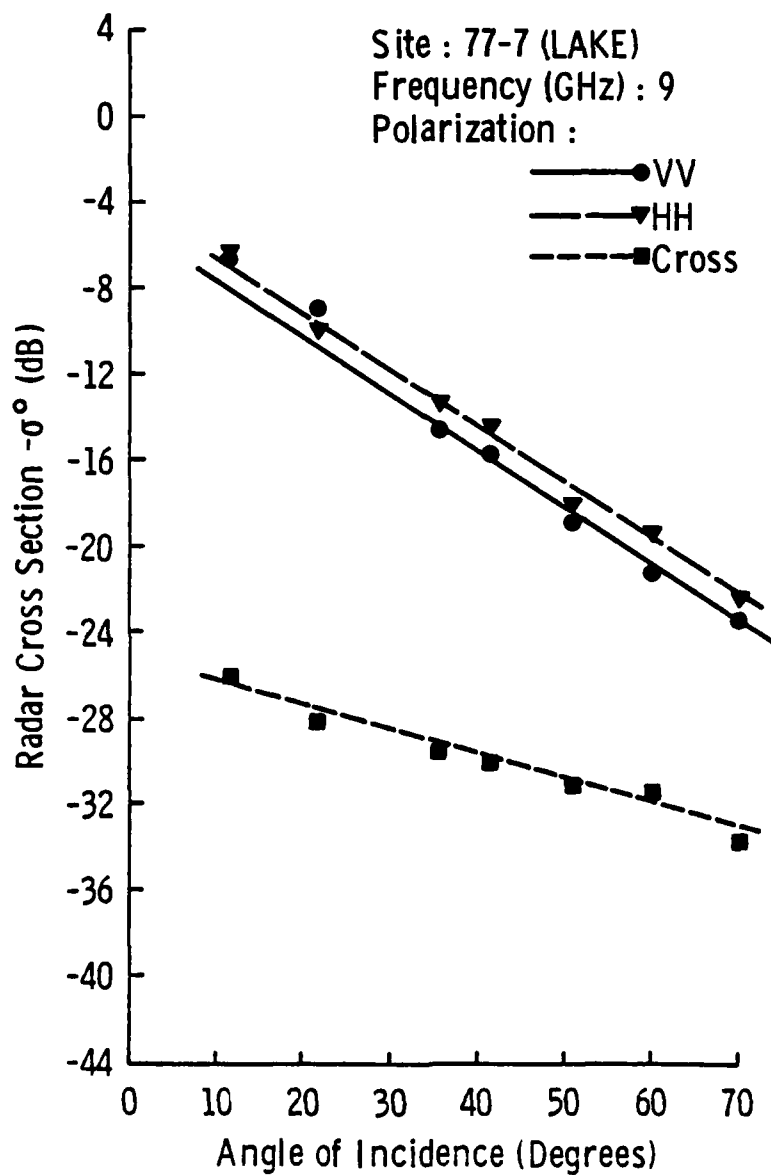


FIGURE 4.5-23 Scattering coefficient of lake ice frozen to its mud bottom, Site 77-7, at 9 GHz.

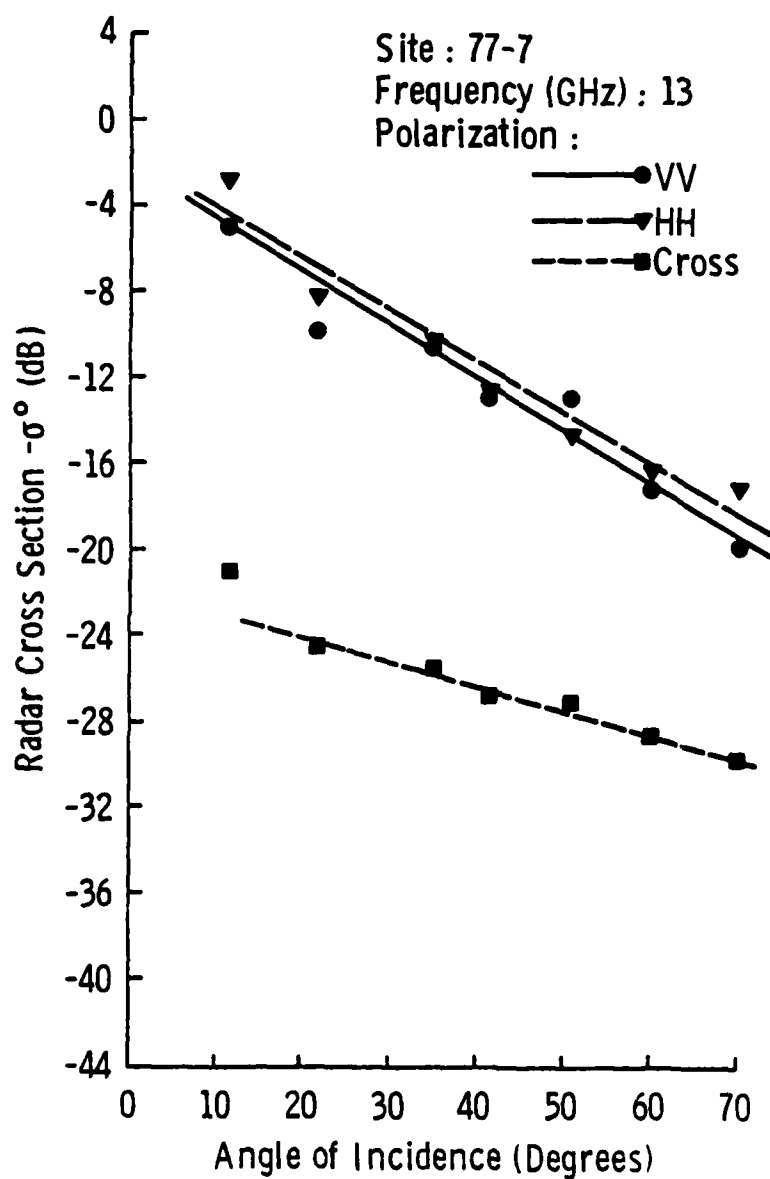


FIGURE 4.5-24 Scattering coefficient of lake ice frozen to its mud bottom, Site 77-7, at 13 GHz.

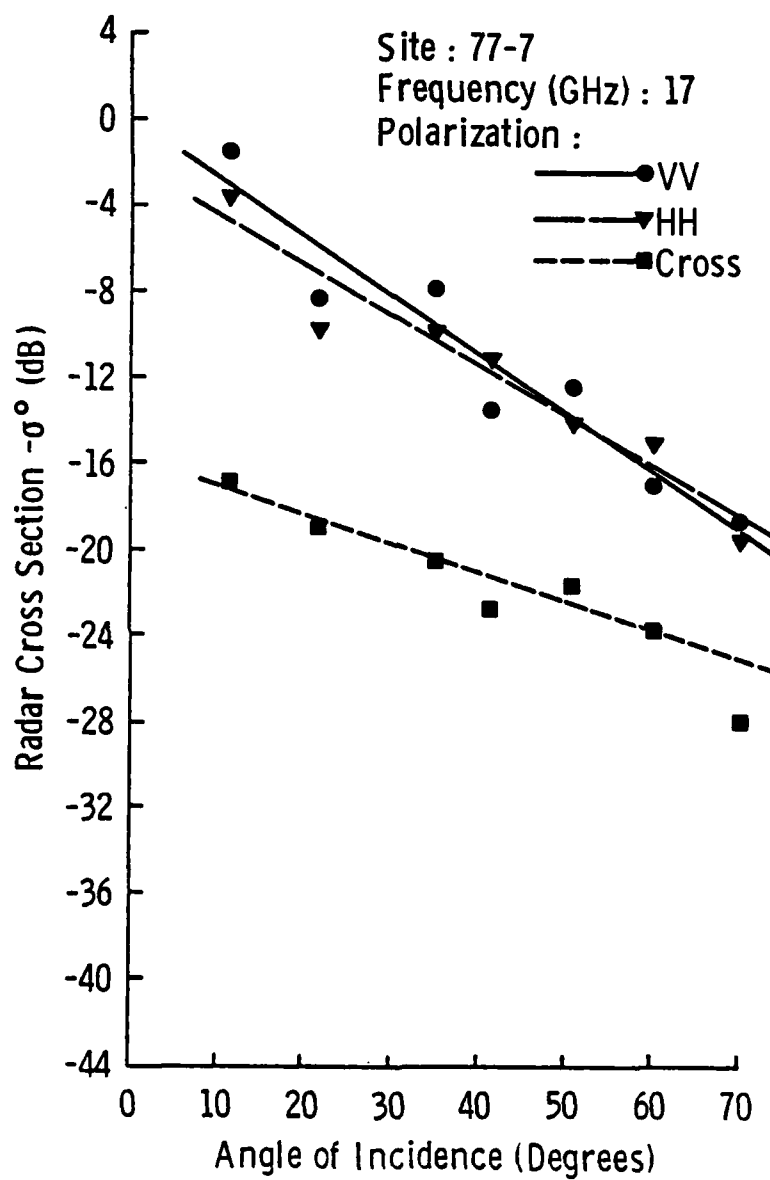


FIGURE 4.5-25 Scattering coefficient of lake ice frozen to its mud bottom, Site 77-7, at 17 GHz.

The cross-polarization response had a slope that was smaller than those for the like-polarization cases. Cross-polarization scatter was also well-separated from like-polarization scatter (14, 14, and 10 dB for 9, 13, and 17 GHz, respectively).

Comparison of VV scatter for Site 77-6 and Site 77-7 (see Figures 4.5-26 to 4.5-28) shows a wide separation between coefficients for these ice categories (5, 6, and 7 dB for 9, 13, and 17 GHz, respectively). In all cases, the return from the lake which was frozen to its mud bottom, which also had a heavy snow cover and higher air and ice temperatures, was found to be the higher. Response trends for 9 and 13 GHz show that both sites had responses that were nearly identical in slope but were separated in absolute level. Cross-polarization scatter from the two sites were not separated as dramatically as for the like-polarization case (1.3, 3.5, and 4 dB at 40° for 9, 13, and 17 GHz, respectively).

#### 4.5.2 Comparison of Scattering Coefficients

Mean scattering coefficient trends of thick first-year and multi-year ice for frequencies in the Ku-X band microwave region are compared in Figures 4.5-29 to 4.5-31. The radar parameters are 9, 13, and 17 GHz frequencies and HH, HV, and VV transmit-receive polarizations. The angular response at 9 GHz is shown in Figure 4.5-29. The minimum spread (HH) which separated returns from these ice types was 6 dB allowing them to be discriminated at all polarizations and angles. Cross-polarization provided the best discrimination, affording 12 dB of separation, which was independent of incidence angle from 20° to 70°. VV polarization was slightly better than HH, afforded 8 dB of separation, and was best from 20° to 45°. The 13 GHz response was similar (Figure 4.5-30).

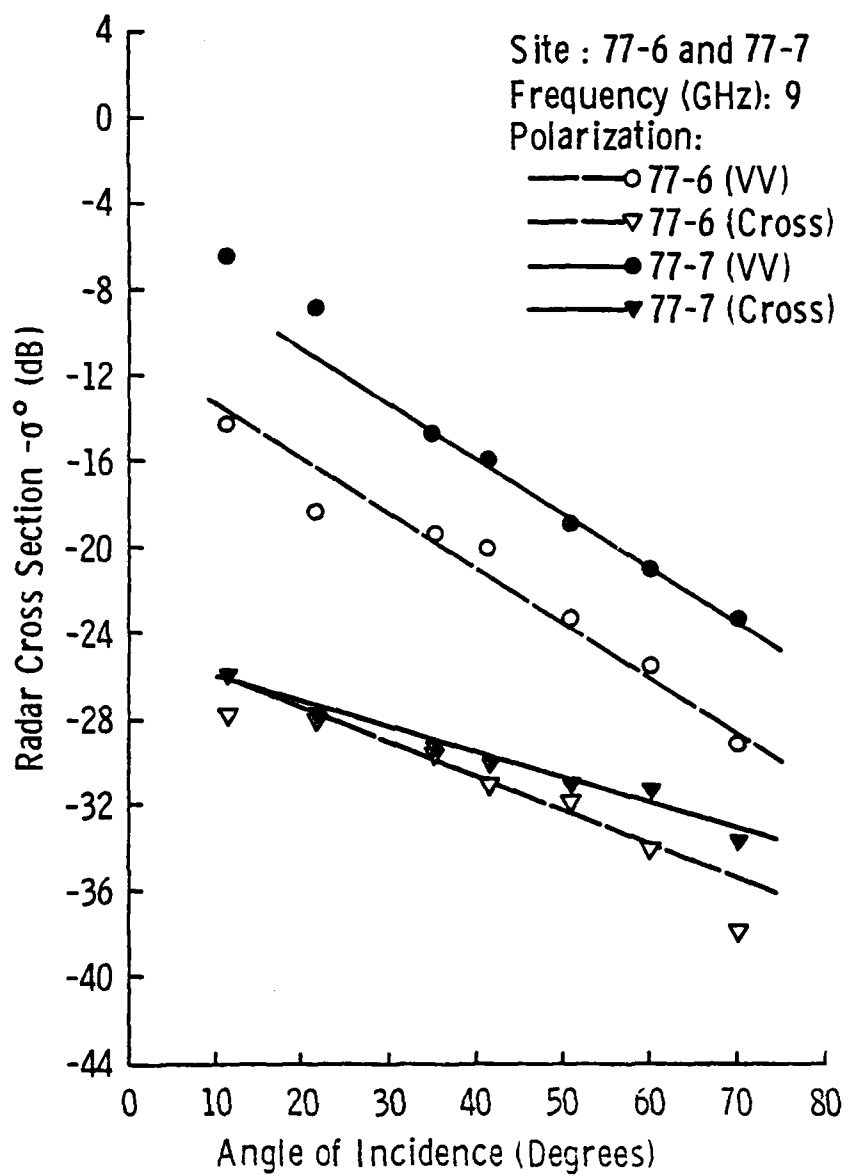


Figure 4.5-26. Scattering coefficient of lake ice, Site 77-6 and Site 77-7, at 9 GHz, VV and Cross.

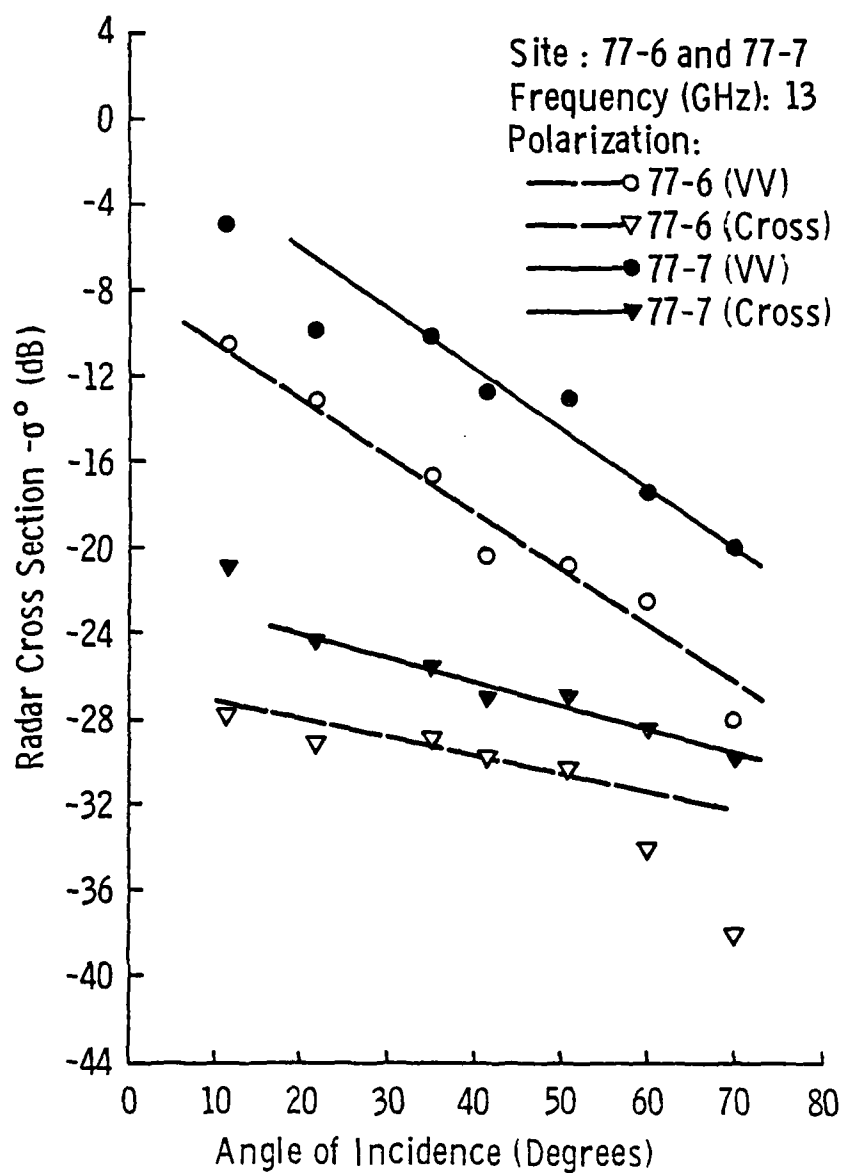


Figure 4.5-27. Scattering coefficient of lake ice, Site 77-6 and Site 77-7, at 13 GHz, VV and Cross.

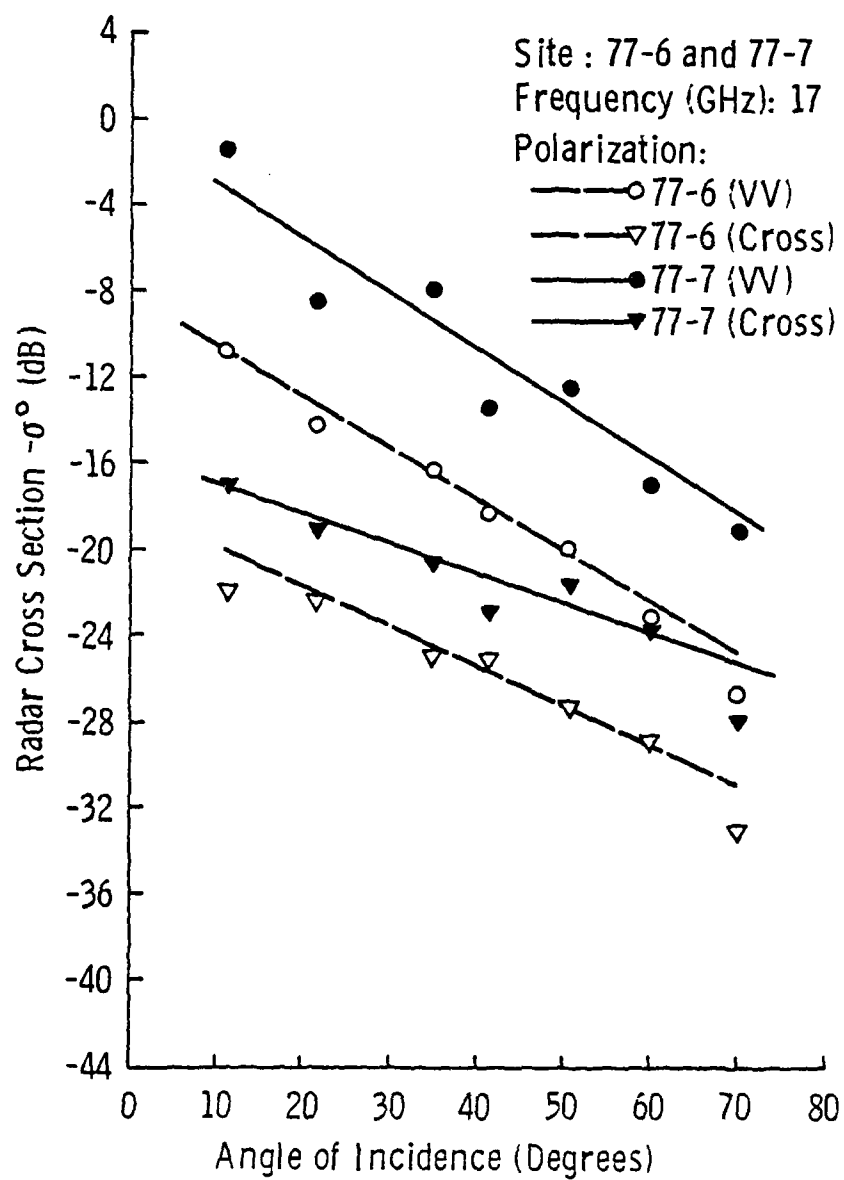


Figure 4.5-28. Scattering coefficient of lake ice, Site 77-6 and Site 77-7, at 17 GHz, VV and Cross.

# Scattering Coefficient of Thick First-Year and Multiyear Ice at 9 GHz

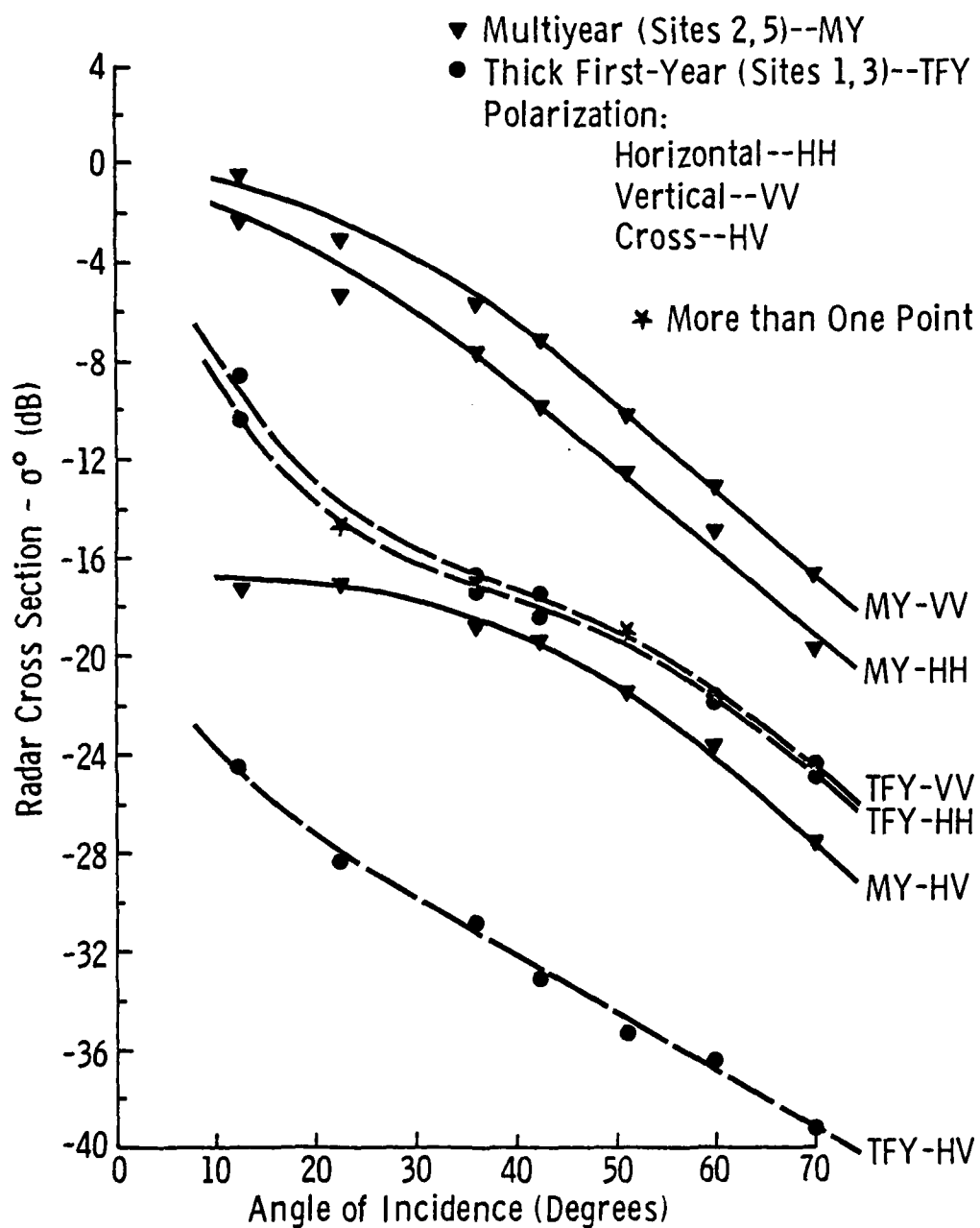


FIGURE 4.5-29 Scattering Coefficient of Thick First-Year  
and Multiyear Ice at 9 GHz.

# Scattering Coefficient of Thick First-Year and Multiyear Ice at 13 GHz

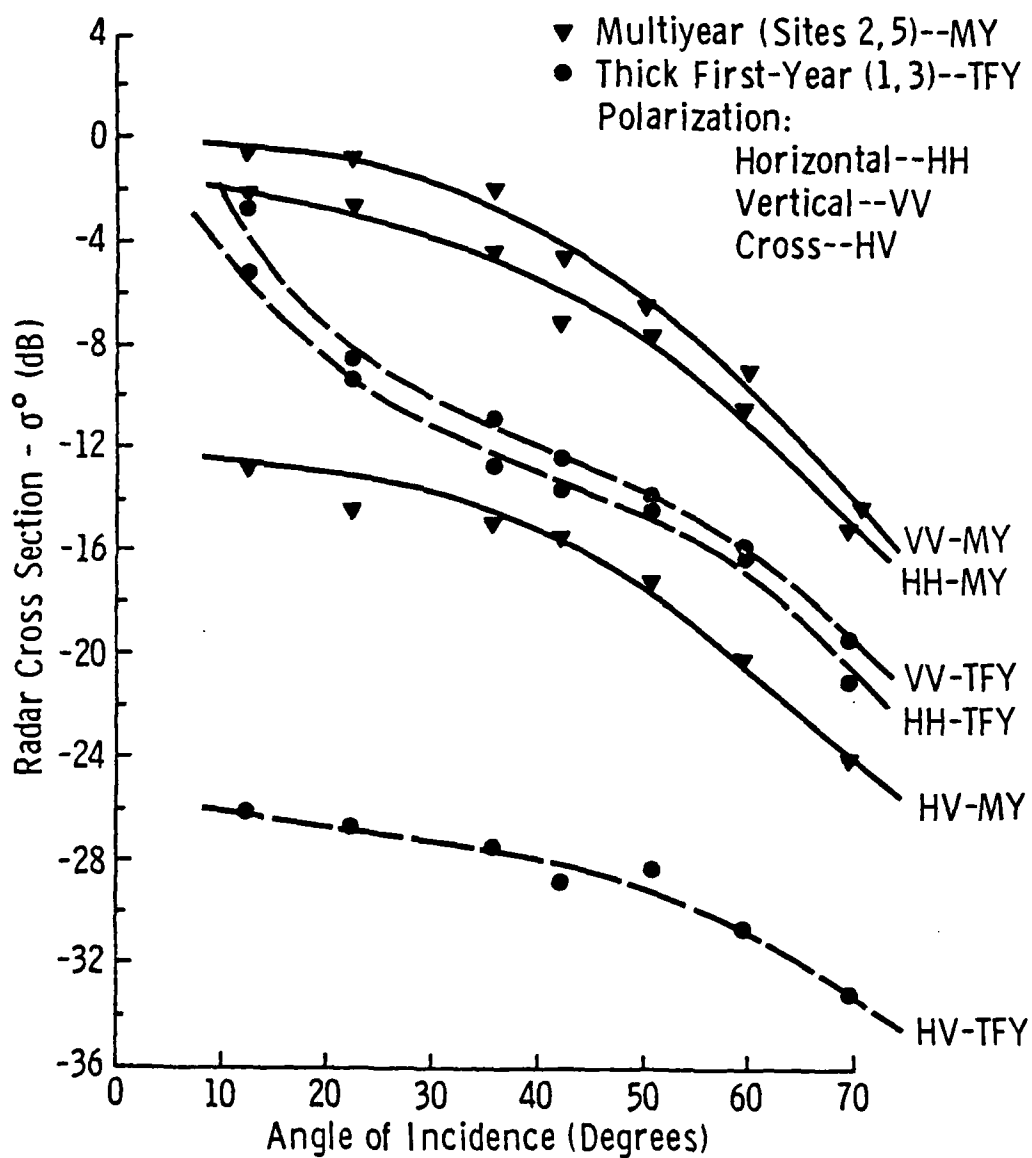


FIGURE 4.5-30 Scattering Coefficient of Thick First-Year and Multiyear Ice at 13 GHz.

# Scattering Coefficient of Thick First-Year and Multiyear Ice at 17 GHz

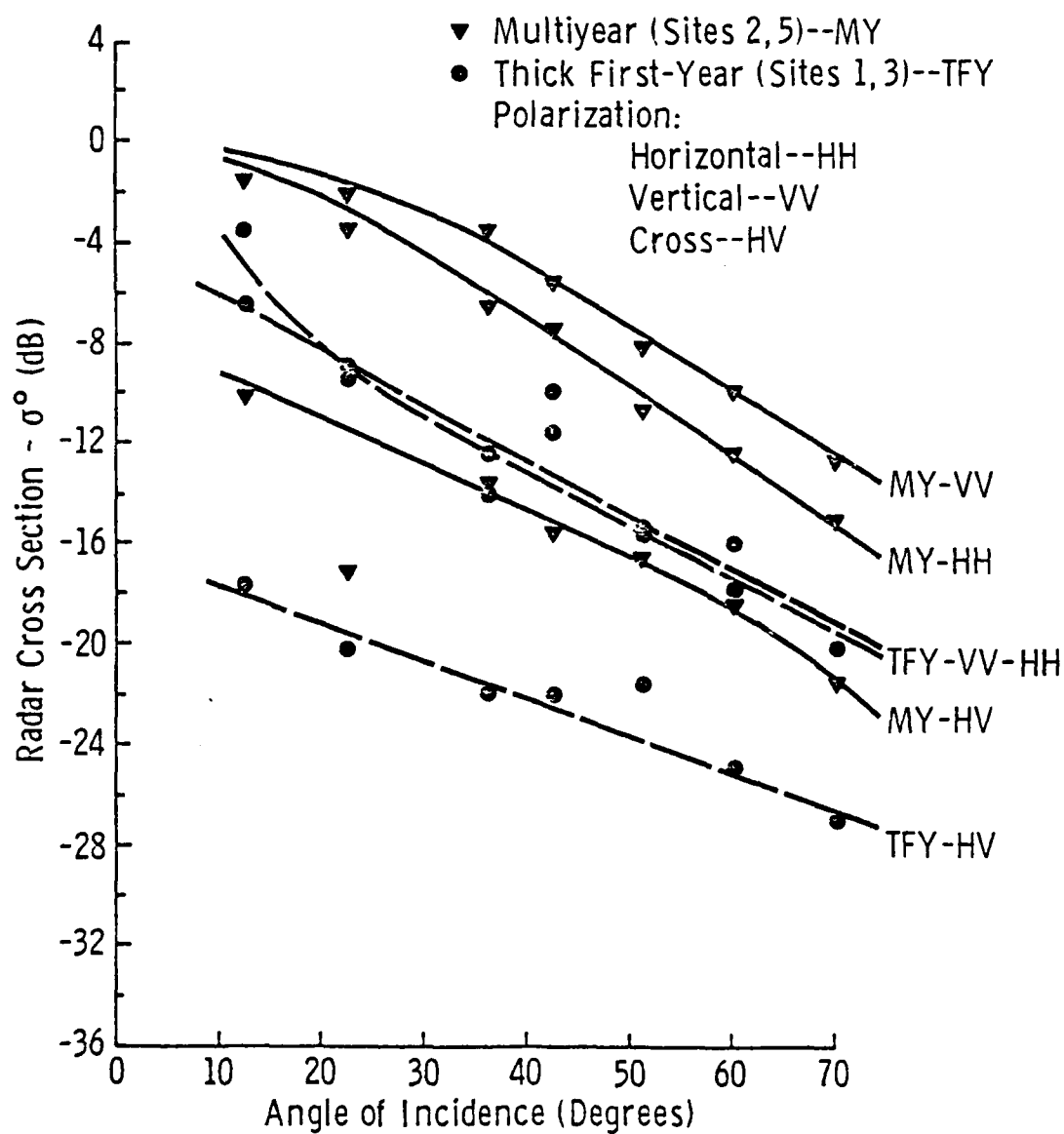


Figure 4.5-31. Scattering Coefficient of Thick First-Year and Multiyear Ice at 17 GHz.

Its angular response was nearly identical to the response at 9 GHz except for a higher absolute level. The 17 GHz response was also similar, but with less separation in the returns from the two ice types (Figure 4.5-31).

Comparisons of the average scattering coefficients of multiyear and thick first-year sea ice (discussed above) with pressure-ridged sea ice and fresh water lake ice are shown vs. angle of incidence in Figures 4.5-32 to 4.5-37 for 9 and 17 GHz (HH) and 13 GHz (HH, VV, and HV). In all cases, multiyear ice had the highest backscatter return and would be easily discriminable from the other ice types. The pressure-ridged ice had the next highest backscatter return. It would be hard to discriminate pressure-ridge ice from thick first-year ice at near grazing angles on the grounds of backscatter return only, but pressure ridges are linear features and thus are readily identifiable in radar imagery of floe features. Lake ice was found to have the lowest backscatter response of these ice categories, with returns well below those of the sea-ice categories. HH and VV polarizations have similar responses for all types of ice. This is demonstrated when one compares Figures 4.5-33 and 4.5-34 which show scatter for 13 GHz HH and VV. Cross-polarization returns are very low compared with VV and HH returns (Figure 4.5-35).

From backscatter alone, one may find that if proper angles were not chosen, difficulty may arise in the ability to discriminate between pressure-ridged and multiyear ice, and also between lake ice and thick first-year sea ice. However, in an actual situation, these problems would not impair the ability to discriminate due to the available information gained through study of the tones and shapes of the features

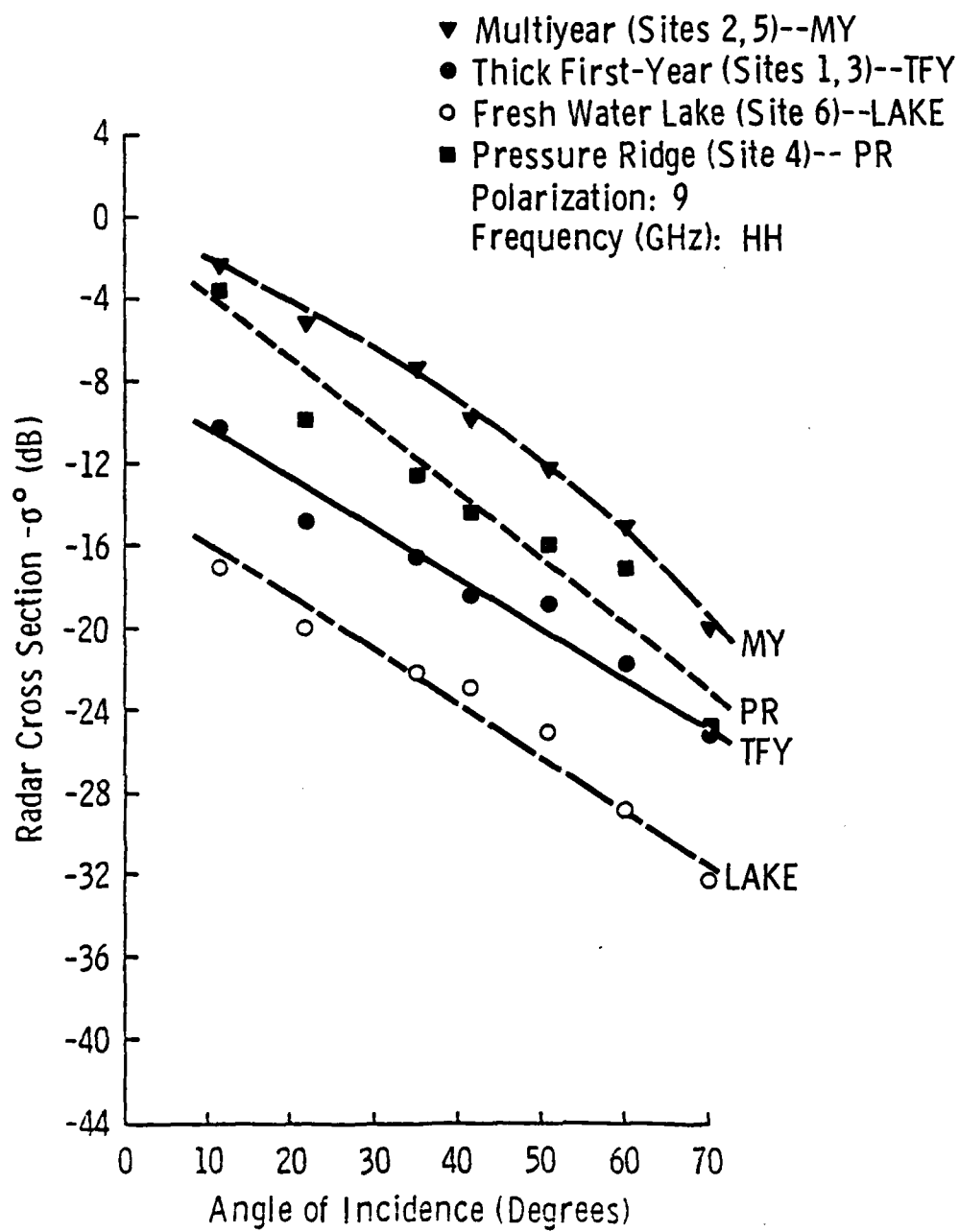


FIGURE 4.5-32 Scattering coefficient of thick first-year, multiyear, lake, and pressure ridge ice at 9 GHz, HH.

# Scattering Coefficient of Thick First-Year, Multiyear, Fresh Water Lake, and Pressure Ridge Ice at 13 GHz

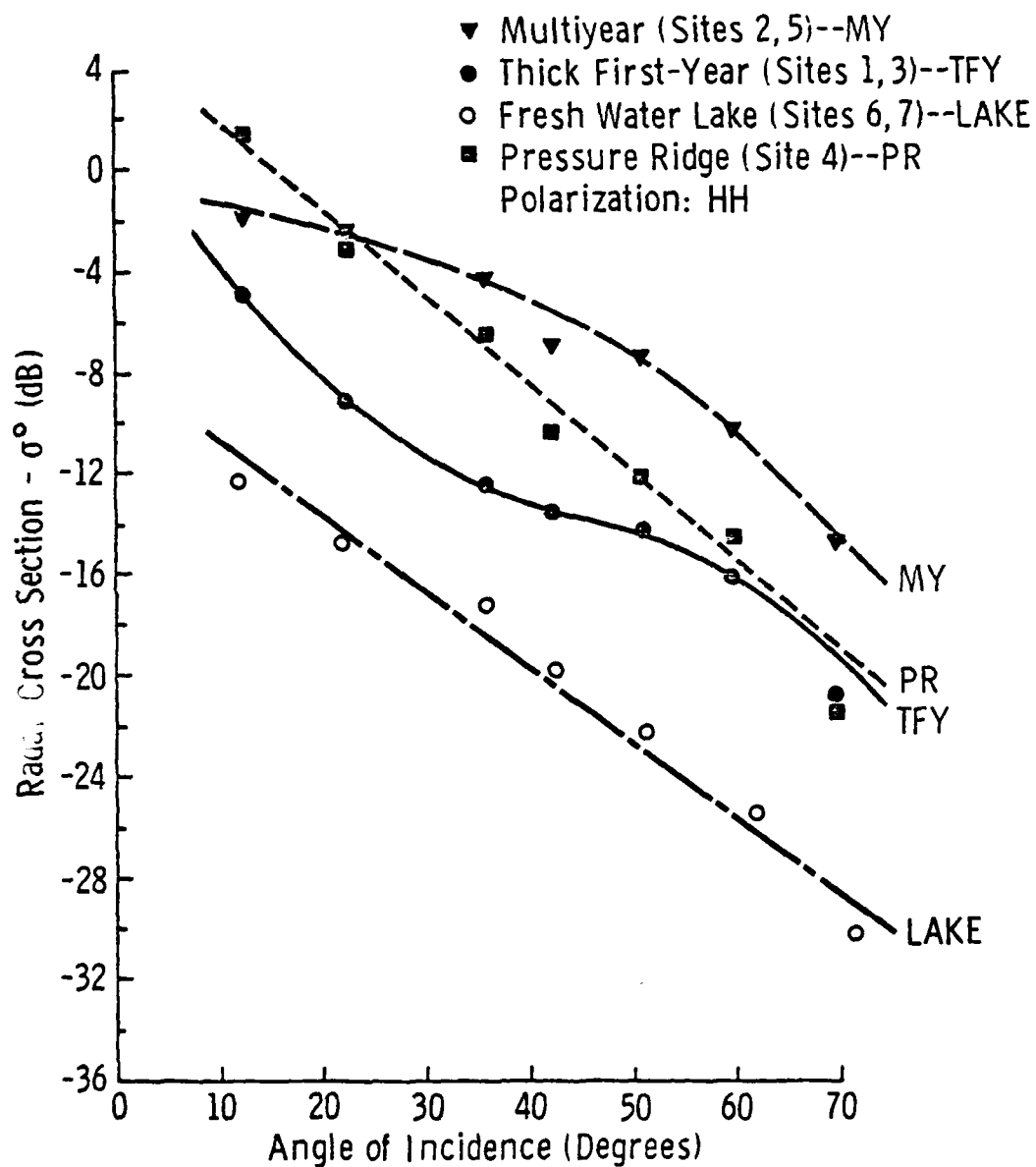


FIGURE 4.5-33 Scattering Coefficient of Thick First-Year, Multiyear, Fresh Water Lake, and Pressure Ridge Ice at 13 GHz.

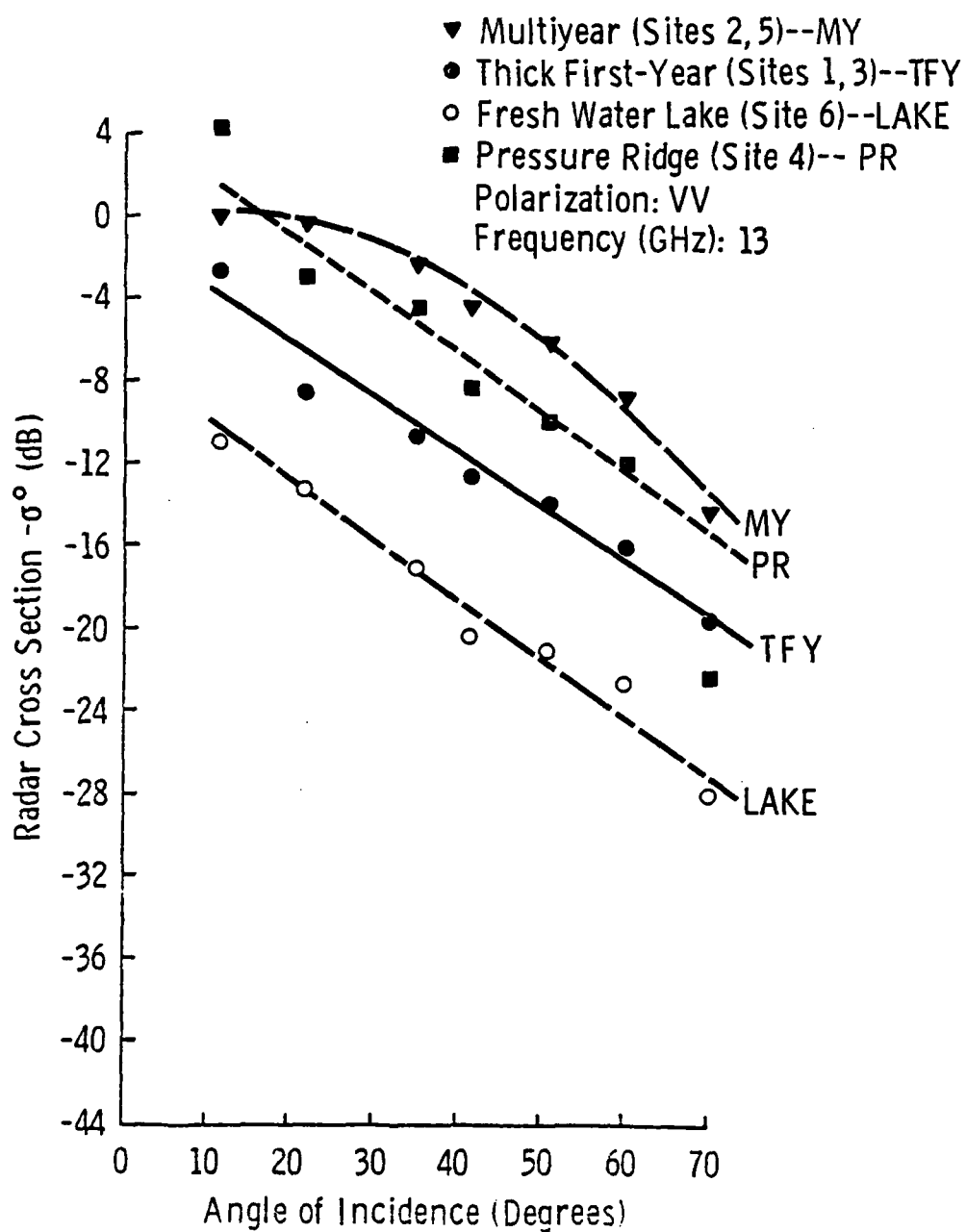


FIGURE 4.5-34 Scattering coefficient of thick first-year, multi-year, lake, and pressure ridge ice at 13 GHz, VV.

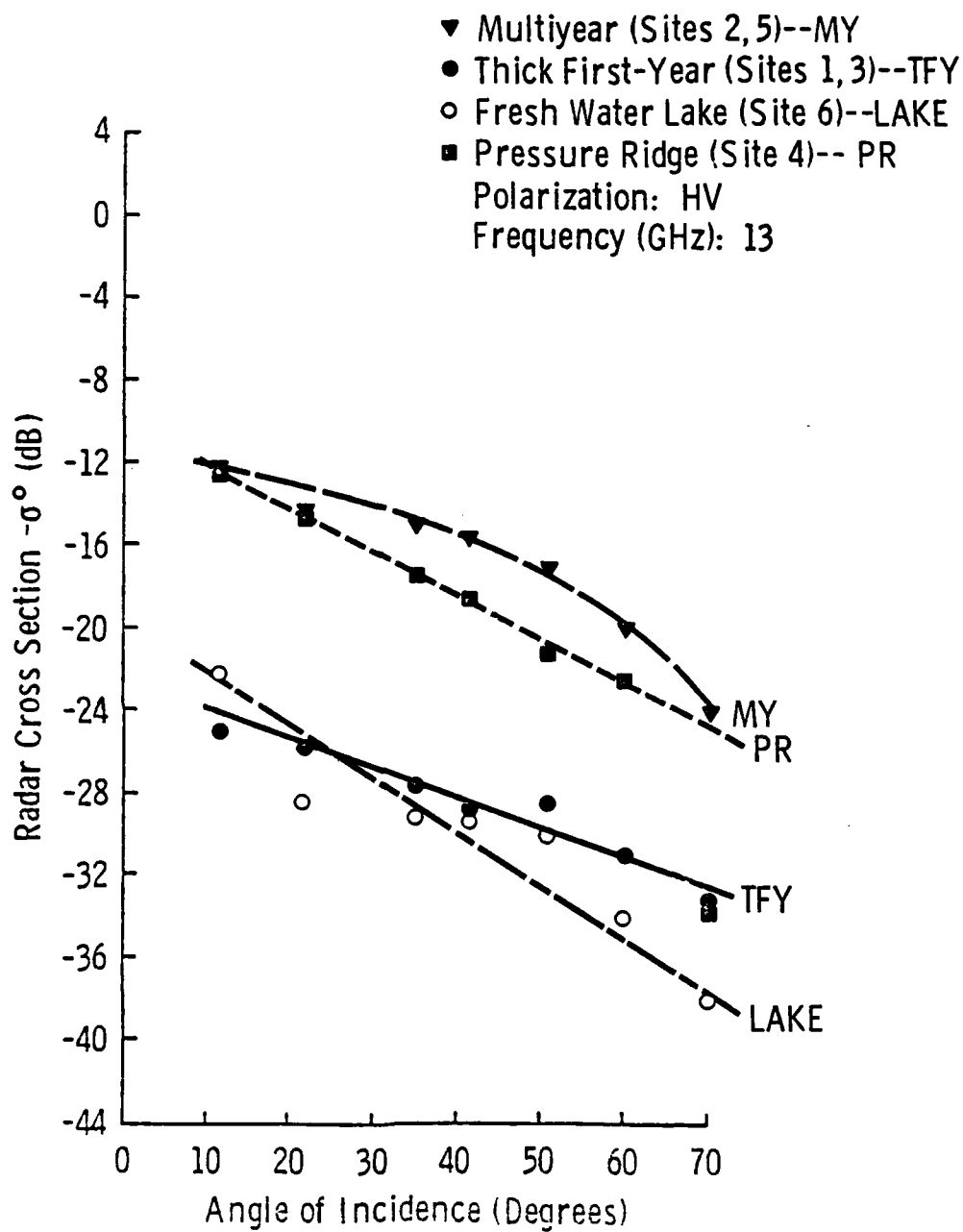


FIGURE 4.5-35 Scattering coefficient of thick first-year, multi-year, lake, and pressure ridge ice at 13 GHz, HV.

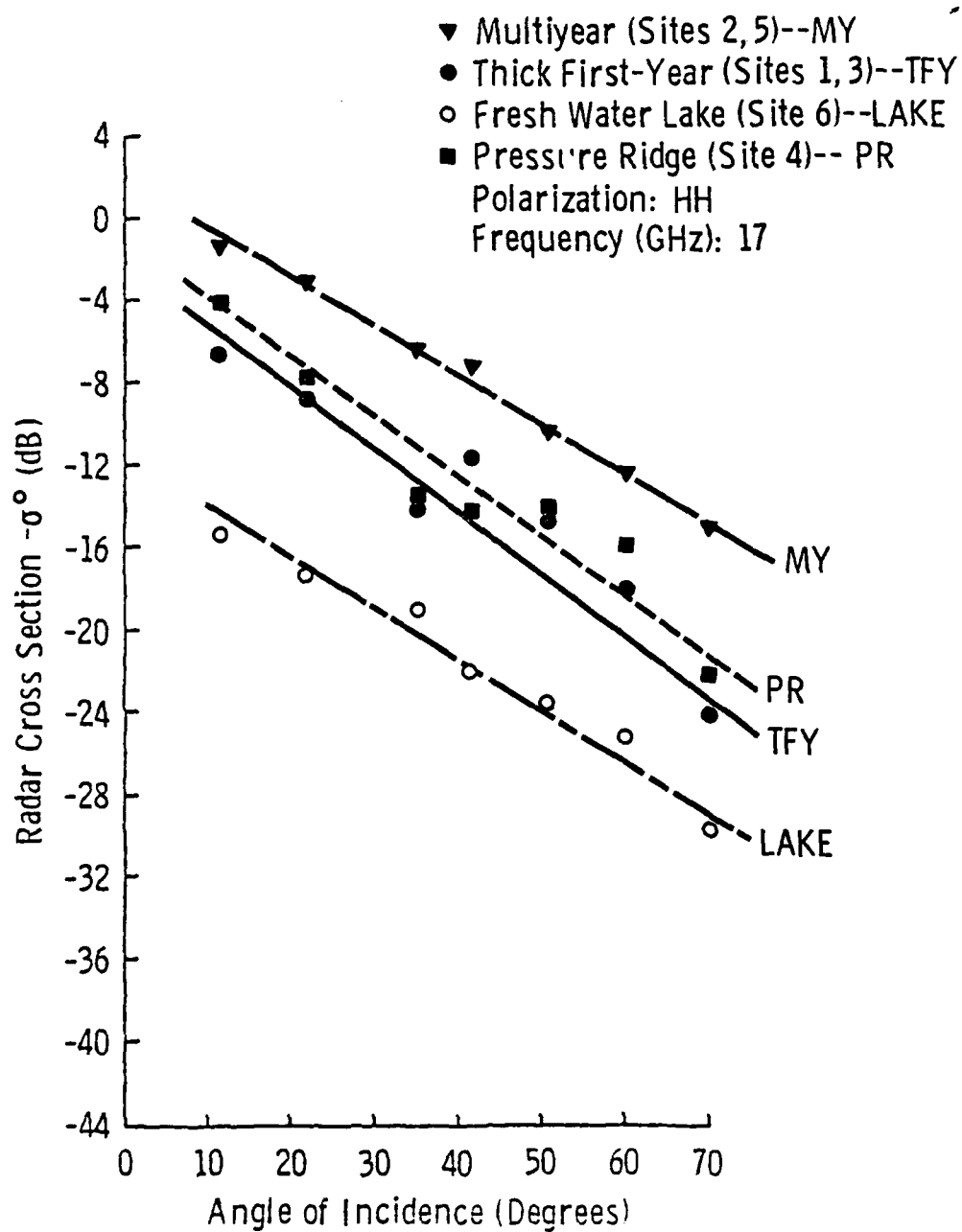


FIGURE 4.5-36 Scattering coefficient of thick first-year, multi-year, lake, and pressure ridge ice at 17 GHz, HH.

under study.

#### 4.5.3 The Effect of Snow Depth on Backscatter Return

Snow was found to affect significantly the absolute level of the radar cross-section of thick first-year sea ice. This effect ranged from 1 to 4 dB depending upon the frequency and angle of incidence. Snow was shown to be a contributing source of backscatter from the sea ice medium. The effect of the snow surface was to enhance the backscatter by modifying the overall absolute level of the scatter, with the shape of the angular response remaining very much the same. The contribution of the snow layer to the backscatter response increased with frequency. These effects are illustrated in Figures 4.5-37 to 4.5-39. Similar results have also been found to be true for scatter from snow-covered ground [56].

A specific example of the scatter from ice with a bare surface is shown in Figure 4.5-40. This figure shows the angular response of Site 78-2 for two looks at 13 GHz. One look had a 4 cm snow cover (natural) and the other had a bare surface. The ice with a bare surface exhibited an 8 dB lower absolute level than the ice with a snow surface. Two interesting effects were also noted in the response from a bare-surface. There was a significant increase in absolute level near nadir ( $12^\circ$ ) and a significant decrease in return at the largest angle ( $70^\circ$ ). These are characteristics of scatter from a smooth surface and were found to be exhibited in many data sets. The overall response of the radar scattering coefficient as it varied with snow depth is shown in Figure 4.5-41. In this figure, the response of the radar cross-section from  $42^\circ$ ,  $51^\circ$ ,  $60^\circ$  and  $70^\circ$  has been averaged (in dB) and this quantitative measure was used to serve as a guide to indicate the degree

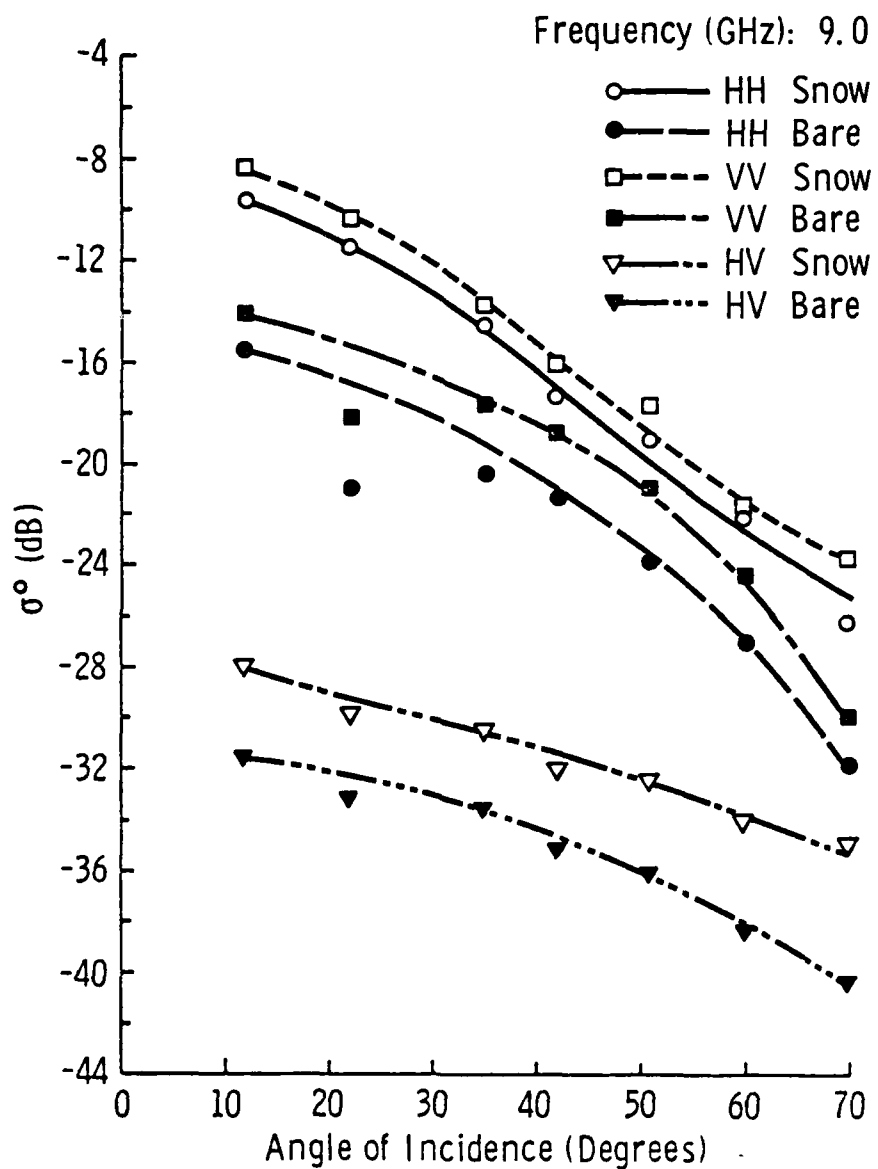


FIGURE 4.5-37 Average  $\sigma^0$  versus angle of incidence ( $\theta$ ) curve for bare-ice and snow-covered first-year sea ice, 9.0 GHz.

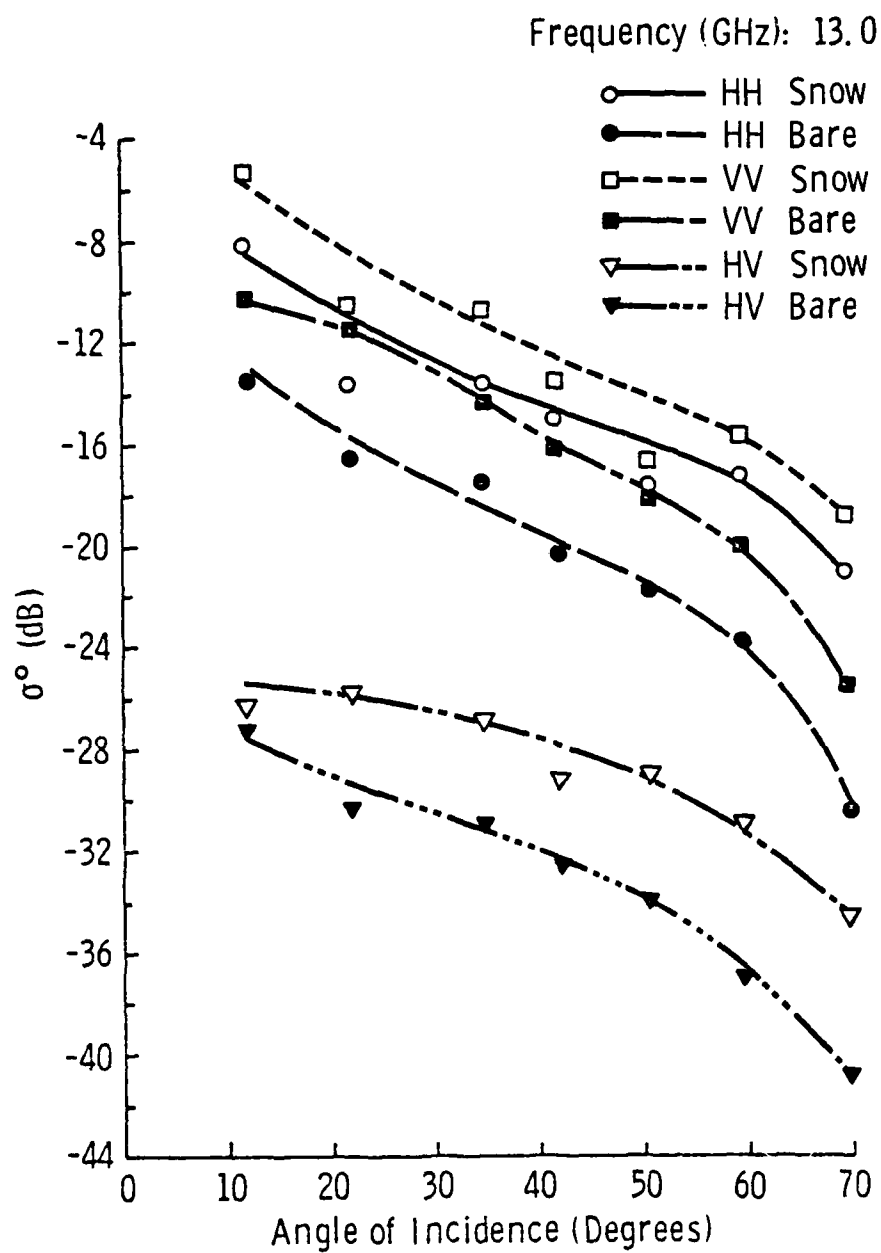


FIGURE 4.5-38 Average  $\sigma^0$  versus angle of incidence ( $\theta$ ) curve for bare-ice and snow-covered first-year sea ice, 13.0 GHz.

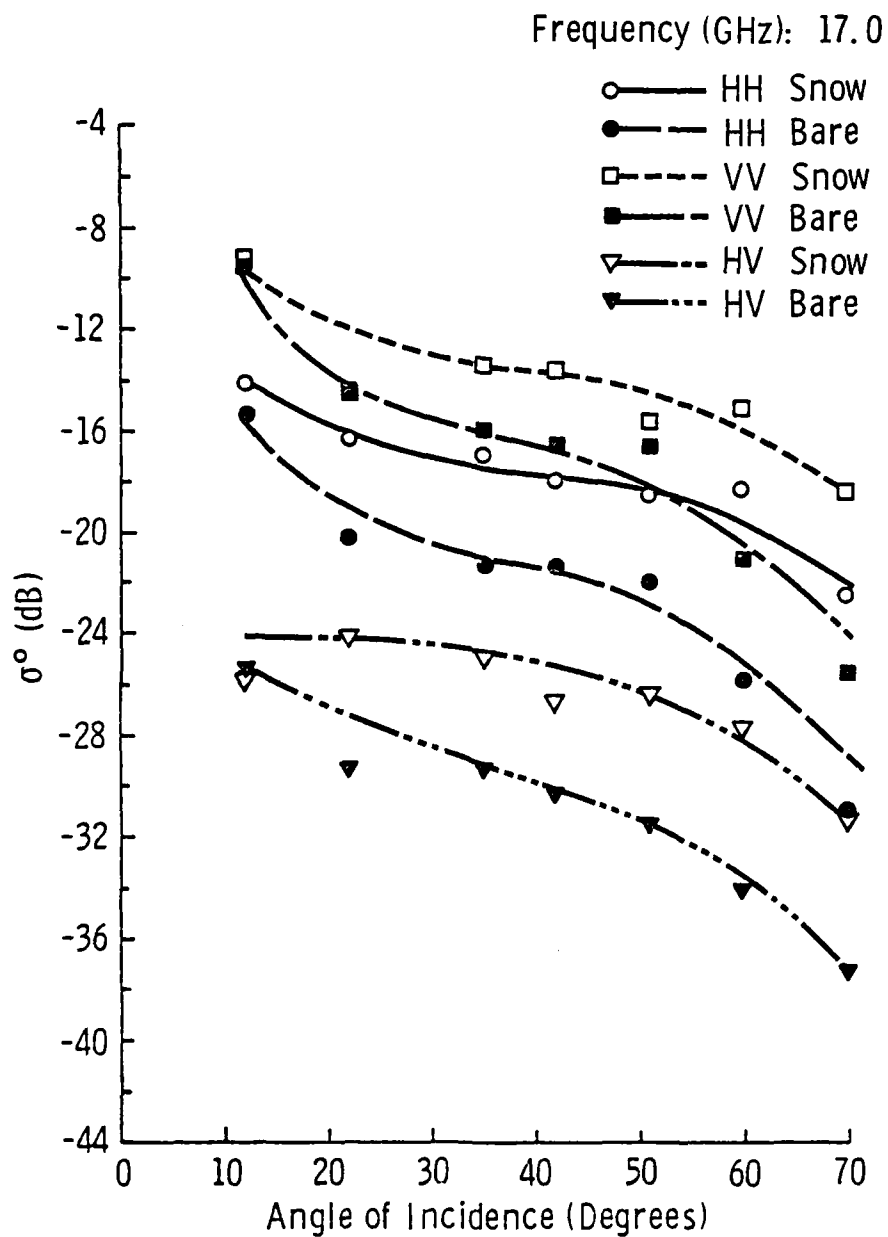


FIGURE 4.5-39 Average  $\sigma^0$  versus angle of incidence ( $\theta$ ) curve for bare-ice and snow-covered first-year sea ice, 17.0 GHz.

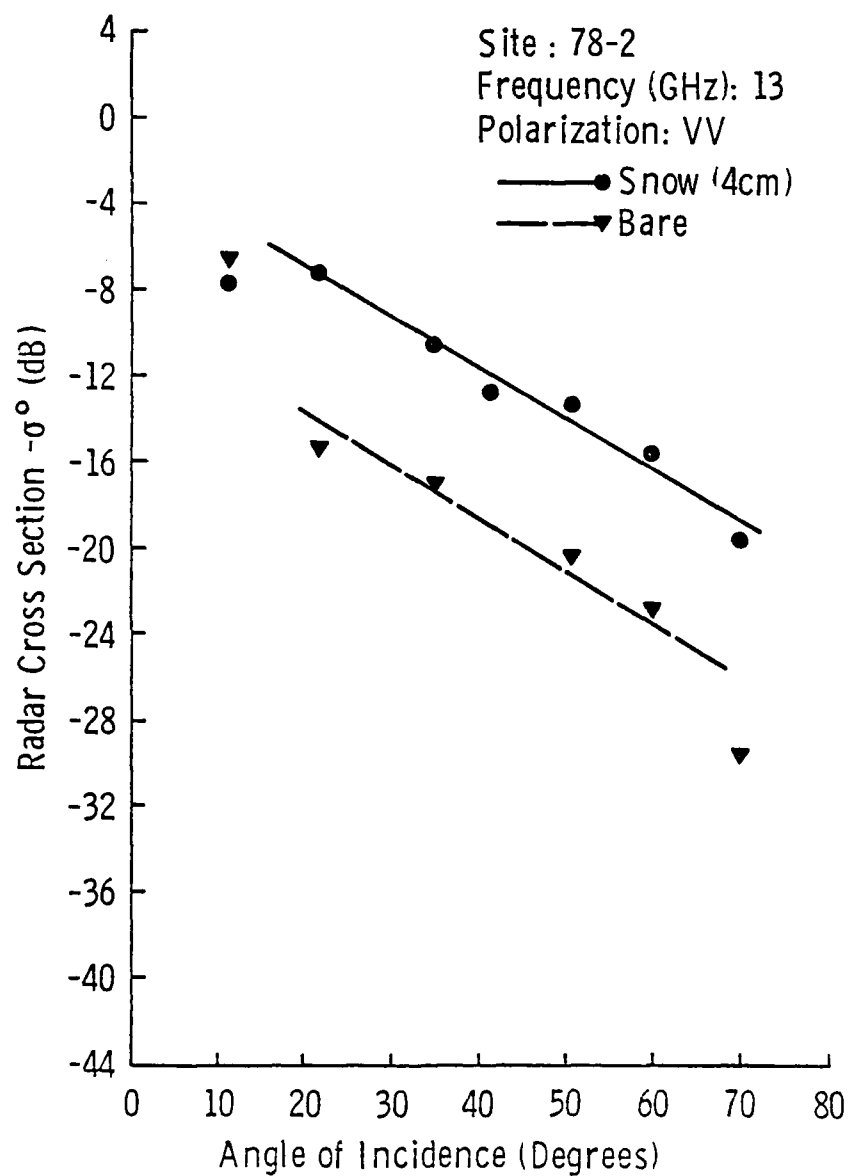


Figure 4.5-40. Scattering coefficient of thick first-year ice, Site 78-2, with a natural 4cm snow cover and a bare surface at 13 GHz, VV.

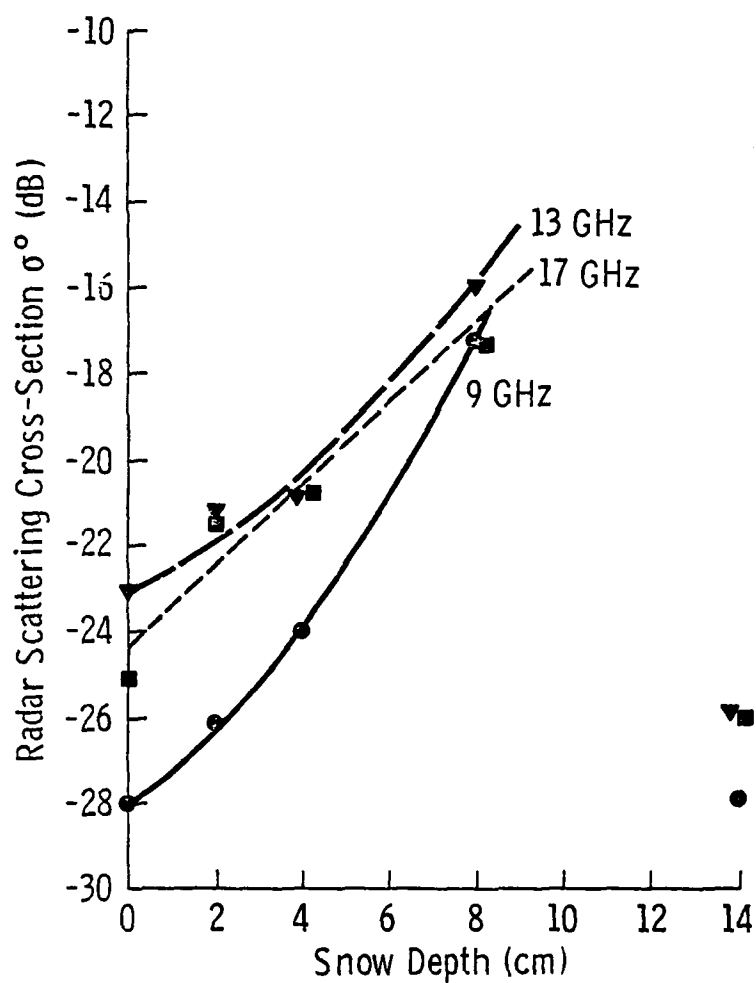


FIGURE 4.5-41 The response of the scattering coefficient of thick first-year ice, Site 78, as a function of snow depth at 9, 13, and 17 GHz, an incidence angle of  $55^\circ$ , and HH polarization.

to which the response of backscatter is effected by snow depth. Results show that ice with a bare surface exhibited lower scatter than ice with a snow cover (at least up to 14 cm), and that ice with snow depths up to 8 cm showed greater absolute levels of scatter than ice with a thinner snow cover. The 14 cm snow cover was generated by shoveling snow from outside of the radar footprint onto the snow in the radar footprint, leveling the piled snow, and slightly packing the snow until the 14 cm depth was obtained; its backscatter was only slightly higher than the scatter measured for bare ice. Thus, the packing apparently reduced the snow backscatter; detailed study of differences in the snow properties was not made.

#### 4.5.4 Temperature Effects on Backscatter Return

Measurements were obtained in 1978 that allowed some study into the effects of temperature on backscatter return. Since the 1978 experiment site was situated on one field of ice with the same history of formation, variations in measurements were correlated with the accompanying variations in temperature. This task was attempted in 1977, but proved difficult due to the limited number of looks at a given site.

Results indicate that, in general, lower radar scattering cross-sections were measured at lower temperatures. This was found to be true for ice with a bare surface (Figure 4.5-42), ice with 2 cm of snow cover (Figure 4.5-43), and ice with a 4 cm snow cover (Figure 4.5-44). Results are not conclusive due to the limited amount of data and a significant amount of scatter in this data, but a similar response has been demonstrated by snow-covered ground [56]. The indication is that temperature effects may be in the 1 to 8 dB range for changes in temperature of 10° C depending upon frequency and snow cover.

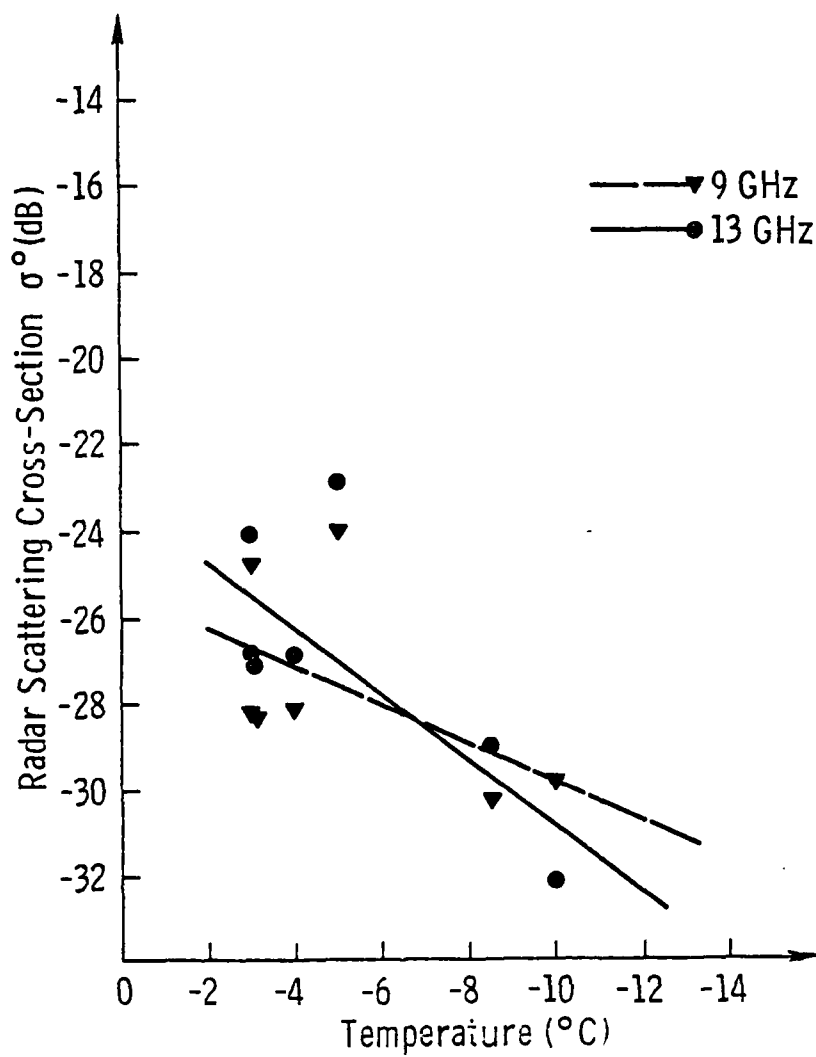


Figure 4.5-42. Effect of temperature on the scattering coefficient of thick first-year ice with no snow cover at 9 and 13 GHz, an incidence angle of  $55^\circ$ , and HH polarization.

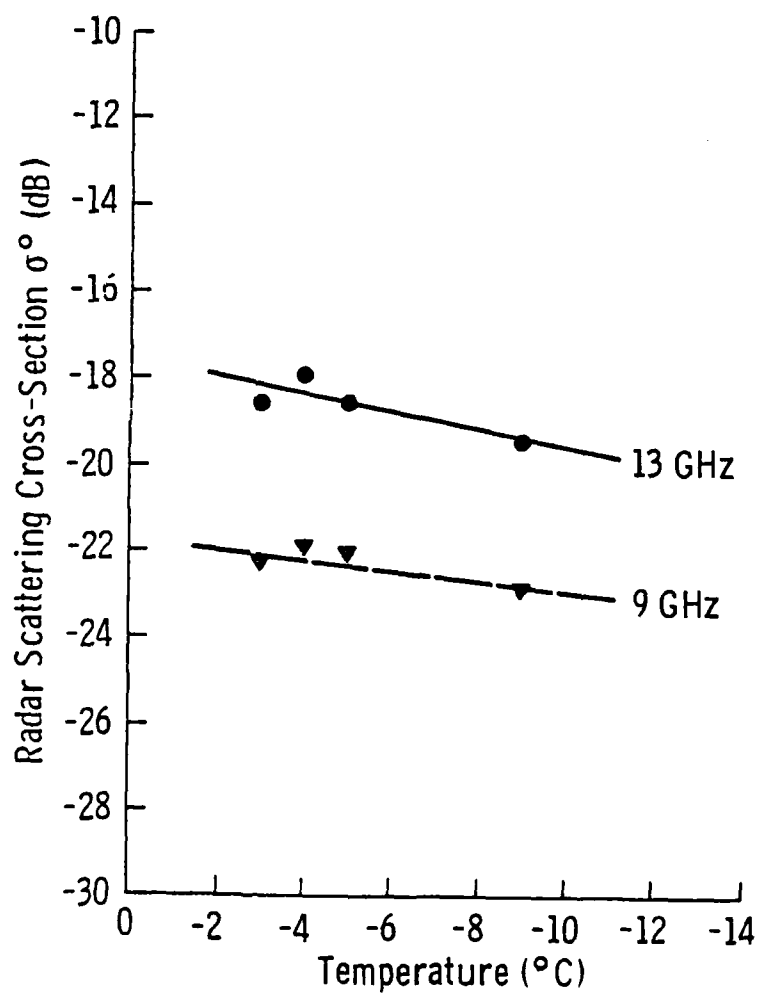


FIGURE 4.5-43

Effect of temperature on the scattering coefficient of thick first-year ice with a 2 cm snow cover at 9 and 13 GHz, and an incidence angle of  $55^\circ$ , and HH polarization.

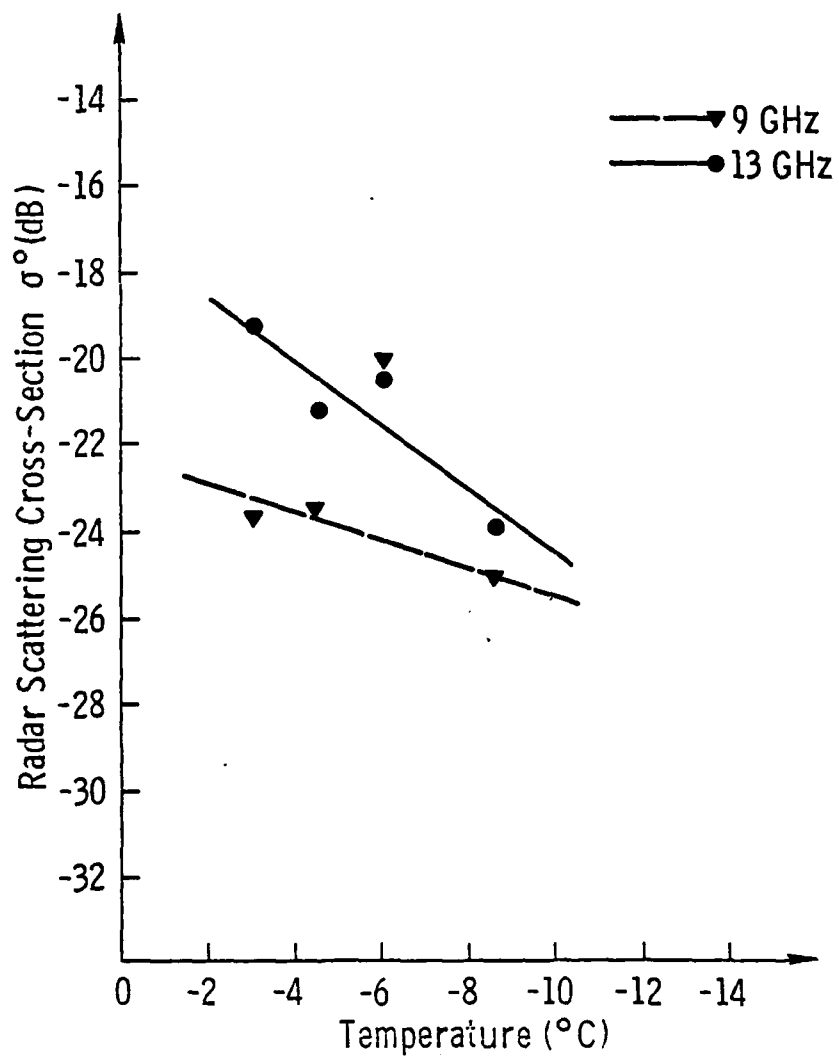


Figure 4.5-44. Effect of temperature on the scattering coefficient of thick first-year ice with a 4cm snow cover at 9 and 13 GHz, an angle of incidence of  $55^\circ$ , and HH polarization.

#### 4.6 Frequency Response

The frequency responses of multiyear and thick first-year sea ice for like-(HH) and cross-(HV) polarization scatter at 70°, 51° and 22° angles of incidence are shown in Figures 4.6-1 to 4.6-4. A comparison of the frequency response of the scatter at 60° for the thick first-year at site 77-3 and Site 78 is shown in Figure 4.6-5. Trends indicate that the radar cross-section at large angles of incidence increases linearly with increasing frequency in the 8.5 to 17.5 GHz region. The response at 1.5 GHz raises some interesting questions. If the backscatter mechanisms that apply at 8 to 18 GHz frequencies were applicable to the 1 to 8 GHz region, one would only need to extend the approximately linearly increasing frequency response used to describe the scatter in the 8 to 18 GHz region into the 1 to 8 GHz region. The response at 1.5 GHz shows that different scattering mechanisms must apply in the case of thick first-year ice. Thick first-year ice backscatter was higher at 1.5 GHz by greater than 4 dB than the extrapolated value. Multiyear ice would be detectably higher than thick first-year ice by extrapolation, whereas it was found that the measured 1.5 GHz return from thick first-year ice (Site 77-3) was higher in absolute level than that from multiyear ice (Site 77-5) by at least 2 dB. The closest that multiyear scatter at 1.5 GHz comes to the extended 8-18 GHz response trend is 4 dB (measured too low). Since VV scatter has been found to be consistently higher in absolute level than HH scatter, this level of separation between the 8 to 18 GHz (HH) trend and the 1.5 GHz measurement may be even more significant. However, an interesting phenomenon occurred in the 9 to 13 GHz regions. Scatter at these frequencies has a frequency response that is very linear in many cases, but with a slope that

# Scattering Coefficient of Thick First-Year and Multiyear Ice at 1.5, 9.0, 13.0, and 17.0 GHz

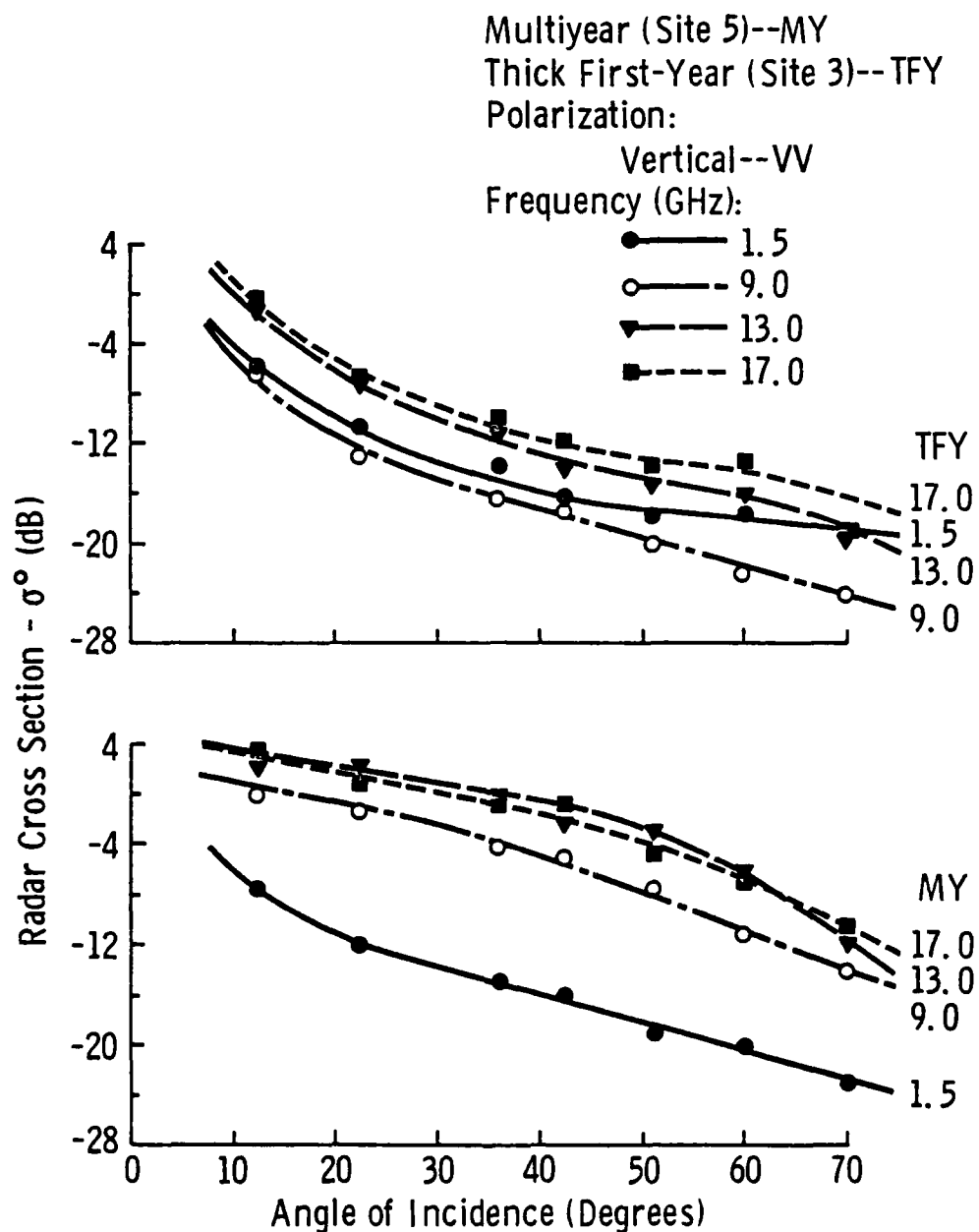


FIGURE 4.6-1 Scattering Coefficient of Thick First-Year and Multiyear Ice at 1.5, 9.0, 13.0, and 17.0 GHz.

# Scattering Coefficient Frequency Response of Thick First-Year and Multiyear Ice

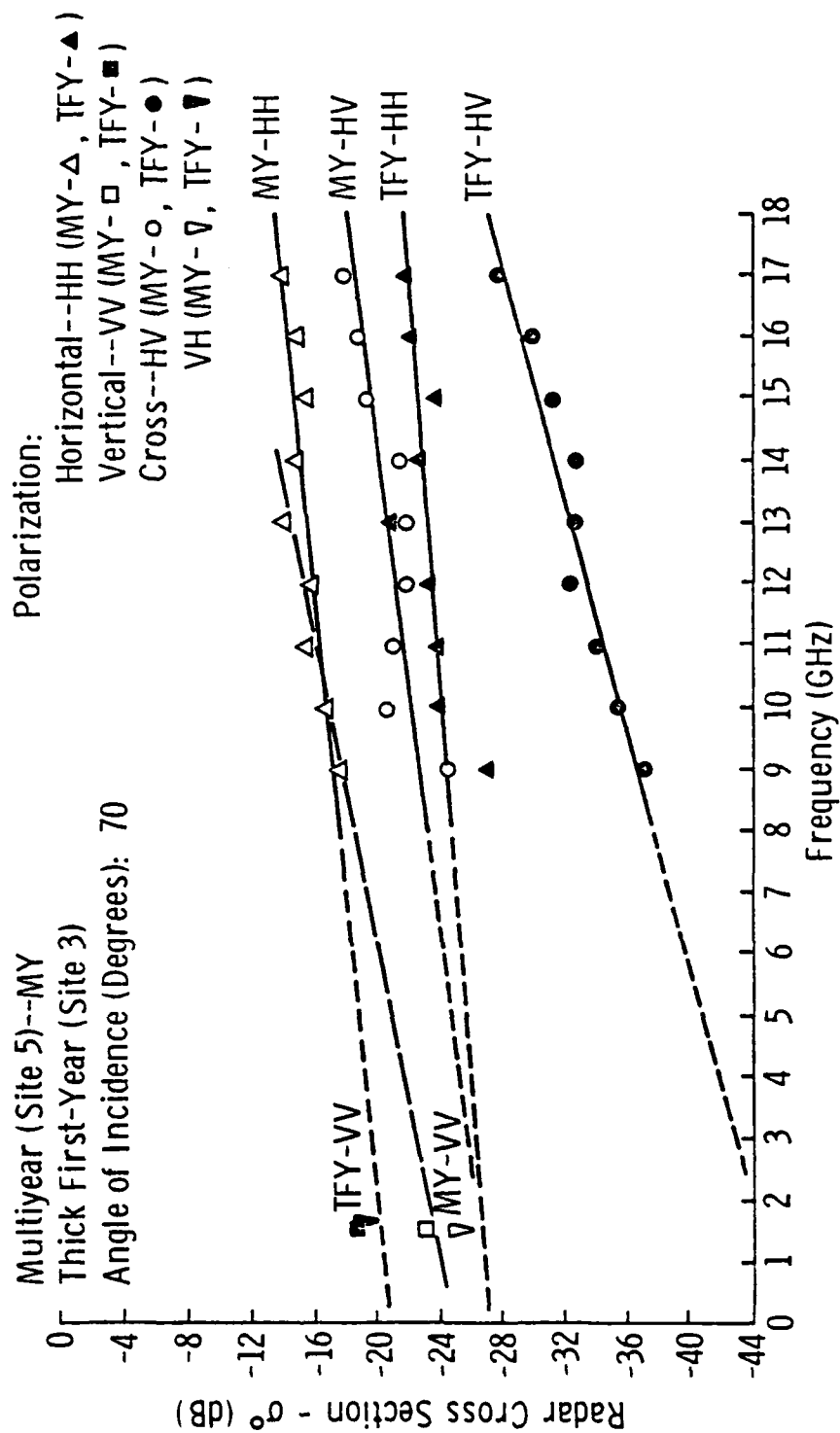


FIGURE 4.6-2 Scattering Coefficient Frequency Response of Thick First-Year and Multiyear Ice.

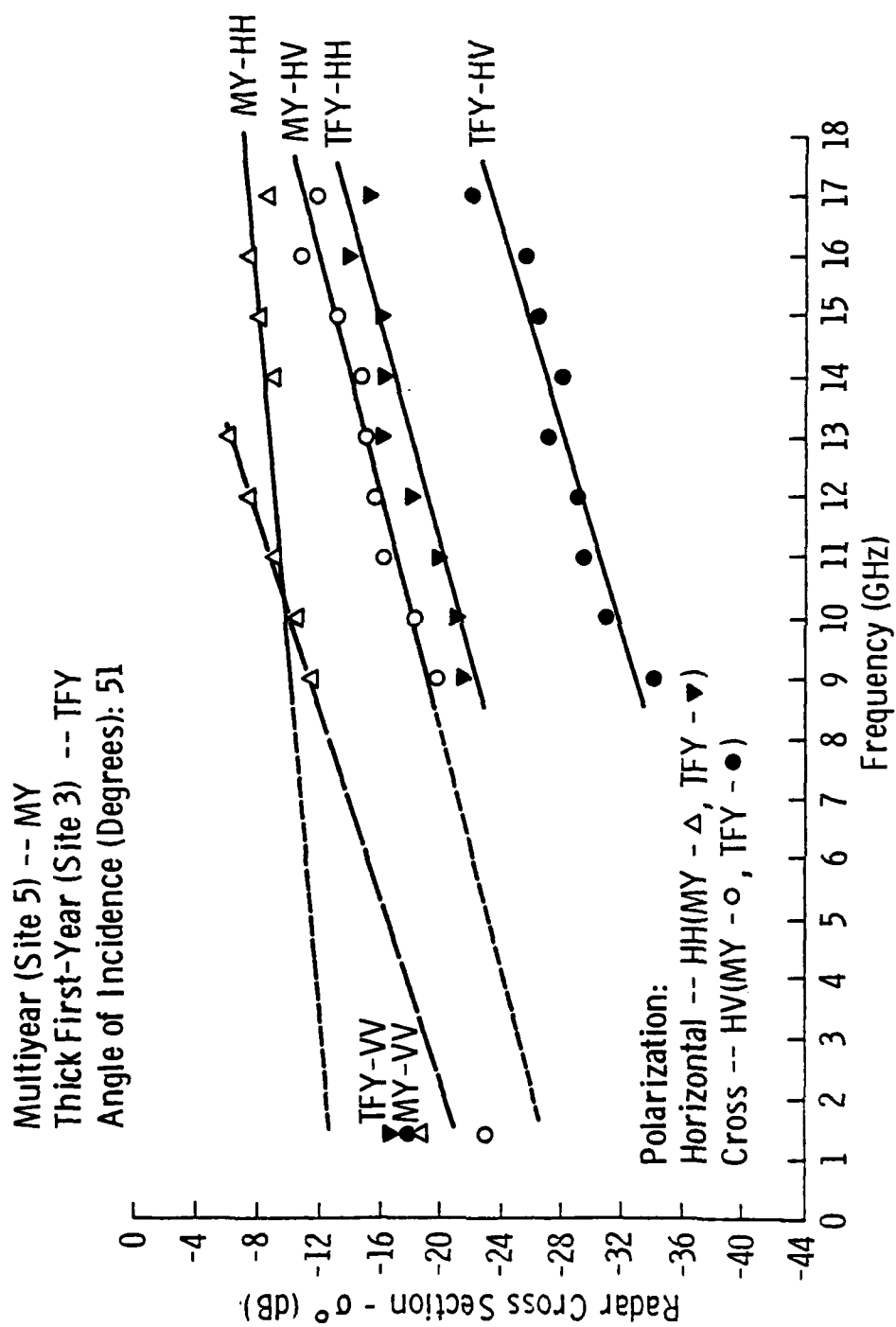


Figure 4.6-3. Scattering coefficient frequency response of thick first-year and multiyear ice.

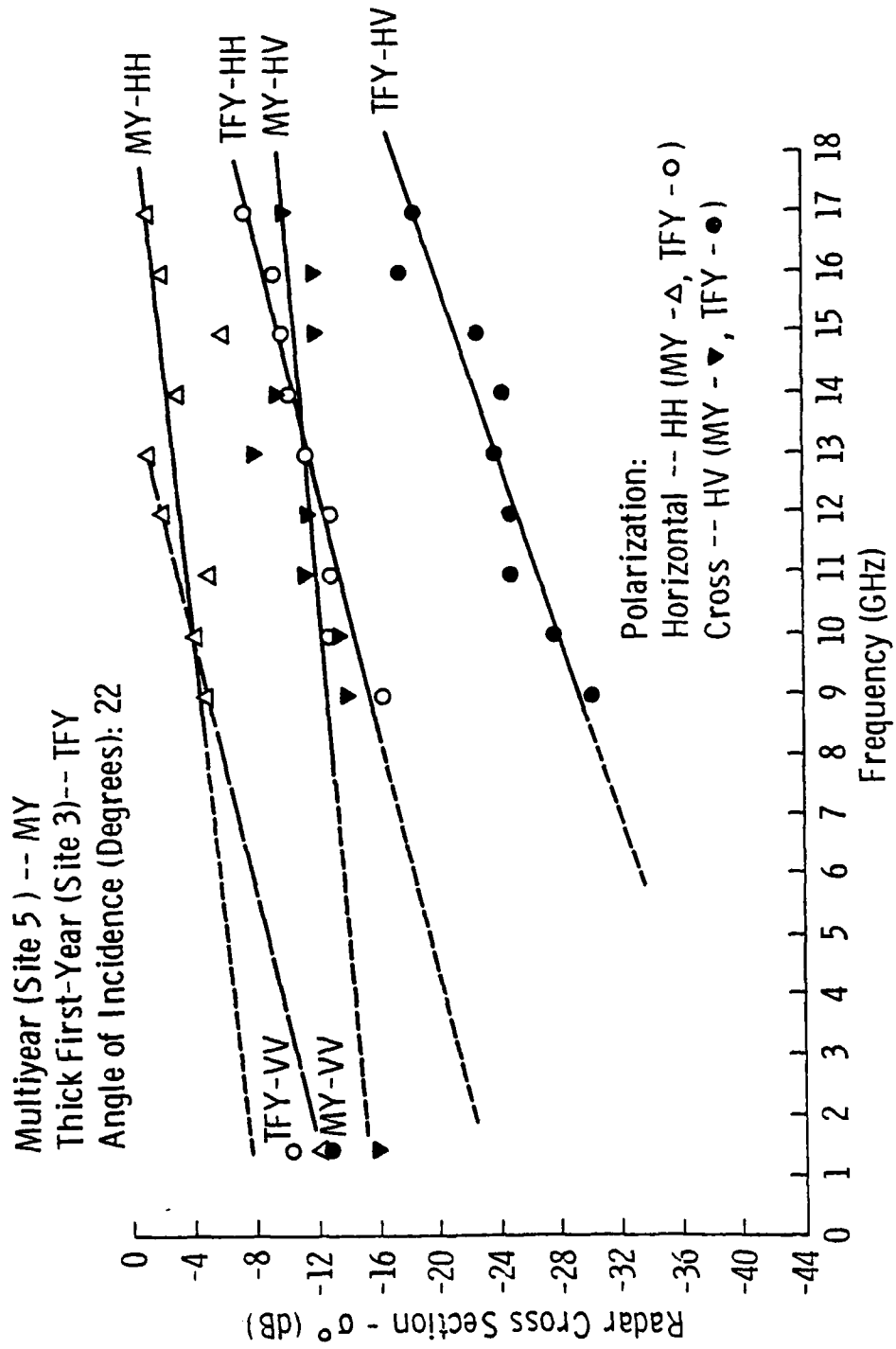


Figure 4.6-4. Scattering coefficient frequency response of thick first-year and multiyear ice.

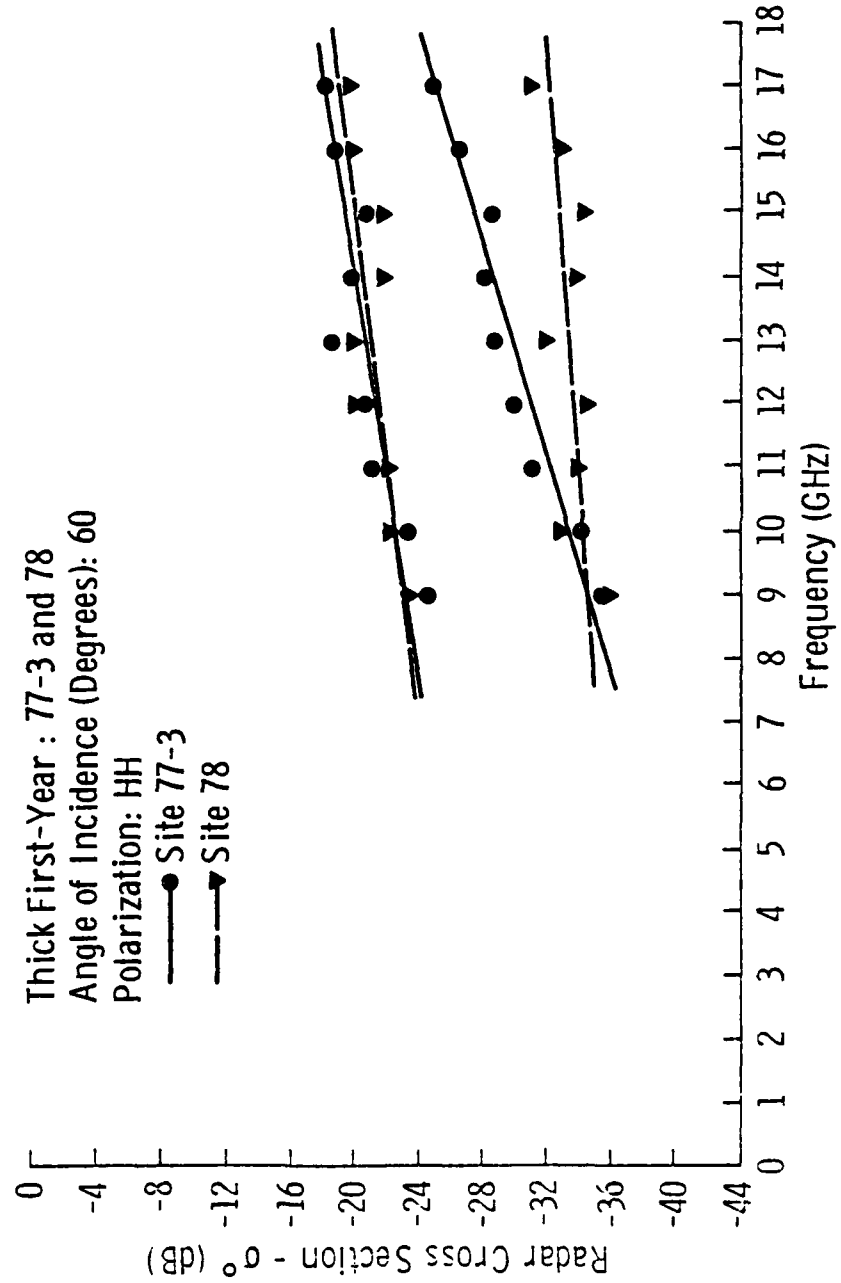


Figure 4.6-5. Scattering coefficient frequency response of thick first-year sea ice, Site 77-3 and Site 78.

is different than the slope of the regression from 8-18 GHz. It is seen that scatter from 1-13 GHz may be best described using a straight line with this slope.

Cross-polarized scatter from multiyear ice was greater in absolute level than like-polarized scatter from thick first-year ice in the 8 to 18 GHz region. The frequency response at the different angles of incidence was found to be much the same, which was an expected result since their angular responses were linear in nature.

In comparing the frequency responses (like-polarization) of the thick first-year ice of Site 77-3 and Site 78 (see Figure 4.6-5), it was found that they correlated well both in frequency variation and absolute level. Cross-polarized scatter for these two sites in two different years, however, differed greatly. This was especially true at the higher frequencies.

#### 4.7 Application to Ice Type/Thickness Identification

A user of an operational ice reconnaissance system needs to be able to use its output in describing the ice distribution of his area of interest. The categories of ice located in the region should be identifiable and relatable to ice thickness ranges. The fraction of ice in each category should also result from the interpretation process. The radar backscatter data obtained in the 1977 and 1978 experiments may be used to provide insight into this capability for a wide range of frequencies, incidence angles, and polarizations. Multiyear, thick first-year, and pressure-ridged sea ice and fresh water lake ice, appear in this limited data set.

At 1.5 GHz frequency, the radar did not have the ability to dis-

criminate between thick first-year and multiyear sea ice for angles between  $12^\circ$  and  $60^\circ$ ; however, discrimination may be possible at angles larger than  $60^\circ$ . With cross polarization these ice types could be more readily distinguished than with like polarization (see Figure 4.7-1). The difference in the radar cross-section of multiyear and thick first-year sea ice at an angle of incidence of  $70^\circ$  was found to be 3 dB for like-polarization (VV) and 5 dB for cross-polarization (VH). Returns at this frequency allowed easy distinction between the flat areas of the pack ice and the more prominent features, such as a pressure-ridge. Lake ice returns were much lower at least than the returns from any of the categories of sea ice that were examined.

Ku-X-Band results indicate that frequencies between 8 and 18 GHz allow discrimination between thick first-year, multiyear, and pressure-ridged sea ice and fresh water lake ice. Both like- and cross- polarizations were found to be useable.

One of the most important needs is the ability to discriminate between thick first-year ice and old ice (multiyear). Old ice is much thicker than first-year ice and therefore concerns most users of the Arctic region. Figures 4.7-1 and 4.7-2 graphically display the difference in backscatter return at frequencies of 1.5, 9, 13, and 17 GHz between these two ice types. Both like-polarization (VV) and cross-polarization (VH) differences are shown in separate graphs. Results indicate that both like- and cross- polarizations were useable. The 9 GHz frequency, for both like- and cross- polarizations, was found to discriminate best. Multiyear ice returns were about 9 dB higher for like-polarization (best angles were  $20^\circ$  to  $48^\circ$ ) and 12 dB higher for cross-polarization (best angles were  $35^\circ$  to  $70^\circ$ ) than the returns from

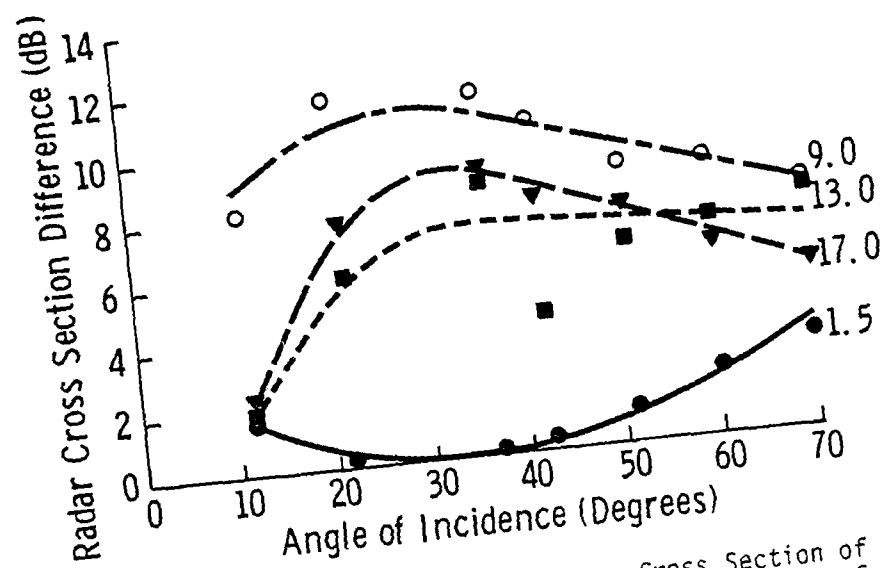


FIGURE 4.7-1 Difference Between Radar Cross Section of Thick First-Year and Multiyear Ice at 1.5, 9.0, 13.0 and 17.0 GHz with Vertical Polarization.

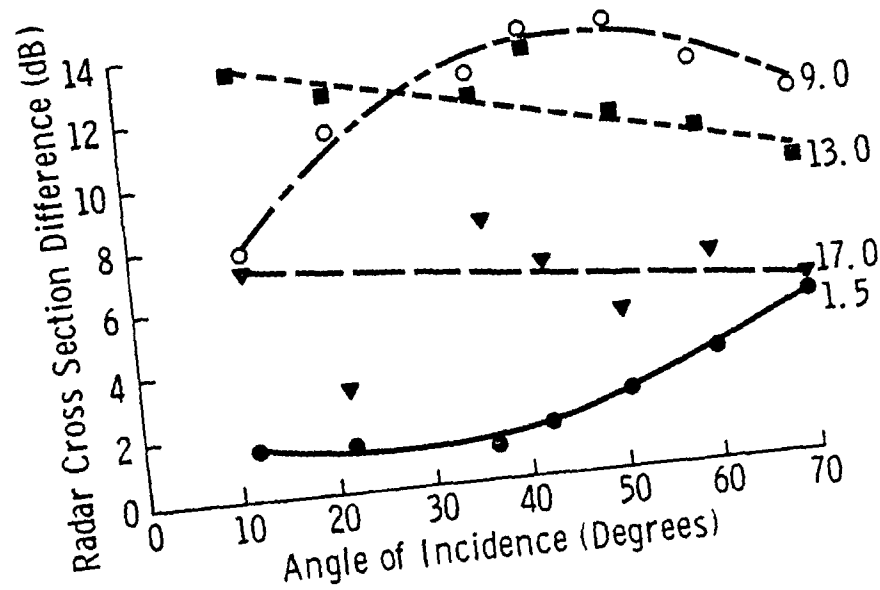


FIGURE 4.7-2 Difference Between Radar Cross Section of Thick First-Year and Multiyear Ice at 1.5, 9.0, 13.0 and 17.0 GHz with Cross-Polarization.

thick first-year ice. Returns at 13 GHz and 17 GHz were found to discriminate about equally well. Both were about 2 dB worse than those at 9 GHz. For cross-polarization returns the difference between thick first-year and multiyear ice was much more sensitive to frequency, with difference in returns for 17 GHz being much less than those for 9 GHz (6 dB).

Another task of an operational system is to provide information about the extent of pressure ridges. Also desired is the ability to estimate the size of the pressure ridge from the width of the bright return and/or the extent of the radar shadow associated with this linear feature. The pressure ridge that was examined in the 1977 experiment was small, and the response, especially at the large incidence angles, may have been affected by the orientation of the ridge with respect to the radar (the radar looked parallel to this linear feature). Pressure-ridges typically provide bright returns on radar imagery at large incidence angles and at these frequencies the backscatter from the small ridge fell between the returns from multiyear and thick first-year ice. Indications are that 20° to 40° incidence angles would be useful in locating ridges from backscatter alone. However, since ridges are linear features with returns greater than those of thick first-year ice, they should be easily identified. Separation of ridges from multiyear ice is done readily since multiyear ice has the characteristics of a floe with angular edges and has a bright radar return.

Little difficulty would exist in discriminating sea ice from fresh water ice (our case was a fresh water lake). The returns for the lake that had very little, if any, snow cover, and had an underlying layer of

water, were found to be at least 6 dB lower than the returns from thick first-year ice (which has the lowest return of any of the sea ice categories that were studied). The lake that was frozen to its mud bottom and had a heavy wet snow cover was found to have returns that were on the order of 8 dB higher than the previously described lake. The uncharacteristically high returns appear to be typical of ice with its snow surface in a melt condition. For example, it has been found for sea ice that returns may increase to a point in which there is little, if any, ability to discriminate among types.

## 5.0 MODELING OF BACKSCATTER RETURN

Theory, as long as it can be confirmed by experiment, provides a useful base from which one may judge the effects of the variation in the dielectric properties of the medium of interest, of wavelength, of the angle of incidence, and of transmit-receive polarizations. Backscatter theory is very useful as an aid to give insight into the understanding of scattering mechanisms.

The validity of the theory depends very heavily on the mathematical model that is used to describe target of interest, as well as on the approximations that may be necessary to be made to obtain some solution to the problem. Since even the simplest ground surfaces are extremely difficult to describe accurately, a true mathematical description of the ground surface or target volume appears impossible. Therefore, it is necessary to measure the radar return from natural and complex targets and then to use theory in a complementary role; i.e., as an aid in interpreting the results of the measurements, and in suggesting how they may be extrapolated.

### 5.1 Parashar's Backscatter Model

Parashar (1974) made an attempt to describe theoretically the radar backscatter cross-section for sea ice by considering the surface roughness of the ice and the amount of brine entrapped in the ice. Since the complex permittivity of sea ice is determined by both the properties of pure ice and the properties and amount of impurities present in the ice, Parashar used these in the description of the vertical profile of the complex permittivity. Random horizontal variations of the complex permittivity were also taken into account. The complex permittivity was considered to have a prescribed mean

vertical profile with random horizontal variation around this mean. The relative random variation was assumed to be small.

The wave scattering was considered to have components both from an irregular air/ice interface and from a continuously varying inhomogeneous medium (sea ice). The salinity profile of the ice was approximated by two intersecting line segments meeting at their end points. It was also convenient to consider the ice to consist of two regions, joined at the breakpoint in the salinity profile. Maxwell's equations were solved using the small perturbation techniques (Fung, 1969), WKB methods (Wait, 1962; and Brekhovskikh, 1960), and variations of parameters (Hildebrand, 1962). Calculations were performed for six categories of ice to obtain radar cross-sections versus incidence angle at 13.3 GHz and 400 MHz for VV and HH polarizations. Correlation lengths and variances were assumed for surface roughness and for the horizontal inhomogeneity within the ice for the different ice categories such that good agreement existed between the theoretical and experimental results. Since surface truth information was not available, parameters such as salinity, temperature, surface roughness and complex permittivity were assumed for each category of ice. Experimental and theoretical results showed similar relative trends from category to category.

## 5.2 Comparison of the Results of the Kansas Experiments with Parashar's Theoretical Model and the Results of Others

The backscatter model correctly predicted that the returns from multiyear ice should be greater than those of thick first-year ice (Figure 5-1). The model indicated a difference in absolute level would be on the order of 2 dB while Parashar's experimental results indicated

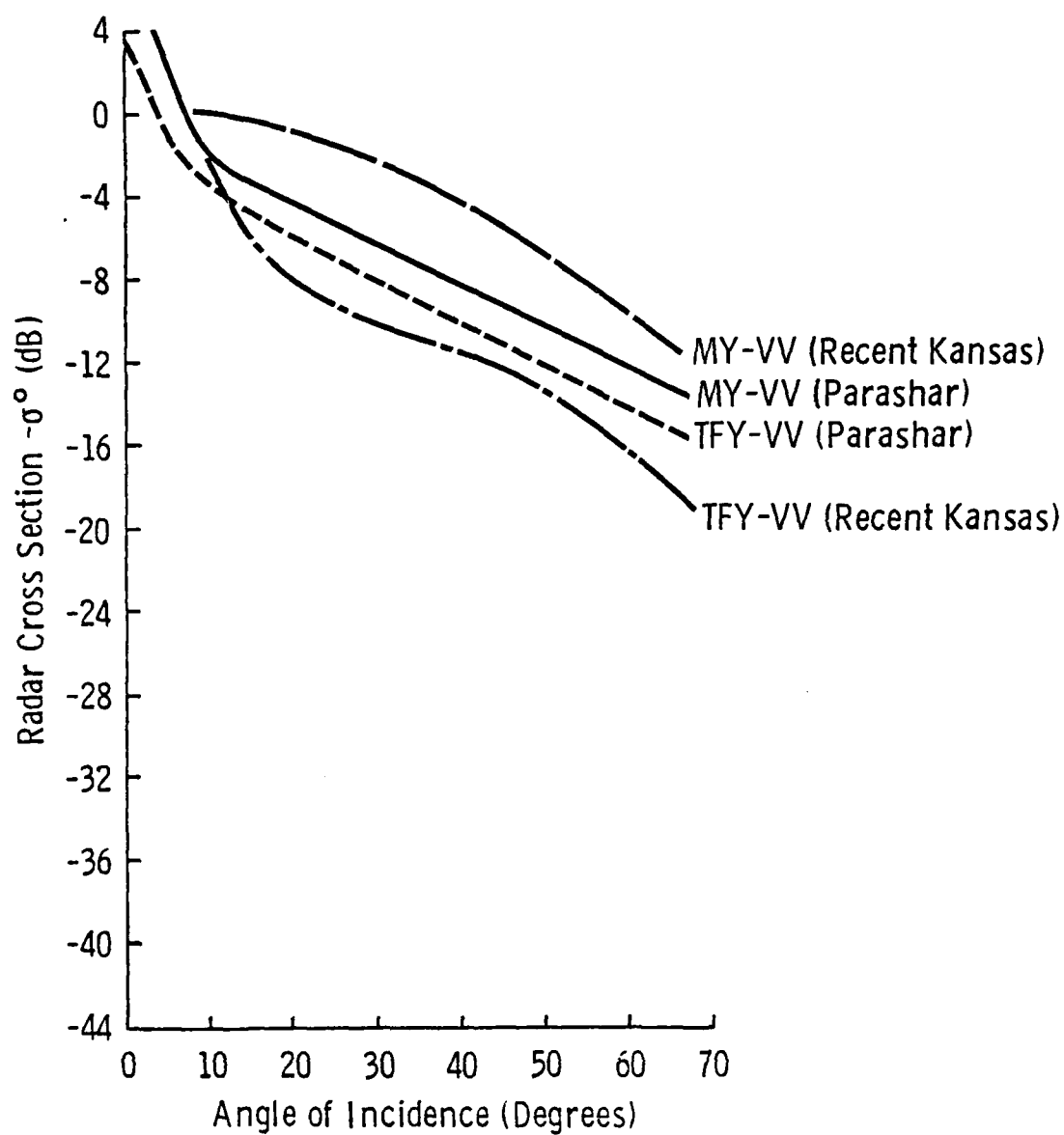


FIGURE 5-1 A comparison of Parashar's Theoretical Results and the Results of the Recent Kansas Experiments at 13 GHz, VV.

4 dB, the recent Kansas results indicated 7 dB, Gray's results indicated 4 to 13 dB, and Rouse's results indicated 6 dB (see Figure 5-2). The model angular responses from  $10^\circ$  to  $60^\circ$  may be fit with a straight line. This was also found to be true in all the experimental data. The model showed returns at VV polarization were consistently higher than returns at HH polarization and their slopes were significantly different. Recent Kansas data had VV returns consistently higher than HH returns, but with similar slopes. The model indicated that the response of multiyear ice and thick first-year ice were effectively the same from  $10^\circ$  to  $60^\circ$  and only differed in absolute level. Parashar's and Rouse's data indicated the same, but our recent data and Gray's data indicated that differences existed in the slopes on the two responses. The absolute levels of our recent results bounded the results of the theoretical model and the absolute levels of the other experimental data varied significantly from one another and from the theoretical model.

Absolute levels and the angular response of experimentally measured radar cross-sections of a target may vary from sensor to sensor as was demonstrated in the results presented above. Inaccuracies may arise due to two problem areas. First, the illumination pattern of the antennas must be known in great detail and second, extreme care must be taken to calibrate the sensor and this calibration must be done periodically. For a further discussion of these problem areas see Chapter 1.

### 5.3 An Empirical Model of Radar Backscatter from Thick First-Year Sea Ice, Multiyear Sea Ice, and Fresh Water Lake Ice

The angular responses of the radar cross-sections at 8 - 18 GHz frequencies of thick first-year sea ice, multiyear sea ice, and a frozen

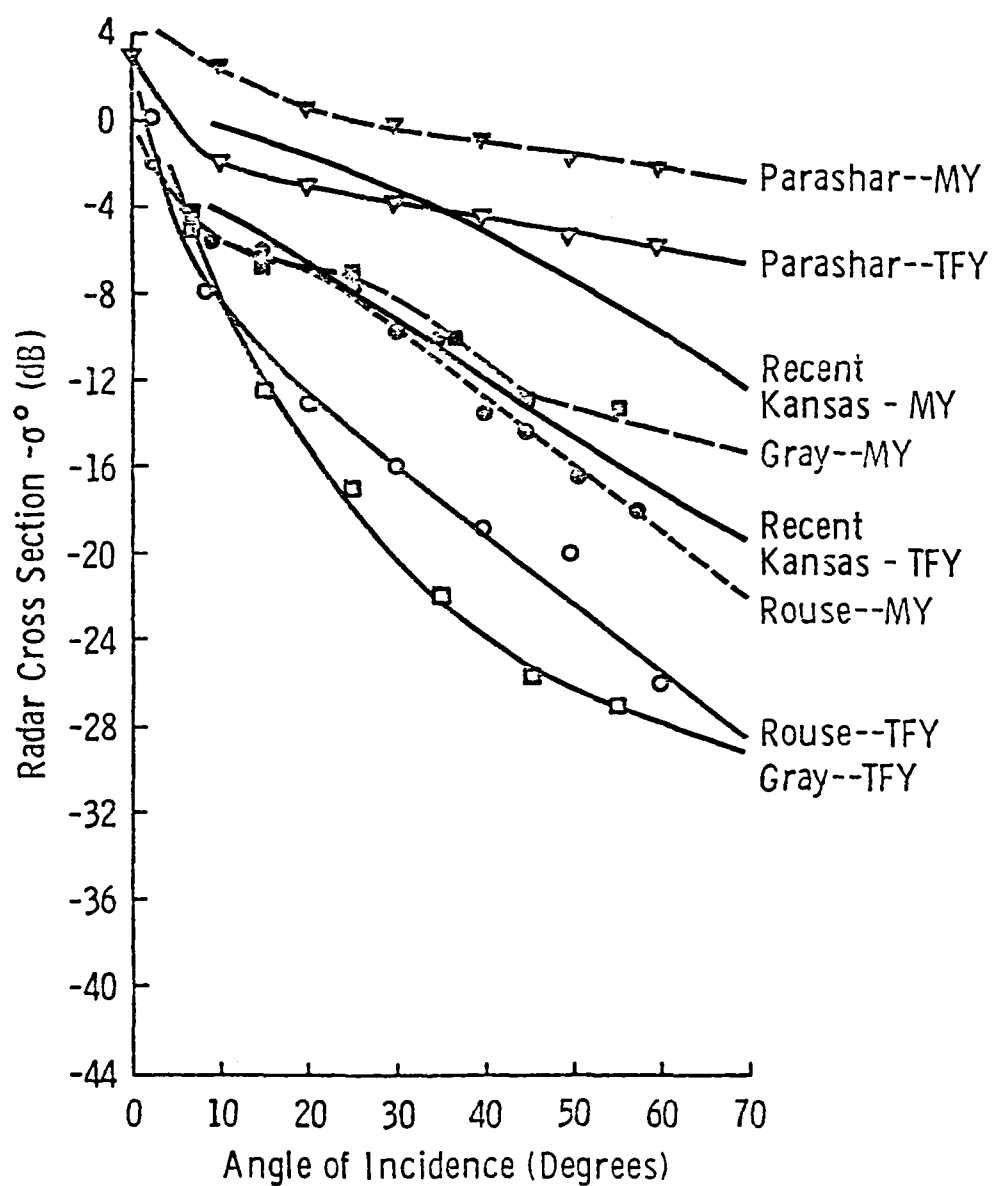


FIGURE 5-2 Comparison of multiyear and thick first-year ice scattering cross-sections (Experimental) according to Rouse (1968), Parashar, et al. (1974), and Gray, et al. (1977).

fresh water lake with an underlying layer of water and light snow cover were found to be reasonably well fit with a straight line at angles of incidences ranging from  $10^\circ$  to  $70^\circ$ . The straight lines were obtained by linear regression using the average (a magnitude average but expressed in dB) scatter obtained from the multiple looks measured at a given site. The scatter was found to fit a straight line for both like- and cross-polarizations. The average correlation coefficient obtained from the regressed data for HH polarization was on the order of .97. Using the critical absolute value test to indicate the significance of the correlation coefficient results in a critical value of .87 for a 1% level of significance. By comparing the correlation coefficient and the critical value it is seen that the null hypothesis that there is zero correlation in these linear trends is not justified. An empirical model has been developed to describe the backscatter for these three types of ice for the 8-18 GHz range of frequencies, angles of incidence ranging from  $10^\circ$  to  $70^\circ$ , and HH polarization. The slopes of VV and HH polarizations were found to be very much the same (both visually and statistically) and thus a model for VV polarization would be found to be basically the same.

The basic regression of the angular response of the data is described by:

$$\sigma_{dB}^0 = Y + M\theta \quad 10^\circ \leq \theta \leq 70^\circ \quad (5-1)$$

where:

$\sigma_{dB}^0$  is the differential scattering coefficient expressed in dB

Y is the intercept value

$M$  is the slope in dB/°  
and  $\theta$  is the angle of incidence expressed in degrees.

This is equivalent to, for real values of the scattering coefficient,

$$\sigma^\circ = a_0 e^{-\theta/\theta_0} \quad 10^\circ \leq \theta \leq 70^\circ \quad (5-2)$$

where:

$\sigma^\circ$  is the differential scattering coefficient in  $m^2/m^2$   
 $a_0$  is the magnitude constant  
 and  $\theta_0$  is the e-folding angle.

For our observation it was found that the regression must take into account both variations in return due to angle and variations due to the operating frequency. The slopes and intercepts obtained from the angular responses were regressed and fit with a straight line. These regression equations were

$$M = A + Bf \quad 8 \leq f \leq 18 \text{ GHz} \quad (5-3)$$

$$Y = D + Cf \quad 8 \leq f \leq 18 \text{ GHz} \quad (5-4)$$

where

- A is the intercept value of the frequency response of the slopes obtained from the angular responses
- B is the slope value of the frequency response of the slopes obtained from the angular responses
- C is the slope value of the frequency response of the intercepts obtained from the angular responses
- D is the intercept value of the frequency response of the intercepts obtained from the angular responses

and  $f$  is the value of the frequency ranging from 8 to 18 (GHz).

The overall expression of the scattering cross-section is then described by the equation:

$$\sigma^0(\text{dB}) = (A+Bf)\theta + Cf + D \quad \begin{array}{l} 8 \leq f \leq 18 \text{ GHz} \\ 10^\circ \leq \theta \leq 70^\circ \end{array} \quad (5-5)$$

The coefficients for the three ice types that were modeled have been included in Table 5-1. Also included is the standard error associated with the model when compared to the averaged data. This error was 2 dB or less and was considered to be reasonable because it maintained the ability to discriminate among ice types and because the error was less than the error associated with the data and the averaged data. The standard error associated with the data was around 3 dB for the worst case. For a comparison of the three ice types using the empirical model and a display of the standard deviation about the angular response, see Figure 5-3.

A statistical test, t-test, was performed to determine if the hypothesis that multiyear sea ice, thick first-year sea ice, and lake ice were statistically different was true. A large angle of incidence,  $60^\circ$ , was chosen for this test because the separation between ice types was less, thus a worst case. Data at 9 GHz (VV) was chosen since a sensor with these parameters is very much of interest. It was found that there was a 100% confidence that multiyear and thick first-year sea ice were statistically different. This was also found to be true for multiyear sea ice and lake ice. There was a 94.7% confidence that thick first-year sea ice and lake ice were statistically different.

TABLE 5.3-1

Regression Model Coefficient for Thick First-Year Sea Ice, Multiyear Sea Ice and Fresh Water Lake Ice with an Underlying Layer of Water and Little Snow Cover for 8-18 GHz Frequencies and Angles of Incidence from 10° to 70°.

Ice Type	Constant A	Constant B	Constant C	Constant D	Standard Error(dB)	Average Correlation Coefficient for Regression of Angular Response
Thick First-Year	-.3764	+.0097	-.1734	- 4.13	+2.02	.974
Multiyear	-.3137	+.0062	-.0047	- 1.70	+1.79	.964
Lake	-.2815	+.0015	+.2381	-13.76	+1.44	.970

#### 5.4 A Qualitative Description of Backscatter

A qualitative description of the backscatter properties of thick first-year sea ice, multiyear sea ice, and fresh water lake ice at Ku-X-Band frequencies has been made. From this description the existing backscatter theory may be modified and extended where needed. The scattering medium will be considered to consist of three major regions. The first is a homogeneous layer of air; the second is a layer of ice which will be described according to its surface roughness, its inhomogeneities, and its dielectric properties; and a homogeneous layer of sea water.

A family of radar cross-section curves, Figure 5-3, has been generated to illustrate, with many qualifications, the complex nature of the interaction of surface roughness and the volume scatter properties of the ice medium on angular response. Five conditions were considered. They are backscatter due to volume scatter alone, to a dominant volume scatter with a contribution of scatter from a slightly rough ( $<\lambda$ ) surface, to scatter from a slightly rough surface with some volume scatter, to scatter from a slightly rough surface, and to scatter from a very slightly rough surface. From this set of curves speculation into the backscatter properties of ice will be made. In Figure 4.5-33, the angular response of three categories of ice is illustrated. In our discussion, backscatter will be described in terms of the contribution of volume scatter, surface scatter, or the interaction of the two.

First we consider multiyear ice. Backscatter is speculated to consist of a significant component of volume scatter and a component of surface scatter. Volume scatter is suggested due to the gradually

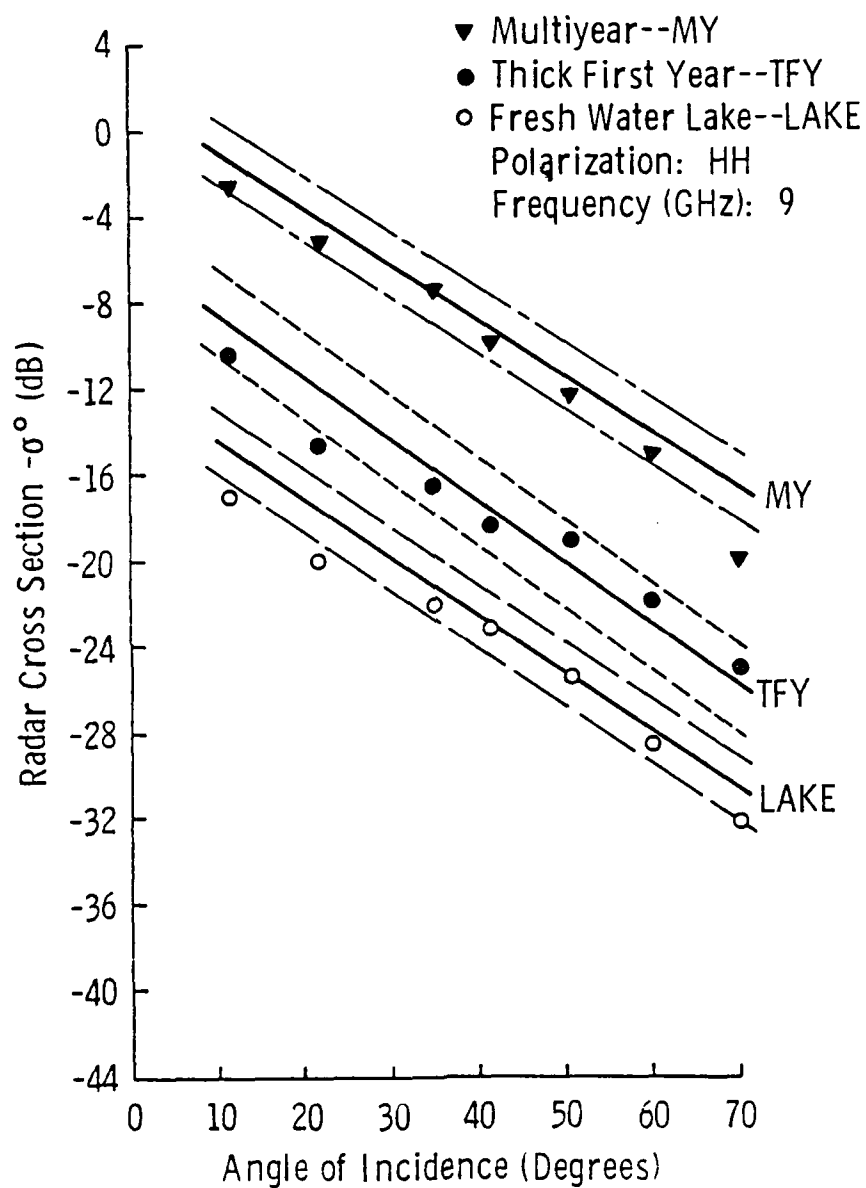


FIGURE 5-3 Scattering coefficients of multiyear, thick first-year and lake ice at 9 GHz, HH, using an empirical model developed from the recent Kansas experiments. Dashed lines indicate  $\pm s_{y/x}$ .

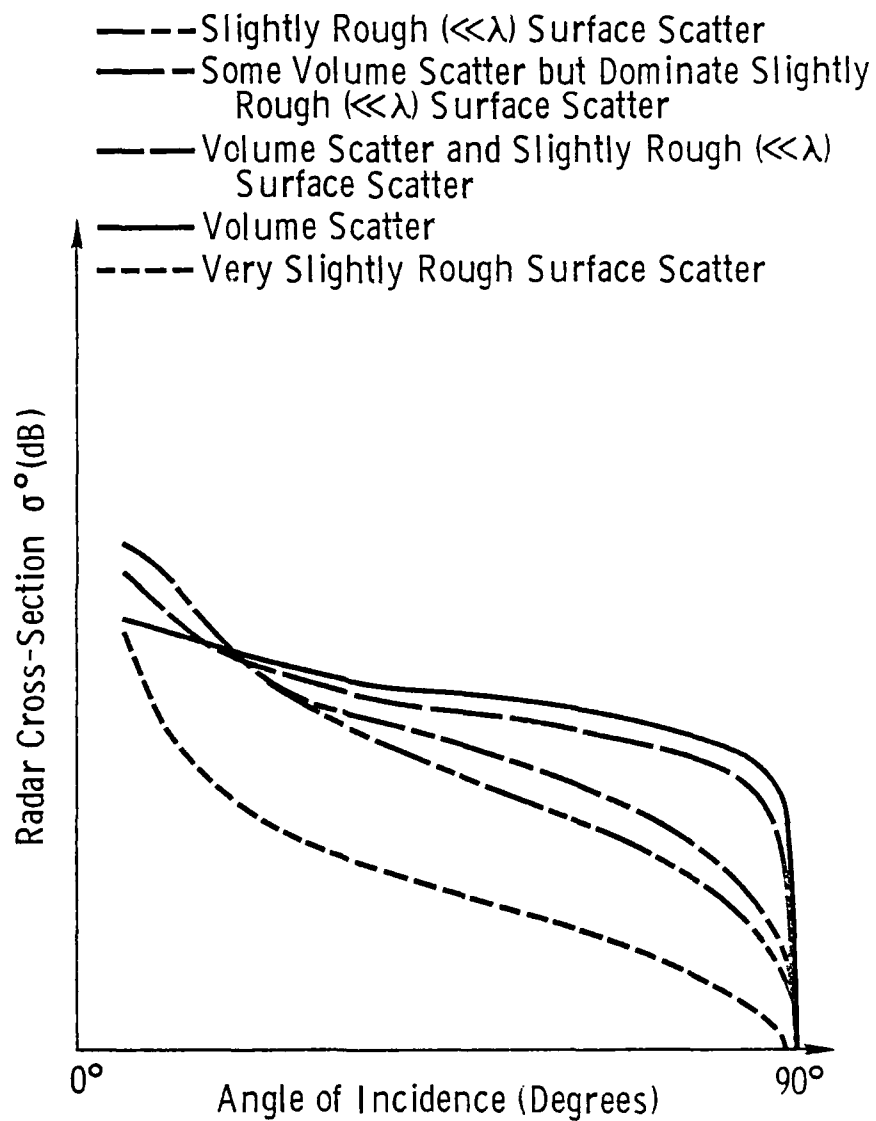


Figure 5-4. A family of radar cross-sections which illustrate the interaction of surface roughness and the volume scatter properties of ice.

decreasing angular response. Returns at large angles fall off too rapidly to be volume scatter alone. The addition of a rough surface has the effect of decreasing the isotropic effect of volume scatter (associated with a smooth surface) which results in a more rapidly decreasing angular response. The speculation that volume scatter is a significant component is seen to be justifiable when the attenuation coefficient and skin depth are examined. According to the literature [60,61], the attenuation coefficient is in the range of 10 dB or less for 1% salinity ice,  $-5^{\circ}$  C, and 10 GHz. The depth at which the electric field in the ice has been attenuated to 37% of its original value is called the skin depth and is 1.2 meter for the conditions given above. Two skin depths shall be considered to be a reasonable choice from which to consider the extent of the scattering volume into the ice. The power at this point is 2% of the power transmitted into the ice. Therefore, the scattering volume for the above conditions would extend into the multiyear ice 2.4 m. Surface truth shows dense distributions of air bubbles of a size less than a wavelength. These serve as the scattering sources in the volume and indicate the capability of the ice to have a large component of volume scatter.

It is speculated that the radar cross-section of thick first-year ice is dominated by surface scatter with some contribution of volume scatter. The rapidly decaying angular response near nadir angles is a shape that is characteristic of scatter from a slightly rough surface. However, a hump occurs at the middle angles and its existence is explained by including a component of volume scatter. The above speculation about backscatter from this type of ice is justified by noting that the surface has a roughness that is on the order of less

than a wavelength, the attenuation coefficient for 8% salinity ice at  $-5^{\circ}\text{C}$  and 10 GHz is 300-500 dB/m, and the skin depth is 2-3 cm [60,62]. Therefore, the scattering volume is small (the top 4-6 cm of the ice sheet) and, as seen from the surface truth photos, bubbles and inclusions on the order of much less than a wavelength exist in this upper layer of the ice sheet and serve as scattering centers.

Lake ice has an even lower return than thick first-year ice. Speculation is that the surface scatter contribution is on the same order of magnitude as that of the volume scattering component. This speculation considers the very uniform and decreasing angular response. The surface is much smoother than the surface of thick first-year ice and roughness is on an order of much-less-than-a-wavelength. Therefore, the absolute contribution due to surface scatter will be less. The attenuation coefficient is on the order of 1 dB/m and a skin depth of 8.7 m. Therefore, the scattering volume extends to the ice/water interface. Small air bubbles, much less than a wavelength in size, are found throughout the ice. Long drain tubes with diameters on the order of .5 mm and lengths on the order of wavelengths are found near the bottom. However, in comparison with multiyear and thick first-year ice the population of scattering centers is light. The reflection from the ice/water interface also serves to enhance the volume scattering effect.

## 6.0 CONCLUSIONS AND RECOMMENDATIONS

### 6.1 Results

The ability to use radar to discriminate ice types has further been demonstrated. Thick first-year, multiyear, and pressure ridged sea ice and fresh water lake ice have been investigated at 1.5 and from 8-18 GHz, at angles of incidence from  $10^\circ$  to  $70^\circ$  (with respect to nadir), and at antenna transmit-receive polarizations of VV and VH for 1.5 GHz and VV, VH, HH, and HV for 8-18 GHz.

The L-Band radar was found to have the ability to discriminate among fresh water ice, the thick categories of sea ice, and pressure ridged sea ice. At angles greater than  $60^\circ$  discrimination between thick first-year and multiyear ice may be possible, especially at cross-polarization. What was found in these experiments confirms what had been concluded from earlier SAR imagery. The practical use of L-Band radar would be in topographical mapping.

The Ku-X-Band radar was able to discriminate among the ice types investigated. The lowest frequency, 9 GHz, was found to provide the greatest separation between two ice types of major concern, thick first-year and multiyear sea ice. Cross-polarization provided a slightly greater separation than VV and HH. Significant levels of separation existed between angles of incidence from  $15^\circ$  to  $70^\circ$ . Pressure ridges are also of great concern. Since they are linear features of high return on a thick first-year background, they should be recognizable due to these characteristics in spite of possible confusion and an absolute scattering level basis with multiyear ice.

Ku-X-Band angular responses from  $10^\circ$  to  $70^\circ$  were regressed with a straight line. An average correlation coefficient of .97 (for 1% confidence the correlation coefficient for our measurements would need to be greater than .89) shows the goodness of the fit. The intercepts and slopes from this straight line were also regressed with straight lines and the results were used in an empirical model which describes the angular and frequency variations for thick first-year and multiyear sea ice and lake ice. The standard deviation between the model and averaged scattering cross-sections was at worst 2 dB. The individual measurements had a worst standard deviation of 3 dB about the average scattering cross-sections. Thus the model effectively describes the data.

## 6.2 Recommendations

There is a great need to investigate further the radar backscatter properties of sea ice. The experiments up to this point have surveyed, in a sense, what may be done with radar. The 1977 and 1978 Kansas experiments were the first of what hopefully will be many carefully staged attempts to describe quantitatively the backscatter properties of sea ice. In these experiments an abundance of surface truth information has been collected which describes the ice under investigation. This information will be used to develop an ice model from which a second generation backscatter model may evolve. Further work desperately needs to be done to pinpoint the locations and elements in the sea ice medium which contribute to the scatter. Recording of the intermediate-frequency returns from the target and processing these returns using Fast-Fourier-transform techniques have been proposed to begin this task.

Study of the effects of temperature on backscatter return is also needed. This must include measurement programs in the growing and melting seasons. These tend to be inherently difficult logistically, but are necessary in a complete description of the radar return of sea ice.

The 1978 experiment was the first experiment to consider quantitatively the role of the snow layer as a contributor to backscatter. Differences between returns from ice with a snow cover and bare ice were in the 3 dB range for thick first-year ice and up to 8 dB for lake ice. These effects need to be considered in the study of the signature of multiyear ice where the ice is almost pure and snow depths vary from none to many tens of cm.

The 9 GHz frequency was found to be the best for discrimination. But what about 2-8 GHz? It follows that these frequencies should also be considered in the puzzle since the lower X-Band frequencies were found to work so well.

Comparison of the measurements taken with the surface-based radar, the airborne SLAR and the SARs would be useful. Besides serving to give a calibration to the airborne imagery it would indicate the peculiarities that may arise due to the differences in what each radar sees.

What has yet to be done and would be extremely valuable is the use of airborne imaging radars in conjunction with a highly mobile scatterometer and ground truth team. The scheme of this type of complementary experiment is the use of an airborne radar to provide real time images, pinpoint areas of greatest interest from these images, fly the surface

Study of the effects of temperature on backscatter return is also needed. This must include measurement programs in the growing and melting seasons. These tend to be inherently difficult logistically, but are necessary in a complete description of the radar return of sea ice.

The 1978 experiment was the first experiment to consider quantitatively the role of the snow layer as a contributor to backscatter. Differences between returns from ice with a snow cover and bare ice were in the 3 dB range for thick first-year ice and up to 8 dB for lake ice. These effects need to be considered in the study of the signature of multiyear ice where the ice is almost pure and snow depths vary from none to many tens of cm.

The 9 GHz frequency was found to be the best for discrimination. But what about 2-8 GHz? It follows that these frequencies should also be considered in the puzzle since the lower X-Band frequencies were found to work so well.

Comparison of the measurements taken with the surface-based radar, the airborne SLAR and the SARs would be useful. Besides serving to give a calibration to the airborne imagery it would indicate the peculiarities that may arise due to the differences in what each radar sees.

What has yet to be done and would be extremely valuable is the use of airborne imaging radars in conjunction with a highly mobile scatterometer and ground truth team. The scheme of this type of complementary experiment is the use of an airborne radar to provide real time images, pinpoint areas of greatest interest from these images, fly the surface

truth team to the sites of interest, investigate the physical properties of these sites, and have a mobile calibrated radar make backscatter measurements. A fundamental problem has existed in past experiments in that imagery has been processed after the experiment is over. Because of this, sites that prove most puzzling and may contain an abundance of information remain unseen by surface parties.

The highly mobile calibrated radar that has been referred to above has been developed by the University of Kansas (HELOSCAT). It is mountable to a helicopter and at present operates at frequencies of 8-18 GHz, HH polarization, and incidence angles of 20°, 40°, and 60°.

### 6.3 Sensor

Description of an ice reconnaissance radar follows from the analysis of the data that is presently available. The operating frequency would be at the lowest X-Band frequencies (example: 9 GHz), operate at VV polarization, and at angles of incidence greater than 25°.

The lowest X-Band frequencies were chosen due to the frequency responses measured in the Kansas experiments. Indications are that separation among sea ice types is greater at this lower X-Ku-Band frequency. VV-polarization was selected according to Parashar's theoretical backscatter model and the results of the recent Kansas experiments. VV returns allow the same degree of discrimination as HH but radar cross-sections are slightly higher (recent experiments) or significantly higher (Parashar) in absolute level. Cross-polarization would allow a couple of dB of added separation to a range of separation that is already large for thick first-year and multiyear ice, but this is at the expense of working with cross-sections that are on the order of

10 dB lower. Nothing can be said at this time to indicate that a real benefit exists in operating at cross-polarization; however, Parashar and CCRC data indicate a possible advantage for thin ice types not studied in the recent experiments. Angles of incidence greater than  $25^\circ$  were chosen by considering both recent results and Parashar's theoretical and experimental results. Least confusion in discrimination occurs at angles away from the region where returns from different categories of ice intersect and change trends ( $15^\circ$  to  $20^\circ$ ). Angles between nadir and this region of overlap also may permit discrimination. However, open water has a high return at these angles and the effects of wind speeds on its backscatter return must be considered in the problem. At angles greater than  $25^\circ$  the angular responses more or less flatten out. The groups of categories of ice that would be discriminable according to the results at hand are multiyear ( $>2\text{m}$ ), thick first-year ( $1\text{-}2\text{m}$ ), new and thin ice ( $0^+ \text{-} 18\text{cm}$ ), and thick young and thin ice ( $18\text{-}100\text{cm}$ ). Open water in many instances would produce very low returns at these angles and be discriminable.

# REFERENCES

1. Anderson, V.H., "High Altitude Side-Looking Radar Images of Sea Ice in the Arctic," Proceedings of the Fourth Symposium on Remote Sensing of Environment, University of Michigan, Ann Arbor, 1966, pp. 845-857.
2. Rouse, J.W. (Jr.), "Arctic Ice Type Identification by Radar," Proceedings of IEEE, Vol. 57, 1969, pp. 605-614.
3. Johnson, J.D. and L.D. Farmer, "Use of Side-Looking Airborne Radar for Sea Ice Identification," Journal of Geophysical Research, Vol. 76, No. 9, 1971, pp. 2138-2155.
4. Glushkov, V.M. and V.B. Komarov, "Side-Looking Imaging Radar System TOROS and Its Application to the Study of Ice Conditions and Geological Explorations," Proceedings of the Seventh International Symposium on Remote Sensing of Environment, University of Michigan, Ann Arbor, 1971.
5. Ketchum, R.D. and S.G. Tooma, "Analysis and Interpretation of Airborne Multi-frequency Side-Looking Radar Sea Ice Imagery," Journal of Geophysical Research, Vol. 78, No. 3, 1973, pp. 520-538.
6. Parashar, S.K., A.W. Biggs, A.K. Fung and R.K. Moore, "Investigation of Radar Discrimination of Sea Ice," Proceedings of the Ninth International Symposium on Remote Sensing of Environment, University of Michigan, Ann Arbor, 1974.
7. Dunbar, M., "Interpretation of SLAR Imagery of Sea Ice, Nares Strait, and the Arctic Ocean," Journal of Glaciology, Vol. 15, No. 73, 1975, pp. 193-213.
8. Dunbar, M. and W.F. Weeks, "The Interpretation of Young Ice Forms in the Gulf of St. Lawrence Using Radar and IR Imagery," DREO Report No. 711, 1975, pp. 1-41.
9. Gray, L., R.O. Ramseier, and W.J. Campbell, "Scatterometer and SLAR Results Obtained Over Arctic Sea Ice and Their Relevance to the Problems of Arctic Ice Reconnaissance," Fourth Canadian Symposium on Remote Sensing, Quebec, Canada, May 1977, pp. 424-443.
10. Ketchum, R.D., "An Evaluation of Side-Looking Radar Imagery of Sea Ice Features and Condition in the Lincoln Sea, Nares Strait, and Baffin Bay <U>," NORDA Technical Note 7, 1977.
11. Moore, R.K., "Radar Scatterometry - An Active Remote Sensing Tool," The University of Kansas Center for Research, Inc., CRES Technical Report 61-11, Remote Sensing Laboratory, Lawrence, Kansas, 1966.

12. Parashar, S.K., "Investigation of Radar Discrimination of Sea Ice," (Ph.D. dissertation), The University of Kansas Center for Research, Inc., Remote Sensing Laboratory, Lawrence, Kansas, RSL Technical Report 185-13, May 1974.
13. Encyclopedia Britannica 1972, Vol. 2, "Arctic", pp. 331-349.
14. Untersteiner, N., K.L. Hunkins, and B.M. Buck, "Arctic Science: Current Knowledge and Future Thrusts," Arctic Science.
15. Gloersen, P., W. Nordburg, T.J. Schmugge, T.T. Wicheit, and W.J. Campbell, "Microwave Signatures of First-Year and Multi-Year Sea Ice," Journal of Geophysical Research, Vol. 78, No. 18, 20 June 1973, pp. 3564-3572.
16. Udin, I. and A. Ullerstig, A Numerical Model for Forecasting the Ice Motion in the Bay and Sea of Bothnia, Vastergotlands Tryckeri, Sweden, Skara 1977.
17. Biggs, A.W., "Volume Scattering from Sea Ice and Glacier Snow," The University of Kansas Center for Research, Inc., CRES Technical Report 137-2, Remote Sensing Laboratory, Lawrence, Kansas, July 1970.
18. Parashar, S.K., "State-of-the-Art -- Radar Measurement of Sea Ice," The University of Kansas Center for Research, Inc., CRES Technical Report 291-1, Remote Sensing Laboratory, Lawrence, Kansas, December 1975.
19. Dunbar, M., "A Glossary of Ice Terms (WMO Terminology)," Ice Seminar, Special Volume 10, The Canadian Institute of Mining and Metallurgy, 1969, pp. 105-110.
20. Campbell, W.J., R.O. Ramseier, W.F. Weeks, and P. Gloersen, "An Integrated Approach to the Remote Sensing of Floating Sea Ice," IAF Proceedings, Lisbon 1975.
21. Hallikainen, M., "Dielectric Properties of Sea Ice at Microwave Frequencies," Helsinki University of Technology, Radio Laboratory Report S 94, 1977.
22. Frankenstein, G. and R. Garner, "Equations for Determining the Brine Volume of SEa Ice from  $-0.5^{\circ}$  to  $-22.9^{\circ}$  C," Journal of Glaciology, Vol. 6, No. 48, 1967, pp. 934-944.
23. Assur, A., "Composition of Sea Ice and Its Tensile Strength," United States Army Snow and Ice and Permafrost Research Establishment, Wilmette, Illinois, December 1960.
24. Kester, D.R., "Comparison of Recent Seawater Freezing Point Data," Journal of Geophysical Research, Vol. 79, No. 30, 20 October 1974, pp. 4555-4556.

25. Weiner, O., "Zur Theorie der Refraktion Skonstater, Berichte Gesellschaft der Wissen Schaften zu Leipzig," Mathematischphysikalische Klasse, Bd. 62, Ht. 5, 1910, pp. 256-268.
26. Evans, S., "Dielectric Properties of Ice and Snow: A Review," Journal of Glaciology, Vol. 5, 1965, pp. 773.
27. Cummings, W., "The Dielectric Properties of Ice and Snow at 3.2 Centimeters," Journal of Applied Physics, Vol. 23, 1952.
28. Ulaby, F., A.K. Fung, and W.H. Stiles, "Backscatter and Emission of Snow: Literature Review and Recommendation for Future Investigation," The University of Kansas Center for Research, Inc., Remote Sensing Laboratory, RSL Technical Report 369-1, Lawrence, Kansas, June 1978.
29. Eder, F., "Das Elecktrische Verhalten von Bis," Annalen den Physik, 6, Folge, Ed. 1, Ht. 7-8, 1974, pp. 381-388.
30. Dorsey, N.E., "Properties of Ordinary Water Substance in All Its Phases: Water Vapour, Water and All the Ices," Reinhold, New York, 1970. (American Chemical Society, Monograph Series, No. 81).
31. Murphy, E.J., "The Temperature Dependence of the Relaxation Time of Polarization in Ice," Transactions of the Electrochemical Society, Vol. 65, 1934, pp. 133-142.
32. Stogryn, A., "Equations for Calculating the Dielectric Constant of Saline Water," IEEE Transactions on Microwave Theory and Technology, Vol. MIT-19, No. 8, August 1971, pp. 733-736.
33. Hoekstra, P. and P. Cappillino, "Dielectric Properties of Sea Ice and Sodium Chloride Ice at UHF and Micro-Wave Frequencies," Journal of Geophysical Research, Vol. 76, No. 20, July 1971, pp. 4922-4931.
34. Byrd, R.C., M. Yerkes, W.M. Sackinger, and T.E. Osterkamp, "Milli-meter Wave Reflectivity of Sea Ice," Ocean '72, IEEE International Conference on Engineering in the Ocean Environment, IEEE Publication, 1972.
35. Bogorodsky, V.V. and G.P. Khokhlov, "Electrical Properties of Ice in the Ice Edge Zone of the Bering Sea at 10 GHz Frequency," USSR/USA Bering Sea Experiment, Proceedings of the Final Symposium on the Results of the Joint Soviet-American Expedition, Leningrad, May 1974, Gidrometeoirdat, Leningrad 1975.
36. Vant, N.R., R.B. Gray, R.O. Ramseier, and V. Makios, "Dielectric Properties of Fresh and Sea Ice at 10 and 35 GHz," Journal of Applied Physics, Vol. 45, No. 11, November 1974, pp. 4712-4717.

37. Hallikainen, M., "Dielectric Properties of  $\text{NzCl}$  Ice at 16 GHz," Helsinki University of Technology, Radio Laboratory Report, 1977.
38. Tayler, L., "Dielectric Properties of Mixtures," IEEE Transactions on Antennas and Propagation, Vol. AP-13, No. 6, November 1965, pp. 943-947.
39. Auty, R.P. and R.H. Cole, "Dielectric Properties of Ice and Solid  $\text{D}_2\text{O}$ ," Journal of Chemical Physics, Vol. 20, No. 8, 1952, pp. 1309-1314.
40. Onstott, R.G. et al., "Backscatter Properties of Sea Ice with Radar --Arctic Operations Description and Preliminary Data Summary," Remote Sensing Laboratory Technical Memorandum, RSL TM 331-1, University of Kansas Center for Research, Inc., Lawrence, Kansas, October 1977.
41. Onstott, R.G., J.S. Patel, C.V. Delker, and R.K. Moore, "Investigation of Backscatter Properties of Sea Ice with Radar: Spring 1978 Arctic Experiment Description and Preliminary Results," Remote Sensing Laboratory Technical Memorandum, RSL TM 331-3, University of Kansas Center for Research, Inc., Lawrence, Kansas, July 1978.
42. Waite, W.P., "Broad-Spectrum Electromagnetic Backscatter," CRES Technical Report 133-17, University of Kansas Center for Research, Inc., Lawrence, Kansas, 1970.
43. Marshall, J.S. and W. Hitchfield, "Interpretation of the Fluctuating Echo from Randomly Distributed Scatterers, Part 1," Canadian Journal of Physics, Vol. 31, No. 6, pp. 962-994, September, 1953.
44. Moore, R.K., W.P. Waite, and J.W. Rouse, Jr., "Panchromatic and Polychromatic Radar," Proc. IEEE, Vol. 57, pp. 590-593, 1969.
45. Moore, R.K., "Radar Return from the Ground," University of Kansas, The Bulletin of Engineering, No. 59, 1969.
46. Moore, R.K., "Ground Return," Radar Handbook, M.I. Skolnik (Editor), McGraw-Hill Book Company, Inc., New York, 1970.
47. Bush, T.F. and F.T. Ulaby, "8-18 GHz Radar Spectrometer," CRES Technical Report 177-43, University of Kansas Center for Research, Inc., Lawrence, Kansas, September 1970.
48. Weeks, W.F. and A. Assur, "The Mechanical Properties of Sea Ice," Cold Regions Res. and Eng. Lab., Cold Regions Sci. and Eng., II-C3, 1967.
49. Weeks, W.F. and A. Assur, "The Fracture of Lake and Sea Ice," Cold Regions Res. and Eng. Lab., Res. Rept. 269, 1969.

50. Weeks, W.F. and A.J. Gow, "Preferred Crystal Orientations in the Fast-Ice Along the Margins of the Arctic Ocean," Journal of Geophysical Research, 1978.
51. Continental Shelf Data Systems, Beaufort Sea-Arctic Coast: Oceanographic and Climatologic Data, Vol. 1, Continental Shelf Data Systems, Rockville, Maryland, 1969.
52. Hufford, G. and 12 others, "Physical Oceanography," Beaufort Sea Synthesis Report, Spec. Bull. 15, Outer Continental Shelf Environmental Assessment Program, Arctic Project Office, Geophysical Institute, University of Alaska, 29-42, 1977.
53. Kovacs, A. and R.M. Morey, "Radar Anisotropy of Sea Ice Due to Preferred Azimuthal Orientation of the Horizontal C-Axes of Ice Crystals," Journal of Geophysical Research, 1978.
54. Weeks, W.F. and A.J. Gow, "Crystal Alignments in the Fast Ice of the Arctic Ocean," Cold Regions Res. and Eng. Lab. Rept. 79, 1979.
55. Fung, A.K., "Mechanisms of Polarized and Depolarized Scattering from a Rough Dielectric Surface," Journal of the Franklin Institute, Vol. 285, No. 2, February, 1968.
56. Stiles, W.H. and F.T. Ulaby, "Microwave Remote Sensing Snowpacks," The University of Kansas Center for Research, Inc., Remote Sensing Laboratory, Lawrence, Kansas, RSL Technical Report 340-3, October 1979.
57. Wait, J.R., Electromagnetic Waves in Stratified Media, The MacMillan Company, New York, 1962.
58. Brekhovskikh, L.M., Waves in Layered Media, Academic Press, Inc., New York, 1960.
59. Hilderbrand, F.B., Advanced Calculus for Applications, Prentice-Hall, Inc., New Jersey, 1962.
60. Vant, M.R., R.O. Ramseier, and V. Makios, "The Complex-Dielectric Constant of Sea Ice at Frequencies in the Range 0.1-40 GHz," Journal of Applied Physics, 49(3), March 1978.
61. Bogorodsky, V.V., "Electromagnetic Characteristics of Sea Ice," Arctic and Antarctic Research Institute, Presented at the International Workshop on the Remote Estimation of Sea Ice Thickness, St. John's Newfoundland, September 25, 1979.
62. Moore, R.K., et al., "Microwave Remote Sensors," Manual of Remote Sensing, R.G. Reaves (Editor), American Society of Photogrammetry, Virginia, 1975, pp. 399-534.

**DAT  
FILM**